Behavior of Bridge Slab Ends at Expansion Joints

by

Elizabeth Michelle Griffith, B.S.

Thesis

Presented to the Faculty of the Graduate School of

The University of Texas at Austin

in Partial Fulfillment

of the Requirements

for the Degree of

Masters of Science in Engineering

The University of Texas at Austin

December 2003

Behavior of Bridge Slab Ends at Expansion Joints

Approved by
Supervising Committee:

_____

Oguzhan Bayrak, Supervisor

_____

Richard Klingner, Supervisor

_____

James Jirsa

Dedication

To Joel, for waiting patiently. I will always love you.

Acknowledgements

I would like to thank Dr. Oguzhan Bayrak for his tireless efforts on this project, his good humor, and his willingness to see others in a flattering light. I would like to thank Dr. Richard Klinger for the generous amount of time and effort he has given this project. His dedication to maintaining high standards was an invaluable contribution to this project and this thesis in particular. I would also like to thank Dr. James Jirsa for always making himself available when his guidance, experience, and advice were needed.

I am grateful to Texas Department of Transportation for providing the funding that made this research study and my graduate education possible. In particular, I would like to thank Dean Van Landuyt, the TxDOT project director for this project, for his enthusiastic involvement and ability to instantly recognize my voice on the phone after months of not hearing it.

I would like to thank the other graduate students who have worked on this project, Jeremy Ryan for paving the way and Christin Coselli for all of her hard work. The talents of the lab staff, Blake Stansey, Mike Bell, Dennis Phillip, and Ray Madonna, and the hard work of undergraduates Corey Redding, Kyle Steuck, and Will Slaughter made the construction of this massive specimen possible. I would also like to thank Hortensia Peoples, Mary Joe Moore, Regina Forward, and Michelle Santos for all of the help and entertainment they provided.

I would like to thank my family for their support. I would especially like to thank my brother, Christopher Woodward, for his efforts to create the drawings

in this thesis. I would like to thank my mother, Judy Woodward, who preserved my sanity by listening to all of my stories on trips to and from Dallas. I would also like to thank Mike and Sylvia Griffith for the countless weekends of volunteer pet-sitting.

Most of all, I wish to thank my kind husband, Joel Griffith, for everything. You made me stay when I wanted to move to Dallas, and you made me stay when you wanted me to move to Dallas. Thank you for reminding me how important this was and why I was here in the first place.

December 2, 2003

Abstract

Behavior of Bridge Slab Ends at Expansion Joints

Elizabeth Michelle Griffith, M.S.E.

The University of Texas at Austin, 2003

Supervisors: Oguzhan Bayrak, Richard Klingner, and James Jirsa

The Texas Department of Transportation (TxDOT) currently uses, for most of its bridges, the "IBTS" standard detail for bridge slab ends at expansion joints. That detail has evolved as a way of achieving increased transverse stiffness at slab ends, without using diaphragms. In the ITBS detail, slab ends are stiffened by a 2-in. (51-mm) increase in slab thickness and a slightly reduced reinforcement spacing for skewed slabs. Although the origin of this detail is unknown, it has been used successfully by TxDOT for decades.

Bridges in Texas are designed in accordance with AASHTO provisions. While AASHTO design loads are typically at the HS-20 level, several TxDOT districts have considered increasing those by a factor of 1.25, to what has been unofficially designated an "HS-25 level." In part, this study seeks to understand the behavior of slab ends under HS-20 and HS-25 applied load levels. Two specimens have been constructed thus far, one constructed with 0º skew slab ends (Ryan 2003) and one constructed with 45º skew slab ends.

An alternate and possibly more economical detail was designed with a flexural capacity similar to that of the IBTS detail but without a thickened edge. Designated the Uniform Thickness Slab End (UTSE) detail, it was also instrumented and tested, and its performance was compared with that of the IBTS detail.

For the 45º skew specimen, a three-bay concrete slab, 21 ft 6 in by 33 ft 7 in. (6.5 by 10.2 m), was built composite with four steel girders. The IBTS and UTSE end details were constructed on opposite sides. Loads were applied to four test areas in the AASHTO design tandem load configuration to HS-20, HS-25 and overload levels, such that negative bending was maximized over the girder in the two 8-ft (2.4-m) bay slab ends, and positive bending was maximized in the two 10-ft (3.0-m) bay slab ends. All test areas were ultimately loaded to failure.

For the 45º skew specimen, the UTSE and IBTS end details performed well at HS-20 and HS-25 load levels. At these loads, reinforcing bar strains were insignificant (less than $0.1\varepsilon_y$) and deflections were extremely small relative to girder spacing (between l/2000 and l/36000). Cracking was not observed at the HS-20 and HS-25 load level in the 8-ft (2.4-m) girder spacing bays. Only the UTSE detail, positive moment test area cracked at the HS-20 load level. The IBTS detail, positive moment test area cracked at the HS-25 load level.

In the 45º skew specimen, test areas had high reserve strength: where negative moment was maximized, the specimen failed at around 6.0 x HS-25, and where positive moment was maximized, the specimen failed at around 4.0 x HS-25. All test areas failed in punching shear, with the exception of the IBTS detail, positive-moment test area, which failed in one-way shear.

Comparisons have been made for the IBTS and UTSE end details constructed at both a 0º skew and 45º skew. An increase in applied loads from HS-20 to HS-25 load levels frequently resulted in a nearly proportional increase in midspan edge deflection and tensile strain in reinforcement. At both HS-20

and HS-25 load levels, tensile strains in transverse reinforcement and the deflection-to-girder-spacing ratio were both extremely small (always less 10% of yield strain and l/800 respectively). Slab ends usually remained uncracked until multiples of the HS-20 design load level, with the exception of the 45º skew, 10-ft (3.0-m) girder spacing, UTSE detail test area, which cracked at 1.0 x HS-20 (13 kips per load point, or 56 kN). When loaded to maximize negative moment, slab ends in 8-ft (2.4-m) bays usually failed around 6.0 x HS-20 (75 kips per load point, or 335 kN). When loaded to maximize positive moment, slab ends in 10-ft (3.0-m) bays failed at load levels higher than 3.8 x HS-25 (48 kips per load point, or 210 kN).

Table of Contents

xiv

List of Tables

List of Figures

CHAPTER 1

Objectives and Scope

1.1 INTRODUCTION

The Texas Department of Transportation (TxDOT) currently uses, for most of its bridges, the "IBTS" standard detail for bridge slab ends at expansion joints. That detail, shown in Figure 1-1and Figure 1-2, has evolved as a way of achieving increased transverse stiffness at slab ends, without using diaphragms. In the ITBS detail, slab ends are stiffened by a 2-in. (51-mm) increase in slab thickness and a slightly reduced reinforcement spacing for skewed slabs. Although the origin of this detail is unknown, it has been used successfully by TxDOT for decades.

Bridges in Texas are designed in accordance with AASHTO provisions. While AASHTO design loads are typically at the HS-20 level, several TxDOT districts have considered increasing those by a factor of 1.25, to what has been unofficially designated an "HS-25 level." This de facto increase has two underlying motivations:

First, trucks may be operated beyond their legal weight limits, and it is useful for TxDOT to understand the possible consequences of such overloads.

Second, the North American Free Trade Agreement (NAFTA), implemented in 1994, has allowed increased trade between the United States and Mexico, and has noticeably increased truck traffic in Texas. This increased traffic has complicated the above concerns over possible consequences of overloaded trucks.
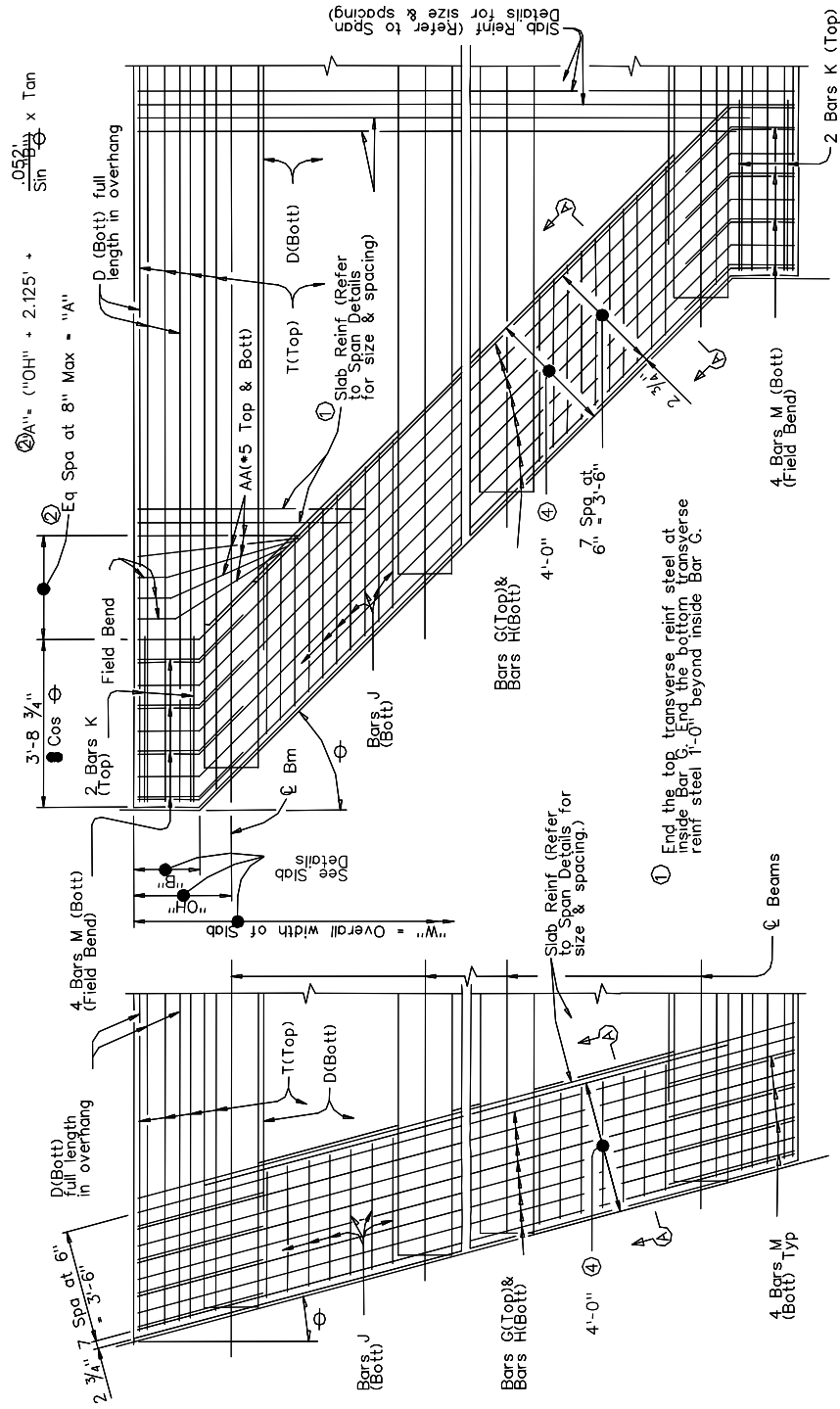
Figure 1-1 IBTS detail, plan view

2
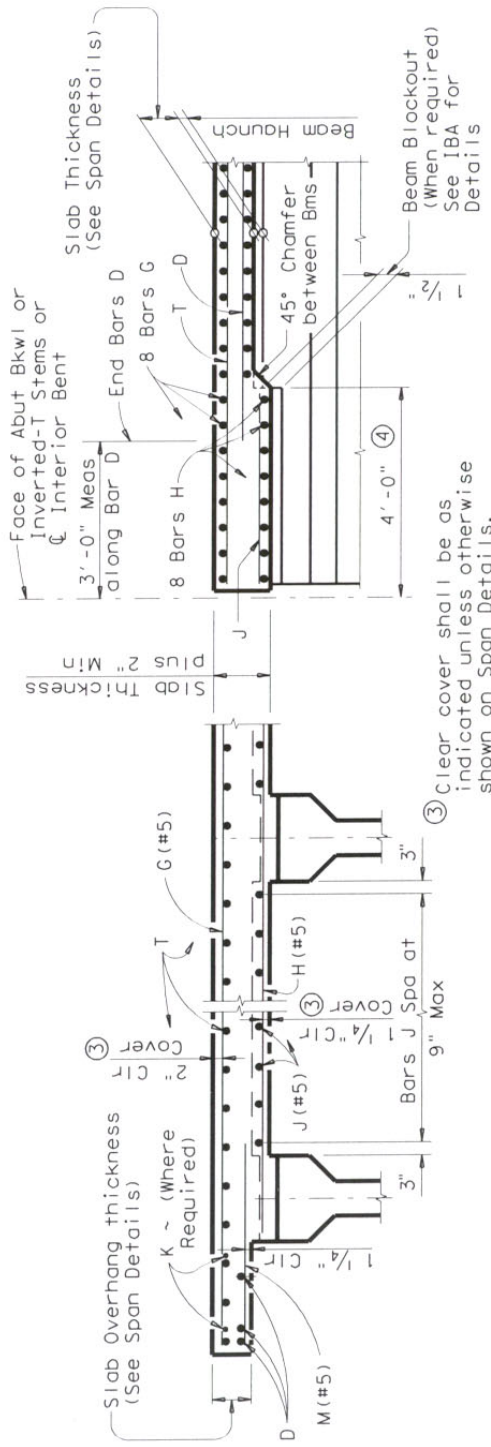
TYPICAL TRANSVERSE SECTION

Slab Overhang thickness (See Span Details)

K ~ (Where Required)

1 1/4" Clr

D

M (#5)

2" Clr Cover ③

T

G (#5)

H (#5)

③ Cover 1 1/4" Clr

J (#5)

Bars J Spa at 9" Max

3"

3"

Slab Thickness plus 2" Min

J

③ Clear cover shall be as indicated unless otherwise shown on Span Details.

SECTION A-A

Face of Abut Bkwl or Inverted-T Stems or ℄ Interior Bent

3'-0" Meas along Bar D

8 Bars H

8 Bars D

End Bars D

D

T

8 Bars G

Slab Thickness (See Span Details)

Beam Haunch

45° Chamfer between Bms

Beam Blockout (When required) See IBA for Details

④

4'-0"

1 1/2"

Figure 1-2 IBTS detail, elevation view

The capacity and behavior of the IBTS slab end detail under applied AASHTO design loads is not known with certainty. Previous related research has focused on the behavior of bridge decks with diaphragms. Tests have indicated that at interior locations, bridge decks fail in punching shear at loads far exceeding their design capacity. This is primarily due to the effects of two-way action and arching action in increasing flexural capacity. At deck edges, where those effects are not as pronounced, capacity would not be expected to be similarly increase as much. The effect of different edge details, and in particular of the IBTS detail, has not been studied.

The research described here is intended to fill that gap. The research is intended to show how loads are carried at free edges of slabs; how skew affects behavior at free edges; how serviceability and capacity are affected by the use of the IBTS end detail and the elimination of diaphragms; and how this behavior can be modeled for design purposes.

Most prior bridge-deck tests have been performed on scaled specimens, and only rarely on full-scale ones. According to Bazant and Cao (1987), results from scaled specimens may be unconservative, however. For models of identical proportions with proportional critical perimeters, the stress at punching shear failure increases with decreasing specimen size. This so-called "size effect" could result in higher punching-shear capacities for smaller-scale models. For this reason, this research study used full-scale specimens.

1.1.1 IBTS End Detail

The IBTS end detail may not be easy to construct, because the thickened edge requires additional formwork. If the reserve strength of the free edge of the bridge deck is adequate, the thickened edge may be unnecessary for capacity. To investigate this, an alternate and possibly more economical detail was designed

4

with a flexural capacity similar to that of the IBTS detail but without a thickened edge. Designated the Uniform Thickness Slab End (UTSE) detail, it was tested, and its performance was compared with that of the IBTS detail.

1.2   OBJECTIVES AND SCOPE

The objectives of the research study are as follows:

- To understand and explain the behavior of slab ends at expansion joints, with special emphasis on skew ends.
- To determine the performance of the IBTS detail when loaded with design loads (HS-20 and HS-25) and typical overloads.
- To determine the ultimate capacity and failure mechanism of the IBTS detail.
- To test an alternate edge detail (UTSE) and compare the behavior with the IBTS detail
- To develop guidelines for TxDOT engineers to follow in designing bridge-deck end details, if current practice is shown to be inadequate.

Two test specimens have been constructed for this study to date. The first specimen, built with 0º skew, had both the IBTS and UTSE end details and was tested to understand the effects of design variables other than skew. Results from tests on this first specimen are given in Ryan (2003). The second specimen, the subject of this thesis, was built with 45º skew at both ends. Because the UTSE detail performed adequately in the 0º skew specimen, that detail was used in the 45º specimen as well. In this thesis, test results from the 45º skew specimen are presented and the comparison of results from the 0º skew specimen.

1.3 **SITE VISITS**

To observe the IBTS detail as constructed in the field, two site visits were made prior to building the 0º skew specimen. The first bridge visited, located on IH-35 in San Marcos, TX, crossed the San Marcos River. The second bridge visited was an overpass on US 290, crossing over US 183. Witnessing the construction of slab ends allowed for observations of differences between the IBTS detail and slab ends, as built.

Typical of most TxDOT bridge construction, prestressed panels were used in both bridges as stay-in-place formwork in the interior of the deck, up to the IBTS detail. Prestressed concrete girders were used in both bridges; Figure 1-3 shows the top of a girder with stirrups extending into the deck.
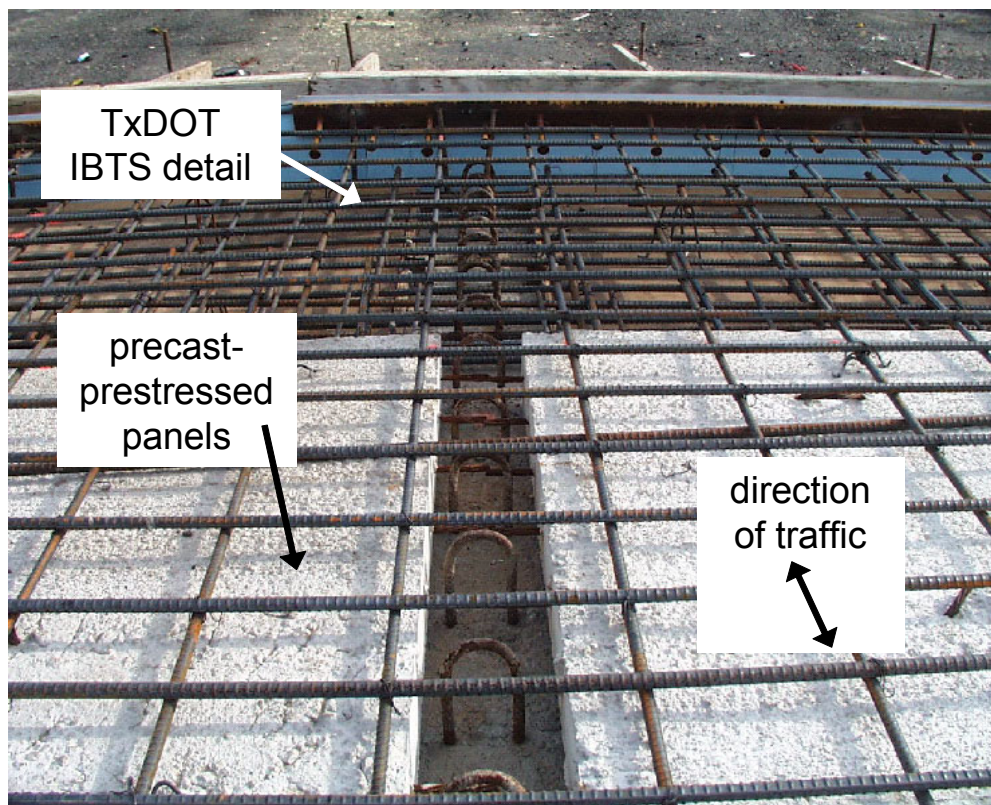
Figure 1-3: Prestressed panels and shear stirrups

Armored joints were cast into the top edge of the decks at the expansion joints (Figure 1-4). Although this is a standard detail in TxDOT designs, it was not included in the 0º skew or 45º skew specimens. The armored joint is assumed to make no contribution to the strength of the slab at the joint in design calculations. While the effects of armored joints are not investigated in this study, it will be included in future studies.
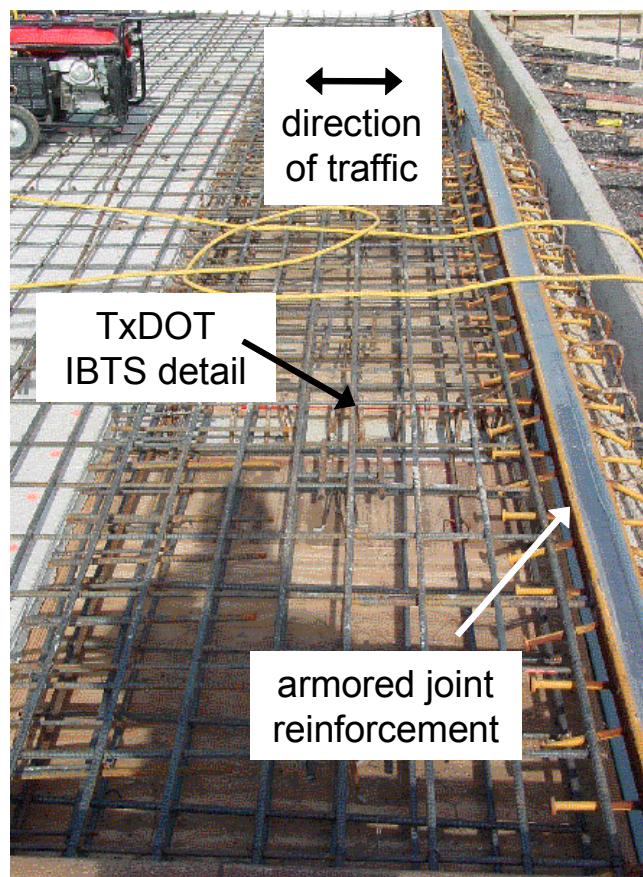
Figure 1-4: IBTS detail prior to concrete placement

In the field, deck concrete was placed using a concrete pump, and was consolidated with mechanical vibrators. It was leveled using a vibrating, movable screed on temporary rails (Figure 1-5), and finished with bull floats. The process was continuous, allowing long lengths of deck to be placed efficiently. These

field construction techniques were modified for constructing the laboratory test specimens (Section 4.2).

Figure 1-5: Placing of concrete in the field

1.4   OUTLINE OF THIS THESIS

In Chapter 2, previous research in areas related to slab ends at expansion joints is summarized, and its relevance to this research program is discussed. In Chapter 3, the development of the 0º skew specimen is briefly addressed, followed by a detailed discussion of the development of the 45º skew specimen. In Chapter 4, test methods and means are discussed. In Chapter 5, results from the 45º skew-specimen slab end tests are discussed, followed by a comparison of the behavior of the four span tests. In Chapter 6, results from tests performed on the 45º skew specimen overhangs are presented and discussed. In Chapter 7, results from the 0º skew and 45º skew specimens are compared, and design

methodology for slab ends is discussed. In Chapter 8, the results from the slab end and the overhang tests in the 45º skew specimen are summarized, along with the conclusions based on those results.

CHAPTER 2

Previous Bridge Deck Research

2.1 INTRODUCTION

In this chapter, research studies contributing to the understanding of bridge-deck behavior at slab ends are summarized. Studies pertaining to the punching-shear capacity of bridge slabs and the effects of arching action on slab capacity, and their relevance to this study is discussed.

2.2 EARLY RESEARCH – BEFORE 1990

The earliest slab research focused on the behavior of slabs in reinforced concrete structures and flexural behavior. In the 1952, Ockleston[26,27] tested a three-story, reinforced concrete building in Johannesburg, loading the flat plate slabs of various sizes to failure. This early research program examined the failure loads and failure mechanisms of slabs, finding that the tested capacities exceeded predictions based on plastic analysis. Several explanations for this were considered. Ockleston stated that although the measured and predicted capacities didn't agree, the observed cracking patterns and slab deflections agreed well with the predicted collapse mechanisms. Deflections were too small to assume that the contribution of catenary action increased the load-carrying capacity, so Ockleston focused on the ability of plasticity-based models to predict flexural capacity. Trying to improve the predictions of yield-line analysis, he assumed that the reinforcement was stressed to its ultimate tensile strength at failure, rather than to yield stress, as was ordinarily assumed. Even incorporating this change, the difference between observed and predicted collapse loads was significant.

10

Ockleston believed that the discrepancy between observed and predicted capacities could be accounted for by the effects of compressive membrane action (also referred to as "arching action"), but he could not predict the extent to which this would increase slab capacity. In 1963, Christiansen[10] published a detailed theory of the mechanics of arching action that could be used to predict the magnitude of membrane stresses and the effects of these stresses on slab capacity.

The phenomenon of arching action refers to in-plane forces generated after flexural cracking of laterally restrained slabs.[31] Once flexural cracking occurs, a compression field emanating from the load point spreads to the supports (Figure 2-1). Equilibrium is maintained by a tension hoop around the compression field, as well as by bottom reinforcement in the slab that acts as tension ties (Graddy, 2002).
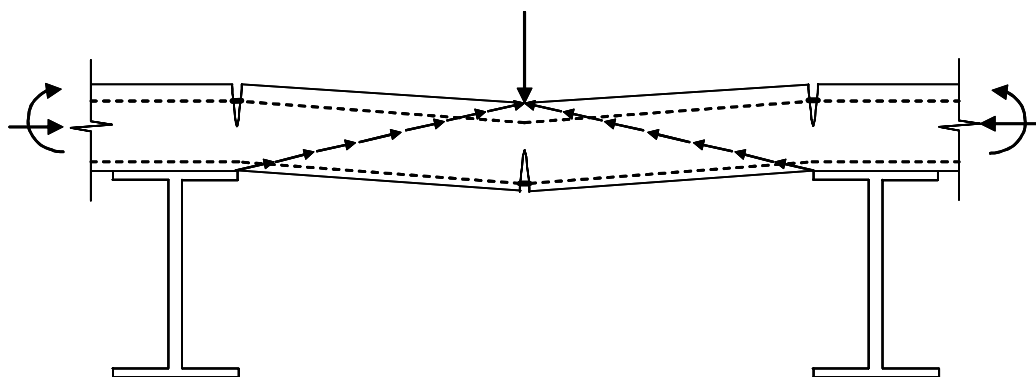
Figure 2-1: Arching action[31]

The extent of arching action depends on a number of factors, including lateral restraint of the supports, material properties and slab thickness. Full lateral restraint of the supports is not necessary to develop in-plane forces, as continuous deck slabs on girders can exhibit arching action, but slab thickness and plan extent must be sufficient.

In the 1960's, the Ontario Ministry of Transportation and Communications sponsored a series of tests on bridge slabs performed at Queen's University in

11

Kingston, Ontario. These tests focused on the presence of compressive membrane action in bridge slabs, the resulting increase in the flexural capacity of those slabs, and their consequent reserve strength. In the 1970's, Batchelor and Hewitt published several articles discussing these studies. Those articles are now discussed here.

2.2.1 Batchelor and Hewitt (1976)

To develop a method to predict the ultimate out-of-plane flexural capacity of bridge slabs, Batchelor and Hewitt performed 31 tests on eight, 1/8th-scale bridge specimens. Those specimens had different percentages and arrangement of reinforcement, and their decks had different span-to-thickness ratios. The test specimens were modeled after two prototype bridge slabs, both 80 ft (24.4 m) long and 7 in. (178 mm) thick, designed for HS-20 and HS-44 loads. Based on these two full-scale designs, eight 4-girder scaled test specimens were fabricated. Indented wire reinforcement with a diameter of 0.0915 in. (2.32 mm) was used to simulate flexural reinforcement, in reinforcement ratios from 0% to 0.6%. Nails 3 in. (8 mm) long simulated shear studs. Four diaphragms were installed in each specimen, at slab ends and at intervals of 2.5 ft (760 mm) along the girders. The average 14-day compressive strength of the concrete was 5000 psi (35 MPa).

Loads were applied to a ½-in. (13-mm) thick, elliptical steel plate, scaled to represent the contact area of tires of large trucks. The loads were applied at midspan between girders in the transverse direction and equidistant between two diaphragms in the longitudinal direction. To study the effects of transverse cracking on punching shear capacity, cracking was deliberately introduced in the deck of one specimen, but the effects of the induced cracks were negligible.

With only two exceptions, loaded areas failed in punching shear. For all tests, the average capacity was approximately 16 kips (71 kN) per load point, 22

12

times the scaled AASHTO HS-20 truck load. A discussion of AASHTO design loads is given in Section 3.2.3.

Results from that test program indicated that the location of the tested panel in the specimen and the magnitude of dead-load stresses had little to no influence on the capacity. They also showed that punching-shear capacity decreased with decreasing percentage of flexural reinforcement. The punching-shear capacity of an unreinforced test section, however, was still 10 times the HS-20 design load.

Because bridge decks, designed for flexure, actually would probably fail in punching shear, Batchelor and Hewitt believed that AASHTO flexural-design provisions were excessively conservative, and that arching action sufficiently increased flexural capacity as to make punching shear the controlling failure mechanism. They advocated the use of only 0.2% isotropic reinforcement placed at the center of the slab, as required by AASHTO provisions for temperature and shrinkage reinforcement.

2.2.2   Arching Action and the Ontario Design Method

Under the auspices of the Ontario Ministry of Transportation, Csagoly, Holowka, and Dorton[11] sought to verify the high reserve strength predicted by Batchaelor and Hewitt by testing in-service bridges in the Province of Ontario. Csagoly et al. agreed with Batchaelor and Hewitt: arching action increased the flexural capacity of slabs, causing them to fail in punching shear. They also agreed that bridge slabs could be adequately reinforced by the use of only 0.3% isotropic reinforcement, placed at mid-depth of the slab. To verify the results of Batchaelor and Hewitt, Csagoly et al. field-tested 40 existing bridge decks in the Province of Ontario, Canada. Based on the results of those field tests and of additional tests of Dorton, Holowka, and King[12] on the Conestogo River Bridge,

constructed with 0.3% isotropic reinforcement, the Ontario Ministry of Transportation developed new design provisions, anticipating vast savings through the significant reduction of flexural reinforcement and potential increase in service life due to diminished corrosion potential.

Most subsequent research studies on bridge decks can be regarded as attempts to further investigate the results of Batchelor and Hewitt and the Ontario design method based on those results. In the 1980's, several studies on isotropic bridge decks were performed, and results were published in the early 1990's. Because much of the research related to isotropic bridge decks has little or no relevance to the behavior of IBTS slab ends at expansion joints, it is not discussed further here.

2.3   RECENT RESEARCH – 1990 TO PRESENT DAY

Recent studies selected for detailed discussion include those contributing to an understanding of the behavior of skewed bridges constructed with the TxDOT IBTS end detail. Though no study focused directly on this issue, many addressed relevant topics.

2.3.1   Kuang and Morley (1992)

While arching action is generally believed to enhance the flexural capacity of slabs, but Kuang and Morley[22] investigated its effect in enhancing punching-shear capacity. They conducted tests of the punching-shear capacities of slabs with varied amounts of support restraint. Twelve 1/5th scale, square slab specimens were supported and restrained on all four sides by monolithic edge beams of varying widths and stiffnesses. Specimens were constructed with 1.6%, 1.0%, and 0.3% ratios of flexural reinforcement. Slabs with thicknesses of 2.4 in. (60 mm) and 1.6 in. (40 mm) were constructed, representing 12-in. (300-mm) and 8-in. (200 mm) full-scale decks respectively. All deck specimens had a clear span

of 47 in. (1.2 m) in both directions, resulting in span-to-depth ratios of 20 and 30. At 28 days, the concrete compressive strength was 6525 psi (45 MPa). The specimens were supported by pedestals at each corner, and were loaded at the center by a square plate measuring 4.7 in. (120 mm) on each side.

All specimens failed in punching shear rather than flexure, and Kuang and Morely observed an increase in punching shear capacity with increased edge restraint for otherwise identical specimens. During testing, lateral bowing of the edge beams was observed during all tests, confirming the existence of compressive membrane action and the associated in-plane lateral deformations of the restrained deck. In addition, Kuang and Morely found that as the percentage of isotropic flexural reinforcement was increased from 0.3% to 1.0% and then to 1.6%, punching-shear capacity also increased, though it increased very little from the 1.0% specimen to the 1.6% specimen. This trend indicated to Kuang and Morely that punching-shear capacity did not increase linearly with increasing isotropic flexural reinforcement ratios. Test results confirmed that while slab thickness was an important factor in punching shear strength, increases in slab thickness did not result in proportional increases in punching-shear capacity. All punching-shear capacities exceeded the punching shear capacity predicted by ACI provisions.

2.3.2 Azad, Baluch, Mandil, Sharif, and Kareem (1993)

Azad et al.[3] hypothesized that the punching-shear capacity of a cracked slab is diminished if the cracks form a zone of weakness near the point of load application. A test program was developed to examine the punching-shear behavior of slab panels with simulated flaws. Three, 0.5 in. (90 mm) deep, square panels were constructed on two parallel girders, spaced 39 in. (1000 mm) between centerlines. All top reinforcement bars were 0.23 in. (6 mm) in diameter. Bottom

reinforcement bars oriented perpendicular to girders were 0.39 in. (10 mm) in diameter, and bars oriented parallel to girders were 0.31 in. (8 mm) in diameter.
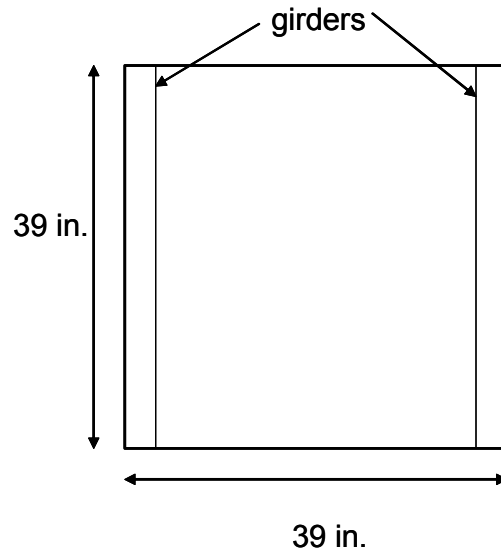
Figure 2-2 Plan view of test specimen (Azad et al. 1993)

(a) bottom mat of reinforcement   (b) top mat of reinforcement
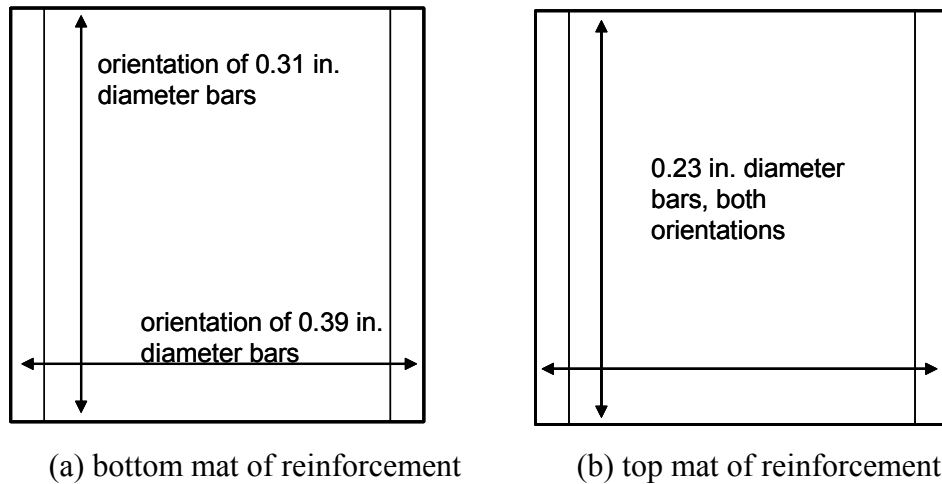
Figure 2-3 Orientation of test specimen reinforcement (Azad et al. 1993)

To introduce crack flaws, a thin-walled conical metallic insert was cast into the panels, beneath the point of load application (Figure 2-4). The angle of

inclination of the insert was varied from 20º to 90º and its height was varied as shown in Figure 2-4.
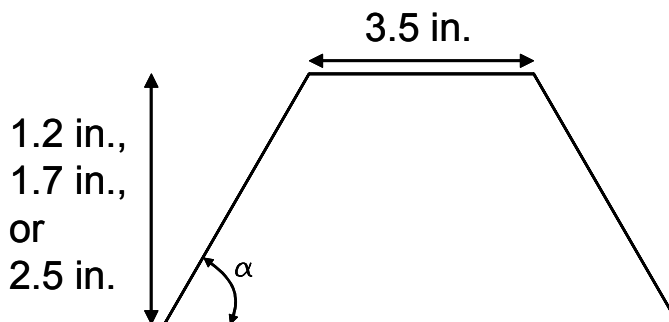
Figure 2-4 Dimensions of metallic insert representing crack flaws (Azad et al. 1993)

All panels failed in punching shear, and Azad et al. observed trends between flaw geometry and punching-shear capacity. As the angle of inclination of the flaw increased, punching shear capacity approached that of a panel with no flaw. For panels with flaws constructed at 90º, punching-shear capacities were similar to that of the panel with no flaw, regardless of the flaw height or diameter. For flaws with diameters smaller than the diameter of the loading plate, punching-shear capacities were similar to that of the panel with no flaw. Most panels failed along the flaw, and for panels with flaws that crossed the failure plane, punching shear capacity was greatly diminished. Azad et al. concluded that progressive crack growth influenced slab capacity, and that there exists a critical crack-surface orientation with regard to loaded area that maximizes the decrease in punching-shear capacity.

2.3.3 Miller, Aktan, and Shahrooz (1994)

Miller, Aktan, and Shahrooz[24] tested a three-span skewed reinforced concrete bridge that was to be decommissioned by the Ohio Department of Transportation. Non-destructive and destructive testing were performed on the

deck to determine its out-of-plane stiffness as a function of distance from the slab end, and also its ultimate capacity.

The test bridge had a three-span, skewed, reinforced concrete deck, 18 in. (457 mm) thick. The outer spans were 32 ft (9.8 m) long, and the interior span was 40 ft (12.2 m) long. Grade 40, no. 9 reinforcing bars were spaced in a 15-in. (381 mm) orthogonal grid in the top mat and a 24-in. (991 mm) orthogonal grid in the bottom mat. The average yield strength of the reinforcement was 48 ksi (335 MPa). The concrete compressive strength of core samples was 7650 psi (53 MPa), and the average splitting strength was 750 psi (5.2 MPa).

To load the bridge to failure, two load plates were anchored with prestressing tendons to bedrock below the bridge. The plates were placed approximately 15 ft (4.6 m) from the edge. A flexural shear failure occurred at a total load of 720 kips (162 kN), approximately 22 times the AASHTO HS-20 design load.

2.3.4   Azad, Baluch, Abbasi, and Kareem (1994)

In 1994, Azad et al.[4] published a discussion of further investigation of the punching-shear capacity of bridge decks. Decks were loaded to failure, and experimental capacities were compared with those predicted by ACI code provisions and the Jiang-Shen model for punching shear (Jiang and Shen 1986). Twelve, 2.7 in. (68 mm) thick decks were constructed with two 28-in. (710-mm) wide bays in the transverse direction, and a longitudinal dimension of 59 in. (1500 mm). Diaphragms were attached at the slab ends. Concrete compressive strength was approximately 3860 psi (26.6 MPa). In the test decks, only the flexural reinforcement ratios were varied: four decks had an isotropic ratio of 0.24%; four had 0.54%; and four had 0.98%. For each reinforcement ratio, the following rectangular load areas were applied to a specimen: 3 by 6 in. (75 by 150 mm); 4

18

by 8 in. (100 by 200 mm); 4 by 16 in. (200 by 400 mm); and 8 by 20 in. (200 by 500 mm).

Punching-shear capacity was predicted using the ACI formula and the plasticity-based approach of Jiang and Shen (Equation 42 in Jiang and Shen 1986). The ACI formula, shown in Equation 2-1, is discussed further in Section 5.6.4 of this thesis. The Jiang-Shen model (Equation 2-2) predicts punching-shear capacity based on the Mohr-Colomb failure criterion, and required a detailed determination of the angle of the slip plane. Instead of that determination, Azad et al. used a simplified version of the model, in which f_c is the 28-day compressive strength of concrete, h is the thickness of the slab, and d_o is the diameter of the loaded area, in effect, making s (Equation 2-3) the perimeter of the section taken at a distance d/2 from the perimeter of the loaded area.

$$P_{ACI} = 4\sqrt{f_c'}b_o d \qquad \text{\textit{Equation 2-1}}$$

$$P_{J-S} = 0.074 f_c' s h \qquad \text{\textit{Equation 2-2}}$$

$$s = \pi(d_o + h) \qquad \text{\textit{Equation 2-3}}$$

All test specimens failed in punching shear, with the failure plane at an inclination between 20º and 35º from the plane of the deck. Azad et al. concluded that the ACI punching shear equation produced conservative results, predicting loads between 98% and 58% of the actual failure load. The Jiang-Shen formulation did not always results in conservative predictions of punching shear capacity, predicting loads between 120% and 76% of the actual failure load. Test specimens with higher percentages of reinforcement had smaller crack widths at similar loads. Increased flexural reinforcement, while beneficial, did not offer an appreciable increase in punching shear capacity. Azad et al. also observed that as the area of the loading footprint was increased, the punching shear capacity increased, though not proportionately.

2.3.5   Ebeido and Kennedy (1996)

Ebeido and Kennedy[13] sought to quantify the effects of several factors on ultimate deck capacity, including girder spacing, angle of skew, reinforcement ratio, deck thickness, load position, shear stud connectors, size of longitudinal girders, and size of cross-bracing.   While their the study was conducted primarily using ABAQUS, seven, 1/8th-scale bridge specimens were constructed to verify the finite-element models.   The scaled specimens were constructed with high early strength concrete and were exaggerated in the vertical direction to accommodate the reinforcement used.   Girder spacings varied from 8 in. (202 mm) to 13.25 in. (337 mm), representing full-scale girder spacings of 5.3 ft (2696 mm) to 8.3 ft (1616 mm).   The slab specimen depths were 2 in. (50 mm) for six of the specimens and 1.5 in. (38 mm) for a single specimen, corresponding to full-scale depths of 16 in. (405 mm) and 12 in. (305 mm) respectively.   Specimens were loaded at multiple locations by a single elliptical plate with major and minor dimensions of 2 in. (52 mm) and 1.4 in. (36 mm) respectively.

Based on their analytical and experimental study results, several trends of slab deck behavior were identified:

- Punching-shear capacity increases as girder spacing decreases.
- Punching-shear capacity decreases as skew angle increases.
- Punching-shear capacity increases as isotropic flexural reinforcement increases.
- Punching-shear capacity increases as deck thickness increases.
- Punching-shear capacity increases as load is applied closer to the end diaphragm.
- Punching-failure capacity is not affected by the presence of cross-bracing.

20

Tested capacities exceeded those predicted by AASHTO, BS-8110, and CEB-FIP punching-shear provisions, and the researchers suggested modifications to the British standard provisions (BS-8110), to account for the effects of skew and the ratio of the longitudinal bending stiffness of a girder to the transverse bending stiffness of the slab.

2.3.6   Petrou and Perdikaris (1996)

In September 1996, Petrou and Perdikaris[30] published a discussion on modeling punching-shear failure in concrete decks as an instability problem in an attempt to describe the characteristics of the sudden failure. The idea originated from the fact that the punching-shear capacity of a deck depends on the loading rate. Petrou et al. claimed that loads placed in the center of the slab could cause flexural or punching shear failures, but failure under loads applied under a high loading rate (such as impact loads at the edge of the slab) usually result in punching shear failures.

In this stability model of punching shear, the applied load is assumed to be transferred in the transverse direction of the deck though a hinge mechanism (Figure 2-5).
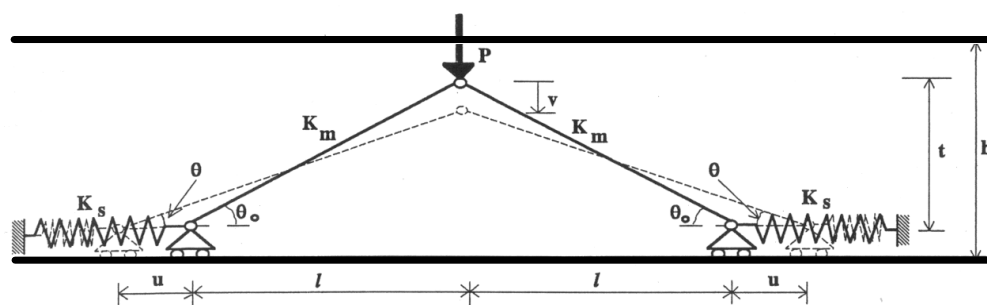
Figure 2-5 Three-hinge strut mechanism model of punching shear (Petrou and Perdikaris 1996)

The goal of that study was to explore the possible relationship between punching shear failure and instability. It was not to predict quantitatively the observed deck response. Although a two-dimensional compressive strut mechanism was assumed for this study, the author believed that a more comprehensive model, possibly incorporating three dimensions, would be more appropriate.

2.3.7 Youn and Chang (1998)

Youn and Chang[32] studied the effects of static and fatigue loading on bridge decks, varying the location of the applied load. Although fatigue is not considered in the study discussed in this thesis, the relationship between punching shear-capacity and the location of applied loads is relevant

In that study, five, $1/3^{rd}$-scale, 1.5-in. (38-mm) deep decks were reinforced with 0.13-in. (5-mm) diameter reinforcing bars. The average 28-day strength of concrete samples taken was 3920 psi (27 MPa). In each specimen, one bay with two overhangs was constructed with two I-shaped steel girders. Diaphragms were installed at the slab ends and at the third-points of the test specimen. Specimen layout is shown in Figure 2-6. To determine how load plate proximity to a girder and deck edge effects punching-shear capacity, a series of tests were performed on the specimens of identical layout at the locations marked in Figure 2-6.
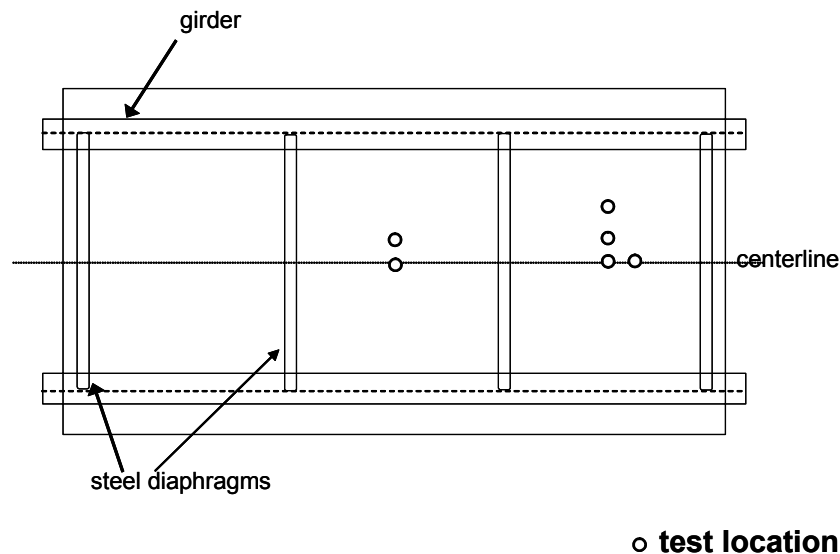
o **test location**

Figure 2-6 Specimen layout and test locations (Youn and Chang 1998)

Test results indicated that punching-shear capacity decreased as the loading position moved away from the center of the supports. The authors attributed this decrease to the reduction in compressive in-plane forces (arching action). They also found that the punching-shear capacity of the exterior panel did not differ significantly that of the interior panel.

2.3.8 Graddy, Kim, Whitt, Burns, and Klingner (2002)

Graddy et al.[18] studied the punching-shear behavior of bridge decks under fatigue loading, using full scale cast-in-place and precast, prestressed panel specimens. Although the effects of fatigue on bridge slabs is beyond the scope of this discussion, static tests were performed on the specimens, the results of which are relevant to this thesis.

Using finite-element models, both cast-in-place concrete and precast-prestressed panels specimens were developed to replicate the behavior of complete bridge decks, whose capacity would be governed by punching shear. Cast-in-place (CIP), test specimens were 6 ft (1.83 m) wide, 7 ft (2.13 m) long,

and 7.5 in (191 mm) thick. Precast-prestressed panel (PCP) specimens, topped with 4 in. (102 mm) of cast-in-place concrete, were 8 ft (2.44 m) long, 6 ft 5 in. (1.96 m) wide, and 7.25 in. (184 mm) thick. Grade 60 reinforcement was used, details of which are shown for a longitudinal section of both types of specimens in Figure 2-7(a) and (b). Concrete used for the CIP specimens and for the topping of the PCP specimens had an average cylinder strength of 6000 and 5000 psi (41 and 34 MPa), respectively. For static tests, a loading footprint of 14 x 24 in. (610 x 356 mm) was applied to the CIP specimen, and a loading footprint of 10 x 17.5 in. (445 x 254 mm) was applied to the PCP specimens. For both specimens, the longer dimension of the loading footprint was parallel to the transverse direction of the specimen.
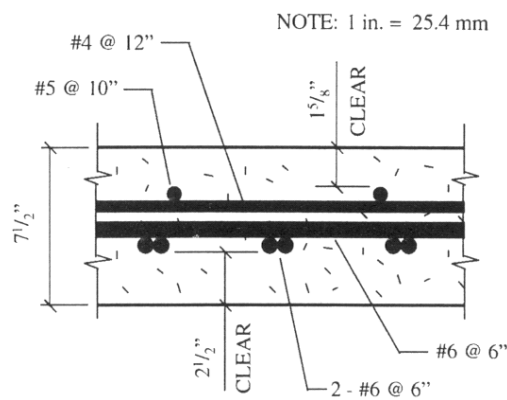
(a) CIP specimens

Figure 2-7 Section of test specimens (Graddy et al. 2002)

STD. 180 DEGREE HOOK — #4 @ 6"
1/2" CLEAR
7 1/4"
PANEL

3/8"-DIAMETER 270-ksi STRANDS
2"
4"
12 x 4 - W2.5 x W7.5 W.W.F. —

NOTE: 1 in. = 25.4 mm
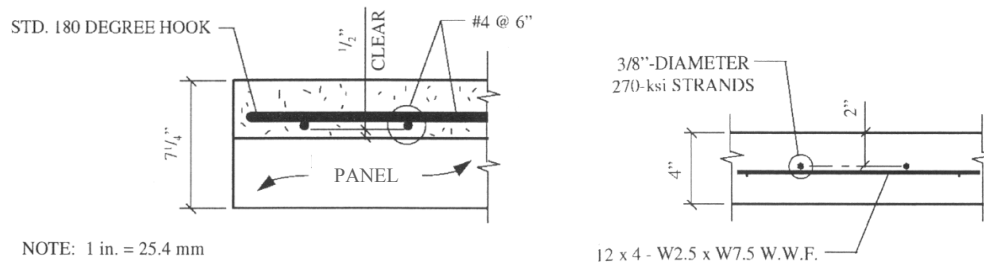
(b) PCP specimens

Figure 2-7 cont'd. Section of test specimens (Graddy et al. 2002)

Flexural capacities were calculated using yield-line analysis, and compressive membrane forces, estimated using finite-element analysis and the results of previous research, were used in calculations of flexural capacity. In addition, predicted AASHTO LRFD and ACI 318-95 punching-shear capacities were calculated for both the predicted and observed failure mode. Resulting predictions and experimental results are shown in Figure 2-8.

25

PREDICTED FLEXURAL CAPACITY
FROM YIELD-LINE THEORY
INCLUDING ARCHING ACTION

239 kips

PREDICTED FLEXURAL CAPACITY
FROM YIELD-LINE THEORY WITHOUT
ARCHING ACTION

232 kips

205 kips — STATIC TEST #2
(PUNCHING SHEAR FAILURE)

PREDICTED PUNCHING SHEAR
CAPACITY FROM GENERAL MODEL

171 kips

173 kips — STATIC TEST #1
(PUNCHING SHEAR FAILURE)

PREDICTED AASHTO AND ACI
PUNCHING SHEAR CAPACITIES

127 kips

ANALYTICAL PREDICTIONS   **EXPERIMENTAL RESULTS**

0

(a) CIP specimens

PREDICTED FLEXURAL CAPACITY
FROM YIELD-LINE THEORY
INCLUDING ARCHING ACTION

143 kips

PREDICTED FLEXURAL CAPACITY
FROM YIELD-LINE THEORY WITHOUT
ARCHING ACTION

139 kips

115 kips — STATIC TEST #2
(COMBINED FAILURE MODE)

112 kips

105 kips — STATIC TEST #1
(COMBINED FAILURE MODE)

PREDICTED PUNCHING SHEAR CAPACITY
FROM GENERAL MODEL ADJUSTED FOR
OBSERVED FAILURE MODE

81 kips

PREDICTED AASHTO AND ACI
PUNCHING SHEAR CAPACITIES
ADJUSTED FOR OBSERVED
FAILURE MODE

ANALYTICAL PREDICTIONS   0   **EXPERIMENTAL RESULTS**

(b) PCP specimens

Figure 2-8 Predicted versus observed failure loads for static tests (Graddy et al.

2002): (a) CIP specimens; (b) PCP specimens

26

Graddy et al. found that AASHTO and ACI punching-shear provisions were conservative, and could be improved based on the shape of the punching shear failure surface. Compared to the flexural capacities predicted from yield-line theory, the beneficial effects of arching action were insignificant.

2.4 SUMMARY AND RELEVANCE OF PREVIOUS RESEARCH

While many studies have investigated the behavior of the interior panels of bridge decks and of flat slabs in structures, no tests have been performed on free edges of bridge decks constructed details similar to the IBTS detail. The earliest slab research was performed on specimens configured to represent flat slabs in reinforced concrete structures. Those studies emphasized the flexural capacity of decks, testing the predictions of plastic analysis methods. That research is of little relevance to the behavior of bridge slabs constructed with the IBTS end detail, as no span tested in this study failed in flexure. As interest in the effects of arching action grew, researchers such as Batchelor and Hewitt studied this phenomenon in bridge slabs. Early tests indicated that at interior locations, bridge decks fail in punching shear, having reserve strengths greatly exceeding the design punching shear capacity. Though this may be true for interior decks panels, the ability of free edges of decks in this regard is unknown. Most research on punching shear in bridge decks has focused on interior locations of bridge slabs with diaphragms; the effects of loads applied at the edge of slabs without diaphragms have not been studied. Slab ends must be studied independently for three reasons: the smaller critical punching-shear perimeter expected for loads applied near an edge; the increase in transverse flexural moments at the slab end expected due to the lack of two-way action there; and the reduction in arching action expected due to decreased in-plane lateral restraint there.

27

Most prior bridge deck tests have been performed on small-scale specimens. Those results (as previously noted) may be unconservative due to size effects.

CHAPTER 3

Design of Test Specimens

3.1 INTRODUCTION

The goal of the experimental program was to investigate the behavior of slabs at expansion joints, with emphasis on skewed slabs. Two full-scale specimens have thus far been constructed and tested. The test specimens were designed to behave as full-scale bridge slabs while permitting investigation of the effects of individual design parameters on behavior at the expansion joints.

The first test specimen was built with 0º skew at both ends. The objective of this specimen was to study the effects of design parameters other than skew, including slab end details, girder spacing, bridge length, and the number of bays. Detailed discussion of the results from this specimen is given in Ryan, 2003.

The second test specimen was built with a 45º skew at both ends. The intent of this specimen was to investigate the effects of end skew angle on slab end behavior. In addition to the four primary span tests, four overhang tests were conducted on this specimen. The development of the specimen included determining how end skew angle affects design load placement, how bridge span affects test outcome, and how the overhangs should be reinforced.

3.2 0º SKEW SPECIMEN

The first test specimen was built with 0º skew at both ends to gain an understanding of how design variables other than skew affect the behavior of slabs ends at expansion joints. The first specimen had four test areas as shown in Figure 3-1. A different combination of slab end detail and girder spacing was tested in each area.

29
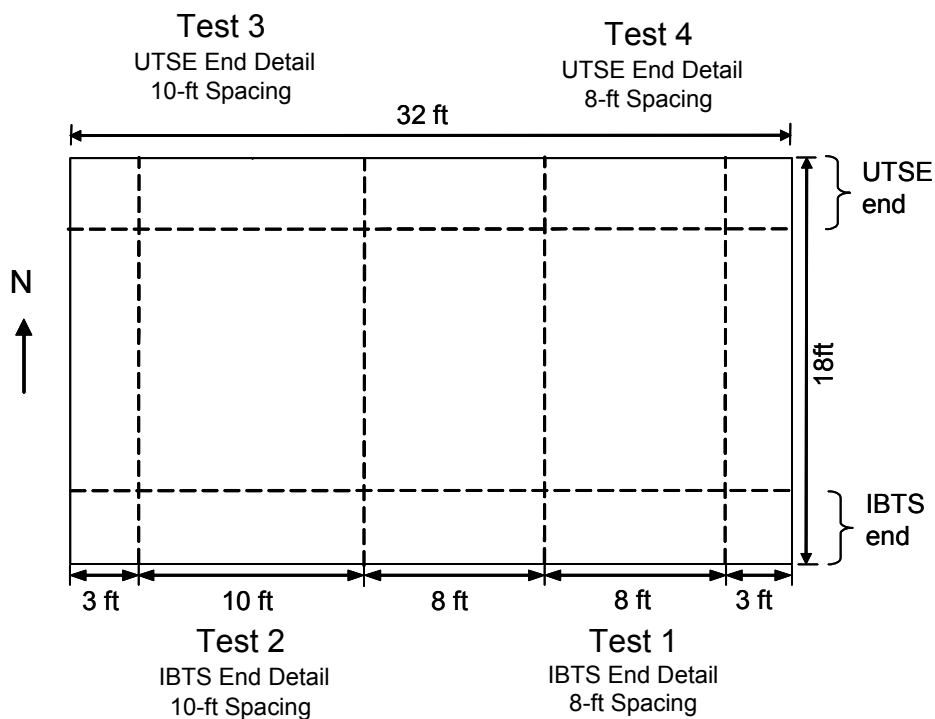
Figure 3-1 0° skew specimen, plan view[31]

3.2.1 Girder Spacing

Although TxDOT bridge standards include bridges with up to six girders, the 0° skew specimen had only four girders. Linear-elastic parametric studies indicated that a four-girder bridge would adequately represent five-girder or six-girder bridge behavior at slab ends. In addition, a six-girder bridge would not have been feasible in the laboratory. A detailed discussion of this analysis is given in Ryan (2003).

The girder spacing of the west-exterior bay was 10 ft (3.0 m). The girder spacing of the east-exterior bay and the interior bay was 8 ft (2.4 m). The 8-ft (2.4-m) girder spacings were used to test a girder spacing commonly used in

TxDOT highway bridges. The 10-ft (3.0-m) girder spacing was used to test the upper end of the range of possible girder spacings used by TxDOT.

3.2.2   End Reinforcement Details

Two end reinforcing details were used, the 10 in (254 mm) deep TxDOT IBTS end detail and a proposed 8 in (203 mm) deep end detail. The IBTS end detail has a total of 16 No. 5 reinforcing bars placed parallel to the slab edge, 8 bars on the top and 8 bars on the bottom. This detail, shown in Figure 3-2, is 4 ft (1.2 m) wide measured perpendicular to the slab end.   As the skew angle increases, the longitudinal length of the end section increases, as shown in Figure 3-3 for a 45º skew. Although the length of the end detail is 4 ft (1.2 m) measured perpendicular to the slab end, it is 5 ft 9 in. (1.75 m) measured parallel to the girders.
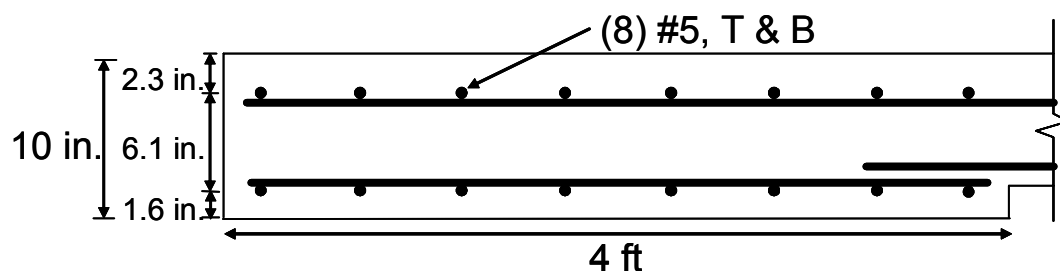
Figure 3-2 Cross-section of IBTS detail[31]
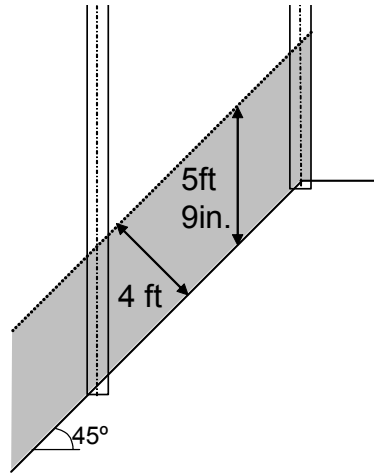
Figure 3-3 Length of end detail

To maximize the information gathered from this specimen, an alternative detail was designed for the edge opposite the IBTS detail. The IBTS detail may not be easy to construct because of the additional formwork required for the 2-in. (51-mm) drop-down. Four-inch thick prestressed panels, topped with 4 in. (102 mm) of cast-in-place concrete topping are often used for bridge s. While this system requires no formwork for most of the , the panels are stopped at the IBTS edge detail, and formwork is constructed in the field to construct the thickened edge. An 8 in. (203 mm) deep edge detail would be expected to improve construction economy by creating a uniform thickness over the entire and eliminating this formwork.

The alternative slab end detail, named the Uniform Thickness Slab End (UTSE) detail, was developed during the first phase of this study. To simplify construction, that detail contains the same size reinforcement bars as the interior of the bridge and in the IBTS end detail, but the number of bars is increased from 8 to 12 in the top mat and 12 in the bottom mat (Figure 3-4).

For both details, a 4 ft (1.2 m) wide section was analyzed. The moment-curvature behavior of the two details is shown in Figure 3-5. The initial portion of the curve is expanded in Figure 3-6 to focus on cracking and yielding of the sections. The reinforcing steel in the UTSE end detail yielded at an 11% and 6% higher moment than the IBTS end detail in positive bending and negative bending, respectively.[31] Because of the increase in reinforcement ratio, the flexural capacity of the UTSE end detail is 5% and 3% higher than the IBTS end detail in positive bending and negative bending, respectively. The UTSE end detail has a lower stiffness, both before and after cracking due to its reduced depth. The sectional analysis was intended to provide a comparison of the two end details, and is not intended to predict behavior. In reality, the continuity of the rest of the will cause cracking to initiate at the edge and penetrate into the . The resulting cracking moments and stiffnesses for both sections would be higher than what is indicated in the analysis discussed here, because the actual is wider than the 4 ft (1.2 m) assumed in the analysis and is restrained along the boundary by the .
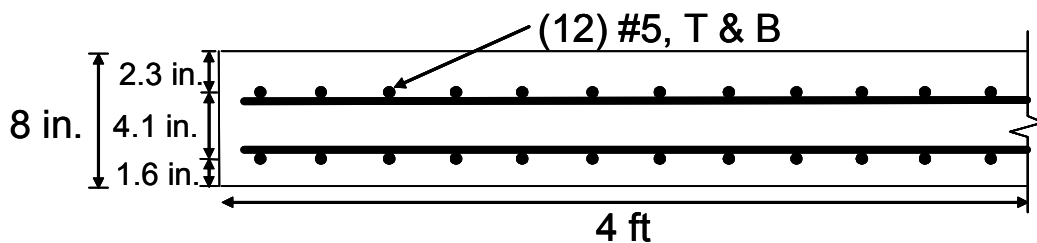
Figure 3-4 Cross-section of UTSE end detail[31]
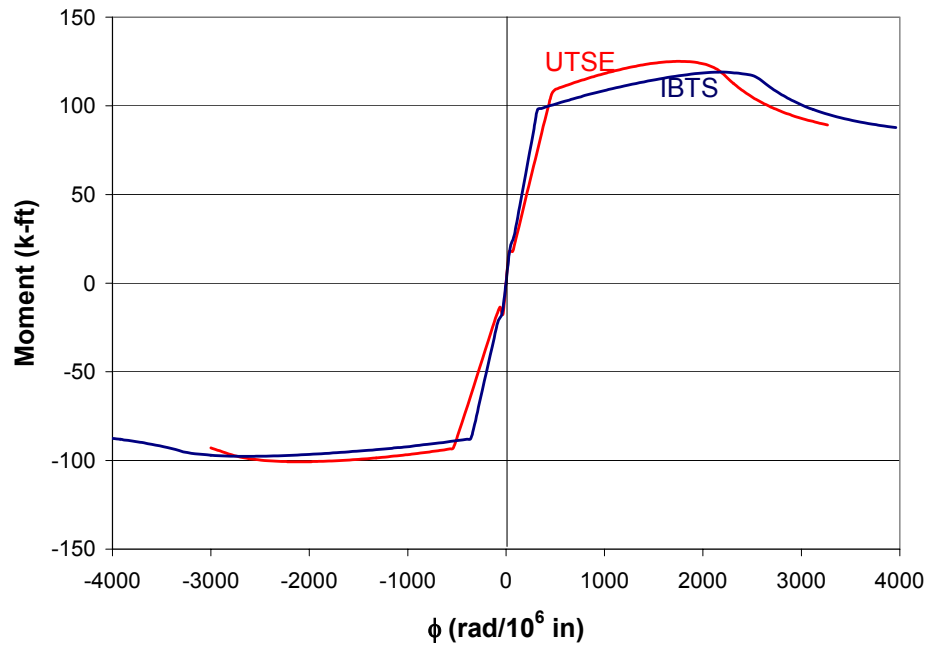
Figure 3-5 Moment-curvature analysis of IBTS and UTSE details[31]
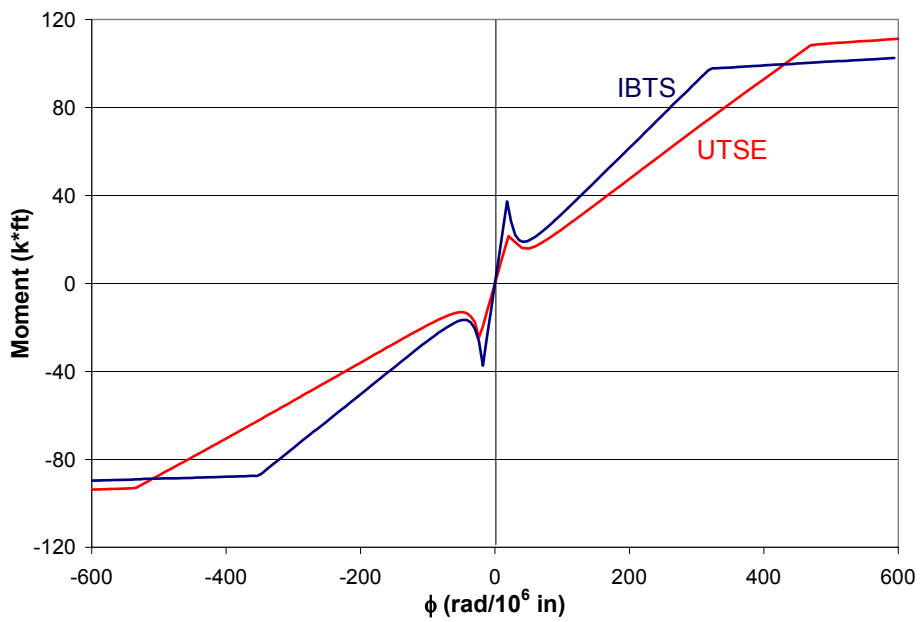
Figure 3-6 Moment-curvature behavior, focused on cracking[31]

34

3.2.3 AASHTO Design Loads as Applied to These Specimens[31]

One of the main objectives of this research was to determine the behavior of the TxDOT IBTS edge detail when subjected to AASHTO design loadings, namely HS-20 and HS-25 (AASHTO LRFD Bridge Design Specifications). Two primary types of vehicle were considered for each design loading (Figure 3-7). The TxDOT Bridge Design Manual uses the same truck vehicle. Instead of the tandem vehicle, there is an alternate military vehicle with 24-kip (107-kN) axles and the same loading configuration. The tandem loading from AASHTO LRFD was applied to the test specimen although the TxDOT alternate military vehicle is almost identical. HS-25 loading utilizes the same vehicle arrangements, but, the load magnitudes are increased by 25%. The loadings shown in Figure 3-7 are axle loads. Half the axle load goes to each set of tires, which are spaced 6 feet apart in the transverse direction (Figure 3-8). For testing, a single load plate was used to represent each set of tires.
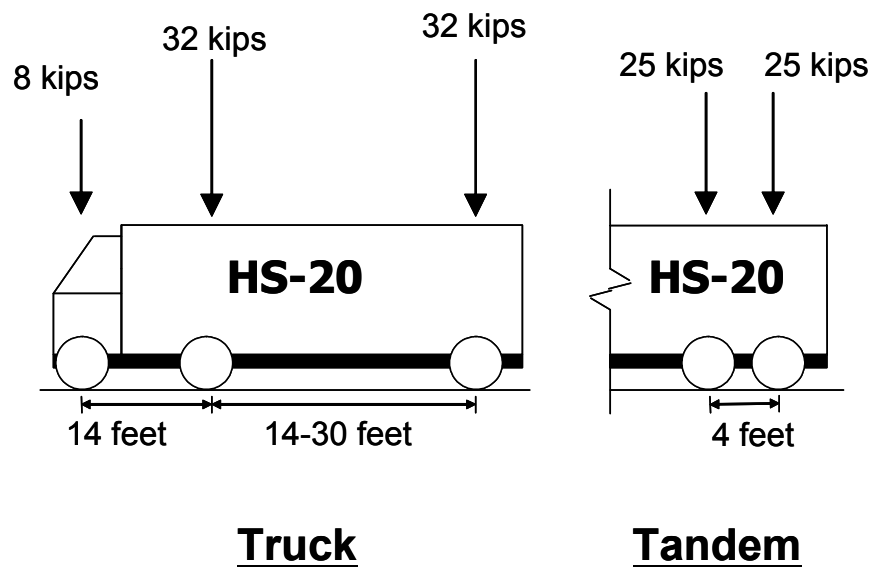
Figure 3-7 AASHTO HS-20 design vehicles[31]

6-ft axle length

set of tires   set of tires
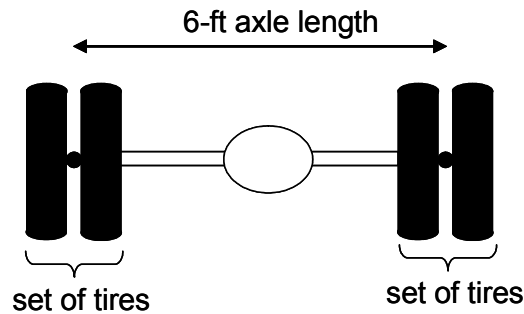
Figure 3-8 AASHTO design vehicle axle

AASHTO LRFD also requires a lane load of 64 psf (4.4 MPa), applied simultaneously with the vehicle loads. Since this comparatively small uniform load is difficult to create in the laboratory and is not likely to have much effect at the edge of the bridge , it was omitted in this study.

Since the AASHTO truck configuration axles are farther apart than the longitudinal dimension of the edge detail, only one axle would load the bridge test specimen at any one time. Therefore, one of the 32-kip (142-kN) axles was applied at the edge of the , and was named truck axle-front; the other, at 4 ft (1.2 m) from the edge, was called "truck axle-back." The AASHTO tandem vehicle axles both affect the edge detail since they are spaced 4 ft (1.2 m) apart. As applied to the bridge specimen, the term "tandem load" describes four load plates on the bridge, and the term "truck load" describes two plates on the bridge.

Section 3.6.2 in the AASHTO LRFD specification establishes a dynamic load allowance, which increases the design vehicle loads by 75% to account for dynamic effects in the bridge at expansion joints.

For the 0º skew specimen, three load configurations were applied at each test area: truck axle-front; truck axle-back; and tandem. In almost every case in every test area, the tandem truck produced the most critical cracking, strain, and deflection response.

36

3.3 45º SKEW SPECIMEN

Following the completion of the test program for the 0º skew specimen, a second test specimen was developed, with 45º skew at both ends (Figure 3-9). Its purpose was to isolate the effects of skew. Skew angle, loading point locations, girder spacing, end detail, and the inclusion of breakbacks were the test variables considered for investigation. In addition, four overhang tests were conducted on this specimen.
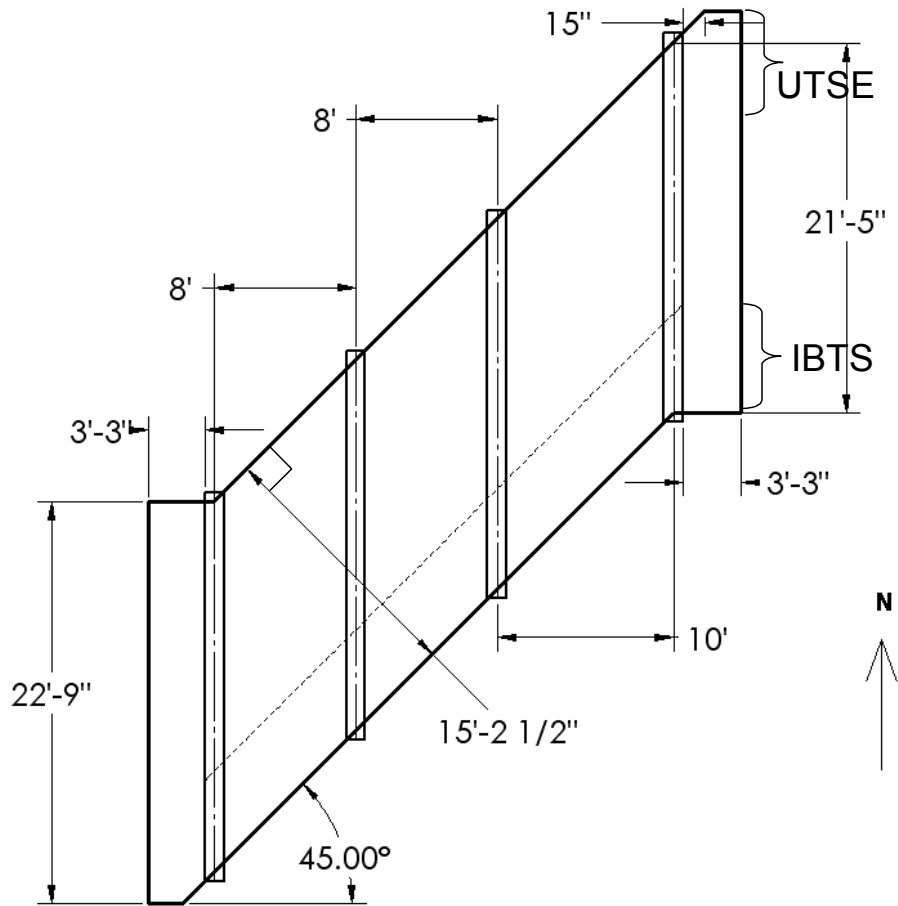
Figure 3-9 45º skew specimen, plan view

3.3.1 Skew Angle and AASHTO Tandem Load Configuration

A major focus of the research project was to understand the behavior of slab end details at expansion joints under AASHTO LRFD design loadings. The details of the AASHTO design loads are discussed in Section 3.2.3. Because the tandem load configuration produced the most critical results in the 0º skew specimen, only that load configuration was considered for the 45º skew specimen. The relationship between skew and the AASHTO load configuration will be discussed. Included will be both a discussion of how the loads can be placed to maximize positive and negative moments in slab ends of varying skew.

3.3.1.1 Skew Angle

The clear span between girder centerlines and the configuration of the tandem truck loading points on the slab is governed by the slab skew angle (Figure 3-10). To maximize negative and positive moments in the end region, the skew angle chosen for the 45º specimen required that the load points be located as close to the slab end as possible, and that the clear span along the slab end be maximized. These choices were made with the intent of maximizing the moments in the end regions, which were the areas being tested.
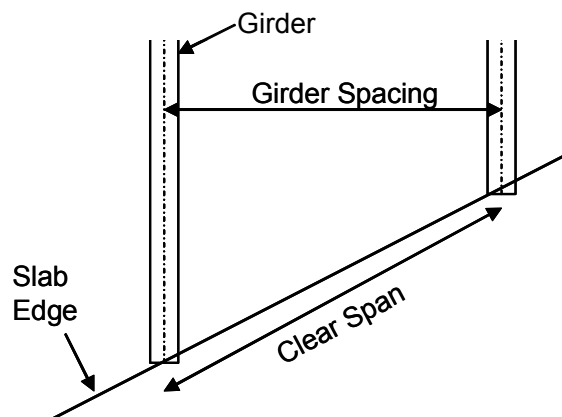
Figure 3-10 Clear span and girder spacing

38

For this specimen, positive moment was maximized in the 10-ft (3.0-m) bay, and negative moment was maximized at the girder in between the two 8-ft (2.4-m) bays. Because increasing girder spacing increases positive moments, positive moments are maximized in the 10-ft (3.0-m) bay, the largest girder spacing constructed in the specimen. Increasing or decreasing the girder spacing has little effect on the maximum negative moments, which are usually controlled by the constant axle length of 6 ft (1.8 m).

3.3.1.2 Positive Moment

In the 10-ft (3.0-m) bays, the transverse orientation of the AASHTO design truck was chosen to maximize transverse positive moments. To accomplish this, one tire from each axle of the tandem load plates was placed at midspan. In the 0º skew specimen, the geometry of the 10-ft (3.0 m) girder spacing results in two load points placed over the girder; these load points were ignored (Figure 3-11a). These plates would have only nominal effects on the overall behavior of the slab end and were not included in the testing of 0º skew specimen. Again in the 45º skew specimen, only two plates were placed midspan in the 10-ft (3.0-m) girder spacing due to the geometry of the skew. Figure 3-11b shows the placement of the AASHTO design truck.

(a) 0º skew   (b) 45º skew
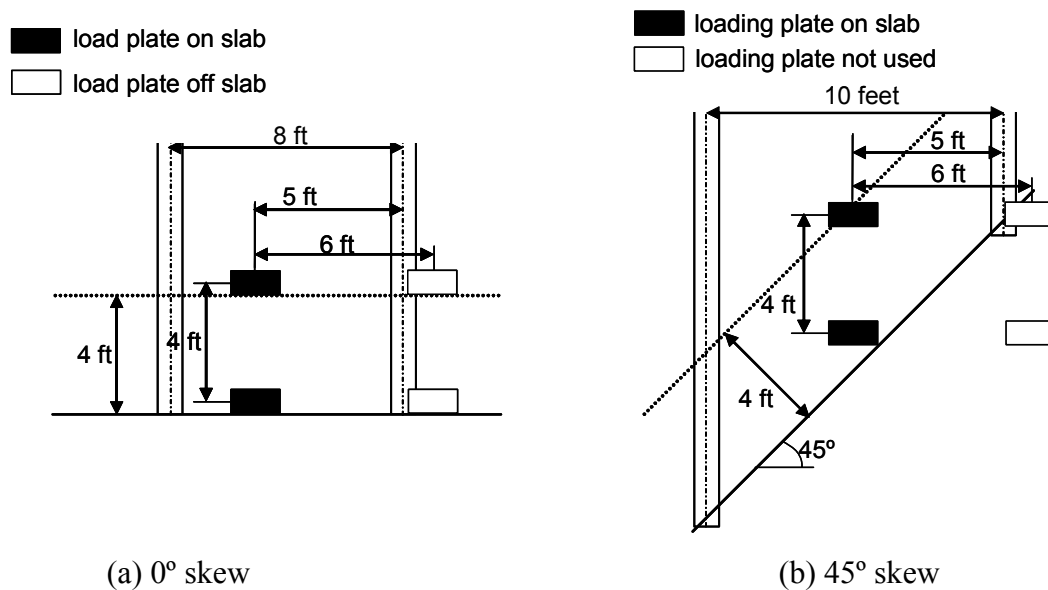
Figure 3-11 Positive load plate location

Increasing the end skew angle increases the maximum transverse positive moments generated in the end region. As previously shown in Figure 3-10, increasing the skew angle increases the clear span between girder centerlines. As this clear span is increased, the positive moment in the end region increases.

3.3.1.3 Negative Moment

Maximum negative moments are produced by placing both axles of a tandem load such that each set of tires is equidistant from the centerline of the girder. All tests maximizing negative moment were performed over the girder between the 8-ft (2.4 m) bays. The choice of skew, not girder spacing, is critical to maximize negative moments. Because the geometry of the HS-20 load points is fixed, increasing the girder spacing has less effect on end section response.

Increasing the end skew angle decreases the transverse negative moments generated over the support in the end region. This decrease is largely caused by the tandem loading configuration and by the geometry of its placement in the end

40

region. Figure 3-12 shows how the tandem truck loading plates can be placed in a negative moment loading configuration on slab ends of varying skew. At zero degree skew, all four of the tandem loading plates can be placed on the slab end (Figure 3-12a). As skew is increased to 15º, one plate of each axle of the tandem truck must now be moved further toward the interior of the slab and away from the test region. Although all four plates can be placed on the slab as shown in Figure 3-12(c), three of the plates are too far from the edge to be of interest in evaluating slab end behavior. Instead, the design truck can be moved slightly off of the bridge such that one load plate would no longer be in contact with the slab as shown in Figure 3-12(b). This moves the remaining three load plates into the slab end region. As the end skew is increased to 30º, three load plates can again be placed in the end region, but in two different configurations (Figure 3-12d, e). One configuration allows three complete plates to be placed in the end region. Though the other allows only two whole plates and one partial plate to be placed in the end region, all three plates are closer to the slab edge. At end skews of approximately 33º or more, two plates can be placed in the end region in a configuration totally omitting the remaining two plates. At 45º end skew, the most critical load plate configuration involves three load plates in the end region as shown in Figure 3-12(f), as (g) is a less critical case, maximizing positive moments. During testing, the small overlap of the fourth plate would be ignored. At an end skew of 55º, only one tire from each axle could be placed on the slab end area (Figure 3-12h). Therefore, at this angle, negative moments are not critical. As a trend, increased skew angle decreases the number of plates that can be placed simultaneously in the slab end region to maximize negative moments over a supporting girder.

41
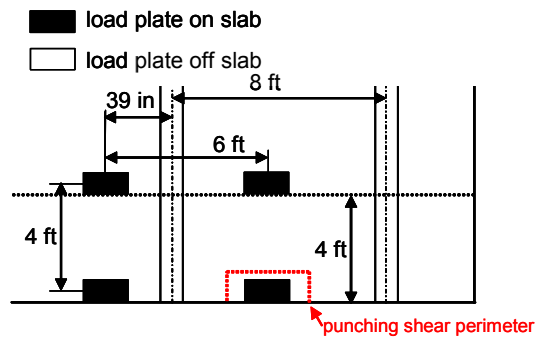
(a) 0º skew, 4 load plates
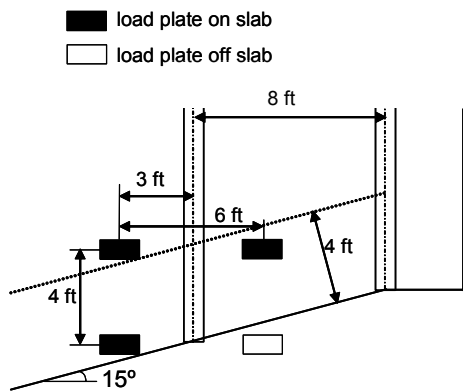
(b) 15º skew, 3 load plates
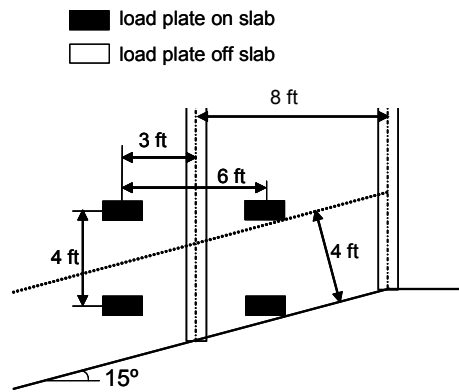
(c) 15º skew, 4 load plates
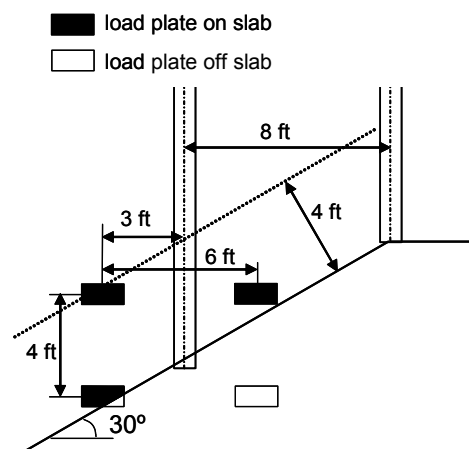
(d) 30º skew, less than 3 load plates
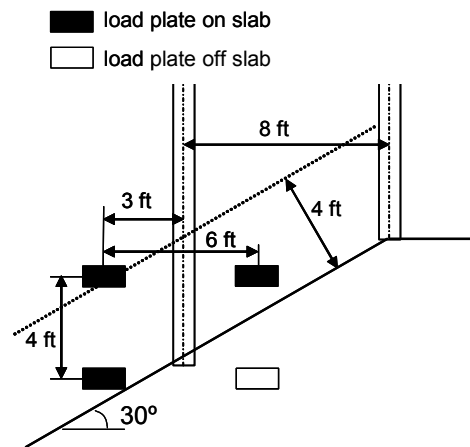
(e) 30º skew, 3 load plates

Figure 3-12 Placement of tandem loading plates, 0º, 15º, 30º, 45º, 55º skew
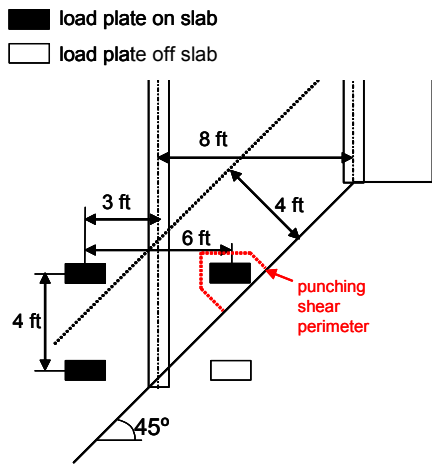
(f) 45º skew, 3 load plates
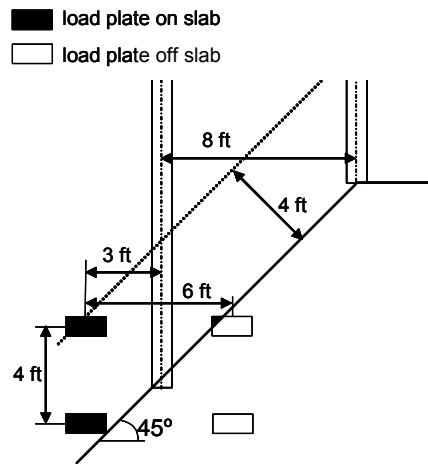
(g) 45º skew, 2 load plates
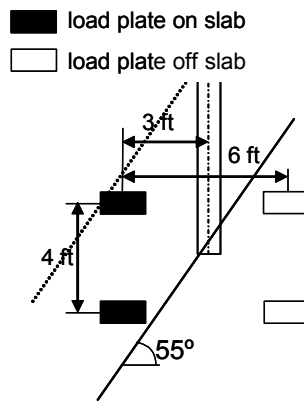
(h) 55º skew, 2 load plates

Figure 3-12cont'd. Placement of tandem loading plates, 0º, 15º, 30º, 45º, 55º

skew

As the skew angle is increased, the punching shear failure loads predicted by ACI 318-02 increase as well (Figure 3-12a and f). As skew angle is increased, the minimum predicted punching shear perimeter around the load plate at the edge increases. Because the punching shear capacity of the plate is directly proportional to the minimum shear perimeter, the predicting punching shear capacity is higher for greater skews.

43

A large end skew was desired to gain a clear understanding of the most critical design cases. Although TxDOT occasionally constructs bridge s with end skew angles as great as 60º, constructing a specimen with this skew was not deemed necessary. Few TxDOT highway bridges are constructed with this skew, while more are constructed at smaller skew angles. A 45º skew was tested to create a large clear span in the positive moment test regions but still be in the range that is likely to be constructed by TxDOT. In addition, a 45º skew was not so large as to make the negative moment test essentially another, but less critical, positive moment test.

3.3.2 Specimen Length

The specimen length, which had been 18 ft (5.5 m) in the 0º skew specimen, was increased to 21.5 ft (6.6 m) in the 45º skew specimen. The increase in length compensated for the decrease in distance between test specimens caused by the skew. Two reasons that increasing the skew of the specimen moved test regions closer to one another are as follows:

- With increasing skew, the end regions increase in length longitudinally. The end region in the 45º skew specimen is shown in Figure 3-3. At 45º skew, the longitudinal length of the end details increased to 5 ft 9 in. (1.8 m), and the bridge span had to be increased to account for the additional total length of the end region.
- The length of the slab measured perpendicular to both slab ends is reduced when skew is increased.

For a slab span increase from 18 ft (5.5 m) to 21.5 ft (6.6 m), the perpendicular length of the slab increased from 12 ft 9 in. (3.9 m) to 15 ft 2.5 in. (4.6 m).

3.3.3   Additional Design Variables

The end details, girder spacings, and number of bays constructed in the 0º skew specimen were repeated in the 45º skew specimen. The IBTS and UTSE end details were constructed at opposite ends of the specimen. A discussion of these details is given in Section 3.2.2. Because the UTSE end detail performed adequately in the 0º skew specimen, the 45º specimen included the same detail. Girder spacings and the number of bays was also unchanged from the 0º skew specimen. Three bays were constructed, one 10-ft (3.0-m) exterior bay and two 8-ft (2.4-m) bays.

3.3.4   Overhang Design

To make full use of the test specimen, four tests were performed on the corners of the overhangs of the 45º skew specimen. Discussion of the design of these test areas and the results of the tests are given in Chapter 6.

3.3.5   Slab Reinforcement

The top mat of slab reinforcement for the 45º skew specimen is shown in Figure 3-13. The bottom mat of slab reinforcement is not shown, because the two mats are largely the same. Slab reinforcement was detailed using the TxDOT IBTS, IBMS and span standards (Figure 1-1 and Figure 3-14). The IBTS detail ends were detailed using the TxDOT IBTS standard. The UTSE detail was unchanged from the 0º skew specimen (Section 3.2.2, Figure 3-4). The IBMS TxDOT standard was used to determine the positions of bars in the acute corners with breakbacks. A portion of the standard is shown in Figure 3-14. The TxDOT span standards were used as a guide for reinforcing the remainder of the slab. Although TxDOT does not have a span standard that details a 45º skew, the details used in a 30º skew standard were adapted as guidelines for construction of a 45º skew.
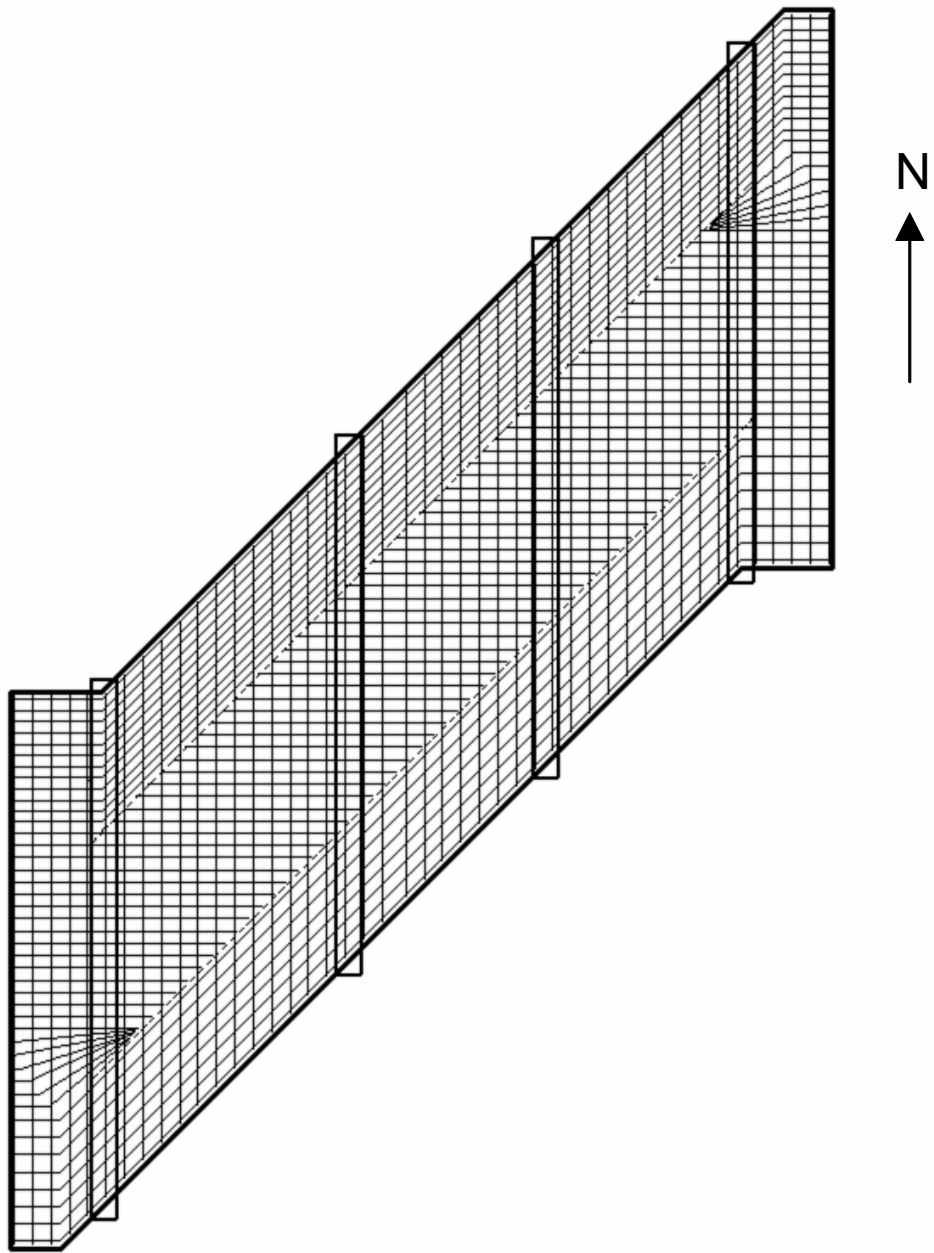
Figure 3-13 45º skew specimen slab reinforcement, top and bottom mats

PARTIAL PLAN OF SLAB END WITH BREAKBACK
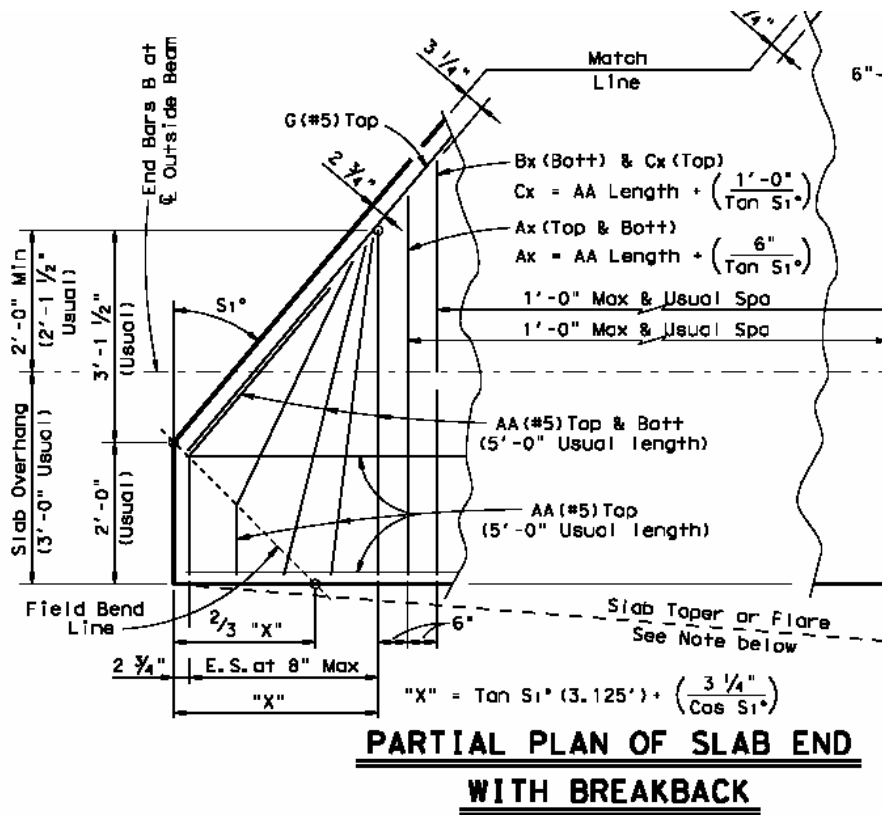
Figure 3-14 TxDOT IBMS detail

3.3.6 Girders[31]

Bridges in Texas are typically built using precast, prestressed concrete girders. Because this research focused on the behavior of slab end details, it was not necessary to replicate the longitudinal behavior of such girders. Since the girders have very little effect on the behavior of the along the edge, steel girders (W24 X 104) were used in the experimental program. The girders used for the 0º skew specimen were reused for the 45º skew specimen.

3.3.6.1 Shear Studs[31]

To obtain composite action between the and the girders, as in an actual concrete girder bridge, shear studs were fabricated using double-nutted bolts (Figure 3-15), which allowed the girders to be reused by removing the bottom nut and lifting the slab off the girders. This shear stud detail proved to be a very efficient method to produce composite action. Figure 3-16 shows the method for creating composite action used by TxDOT as well as the equivalent design used in the test specimen. The shear stud diameter and spacing was designed to match the cross-sectional area of the stirrups that are used with precast, prestressed girders (Table 3-1).
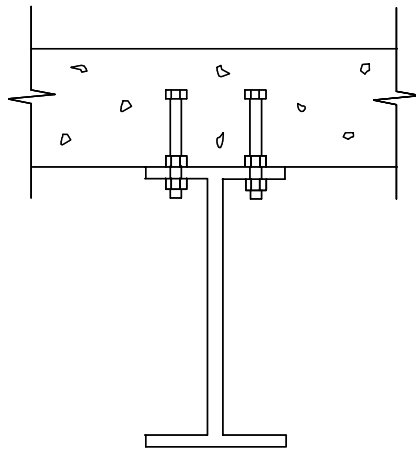
Figure 3-15 Shear stud detail

Prestressed Concrete Girder

#4 HOOPS, TYP

6in   spaced @ 4in   spaced @ 8in

5ft 9in

Test Specimen

3/4∅ BOLTS, TWO ROWS

spaced @ 8in   18in spacing
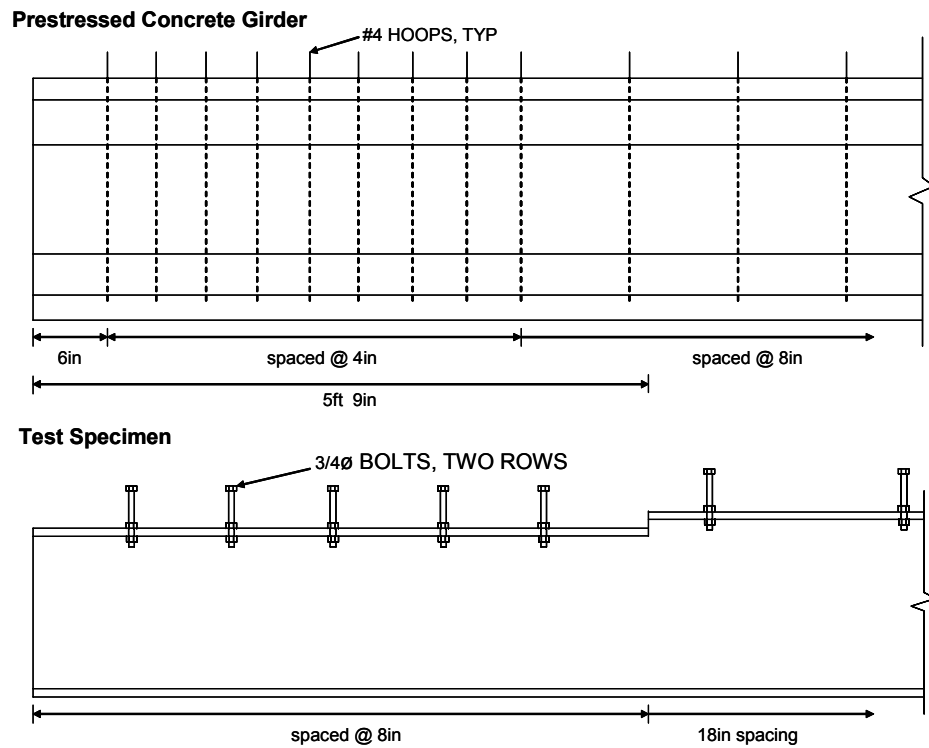
Figure 3-16 Composite shear reinforcement[31]

Table 3-1 Comparison of Composite Shear Reinforcement[31]

Girder type	Shear connection method	Area of composite reinforcement (per 4 ft)	
		IBTS Detail	Typical
Prestressed Concrete	CIP No. 4, hoops	4 in.^{2}	0.6 in.^{2}
Steel	CIP 3/4∅ bolts, two rows	4.4 in.^{2}	0.59 in.^{2}

3.3.7 Prestressed Panels[31]

Prestressed panels are typically used in the field to reduce the required formwork. For the 0º skew and 45º skew test specimens, prestressed panels were not used because they are not placed in the thickened edges in the field.   The panels were expected to have little, if any, effect on the behavior of s at expansion joints.   Construction possibly could be simplified if prestressed precast panels were placed in the thickened slab region. This would eliminate most or possibly all form construction in that region.   The use of prestressed panels will be addressed in future research on this project.

3.4 SUMMARY

Specimens with 0º skew and 45º skew were constructed and tested. Both specimens had three bays with one exterior 10-ft (3.0-m) girder spacing and two 8-ft (2.4-m) girder spacings. The UTSE detail was constructed on the north end of both specimens, and the IBTS detail was constructed on the south end. The full depth of the slab was cast in place, and prestressed precast panels were not used. AASHTO design loads were applied to both s. The 0º skew specimen spanned 18 ft (5.5 m), and the 45º skew specimen spanned 21.5 ft (6.6 m). Details on the development and test results from the 0º skew specimen can be found in Ryan, 2003.

CHAPTER 4

Experimental Program

4.1 INTRODUCTION

Much of the experimental program developed for the 0º skew specimen was repeated for the 45º skew specimen, with only slight modification. For the second specimen, the girders, forms, and load frame were reused with few modifications. While strain gauges were re-located to capture maximum moments over the girders, other instrumentation and the testing protocol remained unchanged.

4.2 CONSTRUCTION

The steel W shapes used as girders in the 0º skew specimen were reused in the 45º skew specimen. The girders were modified to accommodate the change in slab depth from 8 in. (203 mm) to 10 in. (254 mm) at the IBTS slab end. In the 0º skew specimen, this required that the top girder flange be reduced in height by 2 in. (45 mm) over a length of 4 ft (1.22 m) (Figure 4-1). As discussed in Ryan (2003), the top girder flange was cut off, a 2-in. (45 mm) strip of web was cut out, and the top flange was then reattached with a full-penetration weld. For the 45º skew specimen, the longitudinal length of the drop-down was increased from 4 ft (1.22 m) to 5 ft 9 in (1.75 m), and the same procedure was used to reduce the girder depth for an additional 1.75 ft (533 mm) length.
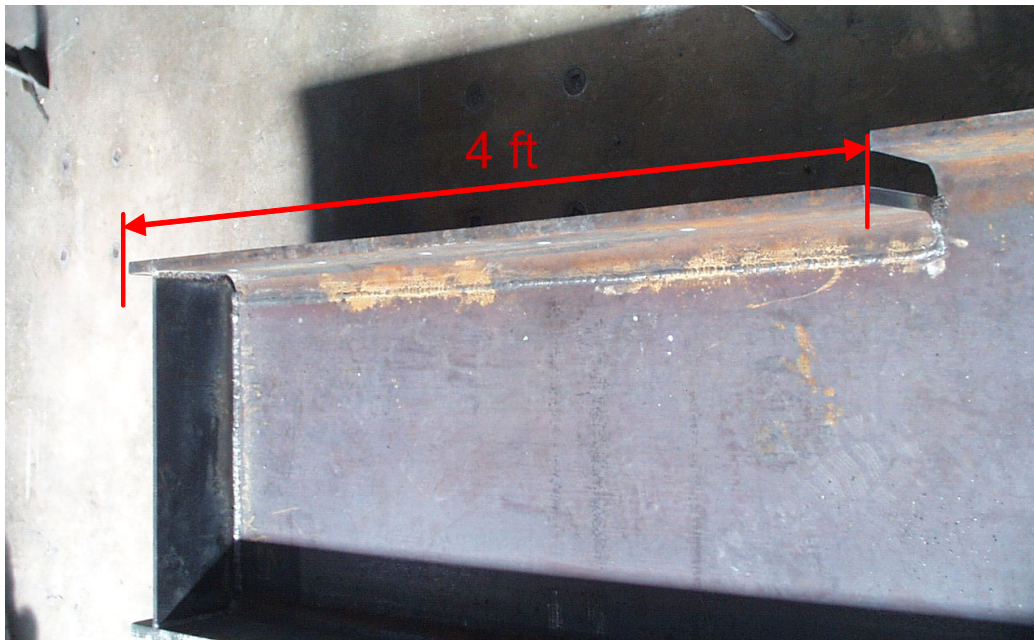
Figure 4-1 Drop-down in top girder flange[31]

As in the 0º skew specimen, the slab and girder assembly was elevated on eight columns, 4 ft (1.22 m) tall and 2 ft (610 mm) in diameter. Elevating the slab was necessary to install the loading frame and instrumentation, and to provide access to view cracking. The columns were positioned on the laboratory floor, and the steel girders were placed on top of them. Underneath the girders were 2-in. thick (45 mm) neoprene pads and a load cell sandwiched between two steel plates. Load cells were installed under the girders on the side of the slab being tested, and steel plates were used to maintain a constant beam elevation on the opposite side.

Once the girders were erected on the columns, elevated formwork was built using 4-ft (1.2 m) by 8-ft (2.4 m) plywood panels, ¾ in. (19 mm) thick.[31] Four 2- x 6-in. (51- x 152-mm) stringers, spaced 16 in. (406 mm) apart, were attached to each panel. The panels were supported from the ground by 4- x 4-in. (102- x 102-mm) posts and from the girder by wooden 2x4's wedged between the

52

bottom girder flange and the 2- x 6-in. (51- x 152-mm) stringers. Posts were braced in two directions with 2x4's. To form the skewed thickened edge, standard panels were built up with additional plywood.

To provide a redundant connection between the girders and the formwork for the overhang forms, fabricated metal clips linked the shear studs to the panels.[31] Edge boards, which formed the sides of the slab, were diagonally braced to the lower formwork. Gaps in the forms were closed with silicone sealant, and the forms were oiled to make them easier to remove. Reinforcing steel, both instrumented and bare, was then placed on chairs and tied together. Block-outs of PVC pipe were placed in the bridge slab where loading rods would pass through the slab. Prior to placing the concrete, the locations of strain gauges were recorded and the strain-gauge wires were routed out of the specimen.

Concrete was transported within the lab with a bottom-drop bucket hoisted by a crane (Figure 4-3), was placed, and was consolidated by electric vibrators (Figure 4-4).[31] An aluminum screed was used to level the top surface of the bridge slab. Finally, bull floats and hand trowels were used to create a smooth, flat surface. The specimen was cured for seven days by placing saturated strips of burlap, covered by plastic sheeting to reduce evaporation, over the entire surface of the slab. After 14 days, the forms were stripped and block-outs were removed; and after 28 days, slab testing began.

Figure 4-2 Forms before pouring

Figure 4-3 Pouring the slab

Figure 4-4 Vibrating concrete

4.3   LOAD APPLICATION[31]

Both test specimens were built on the strong floor of the Ferguson Structural Engineering Lab to allow application of the vehicle loads. Because the test specimen was large and the load frame was to be moved frequently, loading the bridge slab from above with a reaction frame was not feasible. A compact, reconfigurable load frame was designed and built which could fit underneath the test specimen and be moved with hand trucks (Figure 4-5, Figure 4-6).

Threaded rods were routed through the loading assembly on top of the bridge slab and attached to a load arm, labeled in Figure 4-5 as "upper load arm". The upper load arm was connected to two lower load arms by two, 2-in. (51-mm) diameter threaded rods. The rods connecting the two arms were prestressed to

55

eliminate rotation of the arm due to minor misalignment. The upper and lower load arms were constructed by attaching two C10x20 channels back-to-back with steel plate spacers, to allow loading through their shear center. The lower load arm flanges were drilled to match the strong-floor bolt pattern, and were stiffened adjacent to the holes (Figure 4-5, Figure 4-6). Six lower load arms and four upper load arms were built, enabling the application of up to four tire loads at any location under the slab.

4.3.1   Load Plate

Section 3.6.1.2.5 of the AASHTO LRFD Bridge Design Specification, 1999 Supplement specifies that design be carried out using an assumed tire contact area 20 in. wide (transverse direction) and 10 in. long (longitudinal direction). For tests of the 45º skew specimen, steel plates measuring 20 in. long, 10 in wide and 2½ in. thick were used to simulate tire contact areas.

Figure 4-5 Drawing of load frame[31]

Hydraulic Ram

Load Plate

Upper Load Cell

Load Rod

Upper Load Arm

Lower Load Cell

Concrete Support Column

Strong Floor
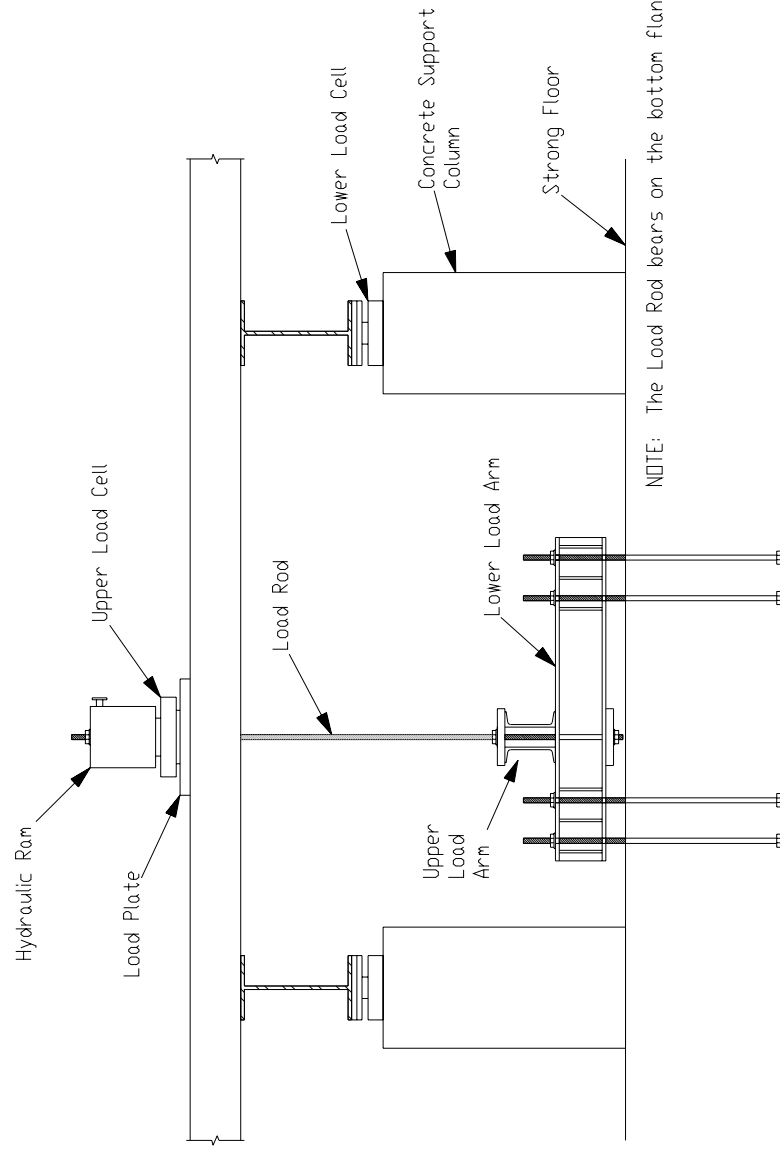
Lower Load Arm

NOTE: The Load Rod bears on the bottom flange of the Upper Load Arm.

57

(a)Facing south (same view as Figure 4-5)

(b)Facing east (perpendicular to view in Figure 4-5)

Figure 4-6 Pictures of load frame[31]

58

4.4   INSTRUMENTATION

To document the behavior of the test specimen during loading, strain gauges, linear potentiometers, and load cell readings were acquired during testing. To decide how to instrument the 45º skew specimen, data acquired for the 0º skew specimen were evaluated.

4.4.1   Strain Measurements

Strain gauges were the primary instrumentation used in the bridge slab of the test specimen.[31]   Since the strain gauges were placed before the concrete was cast, they were located carefully and protected to avoid damage during concrete placement and finishing.

4.4.1.1   Locations of Strain Gauges

Strain gauges were used to measure strains in individual reinforcing bars as a function of applied load, and to determine the corresponding strain profile within the slab. Strain measurements were used to understand how reinforcing bar stresses are distributed in the test area. In the 45º skew specimen, the gauges attached to bars in the UTSE and IBTS details were situated at midspan of both outer bays and on either side of each girder. Strain gauges were attached to every second transverse reinforcing bar in the IBTS and UTSE details. One top and one bottom longitudinal bar was gauged at midspan in the 10-ft bay, UTSE detail. Figure 4-7 shows the locations of strain gauges in the top and bottom mats of reinforcement. Gauges were located identically in the bottom and the top mat.
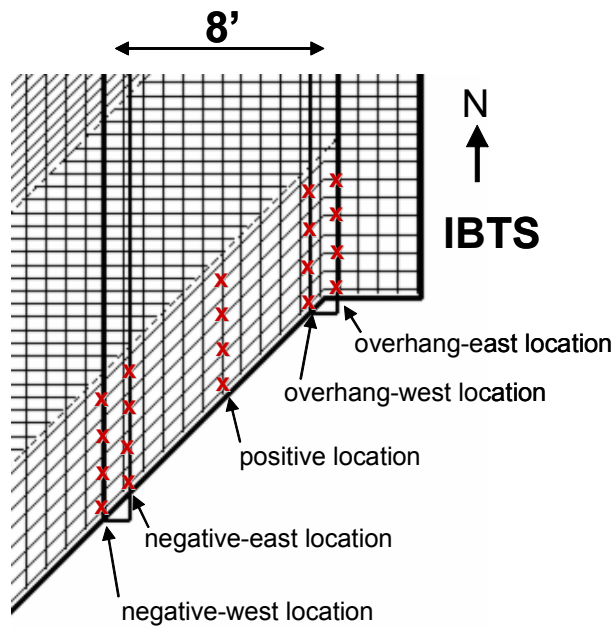
(a) 8-ft girder spacing, IBTS detail
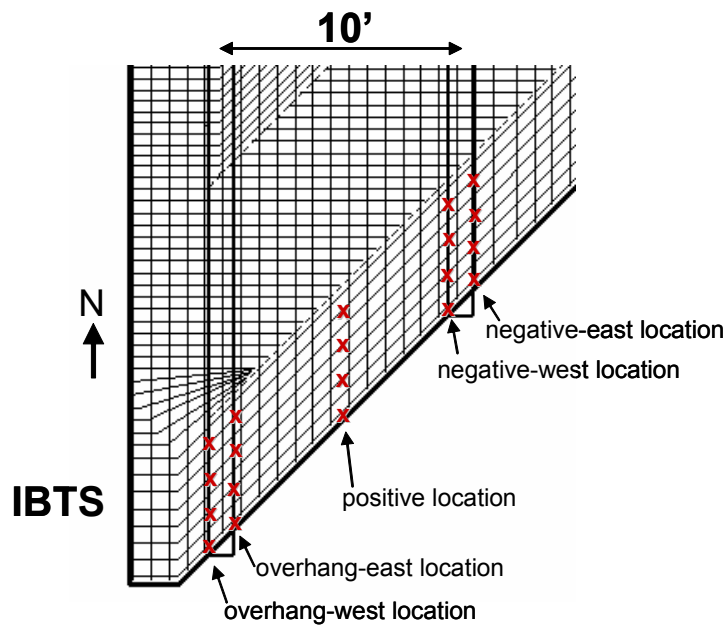
(b) 10-ft girder spacing, IBTS detail

Figure 4-7 Locations of strain gauges, top and bottom mats

60
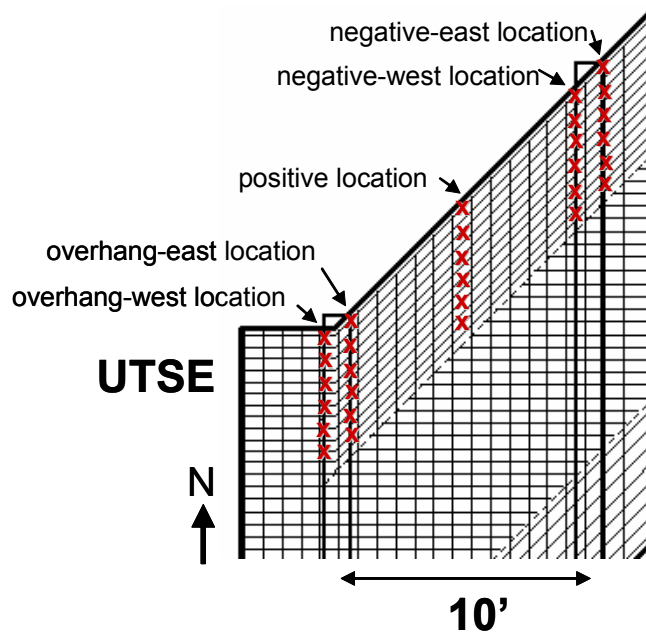
(c) 10-ft girder spacing, UTSE detail
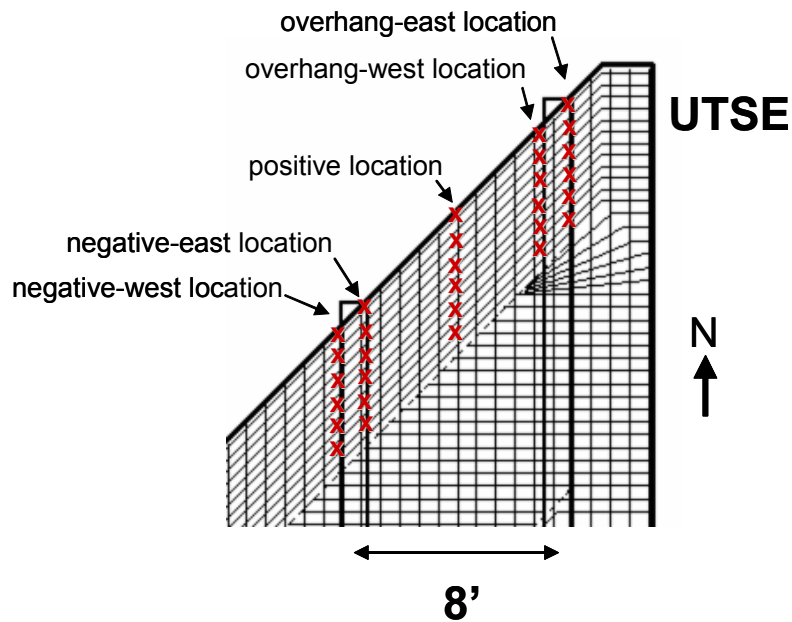
(d) 8-ft girder spacing, UTSE detail

Figure 4-7 cont'd. Locations of strain gauges, top and bottom mat

4.4.1.1.1 Strain Gauge Naming Convention

Strain gauges were identified according to a systematic convention (Figure 4-8). The first two letters were used to indicate the edge detail (UTSE or IBTS). The following number indicated the beam spacing in the bay in which the strain gauge was located. The next letter group denoted "positive," "negative," or "overhang." For gauges installed at girder, an east or west orientation would be added to show the side of the girder on which the gauge was located. The letter "L" was used after "positive" to denote gauges attached to longitudinal bars. The last letter indicated if the bar was in the top or bottom mat of reinforcement. The last number indicated which bar the gauge was on. Gauges were numbered starting at the edge of the slab.

End detail	Girder spacing	Location in span	Rebar mat	Rebar number
IB	8	NE	T	5
IBTS (IB) OR UTSE (UT)	8-ft (8) OR 10-ft (10)	Negative, east or west (NE, NW) OR Positive (P) OR Overhang, east or west (OE, OW)	Top (T) OR Bottom (B)	1 is rebar at the edge
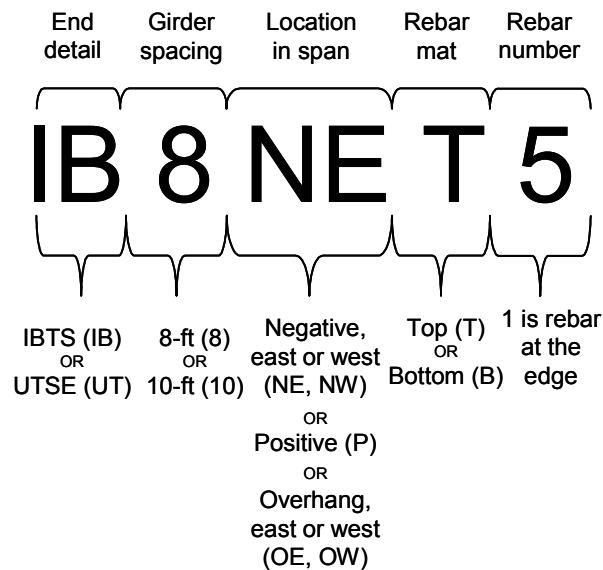
Figure 4-8 Gauge label legend

In the 45º skew specimen, approximately 250 strain gauges were applied to the transverse reinforcing steel in end details. Three major changes from the 0º skew specimen instrumentation plan were made for the 45º skew specimen.

- First, all redundant gauges were eliminated. In the 0º skew specimen, half of the primary gauges had a redundant backup gauge in case one was damaged. Because the very few gauges in the 0º skew specimen were damaged during concrete placement and consolidation, the redundant gauges were eliminated for the 45º skew specimen.

- Second, every second transverse reinforcement bar was instrumented in the 45º skew specimen. Every transverse bar in the 0º skew specimen had been gauged, but the strain variation between adjacent bars was small, and little additional information was obtained from the eliminated gauges.

- Third, in the 45º skew specimen, gauges were installed at both edges of the girder. In the 0º skew specimen, gauges had been installed only at the centerline of the girder. The change was made to place the gauges at the point of expected maximum strain in the bars.

4.4.1.2   *Installation of Strain Gauges[31]*

The strain gauges had a 5-mm gauge length, 3-m pre-attached leads, and were temperature-compensating (3-wire gauges). The procedure used to attach the strain gauges to reinforcement in the 0º skew specimen was repeated for strain gauges in the 45º skew specimen. The reinforcing bars were prepared for strain gauge application by grinding off one rib to create a flat surface.[31] The application area was then cleaned with conditioner and neutralizer. Cyanoacrylate (CN) adhesive was used to bond the strain gauges to the rebar. Then, the gauges were waterproofed with an acrylic coating. Next, a neoprene rubber pad was placed over the gauge as impact protection, and the installation

area was covered with foil tape. Finally, the edges of the foil tape were wrapped with electrical tape to seal out concrete and water.

4.4.2   Load Measurements[31]

Loads were measured by load cells, located underneath the girders (lower load cells) and at the hydraulic rams (upper load cells) (Figure 4-5). The lower load cells were only used under the edge of the bridge slab being tested, as most of the applied load went directly into those supports. The upper, center-hole load cells were the primary transducers for measuring applied load. In addition, a pressure transducer was connected to the hydraulic line at the hydraulic pump, and was used to verify the load-cell readings, as pressure transducers are typically less accurate than load cells. In one case, when applied load nearly exceeded the upper load cell capacity, the load was determined exclusively with the pressure transducer.

4.4.3   Deflection Measurements

Deflection measurements were made under the girders and midspan, using linear and string potentiometers located as shown in Figure 4-9. Under girders and at midspan, deflections measurements were taken at the edge of the slab and at the end of the edge detail, 5.75 ft (1.75 m) from the edge in the longitudinal direction of the slab. String potentiometers were used in congested locations. At some locations, linear potentiometers and string potentiometers were used together to ensure that reliable data. In each test, two linear potentiometers, placed 10 in. (254 mm) apart, were used to measure rotation of the girders. Figure 4-10 shows how the potentiometers were used to measure rotation, and Figure 4-9 shows the locations of the potentiometers.
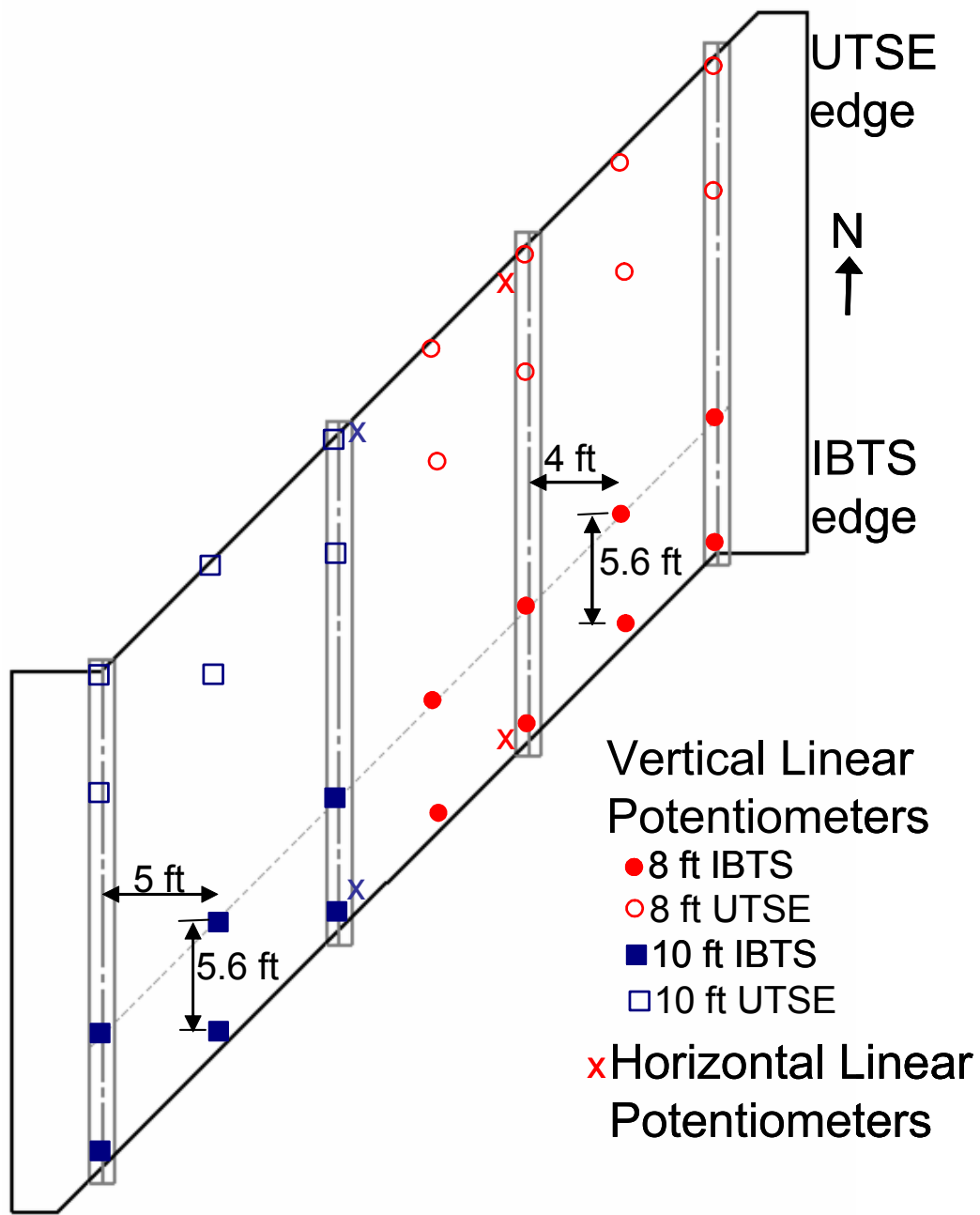
Figure 4-9 Deflection measurement locations, plan view
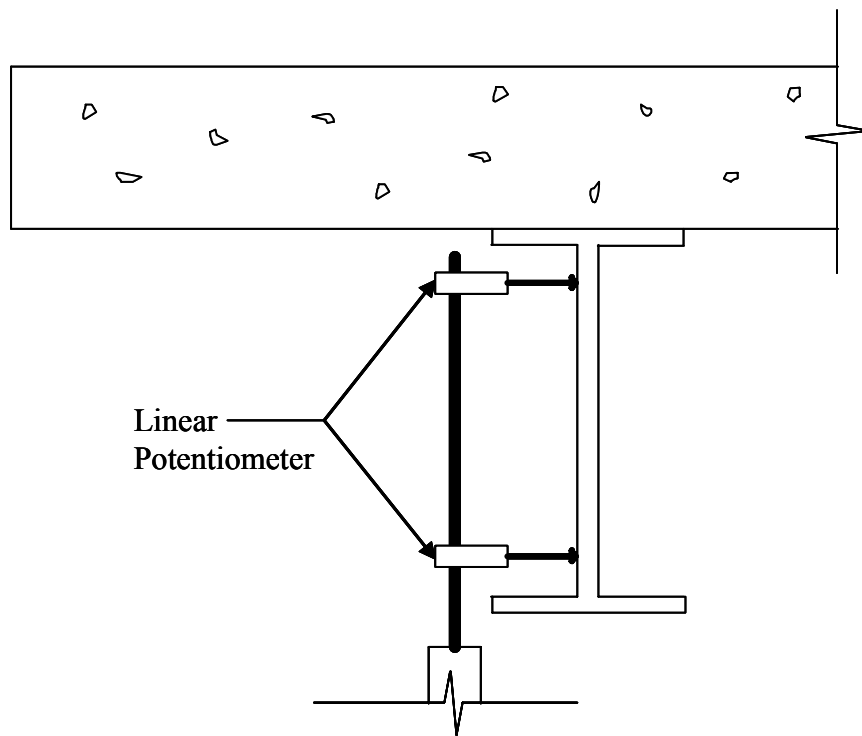
Figure 4-10 Girder rotation measurement[31]

4.4.4   Data Acquisition[31]

The instrumentation output was voltage (analog signal).   The instrumentation was connected to bridge boxes, which direct the current output from the instrumentation to the scanner. The scanner converted the voltages to a digital format, readable by data acquisition software installed on a personal computer. It also plots real-time test data, allowing the specimen's behavior to be monitored while loading.

4.5   MATERIAL PROPERTIES

To aid in the interpretation of the acquired data, tests were performed to measure material properties of the reinforcing steel and concrete used in the

specimen. Results of materials tests were also used to check the strengths reported by the manufacturers.

4.5.1 Reinforcing Steel

The reinforcing steel used in the specimen came from two different heats. The transverse reinforcement in the 10-ft (3.0-m) girder spacing, UTSE end detail region was from the second heat. All other slab reinforcement was from the first heat.

Two lengths of reinforcing bar from each heat were tested in tension. An extensometer and strain gauges were used to determine strains, and load cells in the test machine were used to measure the applied loads (Figure 4-11). After converting the load measurements to stresses, stress-strain plots were created (Figure 4-12).

Figure 4-11 Rebar tension test setup[31]
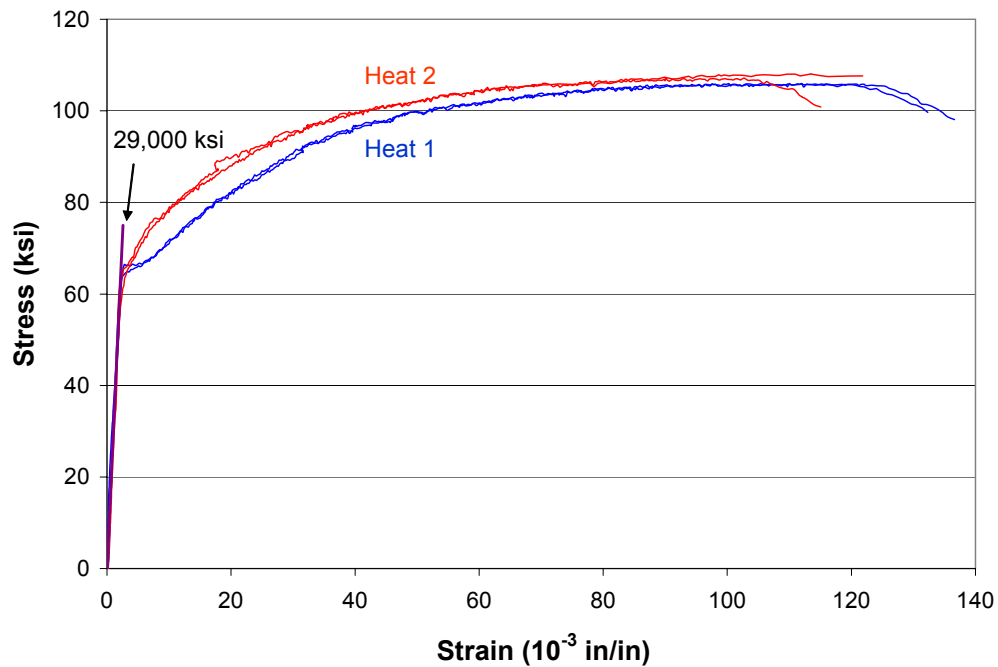
Figure 4-12 Results from rebar tension tests

Reinforcement from both heats had a yield stress higher than the specified 60 ksi (414 MPa). Reinforcement from Heat 1 yielded at about 65 ksi (448 MPa). Reinforcement from Heat 2 had only a very short yield plateau, at around 64 ksi (441 MPa). Yield strains were between 2100με and 2400με, with a mean of 2200με.

4.5.2 Concrete

The TXDOT Bridge Design Manual currently requires a minimum 28-day compressive strength of 4000 psi (27.6 MPa) for concrete used in bridge slabs. To avoid excessive compressive strength, a mix design was ordered with a target compressive strength between 3500 psi (24.1 MPa) and 5000 psi (34.5 MPa).

Table 4-1 Concrete mixture design for bridge slab (one-yard batch)

Mix #	Description	f'$_c$ (psi)	Cement	Fly Ash	Course agg.	Fine agg.	Water	Ad- mixture
225	UT4000A 3/4in	3500 to 5000	470	0	1625	1655	250	20.0

*All quantities are in units of pounds (lbs).

4.5.2.1 Compressive Strength

The 21 yd^3 (16.0 m^3) of concrete used in the slab was delivered in three truckloads; test cylinders were taken from each truck. The concrete in the first truck was placed primarily in the west overhang and the 10-ft (3.0 m) girder spacing bays. Concrete from the second truck was placed in the 8-ft (2.4 m) girder spacing bays and in the portion of the overhang at the southeast corner of the slab. Concrete from the third truck was placed only at the overhang at the northeast corner of the slab. For each point plotted on the strength versus time curve in Figure 4-13, at least two cylinders were tested. If the two strengths were not close, a third cylinder was tested for verification.
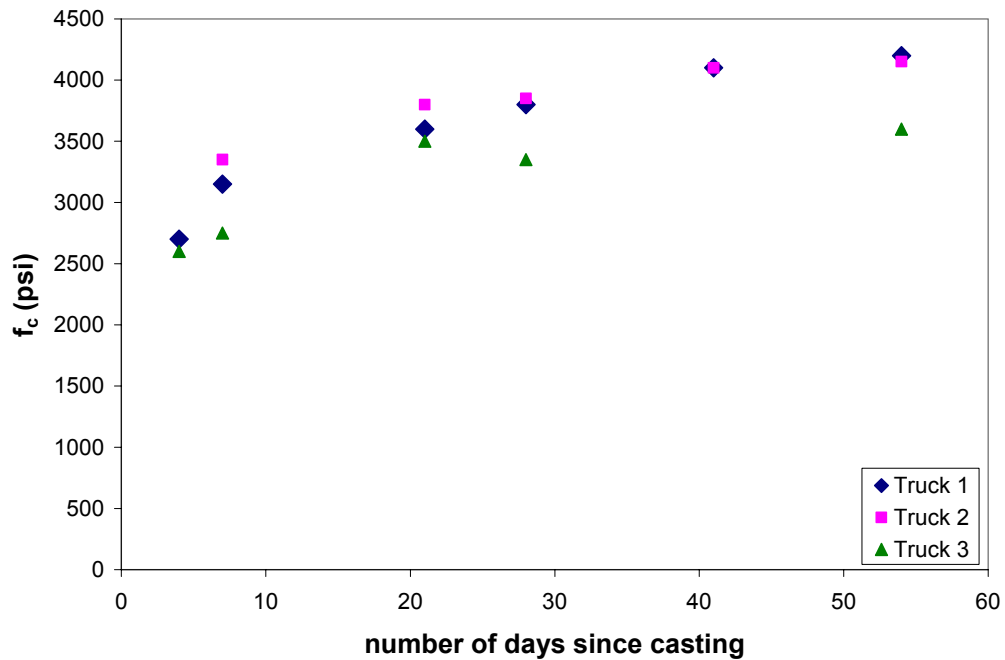
Figure 4-13 History of tested concrete compressive strengths

4.5.2.2 Splitting Tensile Strength

Split cylinder tests were performed four months after casting, on three cylinders from Truck 1 and three from Truck 3. No cylinders from Truck 2 were tested, as the compressive strengths of cylinders from Trucks 1 and 2 were equal. The splitting tensile strength, f_{ct}, was determined using Equation 4-1, with P equal to the failure load. The tensile strength of concrete from Trucks 1 and 3 were 430 psi (3.0 MPa) and 400 psi (2.8 MPa) respectively, essentially the same.

$$f_{ct} = \frac{2P}{\pi l d}$$ *Equation 4-1*

The average of these splitting tensile strengths is equivalent to 6.7 and 6.8 times the square root of f_c for Trucks 1 and 3 respectively, slightly higher than the $6\sqrt{f'_c}$ term often assumed in design.

4.6   TEST PROTOCOL

The specimen was constructed with four test areas, each of which was loaded with the AASHTO tandem load configuration. After the spans were tested, the four overhangs were tested, as discussed in Chapter 6. The span tests are listed in the order in which they were performed:

- 8-ft (2.4-m) girder spacing, IBTS test
- 10-ft (3.0-m) girder spacing, IBTS test
- 10-ft (3.0-m) girder spacing, UTSE test
- 8-ft (2.4-m) girder spacing UTSE test

Figure 4-14 shows a plan view of the locations of the span test areas and the locations of the load plates in each section. In the 8-ft (2.4 m) girder spacing, 11-ft (3.4-m) clear spacing bays, only negative moment was maximized, and load axles were centered over the girder. Positive moment was maximized in the 10-ft (3.0 m) girder spacing, 14-ft (4.3-m) clear spacing bays, and two load plates were placed at midspan.

71
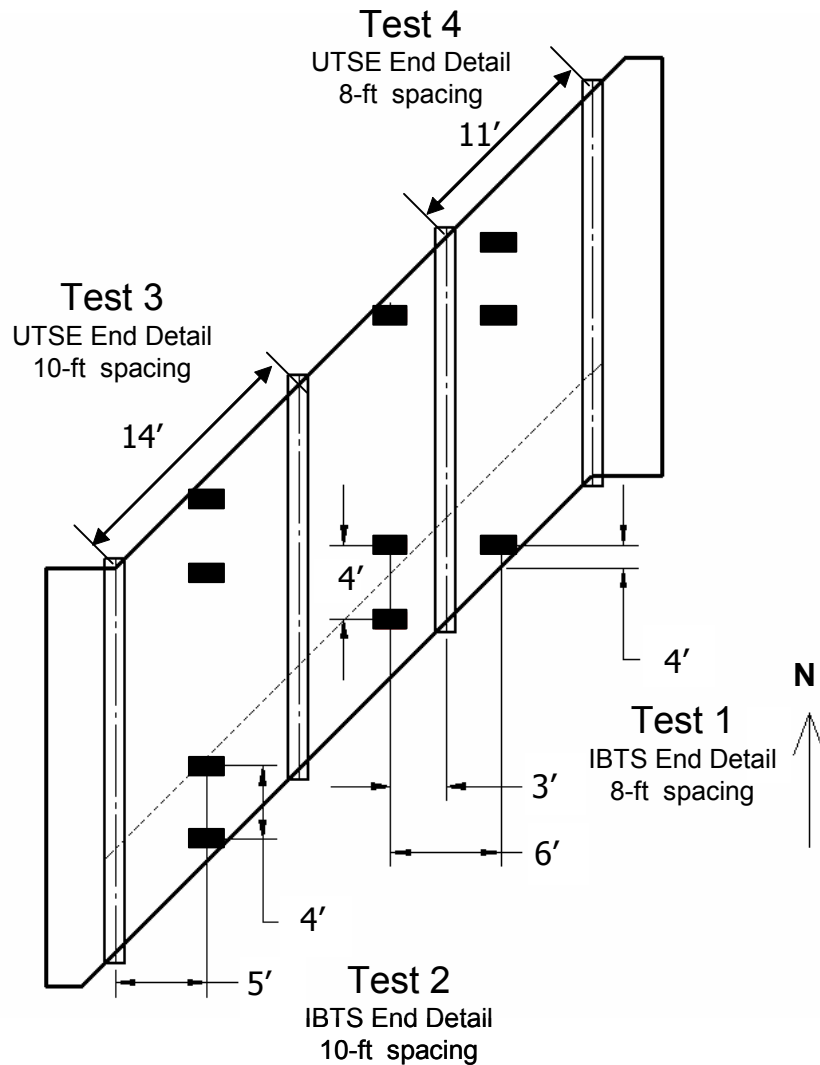
Figure 4-14 Test areas, 45° skew specimen

Load was applied to the test specimen with 60-ton (533 kN) hydraulic rams connected to an air-driven hydraulic pump, applying equal loads to all tires locations.[31]   After verifying that the instrumentation was working properly, the load was increased gradually. Because the scanner took nine seconds to record readings from 90 channels, load was increased in small increments. During testing, a load-strain plot of the most critically strained gauge was generated in

real time to monitor the response of the slab to applied loads. Intermittently, loading was paused, and any cracks that had formed were traced, measured, photographed, and documented.

Service-level tests were first performed on each area to view cracking behavior in each test section before severe damage occurred anywhere in the slab. For each area, loads were applied until cracking began to extend into neighboring test regions. The area was then unloaded, and the load frame was moved to the next test area.

After all service-level tests had been performed, each test area was loaded to design-level load, overloads as multiples of that design-level, and to failure. Each test included load levels HS-20, HS-25, 1.2 HS-25, 1.75 x HS-25, 3.0 x HS-25, and failure, as well as other intermediate load levels. Overload steps were chosen because of their value to researchers and designers. A factor of 1.2 times HS-25 loading may be considered a typical design load increase to account for overloaded trucks. The 1.75 x HS-25 overload was chosen because 1.75 is the value of the live-load factor (Section 3.4.1 in AASHTO LRFD). In addition, the dynamic load allowance in Section 3.6.2 of that document requires the design loading to be increased by 1.75 for expansion joints. An overload level of 3.0 x HS-25 was applied to all test areas because the product of the load factor and the dynamic load allowance is approximately 3.0. When designing the expansion joint of a bridge slab, the required design load is three times the typical value.

CHAPTER 5

Test Results - Slab End Tests

5.1 INTRODUCTION

In this chapter, the results from tests performed on slab ends are presented, including deflections, strains, crack patterns, and failure loads. After the results are presented, they are discussed and compared. In addition, failure modes and capacities are addressed.

Each test area is referred to by the end detail tested and whether positive moment or negative moment was maximized by the placement of the AASHTO design truck. If positive moments are maximized, the test is referred to as a "positive moment test," and if negative moments are maximized, as a "negative moment test." The tests are listed below in the order in which they were performed:

- IBTS, negative-moment region
- IBTS, positive-moment region
- UTSE, positive-moment region
- UTSE, negative-moment region

Positive moment at midspan was maximized in the 10- (3.0 m) bays, and negative moment was maximized over the girder in the 8-ft (2.4-m) bays. Although load points may be placed located in a way that maximizes positive moments, significant negative moments may still be generated in other areas of the test region. The same is true for negative moment tests. In this chapter, results from the negative moment tests are listed together, as are results from the

positive moment tests. Loads are reported as multiples of AASHTO design loads as discussed in Section 3.2.3.

Each area was first loaded until cracking became extensive, and then unloaded. After the four initial tests were performed, the areas were then reloaded to failure.   For the first test in each area, referred to as a serviceability load level test, of the load level was limited so that initial cracking behavior would not be affected by changes in stiffness due to extensive cracking in adjacent test areas.   Table 5-1 shows the largest load applied during the serviceability load level test in each test area.   After all serviceability tests were completed, the test areas were loaded to failure.   Procedurally, there is no difference between the tests. At critical overload values, crack lengths and widths were recorded and pictures were taken.

Table 5-1 Largest load per load point applied during serviceability load level tests

	Load per load point
IBTS, negative moment region	42k / 2.7xHS-25
IBTS, positive moment region	27k / 1.7xHS-25
UTSE, positive moment region	27k / 1.7xHS-25
UTSE, negative moment region	55k / 3.5xHS-25

Figure 5-1 and Figure 5-2 show samples of the graphics used in this chapter to visually identify the area being tested. The sample graphic in Figure 5-1 shows the test region itself, loading points, and gauge locations. To identify

the design parameters being tested, the girder spacing and end detail are shown. A '+' or '-' sign is added to show whether positive or negative moment is being maximized in the test region, and the load points are shown to describe how the area was loaded during testing. The strain gauges are located on the transverse reinforcement bars along the axes drawn and identified as either "positive," "negative," or "overhang." Over the interior girders, negative moments are generated, and these locations are referred to as "negative" locations in the graphics. At midspan, positive moments are generated in the end regions, and these locations are referred to as "positive" locations. The strain gauge locations over the exterior girders are referred to as "overhang" locations. The location of the dashed line on the graphic indicates the orientation of the "negative" and "overhang" gauges relative to the girder.

Figure 5-2 shows a more detailed view of the locations of strain gauges in the tested end region and will be used to show gauge locations in strain profiles. The slab end and transverse reinforcement in the end region are shown, and gauges are depicted by a red 'x'. The smaller graphic indicates the location of the slab being enlarged. Where gauges are installed on either side of the girder, the girder is shown.
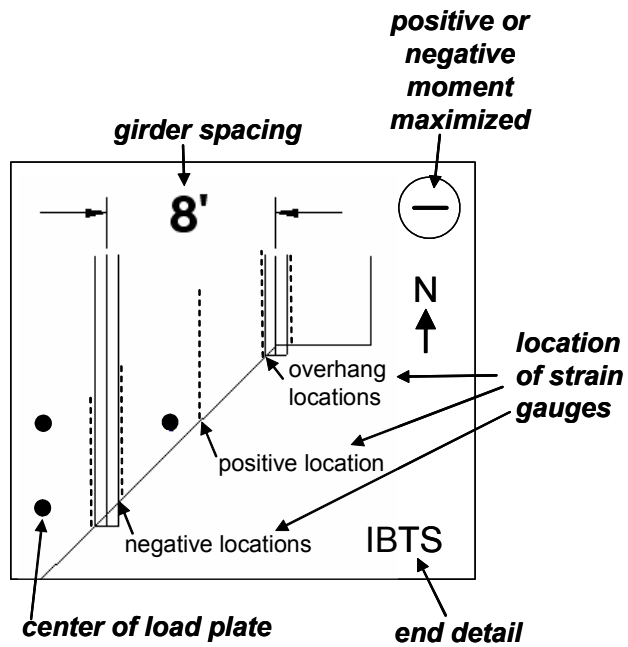
Figure 5-1 Sample test area
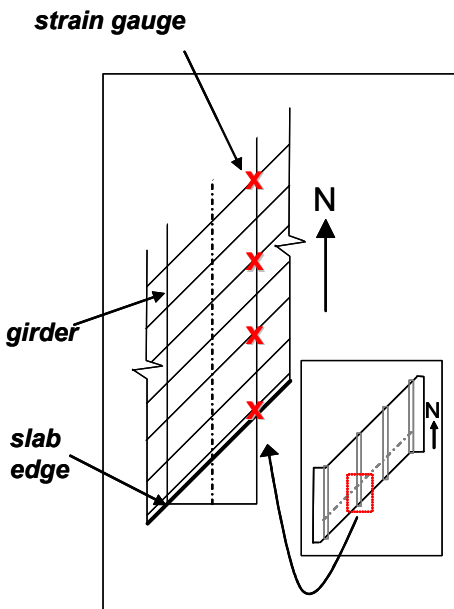
Figure 5-2 Sample strain gauge location

To describe the behavior of the test region, individual load points, girders, and bays must be identified; naming conventions have been adopted to aid in this discussion. Figure 5-3 shows the convention used for identifying girders and bays. As demonstrated in Figure 5-4, a load point is described both by the bay in which it was located, and by its position relative to the edge of the slab.
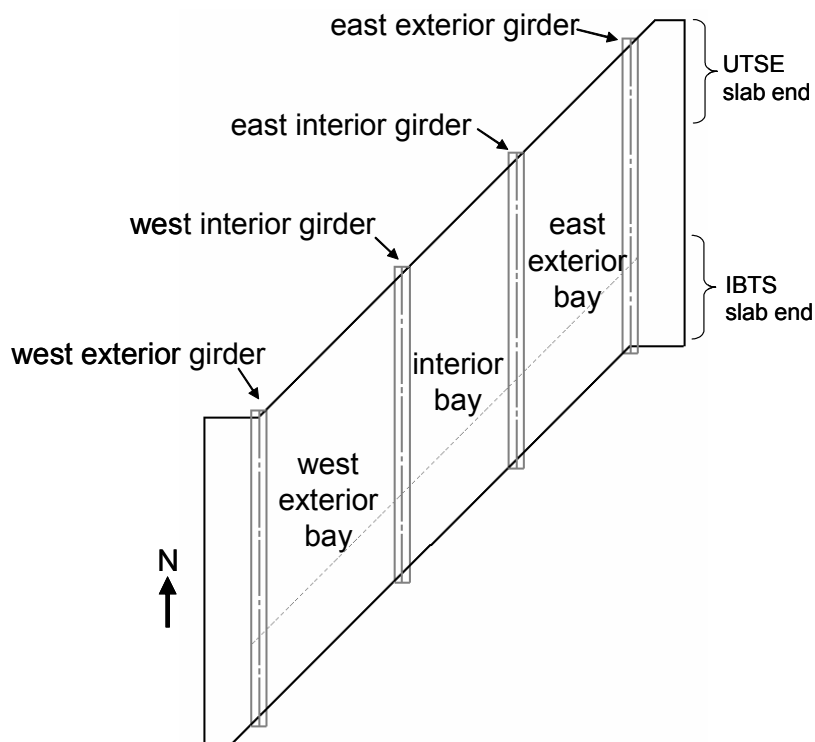
Figure 5-3 Girder and bay naming conventions
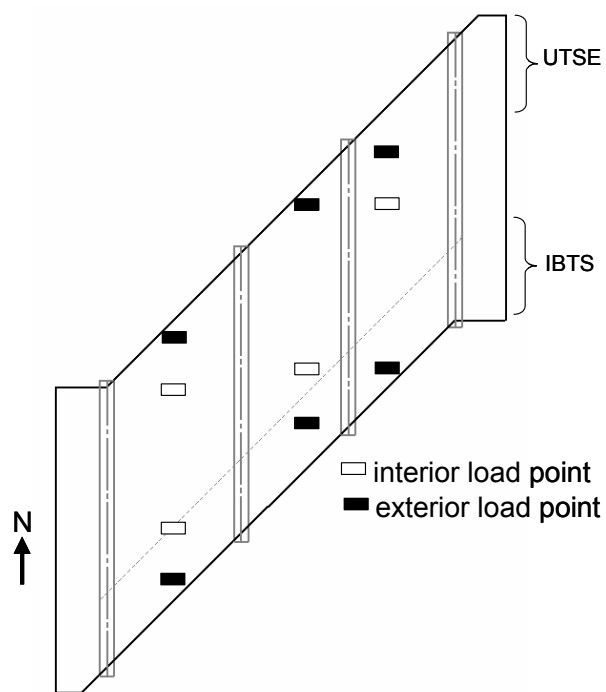
Figure 5-4 Load point nomenclature

5.2   IBTS END DETAIL, NEGATIVE-MOMENT REGION

Negative moments were maximized over the east-interior girder, between the two 8-ft (2.4-m) bays. At the locations shown in Figure 5-5, three 10- by 20-in. (254 by 508-mm) steel plates were placed in the end region on a layer of hydrostone. In the serviceability test, at a load of 42 kips (187 kN) per load point, 2.7 x HS-25. Cracks were observed in the region tested, and a single crack was observed in the west-exterior bay and over the west-interior girder. The test was stopped to evaluate whether the crack should prevent further testing in the region. After, loading was stopped at 3.0 x HS-25 and testing was moved to the next test area.

After serviceability load tests were complete, the IBTS detail, negative-moment test area was loaded to failure. At 94 kips (418 kN) per load point,

approximately 6 x HS-25, a punching shear failure occurred at the interior load point in the interior bay.
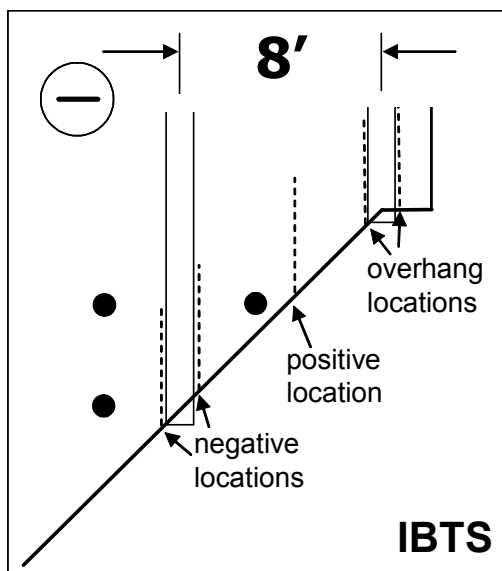
Figure 5-5 IBTS end detail, negative-moment region

5.2.1 Load-Deflection Behavior

Load-deflection plots were created using the readings from the load cells and from the linear and string potentiometers measuring vertical deflection of the bridge slab. The deflection readings from the potentiometers located in the interior of the slab (5-ft, 9-in. (1.75-m) from the edge longitudinally, at midspan of the exterior span transversely) were very small, indistinguishable from the noise produced by the instrumentation (Figure 4-9). Therefore, transverse deflection of the edge is the only deflection measurement reported in subsequent discussions. The relative deflection at the edge was calculated by averaging the two girder deflection readings made underneath the girders near the supports and then subtracting this from the deflection reading at midspan (Figure 5-6). In this way, rigid-body movement of the bridge slab was filtered out, so that

80

deformations causing cause stresses and strains could be reported. For each test, the residual deflection is assumed to be the last deflection measurement taken after unloading in the previous test.
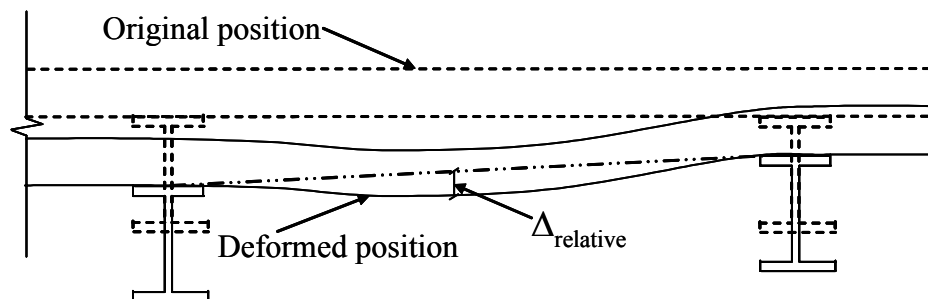
*Deformations are exaggerated.

Figure 5-6 Relative midspan deflection[31]

Two critical transverse edge deflections are reported here, the deflection in the exterior bay and the deflection in the interior bay. Figure 5-7 shows a complete load deflection response as measured during tests in this area. The approximate deflection envelope is also shown. In the HS-20 and HS-25 load ranges, the load deflection response in the interior bay and exterior bay was similar. In this range, all deflections were extremely small relative to the girder spacing. The load-deflection behavior in this range was linear and elastic.

In the interior bay, the relative midspan deflection at HS-20 was approximately 0.025 in. (0.6 mm). At HS-25, the interior bay deflection measured was 0.026 in. (0.7 mm), essentially indistinguishable from the deflection measured at HS-20. In the exterior bay, the relative midspan deflection at HS-20 was 0.009 in. (0.2 mm), and at HS-25, it was approximately 0.015 in. (0.4 mm).

At 1.2 x HS-25, the inner bay deflection was 0.03 in. (0.8 mm), and the outer bay deflection was 0.02 in. (0.5 mm). At this load step, the increase in deflection is proportional to the increase in load from HS-20. At 1.75 x HS-25

the edge deflection was 0.04 in. (1 mm) in the inner bay and 0.033 (0.8 mm) in the outer bay. In both bays, the response at this load level was no longer linear, as slab stiffness reduced. The maximum measured deflection at failure was 0.83 in. (21 mm) in the outer bay and 0.31 in. (8 mm) in the inner bay.

5.2.1.1 Load-Deflection Envelope

Load-deflection envelopes indicate three changes in slab stiffness during all tests in the area. The first change in stiffness, apparent in both bays at approximately 2.8 x HS-25, was caused by developed cracking in the slab. Throughout this thesis, the term "developed cracking" refers to the first major change of stiffness as interpreted from the load-deflection response. Though the load at developed cracking was determined from the load-deflection response, developed cracking is further evidenced by the initiation of multiple new cracks in the test section, and by the propagation and widening of existing cracks. Details on the locations and sizes of the cracks are given in Section 5.2.4.

Load-deflection plots for both bays also indicate a second, smaller change in stiffness at about 5.1 x HS-25, more apparent in the outer bay than the inner one. At approximately 5.9 x HS-25, the slab stiffness approaches zero. This response is largely seen in the outer bay, where deflections nearly doubled due to a load increase of 2 kips (9 kN) per load point.
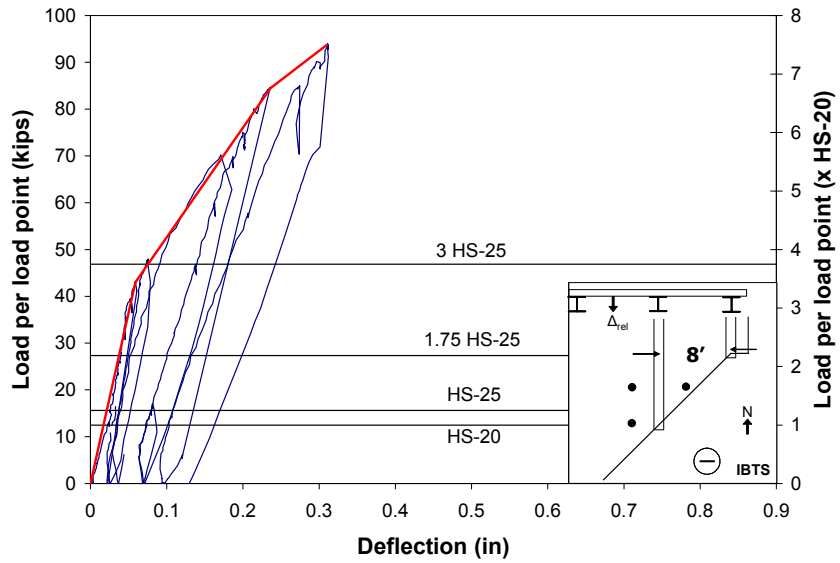
(a)
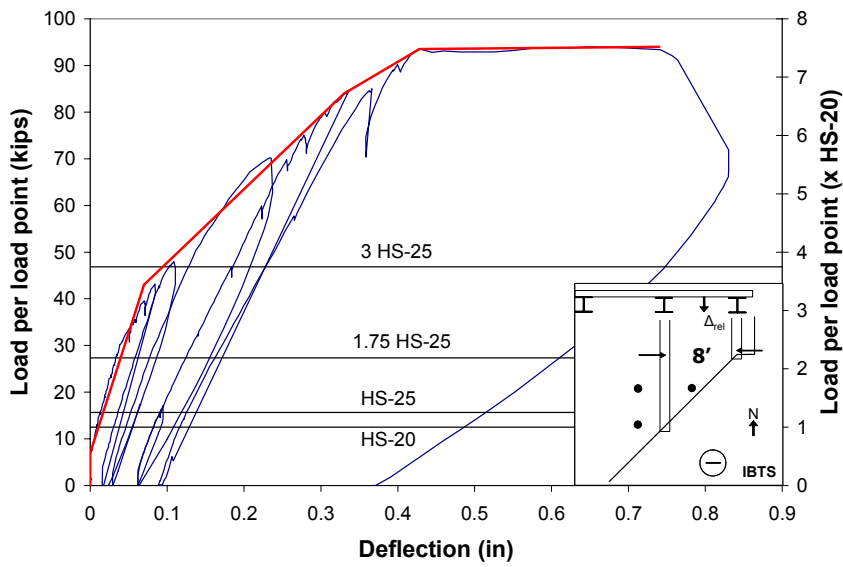
(b)

Figure 5-7 Relative midspan edge deflection, IBTS, negative-moment region:

(a) exterior bay; (b) interior bay

5.2.2   Load-Strain Response

Load-strain plots are shown to analyze cracking and identify loads at which reinforcement yields.   Strain gauges were installed on every other transverse reinforcing bar in the end detail, for a total of four top and four bottom gauges at three locations. Only the data from the most critical strain gauge from each of the three locations are shown here. The critical gauge was that registering the largest strains through most or all of a test. Frequently but not always, the critical gauge is located at the bar closest to the edge. Locations of the critical gauges are shown to the right of the plots. Strain plots for other gauges monitored during testing are shown in Appendix A.

Only gauges installed on transverse reinforcement bars in tension are discussed here. For locations where moment is negative, strains in the top mat of steel are discussed. For locations where moment is positive, strains in the bottom mat of steel are discussed. Strain plots for gauges in compression are shown in Appendix A.

Figure 5-8(a), (b), and (c) show strain measurements recorded on both sides of the girder and midspan.   At serviceability load levels, strains were extremely small, and maximum measured strains were similar on both sides of the girder.

At HS-20, HS-25, and 1.75 x HS-25 load levels, measured strains were less than 5% of yield strain (110 µε). At 3 x HS-25, the load-strain response was no longer linear at any gauge location.   Maximum strains measured at approximately 3.1 x HS-25 were 24% of yield strain (530 µε) on the east side and 14% of yield strain (300 µε) on the west side of the girder where two load points were located. First yield of an instrumented reinforcing bar occurred at 5.3 x HS-25 on the east side of the girder. The maximum recorded strain, 280% of yield strain (6220 µε), was recorded on the west side of the girder, the side where

84

punching shear later occurred. Maximum strain levels on the east side of the girder were 170% of yield strain (3800 με). At midspan, yield strain was not reached by any instrumented reinforcing bar.
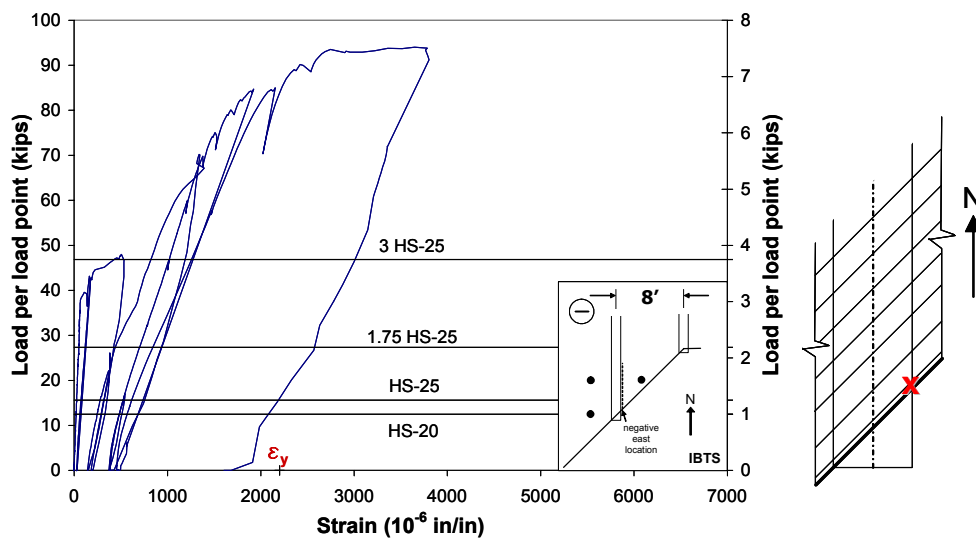
(a)

Figure 5-8 Load-strain response, IBTS, negative-moment region: (a) east side of girder, top mat; (b) west side of girder, top mat; (c) midspan, exterior bay, bottom mat
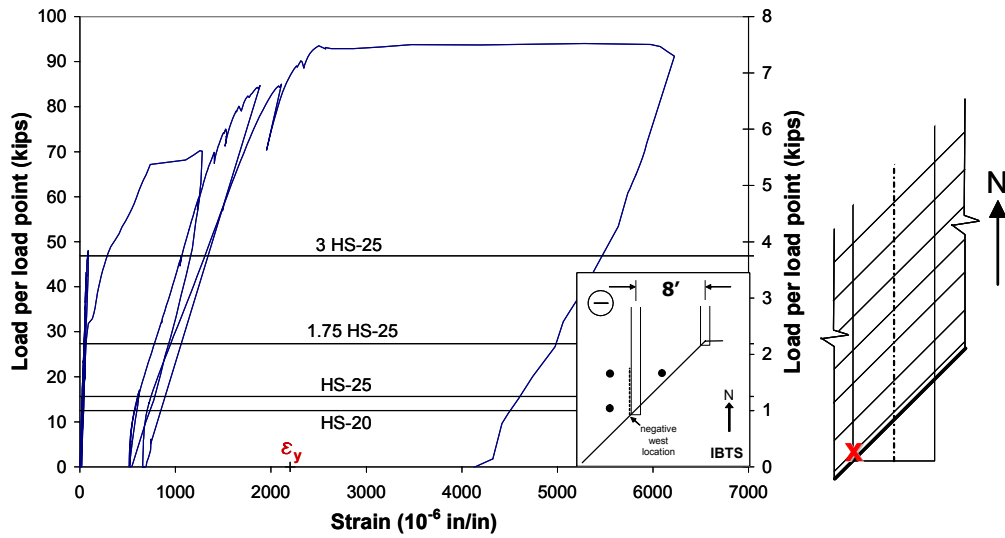
(b)
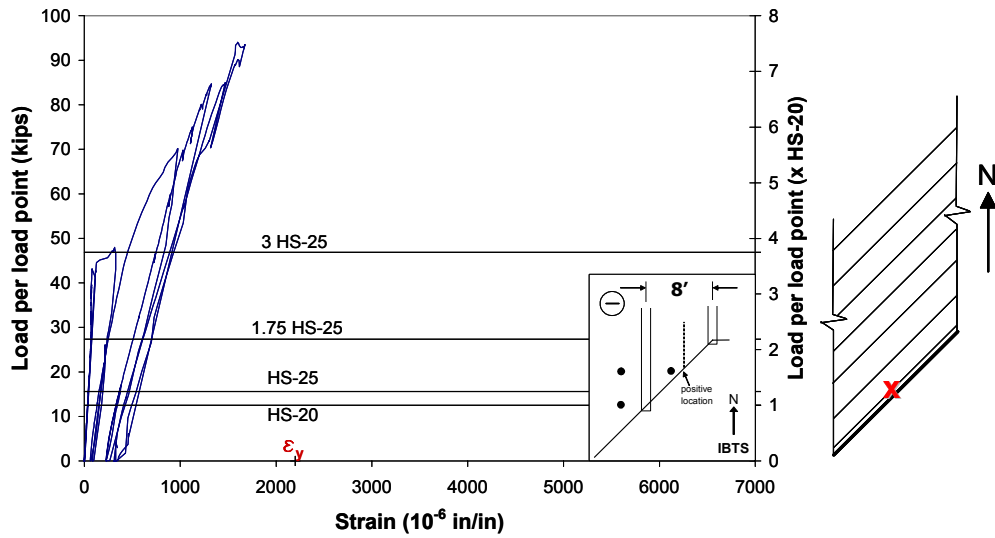
(c)

Figure 5-8 cont'd. Load-strain response, IBTS, negative-moment region: (a)
east side of girder, top mat; (b) west side of girder, top mat; (c) midspan,
exterior bay, bottom mat

5.2.3   Strain Profiles

Strain profiles were used to compare strain readings from reinforcement in the test area at specific locations and loads. The graphic to the right of each profile shows gauge locations in the test specimen. Figures in this section show the strain in the reinforcement at selected load steps in a plan view of the strain measurements from reinforcing steel in the edge detail. The strain profiles were used to compare strains in the bridge slab for the two sections. Since the edge deflection was much greater than the deflection 5.75 ft (1.75 m) into the slab, the expected strain profile would give a maximum strain at the edge reinforcement, gradually decreasing for reinforcement further into the section. The specific shape of the strain profile varies with loading configuration and skew angle, however.

The difference in performance of slabs at HS-20 and HS-25 loads is of particular interest in this project. While the profiles show that strains increase with increasing load, strains at both HS-20 and HS-25 were extremely small, less than 3% of the yield strain (66 $\mu\varepsilon$).

In Figure 5-9(a), (b), and (c), strain profiles are shown for three locations in the IBTS, positive moment test section. In this test area, the largest strains occurred on the west side of the beam, and the smallest occurred at midspan, where maximum positive moment occurs. The increase in strain from HS-20 to HS-25 is extremely small. At 1.75 x HS-25, HS-25, and HS-20 loads, the strain distribution was nearly uniform through the end region. As loads approached the failure load, strains in reinforcement near the slab edge became much larger than strains measured closer to the interior of the section.

87
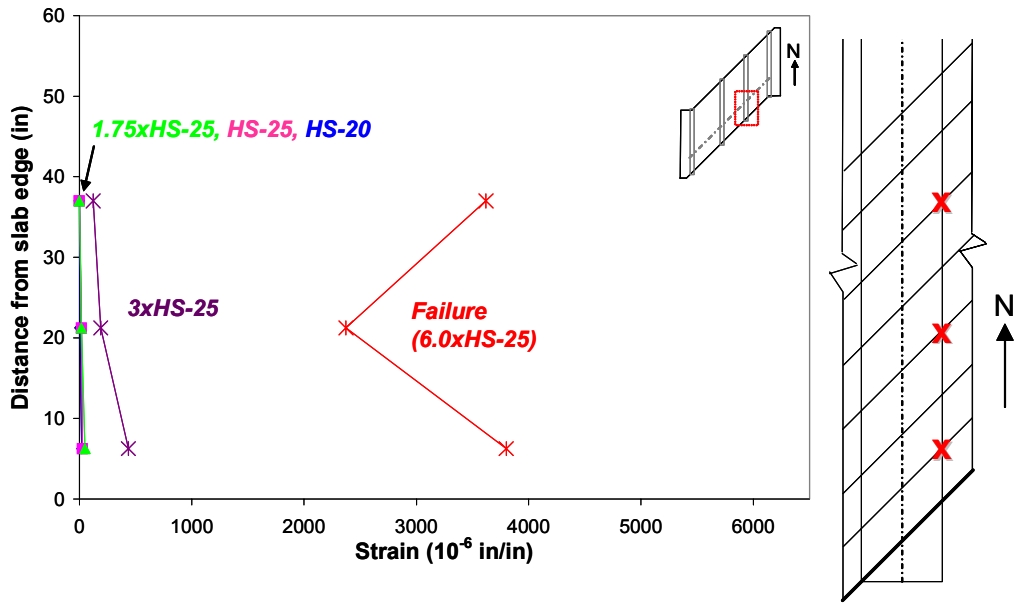
(a)
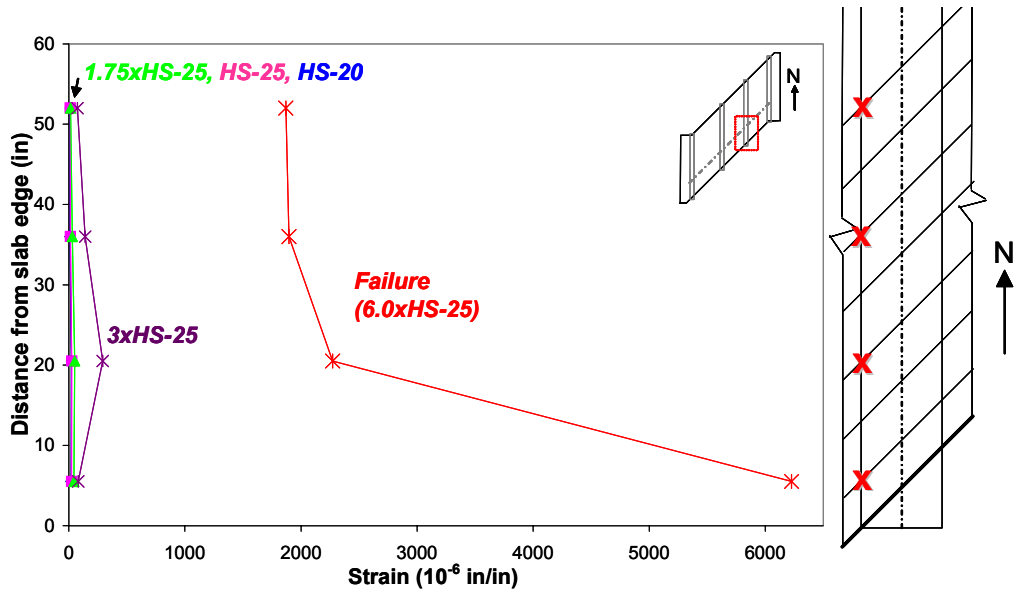
(b)

Figure 5-9 Strain profile, IBTS, negative-moment region: (a) east side of girder, top mat; (b) west side of girder, top mat; (c) midspan, bottom mat

(c)
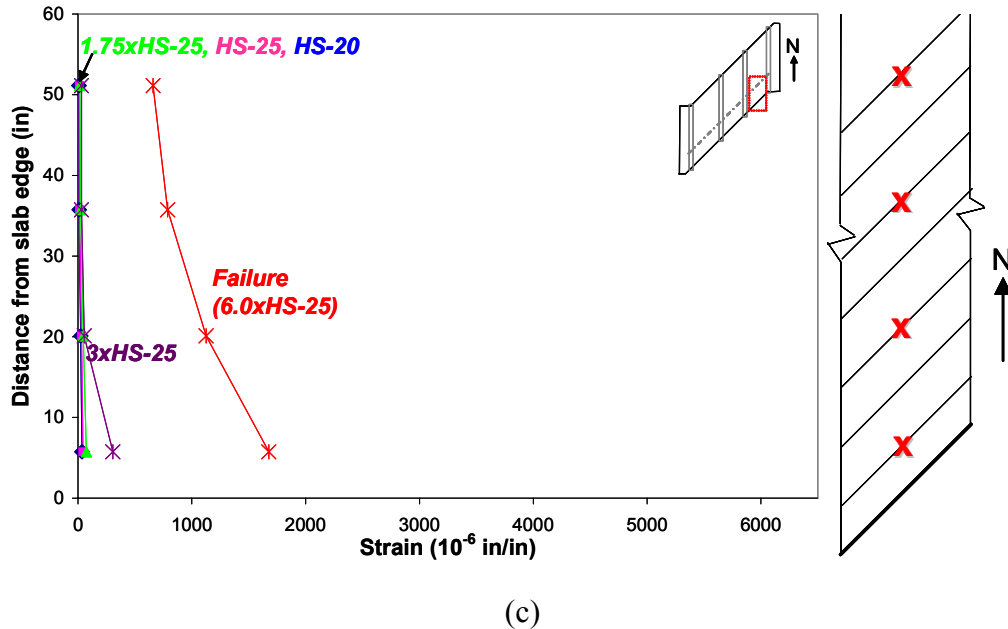
Figure 5-9 cont'd. Strain profile, IBTS, negative-moment region: (a) east side of girder, top mat; (b) west side of girder, top mat; (c) midspan, bottom mat

5.2.4   Crack Maps

At every load step, the locations, widths, and lengths of cracks were photographed and measured and used to produce crack maps that would convey the extent and pattern of cracking at various load levels. Crack maps also show the degradation of the test specimen under applied loads and aid in the identification of failure mechanisms. The crack maps were plotted to display the crack propagation from first cracking to ultimate capacity.

The crack key provides widths and lengths of the cracks as identified by a crack number. This numbering is occasionally non-sequential. The absence of some crack numbers is usually due to the propagation of two cracks into a single crack. When two cracks combine, the two crack records become combined, and

89

some crack names become unnecessary. Original crack numbers, as labeled during testing, are preserved throughout to enable identification of cracks from pictures.

In Figure 5-10, Figure 5-11, and Figure 5-12, crack maps of the top, bottom, and side of the test section are drawn showing cracks at 2.1 x HS-25 (first cracking), 3.1 x HS-25 (load step following developed cracking), and 6.0 x HS-25 (load step before failure). They are organized by view of the slab to show progressive crack growth. The side view of the slab is vertically exaggerated to show detail.

The crack map at 2.1 x HS-25 (first cracking) shows the size and shape of the initial cracks occurring in the slab. Though the load is reported as the load at first cracking, this is load at which cracking was first observed. Load was applied in 5-kip (22kN) increments, so the first visible cracks could have formed up to 5 kips (22 kN) per load point earlier than 2.1 x HS-25. In this test section, the first cracks in the slab occurred on the top of the slab over both girders and on the bottom of the slab at midspan in the interior bay between the load point locations. All cracks were of hairline width at 2.1 x HS-25.

The crack map at 3.1 x HS-25, 48 kips per load point (231kN), shows cracks that were observed at the load step following the first major change in stiffness. Though the change in stiffness was determined from the load-deflection plots, the crack map provides further evidence of a change in slab stiffness; multiple cracks formed and existing cracks opened wide at loads greater than 2.8 x HS-25.

At 3.1 x HS-25, on the top side of the slab, three flexural cracks were visible over the east-interior girder. Over the west-interior girder, a flexural crack formed perpendicular to the slab end. This crack was likely to have initiated before the test was performed, caused by operations necessary to replace load

90

cells beneath the slab. At 3.1 x HS-25, the largest measured crack width on the top side of the slab was 0.005 in. (0.1 mm). On the underside of the slab, all flexural cracks formed approximately parallel to the girders, but were oriented perpendicular to the skew at the slab end. At 3.1 x HS-25, the largest measured crack width beneath the slab was 0.009 in. (0.2 mm).

The crack map at 6.0 x HS-25 shows cracks formed during testing and just after failure. At failure, a large shear crack formed between and around the two load points in the interior bay. Visible on the top of the slab were flexural cracks that formed around the load points in the exterior span and the interior span. Flexural cracks formed parallel to the interior girder on the east side. Additional flexural cracks opened over the interior girder on the west side. On the top of the slab, the largest measured crack width before failure was 0.06 in. (1 mm) for crack T6, a flexural crack in the east-exterior bay. As seen from underneath the slab at failure, a series of flexural cracks formed parallel to the girders in the interior bay, fanning out past the load points. Cracks also formed along the edge of the thickened section. On the bottom of the east-exterior bay, flexural cracks formed perpendicular to the slab end on either side of the loaded point, and did not extend past the thickened end section. Flexural cracks that had formed on the bottom of the slab beneath the east-exterior bay load point could be seen on the side of the slab. At failure, the widest crack visible from the bottom of the slab was Crack B4, which was 0.15 in (4 mm) wide. Additional flexural cracks, on the top of the slab over the girder, extended through the entire depth of the slab. Several flexural cracks also formed beneath the location of the interior load points. Although Crack S8 was the widest crack visible on the side of the slab at 0.03 in. (0.8 mm), Crack S15 opened wide during failure.
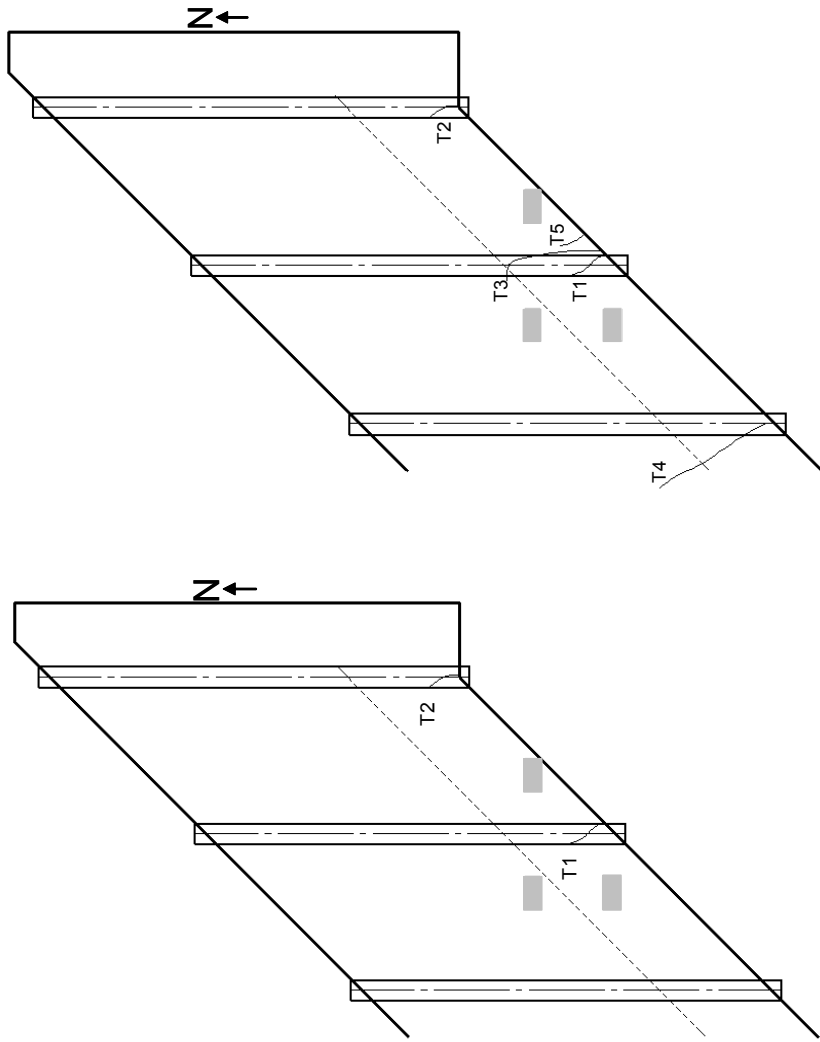
(a) 2.1 x HS-25 (first cracking)   (b) 3.1 x HS-25 (load step after developed cracking)

Figure 5-10 Crack map and key, IBTS, negative-moment region; top view of slab
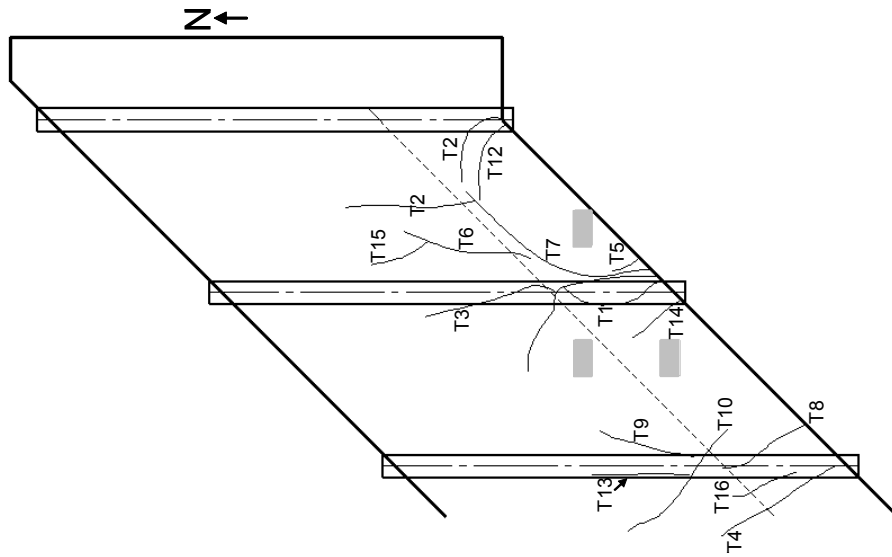
Crack Name	Load = 2.1xHS-25		Load = 3.1xHS-25		Load = 6.0xHS-25	
	Width (in)	Length (in)	Width (in)	Length (in)	Width (in)	Length (in)
T1	HL	13.5	0.005	31	0.04	61
T2	HL	6	0.002	9	0.005	35
T3			0.005	93.5	0.045	124
T4			0.002	74.5	0.01	126
T5			0.003	16.5	0.015	19
T6					0.05	121
T7					0.04	91
T8					0.005	68
T9					0.005	33
T10					0.01	71
T11					0.007	53.5
T12					0.002	12.5
T13					0.003	22
T14					0.005	13
T15					0.005	26.5
T16					0.005	37.5

(d) Key to crack lengths and widths (HL = hairline crack)

(c) 6.0 x HS-25 (failure)

Figure 5-10 cont'd. Crack map and key; IBTS, negative-moment region; top view of slab

93

(b) 3.1 x HS-25 (developed cracking)

(a) 2.1 x HS-25 (first cracking)

Figure 5-11 Crack map and key, IBTS, negative-moment region; bottom view of slab

Crack Name	Load = 2.1xHS-25 Width (in)	Length (in)	Load = 3.1xHS-25 Width (in)	Length (in)	Load = 6.0xHS-25 Width (in)	Length (in)
B1	HL	56	0.009	75.5	0.030	75.5
B2	HL	6.5	0.002	34	0.010	48
B3			0.009	36	0.020	128
B4			0.002	41	0.150	54
B5			HL	8	0.010	34
B6			0.002	24	0.020	44
B7					0.010	20.5
B8					0.010	20.5
B9					0.025	48
B10					0.020	58.5
B11					0.040	23
B12					0.010	20.5
B13					0.005	77
B14					0.005	103
B15-16					0.005	46
B17					0.005	57
B18					0.015	27
B19					0.010	24
B20					0.010	29
B21-22					0.005	51
B23					0.010	54
B24					0.005	55
B25					0.002	46
B26					HL	48

(c) 6.0 x HS-25 (failure)

(d) Key to crack lengths and widths (HL=hairline crack)

Figure 5-11 cont'd. Crack map and key, IBTS, negative-moment region; bottom view of slab

(a) 2.1 x HS-25 (first cracking)

(b) 3.1 x HS-25 (developed cracking)

(c) 6.0 x HS-25 (failure)
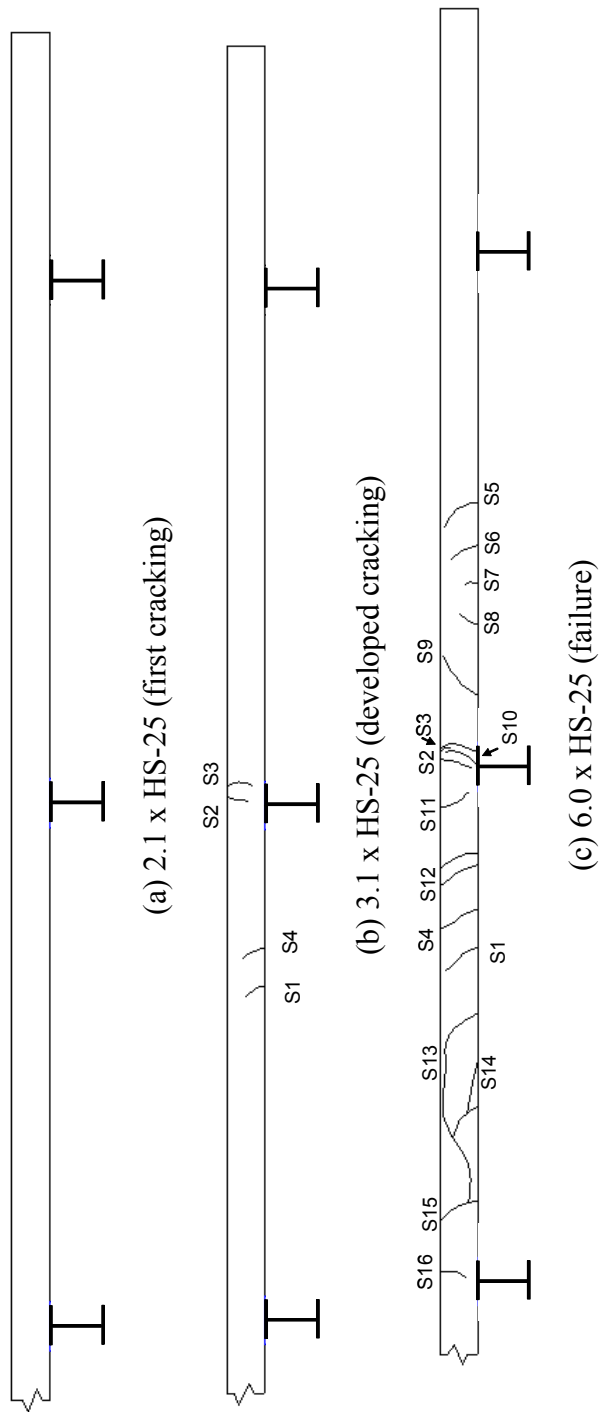
Figure 5-12 Crack map and key, IBTS, negative-moment region; side view of slab

	Load = 2.1xHS-25		Load = 3.1xHS-25		Load = 6.0xHS-25	
Crack Name	Width (in)	Length (in)	Width (in)	Length (in)	Width (in)	Length (in)
S1			0.003	7.5	0.015	9
S2			0.002	7	0.01	9.5
S3			0.002	7.5	0.02	13.5
S4			0.002	6.5	0.015	9
S5					0.01	11
S6					0.005	6
S7					0.004	4.5
S8					0.003	5
S9					0.005	13.5
S10					0.015	10
S11					0.02	8.5
S12					0.01	11
S13					0.01	9
S14					0.01	5.5
S15					0.005	19
S16					0.005	3.5

(d) Key to crack lengths and widths

Figure 5-12 cont'd. Crack map and key, IBTS, negative-moment region; side view of slab

5.2.5   Appearance after Failure

At 6.0 x HS-25, a punching shear failure occurred on the east side of the load points in the interior bay. Pictures were taken of the failure surface (Figure 5-13, Figure 5-14, Figure 5-15).   Cracks formed between the two load points and around the exterior load points. Because the area around the interior load point was more extensively damaged than the area around the exterior load point, failure was probably initiated by punching shear at the interior load point, where the slab thickness was 8 in. (203 mm) instead of 10 in. (254 mm).   Existing

flexural cracks opened on the top surface, but little evidence of failure was visible on the bottom or side surfaces of the slab.

(a) Facing north

Figure 5-13 Interior bay failure surface at top of slab

(b) Facing southeast

Figure 5-13 cont'd. Interior bay failure surface at top of slab

Figure 5-14 Interior bay failure surface at side of slab, facing north
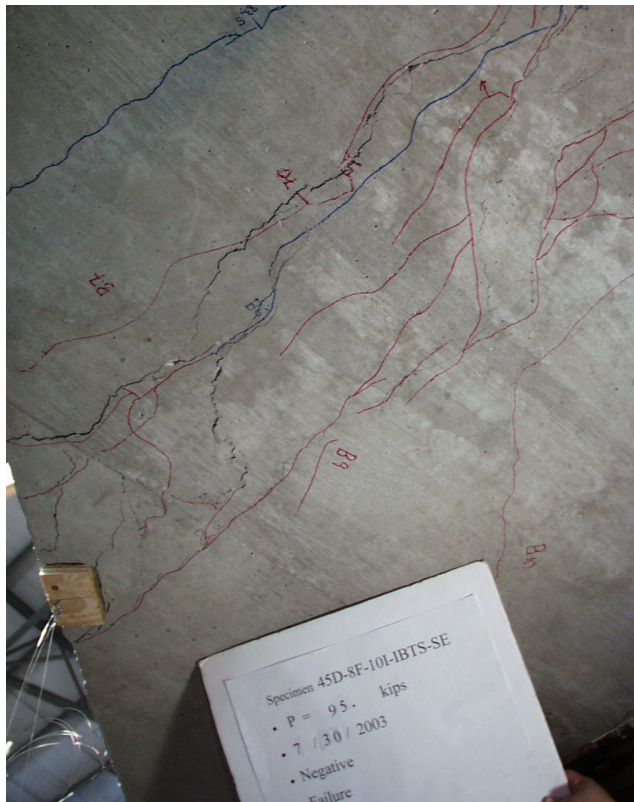
Figure 5-15 Interior bay failure surface at bottom of slab, facing west

5.2.6 Failure of the Exterior Bay

Because only the interior bay of the test area failed in punching shear, the remaining load point in the exterior bay was also loaded to failure, which occurred by punching shear at a load of 6.2 x HS-25. Figure 5-16 and Figure 5-17 show the failure surface after the test.

At the top surface of the slab, shear cracks around the load point indicate punching shear failure. The crack closely followed the perimeter of the load point on the west and north sides of the plate, and propagated to the slab edge on both sides. The failure surface that was visible on the bottom surface had a shape similar to that of cracks on the top surface.
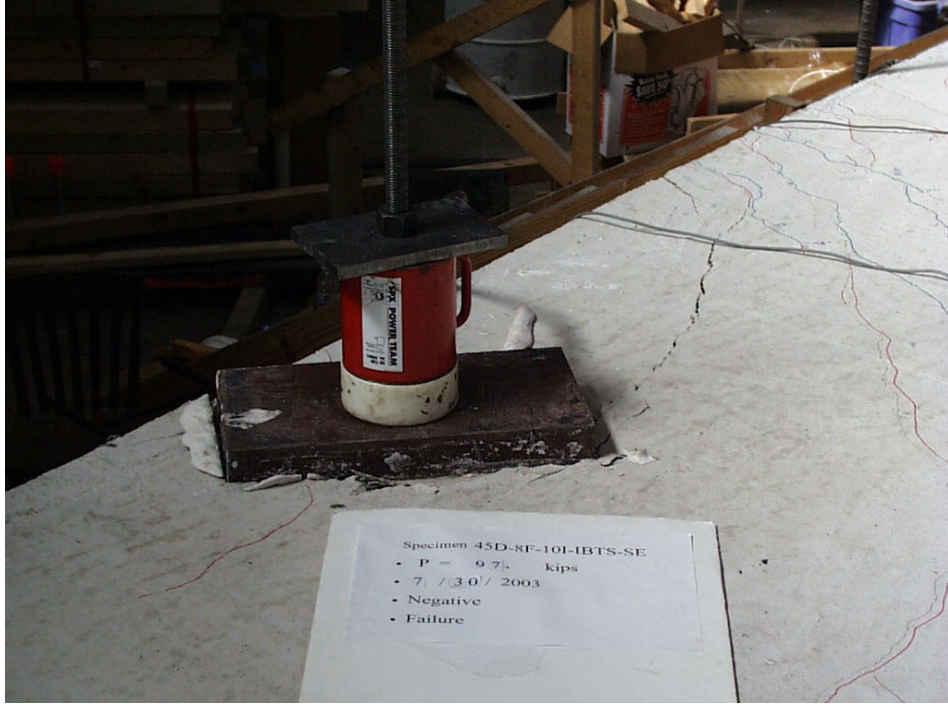
(a) Facing south

(b)Facing south

Figure 5-16 Exterior bay failure surface at top of slab
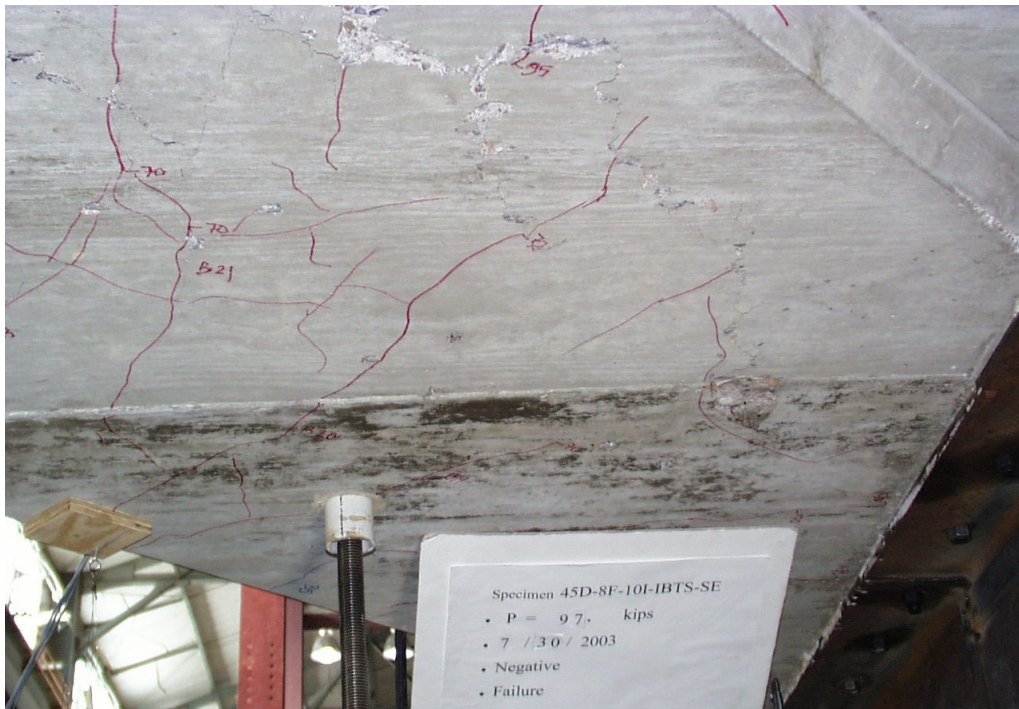
(a) Facing south
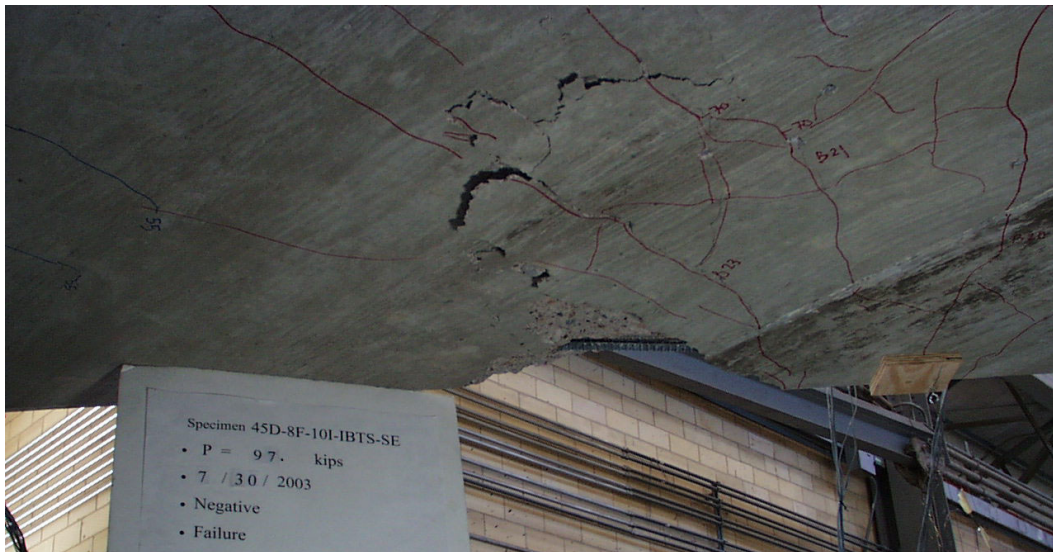
(b) Facing south

Figure 5-17 Exterior bay failure surface at bottom of slab

5.2.7 Summary of IBTS End Detail, Negative-Moment Region Test

The IBTS detail test area was loaded to design and overload levels with the AASHTO tandem load configuration placed to maximize negative moments in the end detail.

At 2.1 x HS-25, cracks were first observed on both the underside and top side of the slab. The top cracks formed over the east-interior girder, and propagated parallel to that girder. The bottom cracks formed in the interior span, and also propagated parallel to the girder. Developed cracking occurred around 3.1 x HS-25. The cracking loads in this test area were higher that the design load level, and this test area performed well at serviceability load levels. At 6.0 x HS-25, a punching shear failure initiated at the interior load point in the interior bay. The exterior load point in the exterior bay was reloaded to failure; a punching shear failure initiated in the exterior bay at 6.2 x HS-25.

The relative midspan edge deflection at failure was 0.83 in. (21 mm) in the exterior bay and 0.31 in. (8 mm) in the interior bay. First reinforcement yield occurred at 5.3 x HS-25 at a location on the east side of the girder. The maximum recorded strain was 280% of yield strain (6160 $\mu\varepsilon$), measured on the west side of the girder at failure.

5.3 UTSE END DETAIL, NEGATIVE-MOMENT REGION

The UTSE end detail, negative-moment region was loaded at the locations shown in Figure 5-18 by three 10- by 20-in. (254- by 508-mm) steel plates placed in the AASHTO design load configuration. When the slab was loaded to 55 kips (245 kN) per load point, 3.5 x HS-25, cracks formed began to initiate in the south side of the east-exterior bay, in the negative-moment region of the adjacent neighboring IBTS, negative moment region. Loading the IBTS detail to failure before severe damage occurred to the section was desired, so the UTSE, negative

moment region was unloaded. After the three remaining test areas were loaded to failure, the UTSE, negative moment test area was reloaded to failure. A punching shear failure initiated around the load point in the interior bay at 68 kips (302 kN), 4.3 x HS-25.
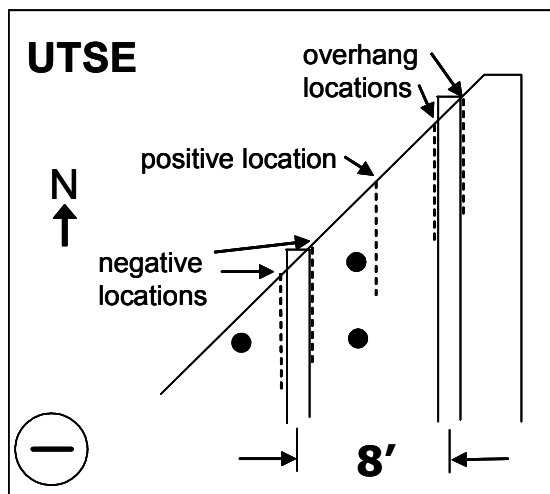
Figure 5-18 UTSE end detail, negative-moment region

5.3.1 Load-Deflection Behavior

Load-deflection plots show relative deflections measured at the slab edge, midspan, corrected to remove rigid-body movement as discussed in Section 5.2.1 (Figure 5-19).

Deflections measured under HS-20 and HS-25 loads in the exterior and interior bays are extremely small compared to the girder spacing. At HS-20, practically no relative deflection was measured in the exterior bay; and 0.006 in. (0.2 mm) of relative deflection was measured in the interior bay. At HS-25, 0.004 in. (0.1 mm) of relative deflection was measured in the exterior bay, and 0.007 in. (0.2 mm) of relative deflection was measured in the interior bay. In this range, load-deflection behavior was linear in both bays. At 1.75 x HS-25, the relative deflection in the exterior bay was 0.032 in. (0.8 mm) and 0.024 in. (0.6 mm) in

the interior bay. This is a proportional increase from HS-25 and HS-20 loads, indicating that the load-deflection response is still linear at 1.75 x HS-25. At 3 x HS-25, the relative deflection in the exterior bay was 0.16 in. (4 mm) and 0.06 in. (1.5 mm) in the interior bay. At failure, the relative deflection in both the exterior bay and the interior bay was 0.32 in. (8 mm).
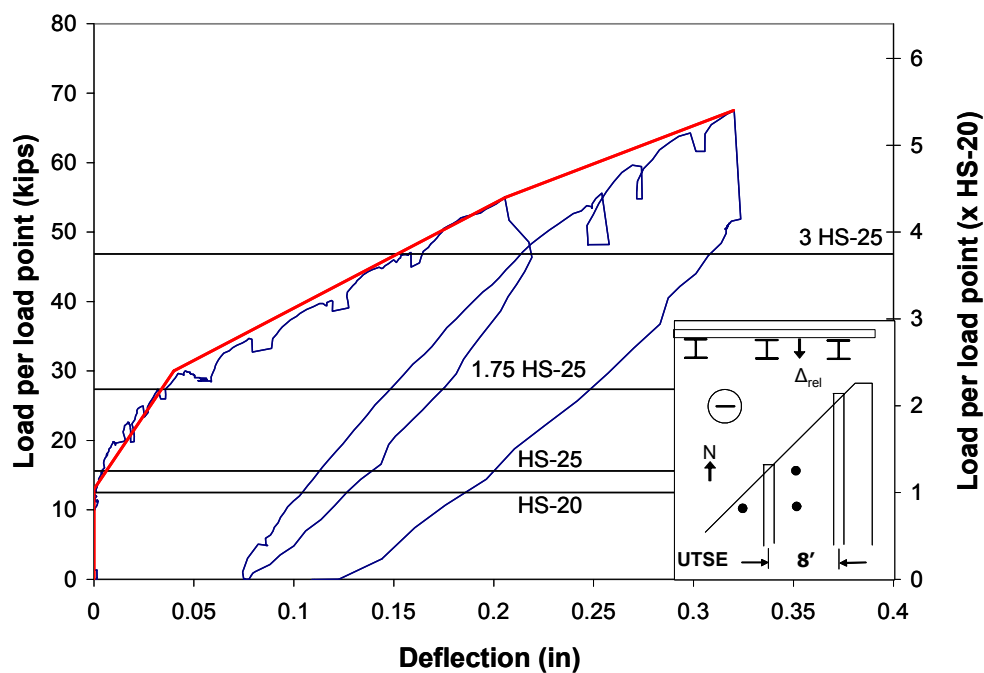
(a)

Figure 5-19 Relative midspan edge deflection, UTSE, negative-moment region: (a) exterior bay; (b) interior bay
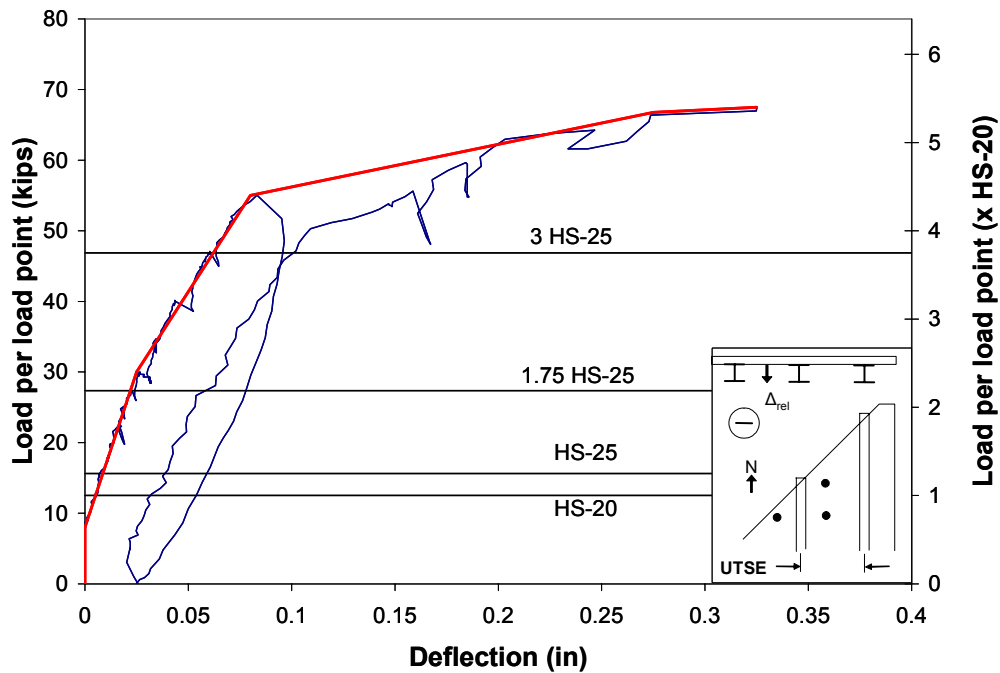
(b)

Figure 5-19 cont'd. Relative midspan edge deflection, UTSE, negative-moment region: (a) exterior bay; (b) interior bay

5.3.1.1   Load-Deflection Envelope

Based on the load-deflection response of both bays, three major changes in stiffness can be identified before failure. The first change in stiffness is apparent in both bays at 1.9 x HS-25. This change in stiffness, caused by multiple cracks initiating and propagating in the test area, is corroborated by the crack history recorded during testing. At 1.9 x HS-25, new cracks first initiated on the top side of the slab, possibly accelerating the decrease in slab stiffness. Plots of deflection in both bays also indicate a second, smaller change in stiffness at about 3.5 x HS-25, more apparent in the exterior bay than the interior one. At approximately 4.2 x HS-25, the stiffness of the interior bay drops to nearly zero.

5.3.2   Load-Strain Response

Load-strain plots are included to evaluate cracking and identify the loads at which reinforcement yielded. Strain gauges were installed in the end detail on every other transverse reinforcing bar, for a total of six top and six bottom bars at three locations, and only the data from the most critical strain gauge are shown in this section. Additional plots are shown in Appendix A, and additional discussion of strain-gauge plots is given in Section 5.2.2.

Figure 5-20(a), (b), and (c) show strain measurements from the most critical gauge on both sides of the girder and midspan. Strains induced during serviceability tests were extremely small, and maximum measured strains were similar on both sides of the girder at serviceability-level loads.

At the HS-20, HS-25, and 1.75 x HS-25 load levels, strains were less than 5% of the yield strain. At 3 x HS-25, the maximum strain was 42% of yield strain (930 $\mu\varepsilon$) on the west side of the girder. The maximum strain at midspan was 35% of yield strain (760 $\mu\varepsilon$), and the maximum strain on the east side of the girder was 9% of yield strain (200 $\mu\varepsilon$). At the instrumented locations, no reinforcement reached yield strain in this test area. The critical strain gauge on the west side of the girder malfunctioned at 64 kips (285 kN) per load point, just before failure. Though the gauge malfunctioned, the largest strains in this test area were measured at that location at 4.1 x HS-25. The maximum strain measured before failure was 89% of yield strain (1960 $\mu\varepsilon$) on the west side of the girder, near the location of punching shear failure.
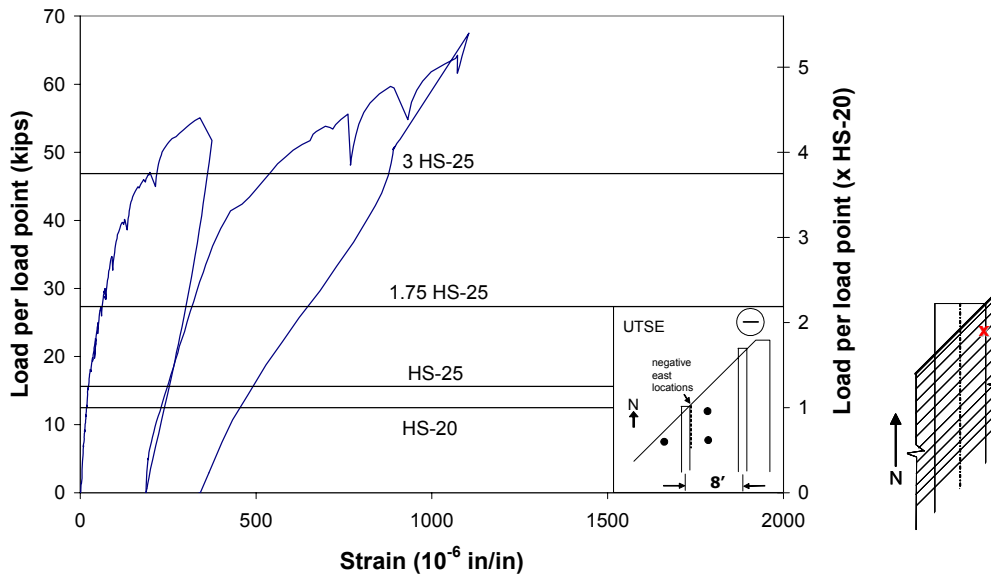
(a)
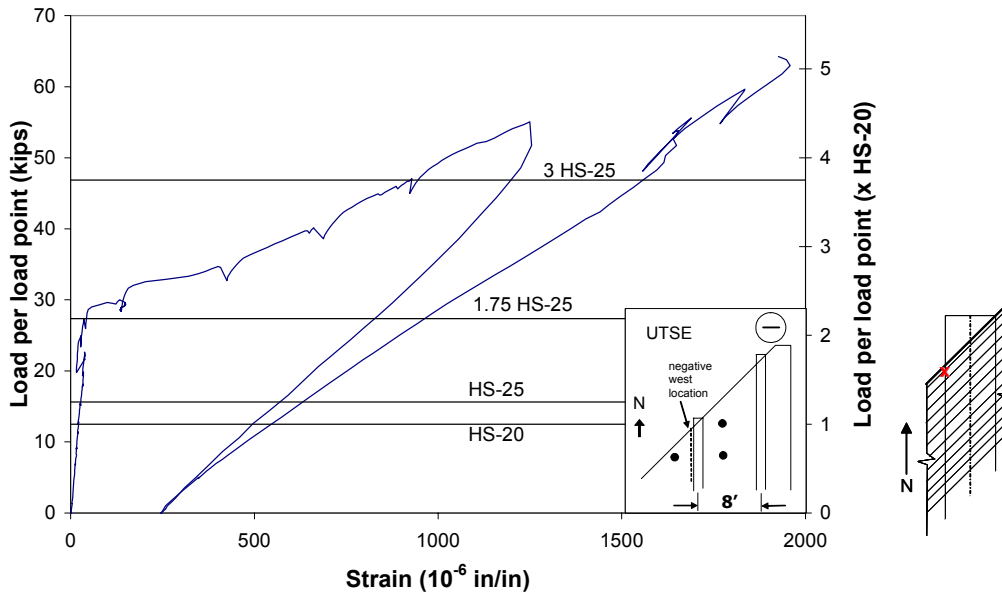
(b)

Figure 5-20 Load-strain response, UTSE, negative-moment region: (a) east side of girder, top mat; (b) west side of girder, top mat; (c) midspan, bottom mat

108
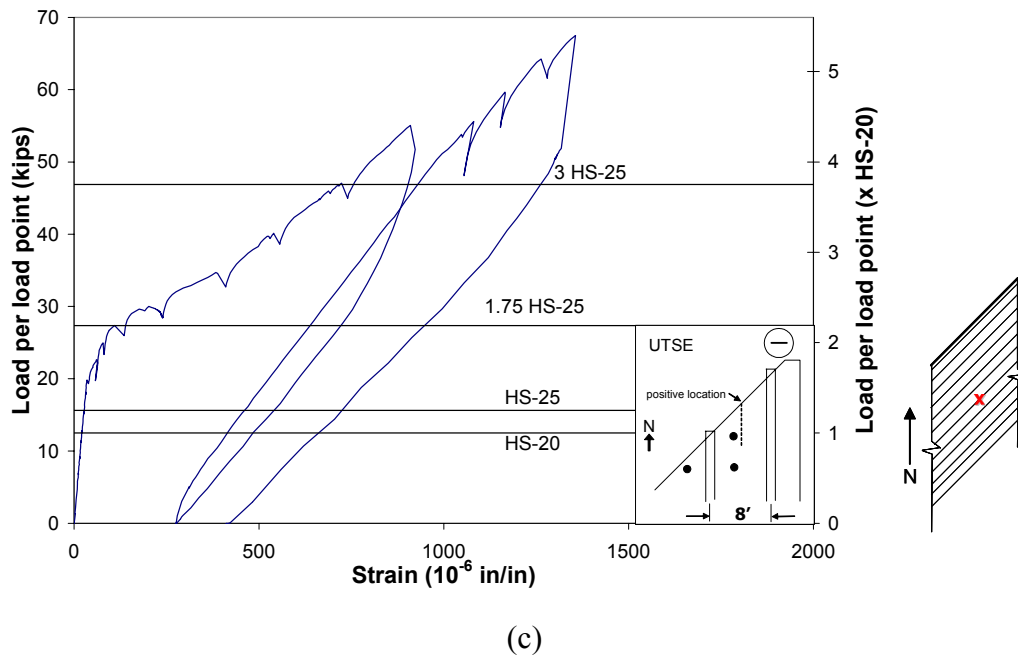
(c)

Figure 5-20 cont'd.   Load-strain response, UTSE, negative-moment region:
(a) east side of girder, top mat; (b) west side of girder, top mat; (c) midspan,
bottom mat

5.3.3   Strain Profiles

Strain profiles were used to compare strain readings from reinforcement in the test area at a specific location (positive- or negative-moment sections). Figures in this section show the strain in the reinforcing bars at explicit load steps (Section 5.2.3).

In Figure 5-21(a), (b), and (c), strain profiles are shown for three locations in the UTSE, negative-moment region.   In this test area, the largest strains occurred on the west side of the beam, and the smallest, at midspan. At HS-20 and HS-25, all strains were less than 5% of yield strain. At all three strain profile locations, the profiles are almost indistinguishable at these two load levels. At 1.75 x HS-25, HSx25, and HS-20 load levels, strains were distributed uniformly

109

through the end section. As applied loads increased, response was increasingly non-uniform though the section.
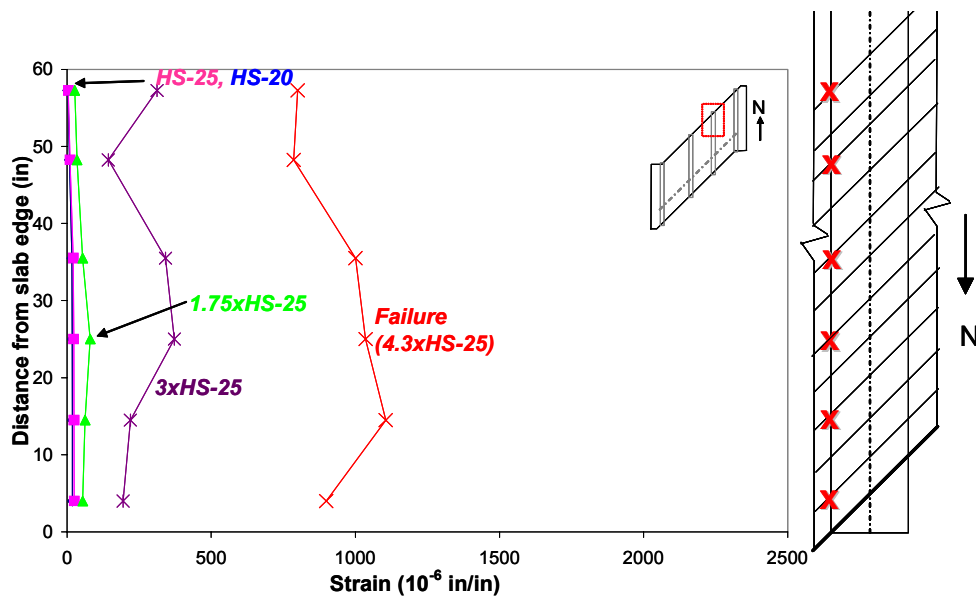
(a)

Figure 5-21 Strain profile, UTSE, negative-moment region: (a) east side of girder, top mat; (b) west side of girder, top mat; (c) midspan, bottom mat
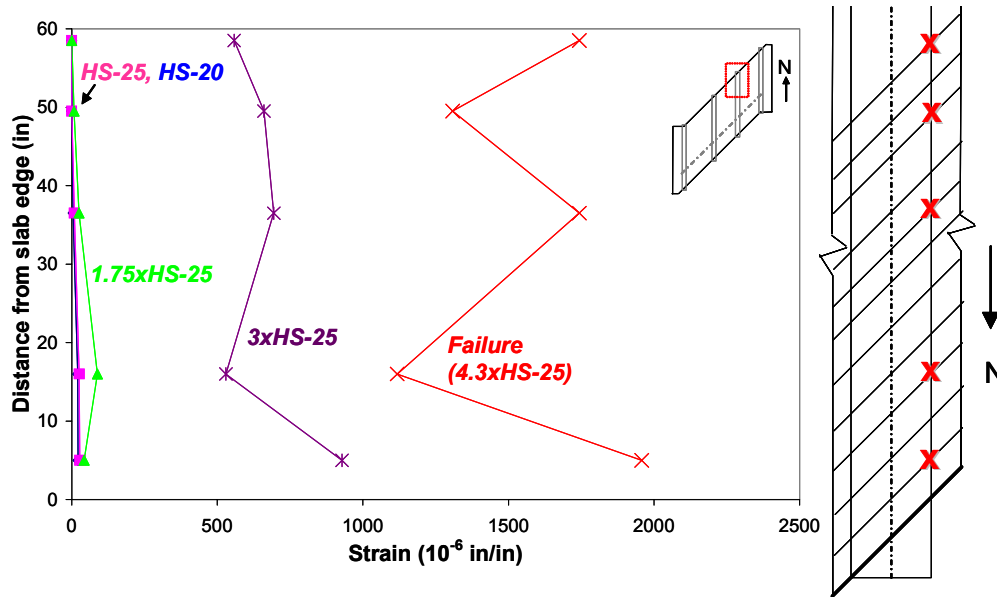
(b)
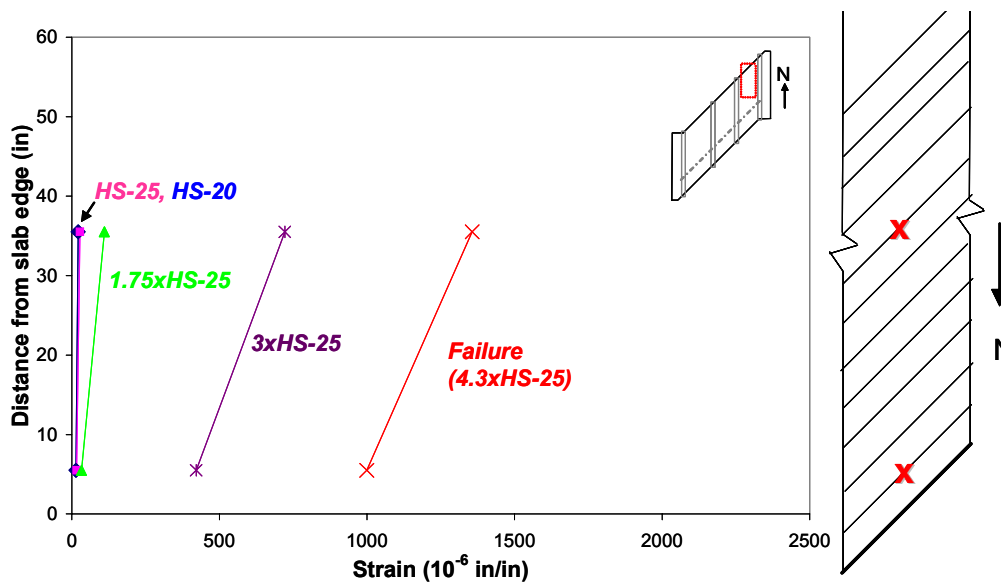
(c)

Figure 5-21 cont'd. Strain profile, UTSE, negative-moment region: (a) east side of girder, top mat; (b) west side of girder, top mat; (c) midspan, bottom mat

5.3.4 Crack Maps

Figure 5-22, Figure 5-23, and Figure 5-24, show crack maps of the top, bottom, and side of the test section, drawn at 1.5 x HS-25 (first cracking), 1.9 x HS-25 (load step after developed cracking), and 4.3 x HS-25 (failure). To create crack maps, the locations, widths, and lengths of cracks were measured at every load step during testing. Additional discussion of crack maps is given in Section 5.2.4.

At 1.5 x HS-25, flexural cracks were first observed on the top of the slab over the interior girder, and on the bottom of the slab at midspan in the exterior bay between the loaded points. The cracks at midspan could be seen from the side of the slab as well. All cracks were of hairline width at 1.5 x HS-25.

The load-deflection response indicated a decrease in slab stiffness around 1.9 x HS-25, a load step at which crack widths and lengths were recorded. On the top of the slab, three flexural cracks were visible over the interior girder. Cracks visible on the top were short relative to those on the bottom, with the longest being 20 in. (508 mm) on the top and 89 in. (2261 mm) on the bottom. The widest top crack was 0.003 in. (0.1 mm). On the bottom, flexural cracks formed perpendicular to the slab end and propagated parallel to the girders. The widest bottom crack was 0.002 in. (0.05 mm).

At 4.3 x HS-25, punching shear failure occurred, with a wide shear crack around the loaded point in the interior bay. Before failure, flexural cracks such as T6, T7, T1, T2, and T3 formed perpendicular to the slab edge over each of the girders. On the top of the slab, the widest crack before failure was Crack T4-T5, a flexural crack 0.05 in. (1 mm) wide, oriented parallel to the east interior girder. As seen from underneath the slab, additional flexural cracks formed parallel to the girders in the exterior bay, fanning out past the load points. In the interior bay, parallel flexural cracks formed perpendicular to the slab end on either side of the

112

load point location. The widest crack visible from underneath the slab was Crack B3, which was 0.04 in. (1 mm) wide before failure. The flexural cracks visible from the side of the slab formed primarily in three locations: from the bottom of the slab beneath the exterior bay load point; over the east interior girder; and propagating from the bottom of the slab beneath the loaded point in the interior bay. Cracks S3, S13, and S17 extended through the full depth of the slab. The shear Crack S13, visible from the side of the slab, was the widest crack at the last recorded load step at 0.05 in. (1 mm), and became the location of punching shear failure on the east side of the plate.

N ←

N ←
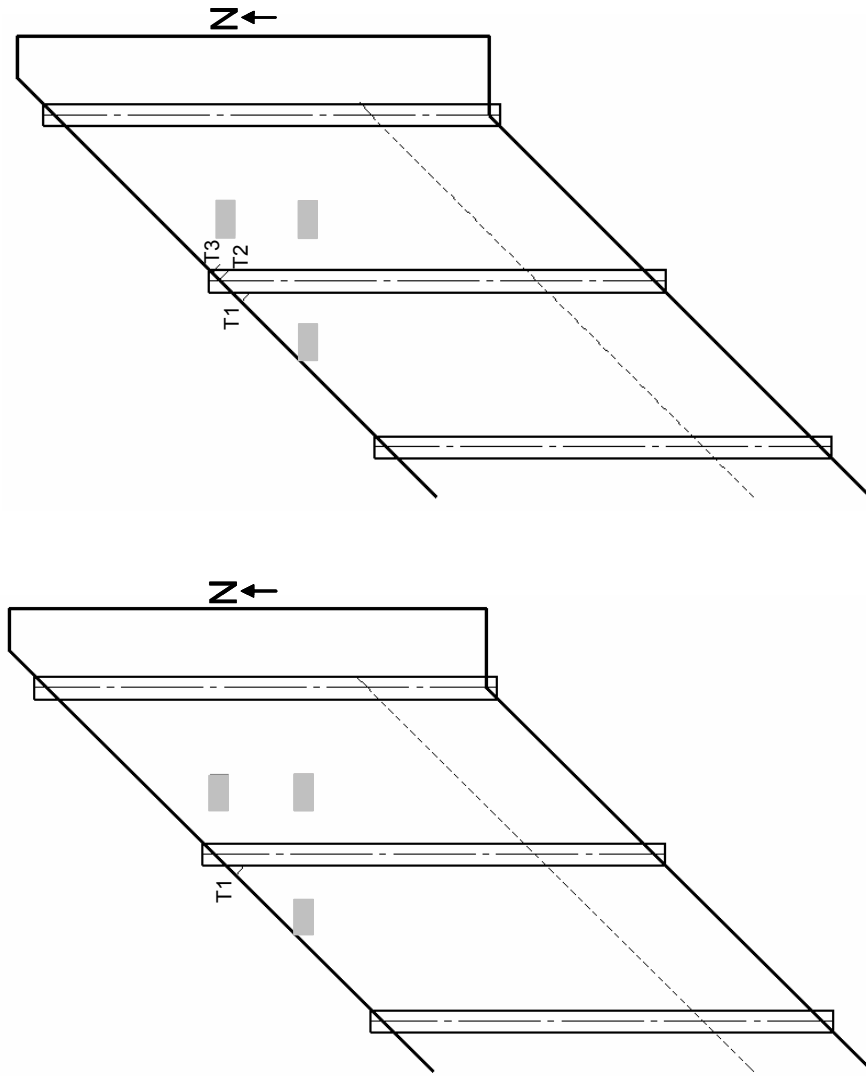
(a) 1.5 x HS-25 (first cracking)

b) 1.9 x HS-25 (developed cracking)

Figure 5-22 Crack map and key, UTSE, negative-moment region; top view of slab

114
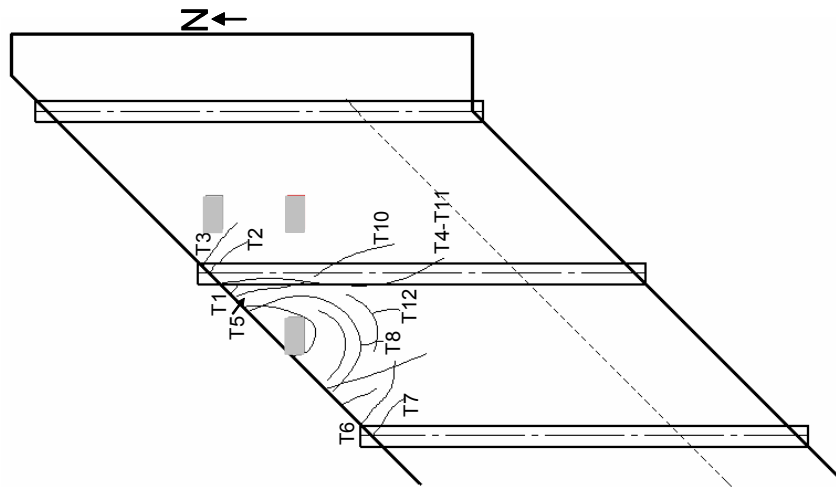
Crack Name	Load = 1.5xHS-25		Load = 1.9xHS-25		Load = 4.3xHS-25	
	Width (in)	Length (in)	Width (in)	Length (in)	Width (in)	Length (in)
T1	HL	2	0.003	4	0.003	4
T2			0.002	20	0.025	48
T3			0.002	7.5	0.015	23
T4					0.05	92
T5					0.05	89.5
T6					0.025	21
T7					0.01	13.5
T8					0.005	22
T10					0.01	48.5
T11					0.005	46
T12					0.005	23

(d) Key to crack lengths and widths (HL=hairline crack)

(a) 4.3 x HS-25 (failure)

Figure 5-22 cont'd. Crack map and key, UTSE, negative-moment region; top view of slab

115
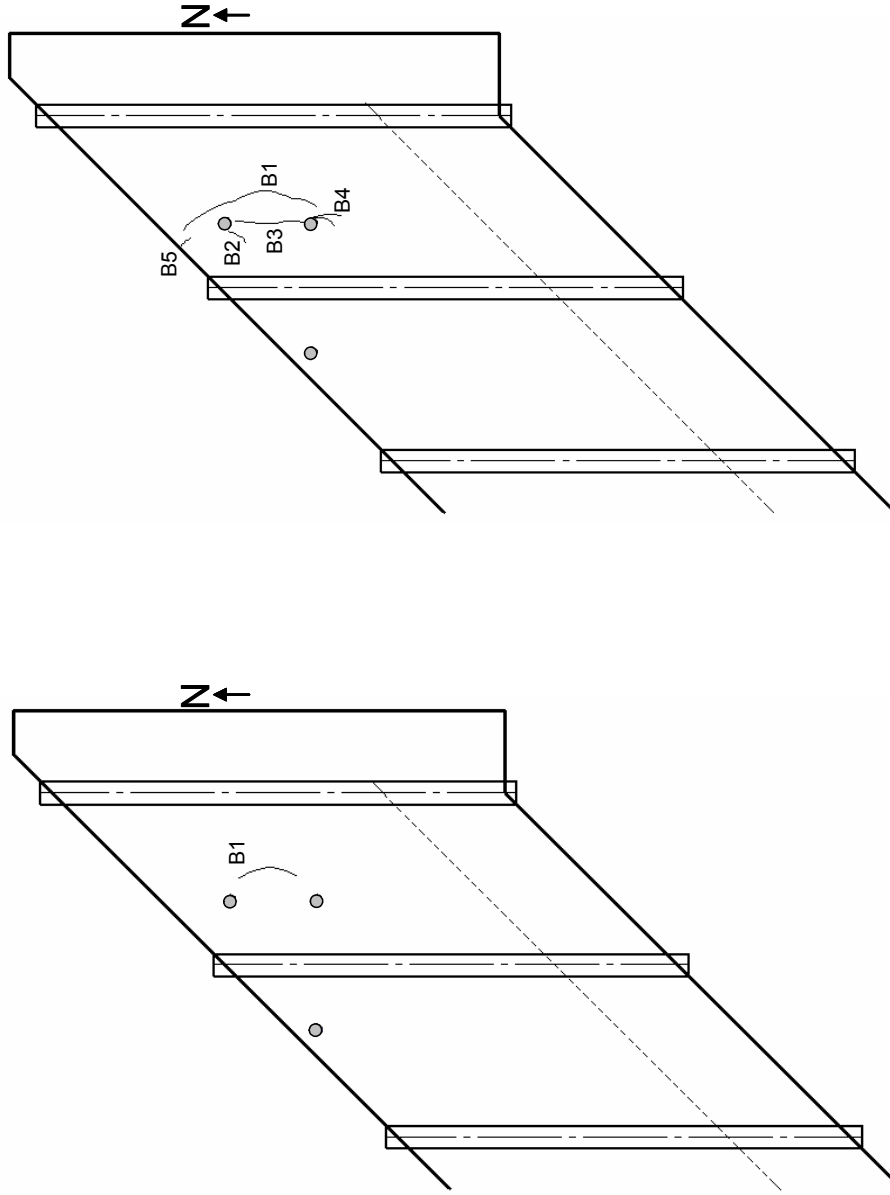
(a) 1.5 x HS-25 (first cracking)

(b) 1.9 x HS-25 (developed cracking)

Figure 5-23 Crack map and key, UTSE, negative-moment region; bottom view of slab

Crack Name	Load = 1.5xHS-25 Width (in)	Length (in)	Load = 1.9xHS-25 Width (in)	Length (in)	Load = 4.3xHS-25 Width (in)	Length (in)
B1	HL	29	0.002	89	0.030	155
B2			HL	8.25	0.035	44.5
B3			0.002	32	0.040	64.5
B4			HL	16.5	HL	72
B5			HL	17.5	0.007	34
B6					0.005	22.5
B7					0.009	29
B8					0.007	77
B10					0.013	61
B12					0.003	22
B14					0.005	32
B15					0.002	63
B16					0.000	11
B17					HL	26
B26					0.010	40.5
B27					0.010	52
B29					0.003	39
B31					0.003	55
B32					0.003	53
B33					0.002	13.5
B34					0.013	10.5
B35					0.002	15
B36					0.005	9

(d) Key to crack lengths and widths (HL=hairline crack)

(c) 4.3 x HS-25 (failure)

Figure 5-23 cont'd.   Crack map and key, UTSE, negative-moment region; bottom view of slab

117

(a) 1.5 x HS-25 (first cracking)

(b) 1.9 x HS-25 (developed cracking)

(c) 4.3 x HS-25 (failure)

(d) Key to crack lengths and widths (HL=hairline crack)

Figure 5-24 Crack map and key, UTSE, negative-moment region; side view of slab

118

	Load = 1.5xHS-25		Load = 1.9xHS-25		Load = 4.3xHS-25	
Crack Name	Width (in)	Length (in)	Width (in)	Length (in)	Width (in)	Length (in)
S1	HL	1.5	0.002	3	0.002	4
S2			HL	1.5	0.010	7
S3			HL	2.5	0.005	6
S4					0.030	10
S5					0.015	7.5
S6					0.010	7.5
S7					0.005	4
S8					0.010	8.5
S9					0.010	5.5
S10					0.010	5
S12					0.010	8.5
S13					0.050	17
S14					0.005	7.5
S15					HL	2.5
S17					0.025	14
S18					0.002	4
S20					0.002	3.5
S21					0.005	7

(d) Key to crack lengths and widths (HL=hairline crack)

Figure 5-24 cont'd. Crack map and key, UTSE, negative-moment region; side view of slab

5.3.5 Appearance after Failure

At 4.3 x HS-25, punching shear failure occurred around the exterior loaded point in the interior bay. After failure, pictures were taken of the failure surface (Figure 5-25, Figure 5-36, Figure 5-27).

At failure, cracks formed around the load point and extend to the slab edge of either side, in a pattern suggestive of punching shear failure. Figure 5-37 shows the failure surface as seen from the side of the slab. A large shear crack, labeled S13 during testing, opened wide during failure. Only a short section of the failure surface could be seen from the bottom of the slab. At the east-interior girder, the failure surface, as seen on the side of the slab, extends beneath the slab for a short distance.

Figure 5-25 Interior bay failure surface at top of slab, facing north

(a) Facing south

Figure 5-26 Interior bay failure surface at side of slab

(b) Facing south

Figure 5-26 cont'd. Interior bay failure surface at side of slab

Figure 5-27 Interior bay failure surface at bottom of slab, facing north

121

5.3.6 Failure of the Exterior Bay

Because only the interior bay of the test area failed in punching shear, the load points in the east-exterior bay were subsequently loaded to failure as well. Figure 5-28, Figure 5-29, and Figure 5-30 show the failure surface after failure occurred in the exterior bay. Failure initiated on the west side of the load plates simultaneously at 5.1 x HS-25. Simultaneous punching shear failures occurred near both plates, with the failure surfaces merging to form a single failure surface with an appearance like that corresponding to a one-way shear failure. The failure surface, as seen from the top of the slab, shows a shear crack around the exterior loaded point, to the slab edge (Figure 5-28). Figure 5-29 shows the failure surface from the side of the slab, including shear cracks with a small angle to the plane of the slab. Underneath the slab, the failure surface is visible around the interior load point and near the girder (Figure 5-30).
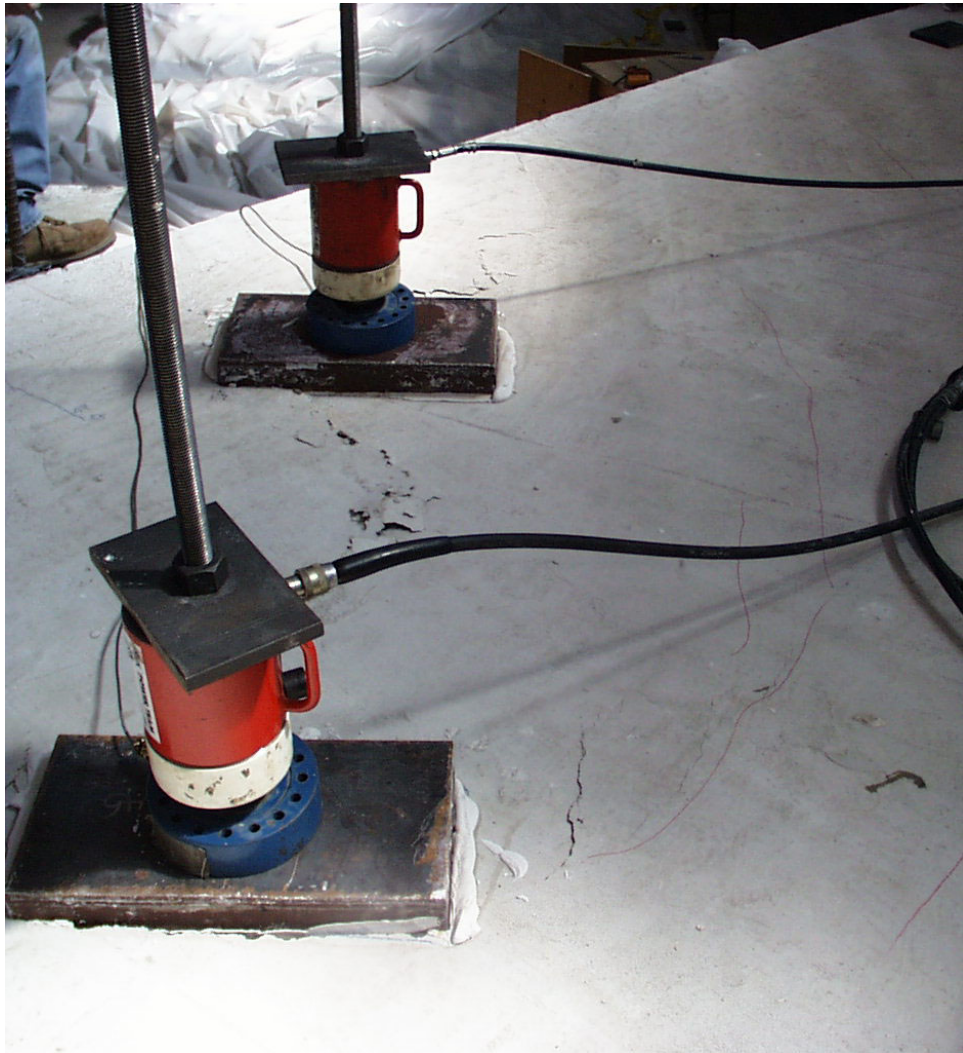
(a) Facing north

Figure 5-28 Exterior bay failure surface at top of slab
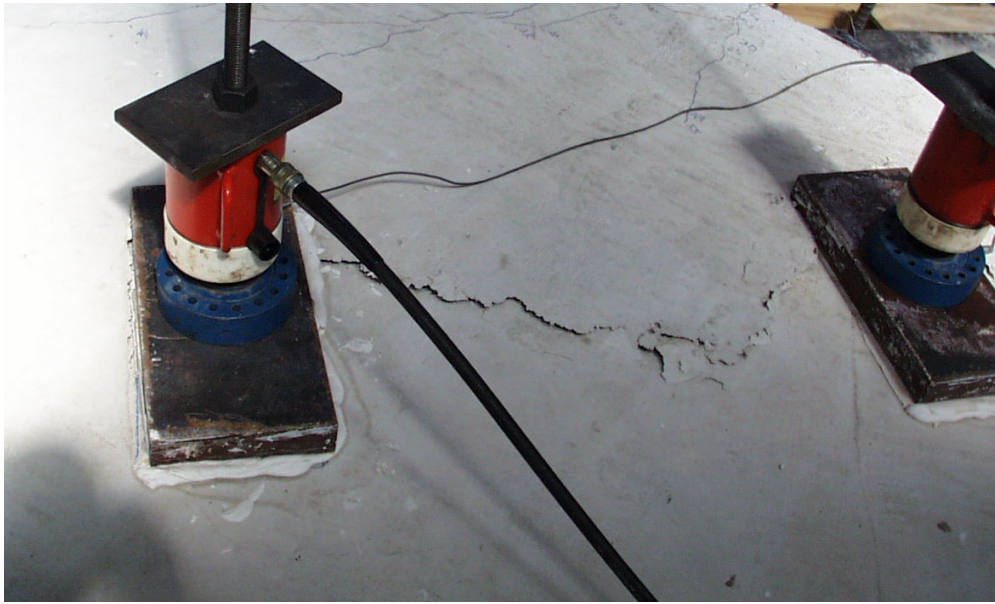
(b) Facing west

Figure 5-28 cont'd. Exterior bay failure surface at top of slab

Figure 5-29 Exterior bay failure surface at side of slab, facing south

Figure 5-30 Exterior bay failure at bottom of slab, facing north

5.3.7   Summary of UTSE End Detail, Negative-Moment Region Test

The UTSE detail, negative-moment region was loaded with the AASHTO tandem load configuration to typical design levels and then to overload levels.

At 1.7 x HS-25, flexural cracking was first observed on the bottom, top, and side of the slab.   Top cracks formed over the east-interior girder, perpendicular to the slab edge.   The bottom crack was in the exterior bay and parallel to the girders. Developed cracking occurred around a load level of 1.9 x HS-25. The cracking loads in this test area were higher than design loads, and

this test area performed well under service-level loads. At 4.3 x HS-25, a punching shear failure occurred at the loaded point in the interior bay.

The loaded point in the interior bay failed in punching shear at 4.3 x HS-25. Although the failure occurred at a high multiple of service-level load, it was brittle. At failure, the relative midspan edge deflection was 0.32 in. (8 mm) in both the interior and exterior bays. No instrumented reinforcement reached yield strain in this test area. The maximum recorded strain was about 89% of yield strain (1960 $\mu\varepsilon$), measured on the west side of the girder at 4.2 x HS-25.

5.4 IBTS END DETAIL, POSITIVE-MOMENT REGION

The 10-ft (3.0-m) girder spacing bay constructed with the IBTS end detail was loaded by two 10- by 20-in. (254- by 508-mm) steel plates, placed midspan in the west exterior bay (Figure 5-31). During the service-load test, the slab was loaded to approximately 27 kips (120 kN) per load point, 1.7 x HS-25. Flexural cracks on the top of the slab extended into the north side of the west exterior bay. The area was unloaded to prevent further damage to neighboring test regions. When loaded to failure, the 5.75-ft (1.75-m) thickened end region failed in one-way shear at 3.0 x HS-25.
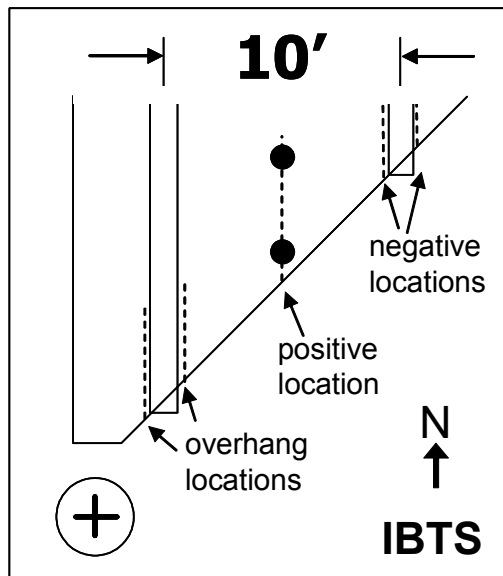
Figure 5-31 IBTS end detail, positive-moment region

5.4.1 Load-Deflection Behavior

Deflections measured under HS-20 and HS-25 loads were extremely small compared to the girder spacing (l/4000 and l/2000 respectively). The edge at midspan deflected 0.03 in. (0.8 mm) at HS-20, and 0.06 in. (1.5 mm) at HS-25 (Figure 5-32). Because cracking began at the latter load level, deflection did not increase proportionately with the load, to 0.23 in. (5.8 mm) at 1.75 x HS-25, and to 1.52 in. (39 mm) at failure.
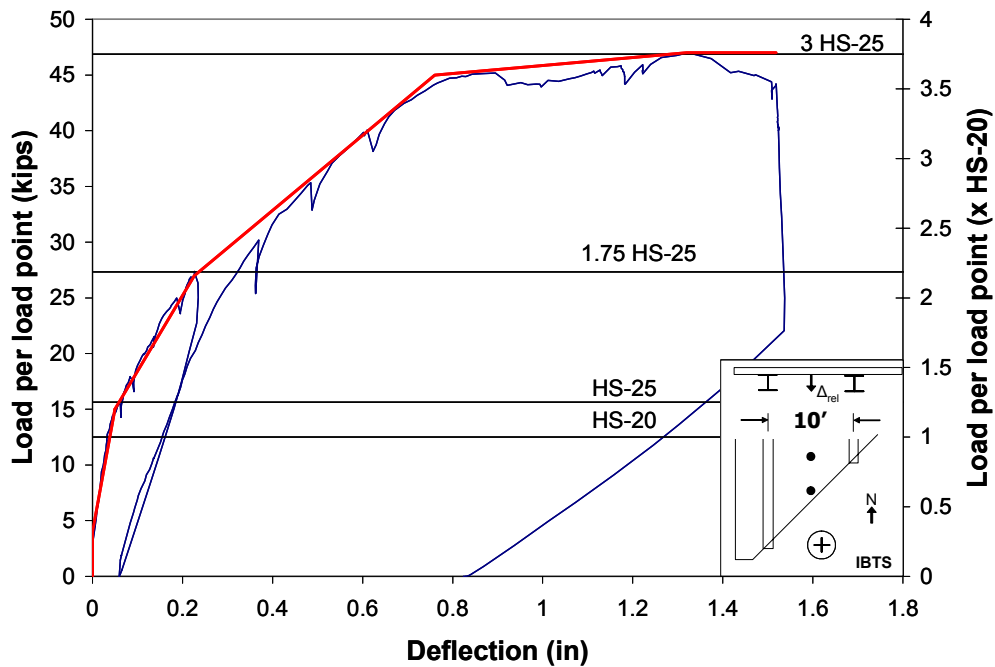
Figure 5-32 Relative midspan edge deflection, IBTS, positive-moment region

5.4.1.1 Load-Deflection Envelope

The load-deflection response can be idealized as linear with four major changes in stiffness before failure. The first change in stiffness occurred at approximately 0.9 x HS-25, just prior to the first observed cracking in the slab at 1.0 x HS-25. The second change in stiffness occurred at 1.6 x HS-25. At approximately 3.0 x HS-25, the stiffness reduced to nearly zero as failure progressed. At 3.0 x HS-25, the slab end failed in one-way shear.

In the tests maximizing negative moment, first cracking did not coincide with an observed change in stiffness in the load-deflection response. The overall slab stiffness decreased after the formation of multiple cracks. For the tests maximizing positive moment, initial cracking in the slab did cause a very slight change in stiffness, but these initial cracks were short, narrow, and few in

comparison to initial cracking in the negative test regions. As defined earlier, developed cracking is identified as the load stage at which the first significant change in the load-deflection response stiffness can be identified. Thus, developed cracking occurred at the same load as first cracking in the positive moment test regions. Because the "cracks at developed cracking" are identical to the "cracks at the first cracking," only the latter need to be discussed.

For positive moment, the term "major change in stiffness" is used to describe the load at which the second change in stiffness can be identified in the load-deflection response. The second change coincided with the initiation of multiple cracks and a subsequent decrease in slab stiffness, so the "cracks at major change in stiffness" will be discussed for test regions where positive moment was maximized.

5.4.2   Load-Strain Response

Figure 5-33(a), (b), and (c) show measured strains at both sides of the girder and at midspan. Tensile strains at midspan were significantly larger those at the girder, so only the former are discussed here. At the HS-20 load level, the maximum strain was 4% of the yield strain (90 $\mu\varepsilon$). At the HS-25 load level, the maximum strain was 6.3% of yield strain (140 $\mu\varepsilon$). At 1.75 x HS-25, the maximum strain was 41% of yield strain (900 $\mu\varepsilon$). First yield of instrumented reinforcement occurred at midspan at 2.8 x HS-25. During this test, yield strain was not reached by any reinforcement at the locations at the girder. At failure, the maximum strain at midspan was 395% of yield strain (8690 $\mu\varepsilon$). On the west side of the girder, the maximum strain was 82% of yield (1800 $\mu\varepsilon$), and on the east side, the maximum strain was 72% of yield (1590 $\mu\varepsilon$).
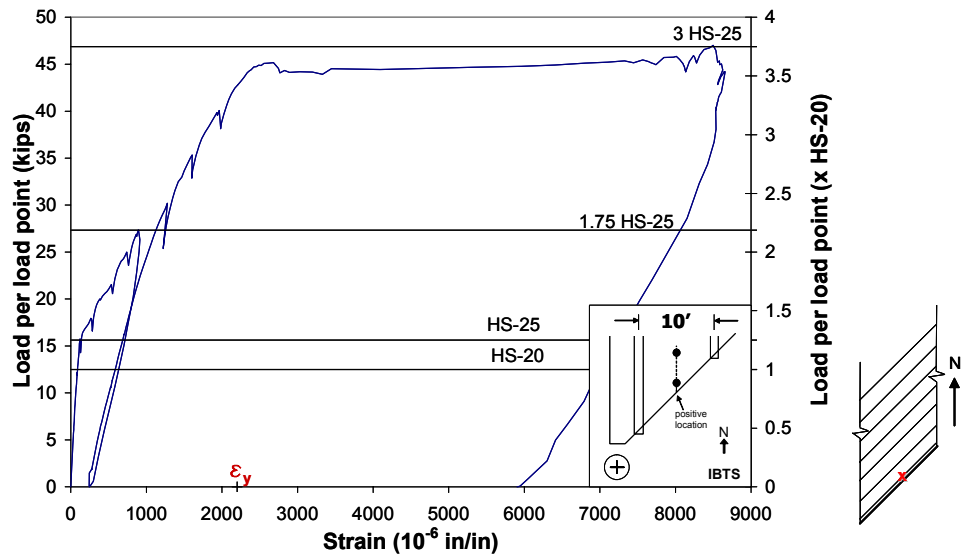
(a)
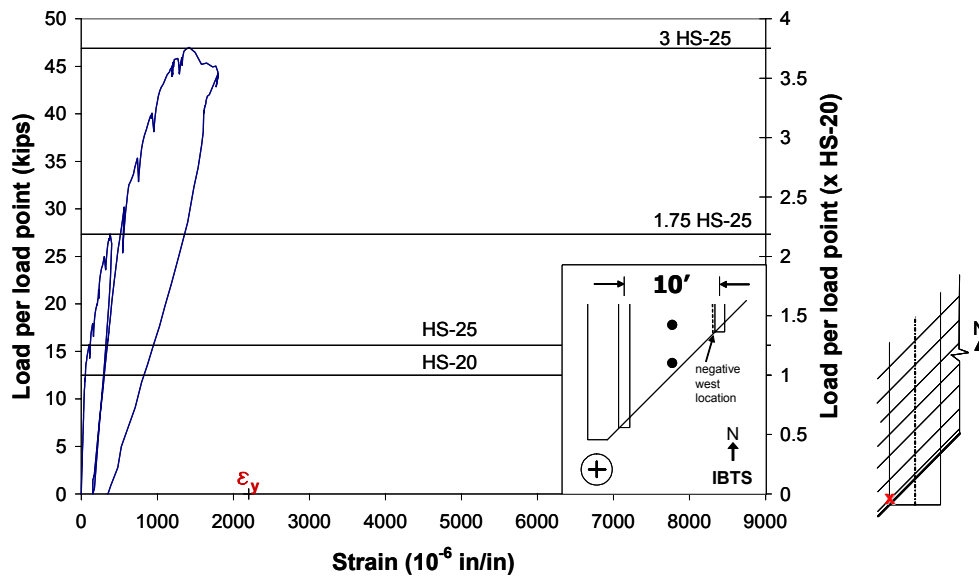
(b)

Figure 5-33 Load-strain response, IBTS, positive-moment region: (a) positive moment location, bottom bar; (b) west side of girder, top bar; (c) east side of girder, top bar

130
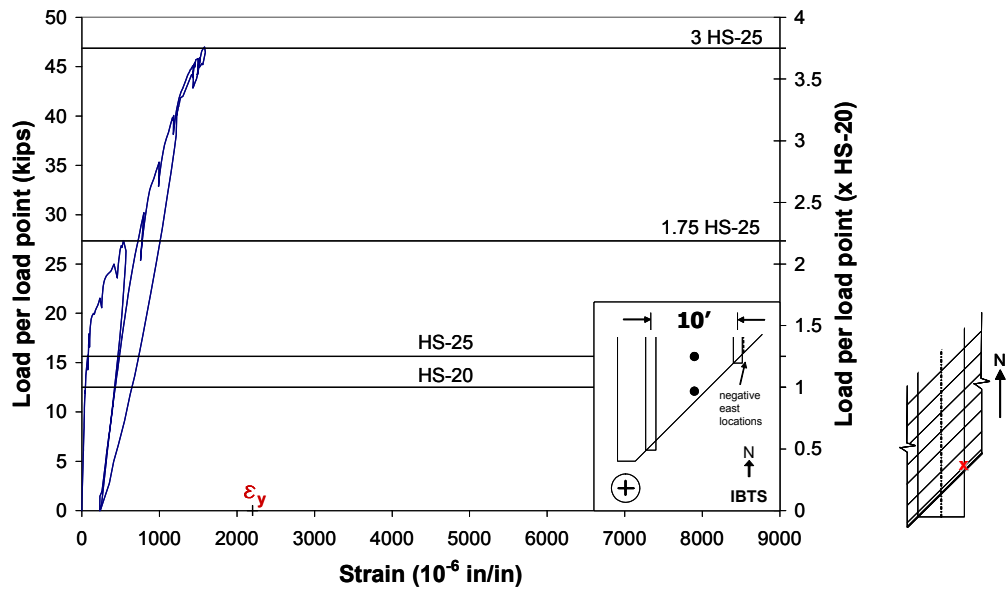
(c)

Figure 5-33 cont'd. Load-strain response, IBTS, positive-moment region: (a) positive moment location, bottom bar; (b) west side of girder, top bar; (c) east side of girder, top bar

5.4.3 Strain Profiles

In Figure 5-34(a), (b), and (c), strain profiles are shown for three locations in the IBTS, positive-moment region. The largest strains were measured in the gauges located at midspan, closest to the one-way shear failure plane and the location of maximum positive moment. Gauges installed at midspan measured increases ranging from 35% to 50% as loads were increased from HS-20 to HS-25. Tensile strains measured at midspan at 1.75 x HS-25 were 500% to 1000% of those measured at HS-20. On both sides of the girder, strain distribution is nearly uniform through the end region though the entire test. At midspan, the strain distribution is uniform at HS-20 and HS-25 load levels, but strains are larger near the slab edge at higher load levels.

131
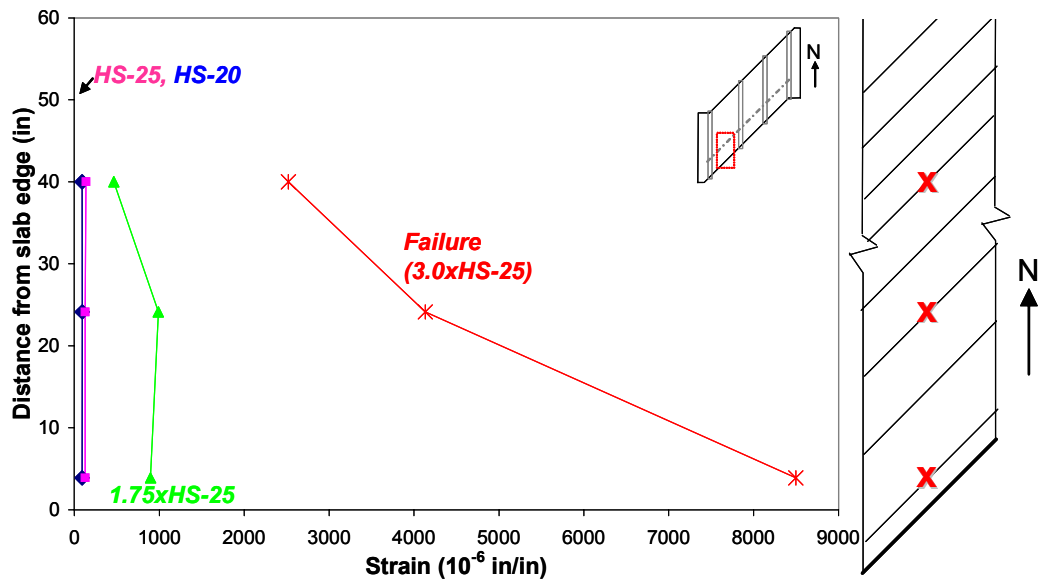
(a)
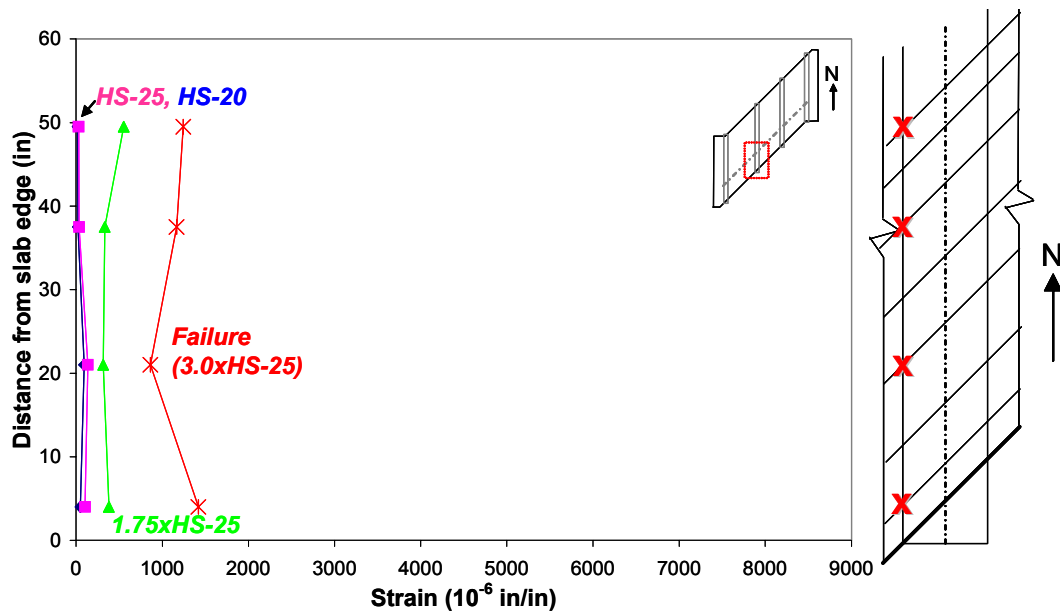
(b)

Figure 5-34 Strain profile, IBTS, positive-moment region: (a) midspan, bottom bars; (b) west edge of girder, top bars; (c) east edge of girder, top bars

132
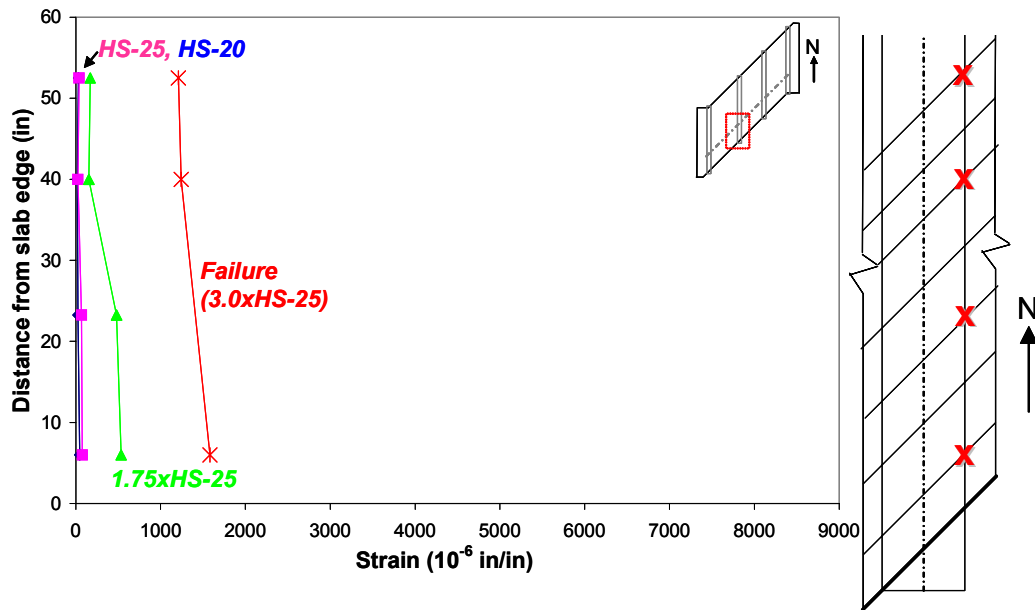
(c)

Figure 5-34 cont'd. Strain profile, IBTS, positive-moment region: (a) midspan, bottom bars; (b) west edge of girder, top bars; (c) east edge of girder, top bars

5.4.4 Crack Maps

In Figure 5-35, Figure 5-36, and Figure 5-37, crack maps of the top, bottom, and side of the test section are drawn for 1.0 x HS-25 (first cracking), 1.6 x HS-25 (load step after major change in stiffness), and 3.0 x HS-25 (failure). The crack map corresponding to developed cracking has been eliminated and replaced with a crack map corresponding to the load at which a major change in slab stiffness occurs. The terms "major change in stiffness" and "developed cracking" are discussed in Section 5.4.1.1.

At 1.0 x HS-25, the only flexural crack visible on the top of the slab was one previously initiated during the testing of the neighboring IBTS, negative-moment region. That crack, designated T4 on the drawing, was hairline, and did

not widen until 1.2 x HS-25 (18 kips). New flexural cracks in the slab were visible on the bottom and side of the slab. The bottom flexural crack formed perpendicular to the slab end and propagated parallel to the girders. A single side flexural crack extended from the crack visible on the bottom (B1 and S1, Figure 5-36 and Figure 5-37). All cracks were of hairline width at 1.0 x HS-25.

The second change in stiffness occurred at 1.6 x HS-25, and crack widths and lengths were recorded at this load level. At this load, the major change in stiffness is corroborated by the formation and propagation of several new cracks. Flexural cracks visible from the top of the slab formed perpendicular to the slab end over the west interior girder. Beneath the slab, cracks formed perpendicular to the slab end, turning parallel to the girders further into the slab. At 1.6 x HS-25, the largest crack width was 0.007 in. (0.2 mm) for Cracks B1 and B2 beneath the slab.

At 3.0 x HS-25, flexural cracks formed on the top of the slab over the west-interior girder and underneath the slab at midspan. The widest crack before failure was Crack B2 beneath the slab, with a width of 0.025 in. (0.6 mm).
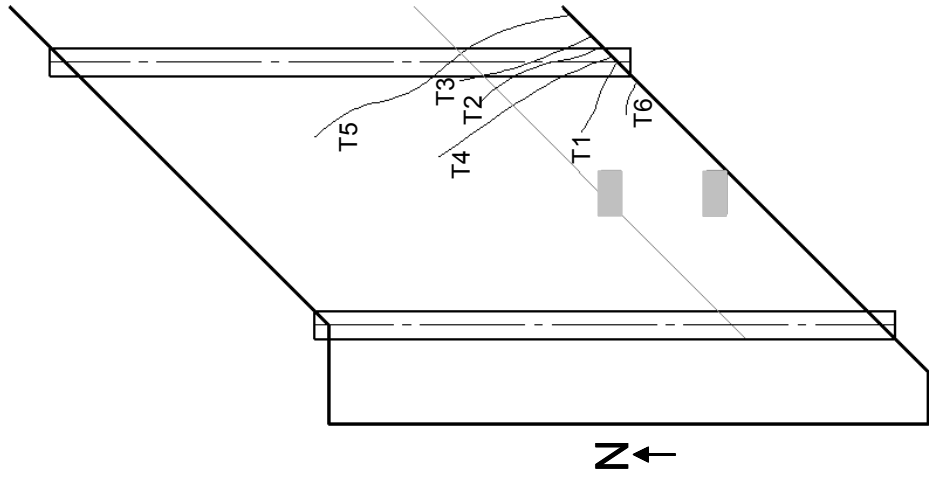
(a) 1.0 x HS-25 (first cracking)

(b) 1.6 x HS-25 (major change in stiffness)
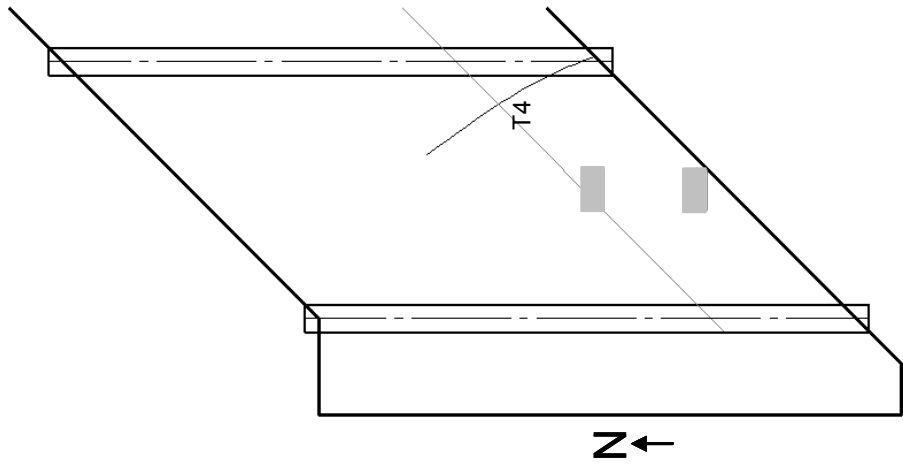
Figure 5-35 Crack map and key, IBTS, positive-moment region; top view of slab
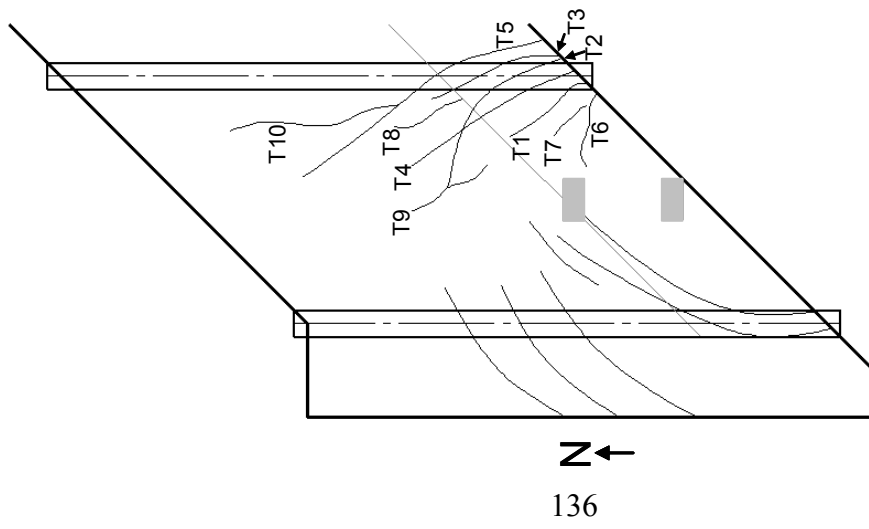
135

(c) 3.0 x HS-25 (failure)

Crack Name	Load =1.0xHS-25		Load = 1.6xHS-25		Load = 3.0xHS-25	
	Width (in)	Length (in)	Width (in)	Length (in)	Width (in)	Length (in)
T1			0.005	44	0.015	49.5
T2			0.002	54	0.01	116
T3			HL	17	0.015	60.5
T4	HL	118	0.004	121.5	0.015	126
T5			0.002	114	0.02	182
T6					0.015	35
T7					0.005	33.5
T8					0.008	32
T9					HL	42
T10					HL	81.5

(d) Key to crack lengths and widths (HL=hairline crack)

Figure 5-35 cont'd. Crack map and key, IBTS, positive-moment region; top view of slab

136
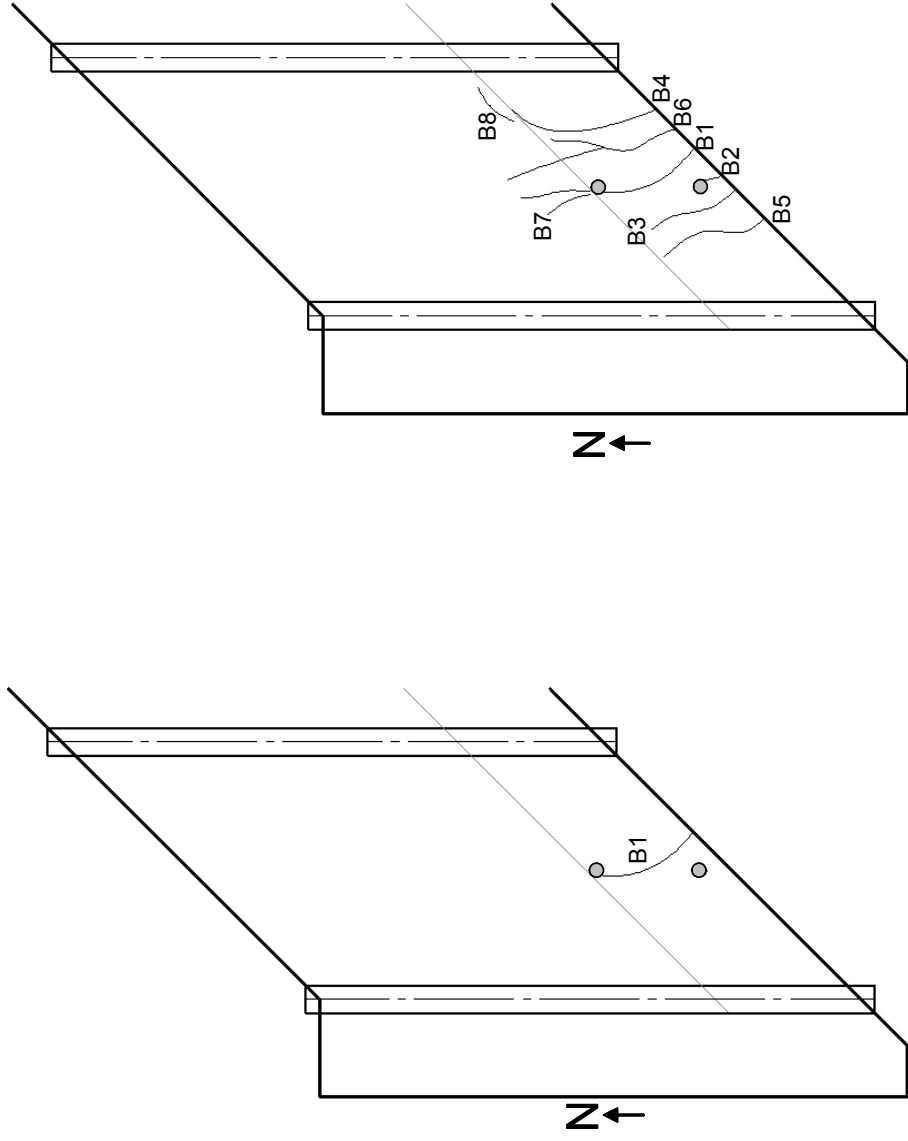
(a) 1.0 x HS-25 (first cracking)

(b) 1.6 x HS-25 (major change in stiffness)

Figure 5-36 Crack map and key, IBTS, positive-moment region; bottom view of slab
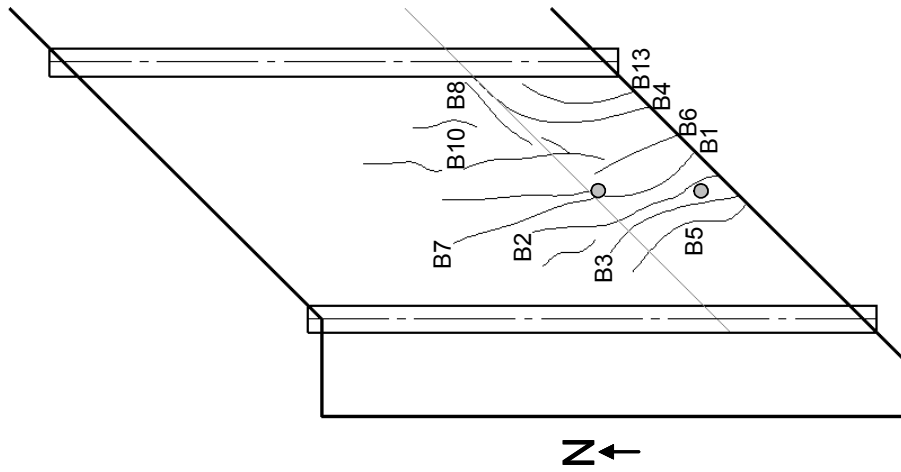
(c) 3.0 x HS-25 (failure)

Crack Name	Load =1.0xHS-25		Load = 1.6xHS-25		Load = 3.0xHS-25	
	Width (in)	Length (in)	Width (in)	Length (in)	Width (in)	Length (in)
B1	HL	57	0.007	84	0.020	137
B2			0.007	85	0.025	163
B3			0.003	29	0.020	114
B5			HL	29	0.015	71.5
B6			HL	33	0.020	37
B7			HL	35	0.005	94.5
B8			HL	32	0.005	107
B10			HL	13	0.005	96
B11					0.015	28
B13					0.020	58

(d) Key to crack lengths and widths (HL=hairline crack)

Figure 5-36 cont'd. Crack map and key, IBTS, positive-moment region; bottom view of slab

138

(a) 1.0 x HS-25 (first cracking)

(b) 1.6 x HS-25 (major change in stiffness)

(c) 3.0 x HS-25 (failure)
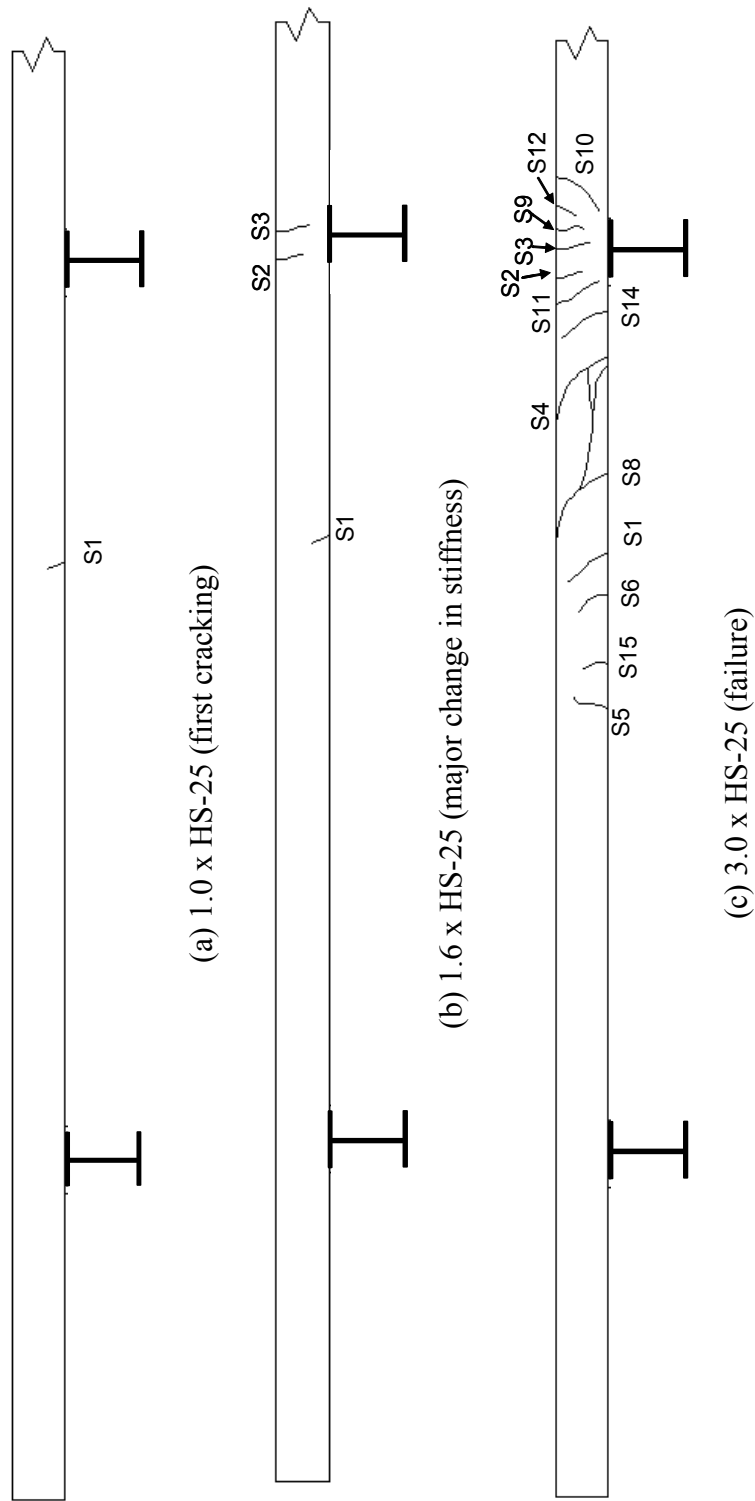
Figure 5-37 Crack map and key, IBTS, positive-moment region; side view of slab

139

	Load =1.0xHS-25		Load = 1.6xHS-25		Load = 3.0xHS-25	
Crack Name	Width (in)	Length (in)	Width (in)	Length (in)	Width (in)	Length (in)
S1	HL	3	0.002	6	0.01	7.5
S2			0.002	6.5	0.015	8
S3			0.002	7	0.015	8
S4			0.005	6.5	0.015	13.5
S5			HL	3.5	0.015	5.5
S6			HL	5.5	0.01	6
S8			HL	4.5	0.013	14
S9			HL	3.5	0.02	7.5
S10			HL	3.5	0.015	10.5
S11					0.02	11
S12					0.005	4.5
S14					0.015	13.5
S15					HL	5.5

(d) Key to crack lengths and widths (HL=hairline crack)

Figure 5-37 cont'd. Crack map and key, IBTS, positive-moment region; side view of slab

5.4.5   Appearance after Failure

Photographs of the failure surface are shown in Figure 5-38, Figure 5-39, and Figure 5-40. At 3.0 x HS-25, one-way shear failure occurred. The extension of the failure plane through the thickened end indicates that the section acted as a wide beam. As visible from the top of the slab, the one-way shear failure was parallel to the girders on the east side of the loaded points, and extended to the interior loaded point.   The failure surface on the bottom of the slab was approximately parallel to the failure surface on the bottom of the slab. Beneath the slab, the failure surface extended through the end region, turned, and followed the end of the thickened section to the girder. As seen from the side of the slab, a large shear crack, labeled S8 during testing, opened wide during failure. As

corroborated by the three views, the failure surface extends through the full depth of the thickened end region.

(a) Facing southwest

Figure 5-38 Failure surface at top of slab

(b) Facing south

Figure 5-38 cont'd. Failure surface at top of slab

Figure 5-39 Failure surface at side of slab, facing north

Figure 5-40　Failure surface at bottom of slab, facing south

5.4.6　Summary of IBTS End Detail, Positive-Moment Region Test

The 10-ft (3.0-m) bay constructed with the IBTS end detail was loaded with the AASHTO tandem load configuration placed to maximize positive moments in the end detail region. During the service-load test, at 1.75 x HS-25, flexural cracks on the bottom surface began to propagate into the UTSE, positive-moment test region. To prevent further damage to the neighboring test area, the specimen was unloaded.

At 1.0 x HS-25, only a few flexural cracks were observed on the bottom and the side of the slab. The first change in stiffness in the load-deflection

response occurred around 1.0 x HS-25, coinciding with first cracking. The second major change in stiffness at 1.6 x HS-25 (25 kips) was the result of numerous cracks forming and existing cracks propagating in the slab. Cracking did not occur on the top surface until the second major change in stiffness at 1.6 x HS-25.

The interior bay failed in beam shear at 3.0 x HS-25. The IBTS, positive-moment region had adequate strength, but the least reserve strength of all the sections tested thus far in this research program. The midspan edge deflection was 0.03 in. (0.8 mm) at HS-20 and 0.06 in. (1.5 mm) at HS-25. At failure, the midspan edge relative deflection was 1.5 in. (38 mm). The maximum recorded strains occurred at midspan in the transverse reinforcement. At HS-20, the maximum strain was 4% of yield strain (90 με), and at HS-25 was 6% of yield strain (140 με). During failure, the maximum recorded tensile strains at midspan were 4 times the yield strain (8690 με).

5.5   UTSE End Detail, Positive-Moment Region

The 10-ft (3.0-m) girder spacing bay constructed with the UTSE end detail was loaded in the configuration of the AASHTO design truck, placed to maximize positive moment (Figure 5-41). During the service-load test, the slab was loaded to approximately 27 kips (120 kN) per load point, approximately 1.7 x HS-25. The IBTS, positive-moment region eventually failed in punching shear at 3.5 x HS-25.
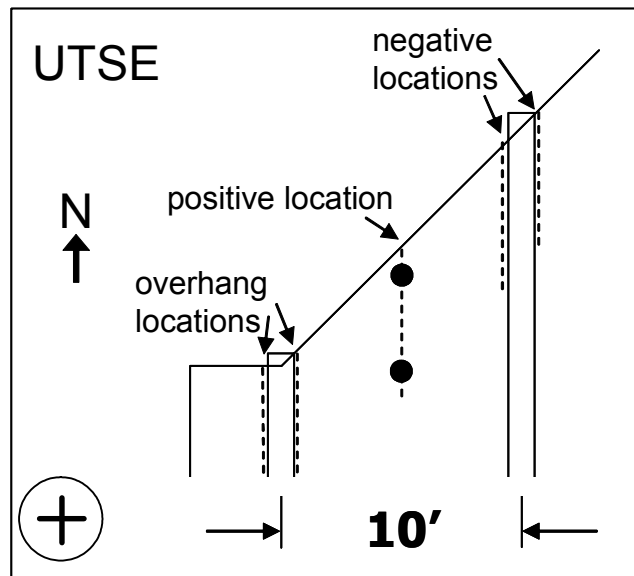
Figure 5-41 UTSE end detail, positive-moment region

5.5.1   Load-Deflection Behavior

Deflections measured under HS-20 and HS-25 loads were extremely small compared to the girder spacing (l/2400 and l/1500 respectively) (Figure 5-42). At HS-20, the edge at midspan deflected 0.05 in. (1.3 mm). At HS-25, the deflection was 0.08 in. (2.0 mm).   The measured edge deflection did not increase proportionately with the load between these two load steps. At 1.75 x HS-25, the relative deflection was 0.22 in. (5.6 mm), and at 3 x HS-25, it was 0.82 in. (21 mm). At failure, the relative deflection at the edge was 1.74 in. (44 mm).
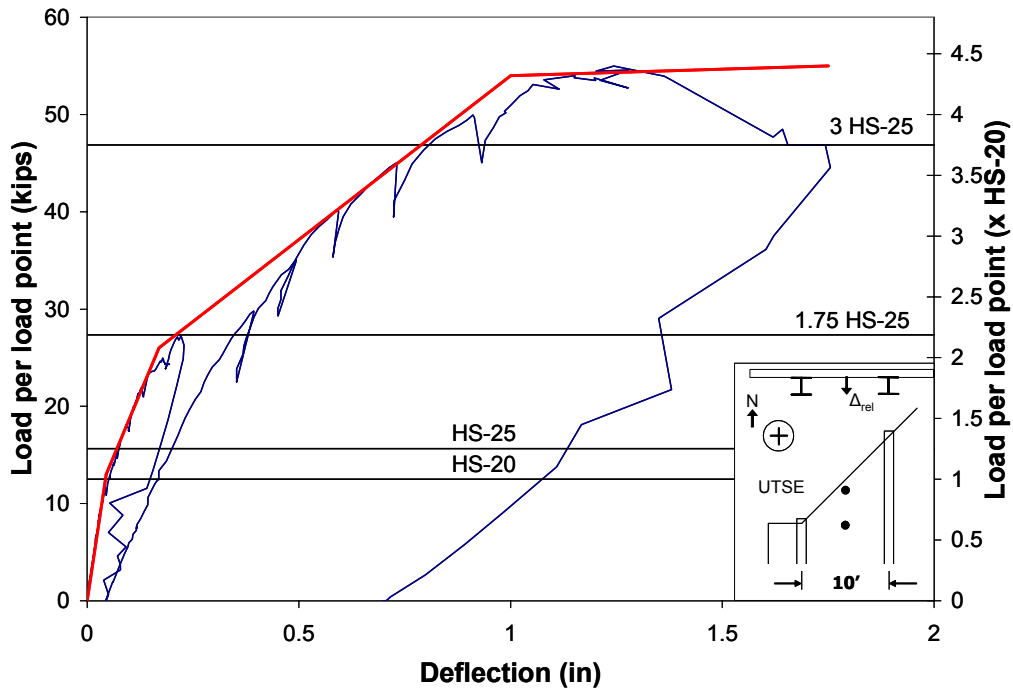
Figure 5-42 Relative midspan edge deflection, UTSE, positive-moment region

5.5.1.1   *Deflection Envelope*

The load-deflection response can be idealized as linear with three major changes in stiffness before failure. At first cracking, three flexural cracks formed on the top of the slab only. Coinciding with the incidence of first cracking, the first change in stiffness in the load-deflection response occurred around 0.8 x HS-25. The second major change in stiffness at 1.7 x HS-25 was the result of numerous cracks forming and propagating in the slab. The term "major change in stiffness" is used to describe the load at which the second change in stiffness occurred. Definition of this term is discussed in Section 5.4.1.1. At approximately 4.3 x HS-25, the slab stiffness decreased drastically as failure progressed.

5.5.2 Load-Strain Response

Figure 5-43(a), (b), and (c) show strain measurements from the most critical gauge on both sides of the girder and at midspan. The gauges on either side of the girder do not show the full strain response. Possibly due to equipment malfunction or extensive cracking near the gauges, all gauges installed over the girder registered erratically at loads above 50 kips (222 kN) per load point. At failure, the reinforcement at those sections probably experienced greater strains than were recorded.

At the HS-20 load level, the maximum tensile strain was 5% of yield strain (115 $\mu\varepsilon$) at midspan. On either side of the girder, the measured tensile strains were less than 5% of the yield strain. At the HS-25 load level, the maximum strain was 10% of yield strain (220 $\mu\varepsilon$) at midspan. An increase in load from HS-20 to HS-25 resulted in a more than proportional increase in strain at all monitored gauges. At 1.75 x HS-25, the maximum strain was 25% of yield strain (560 $\mu\varepsilon$) at midspan. At the locations where strain was measured, no reinforcement in this test area reached yield strain. At failure, the maximum strain was 99% of the yield strain (2170 $\mu\varepsilon$) at a single gauge at midspan. On the west side of the girder, the maximum strain measured before gauge malfunction was 55% of yield strain (1200 $\mu\varepsilon$), and on the east side, 44% of yield strain (960 $\mu\varepsilon$).

147
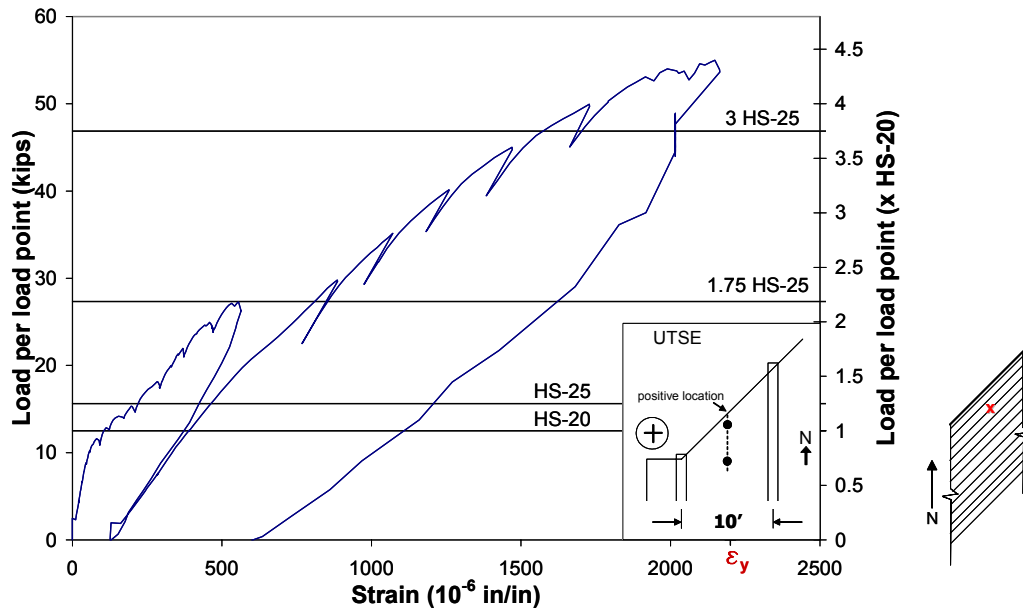
(a)
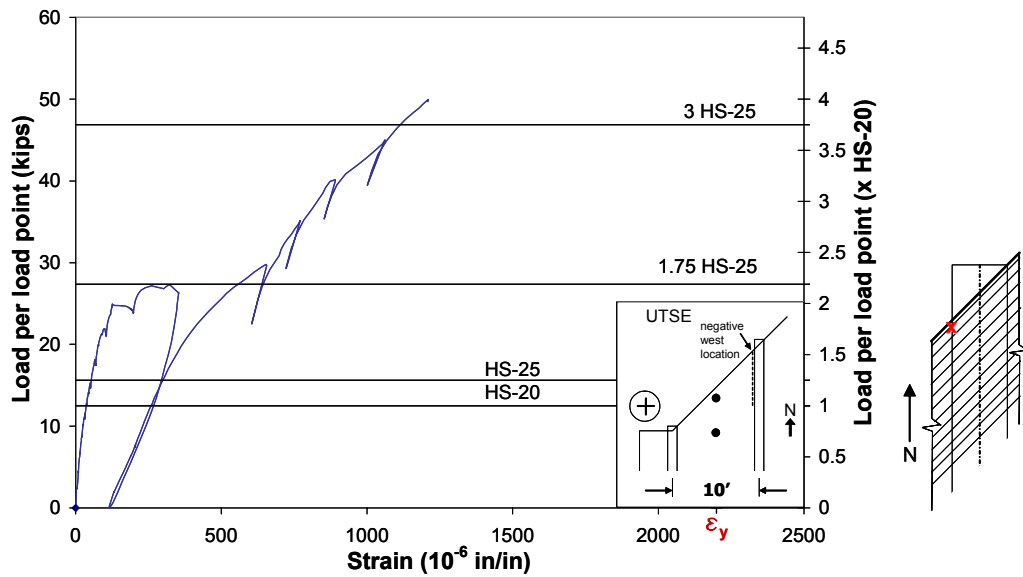
(b)

Figure 5-43 Load-strain response, UTSE, positive-moment region: (a) midspan,

bottom bar; (b) west side of girder, top bar; (c) east side of girder, top bar

148
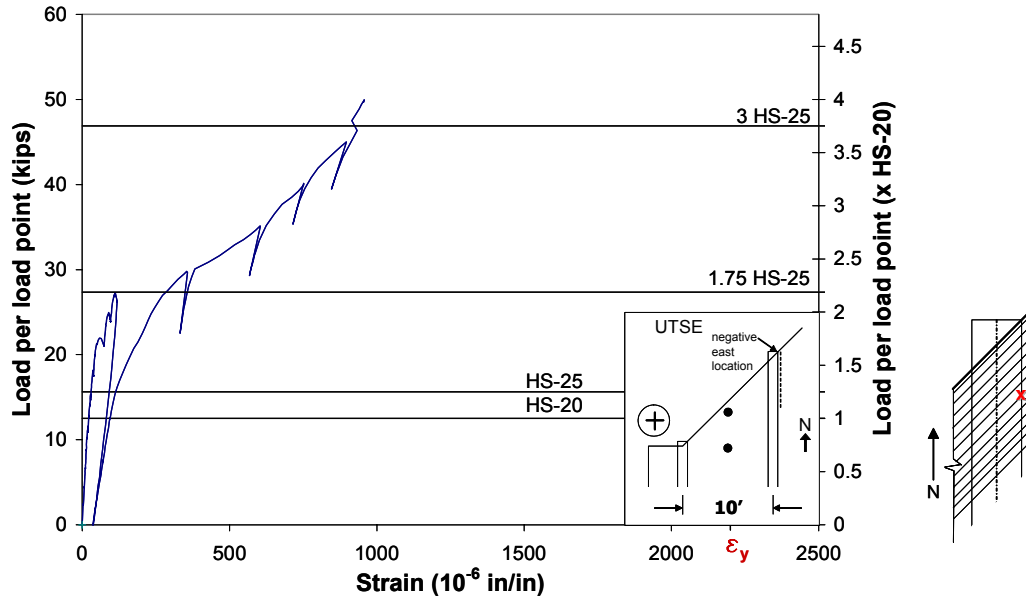
(c)

Figure 5-43 cont'd. Load-strain response, UTSE, positive-moment region: (a) midspan, bottom bar; (b) west side of girder, top bar; (c) east side of girder, top bar

5.5.3   Strain Profiles

In Figure 5-44(a), (b), and (c), strain profiles are shown for three locations in the IBTS, positive-moment test section. At each load level, the largest strains were measured at the gauges at midspan. As load levels were increased from HS-20 to HS-25, measured midspan strains increased 110% to 210%. At load levels of 1.75 x HS-25 and below, the strain distribution is nearly uniform through the end region. At 3 x HS-25 and greater loads, reinforcement close to the slab edge experienced slightly greater strains.
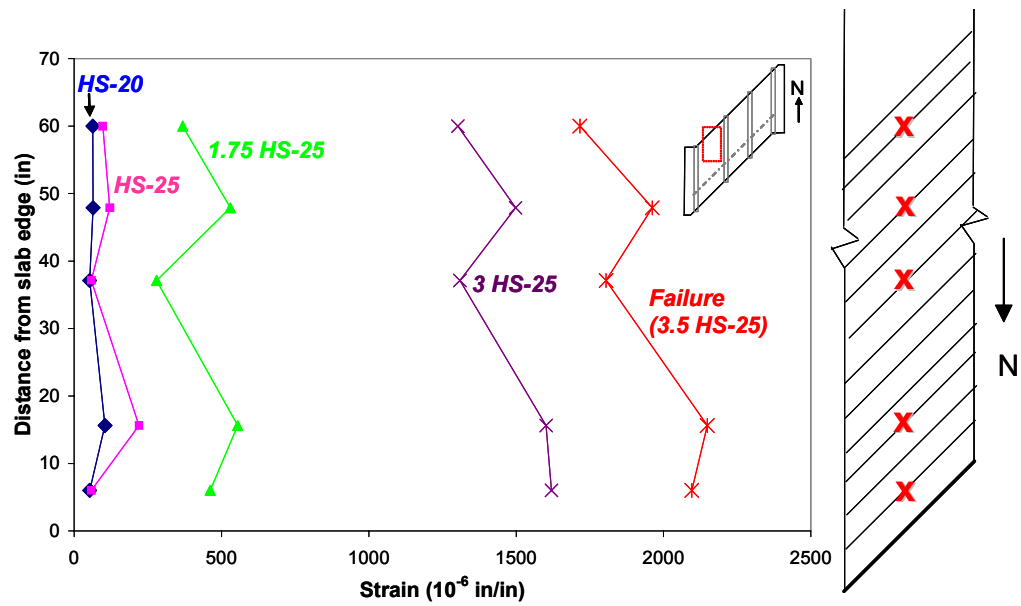
(a)
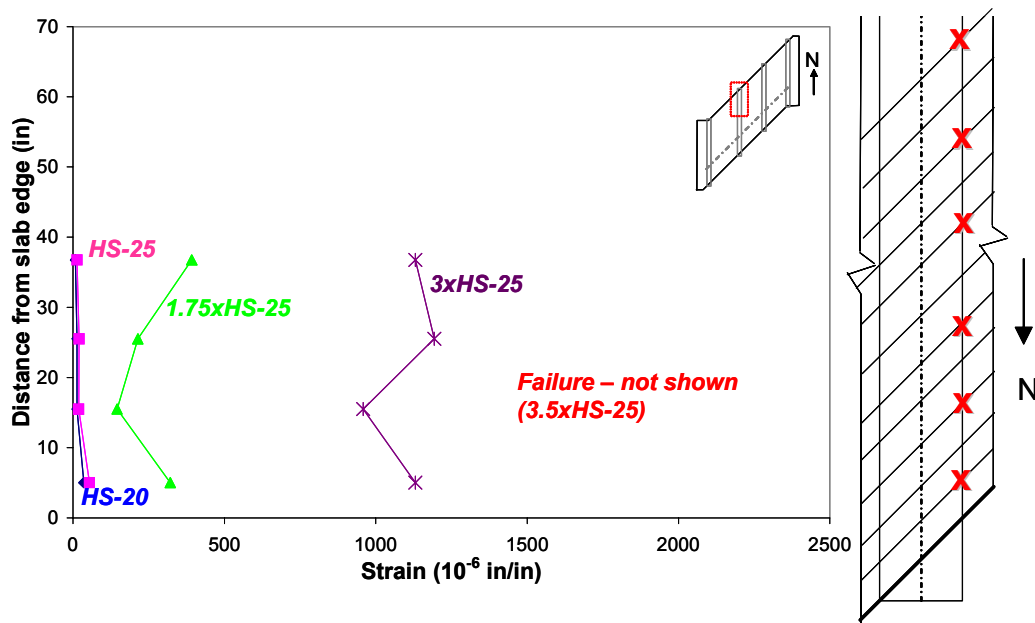
(b)

Figure 5-44 Strain profile, UTSE, positive-moment region: (a) midspan,

bottom bars; (b) west side of girder, top bars; (c) east side of girder, top bars
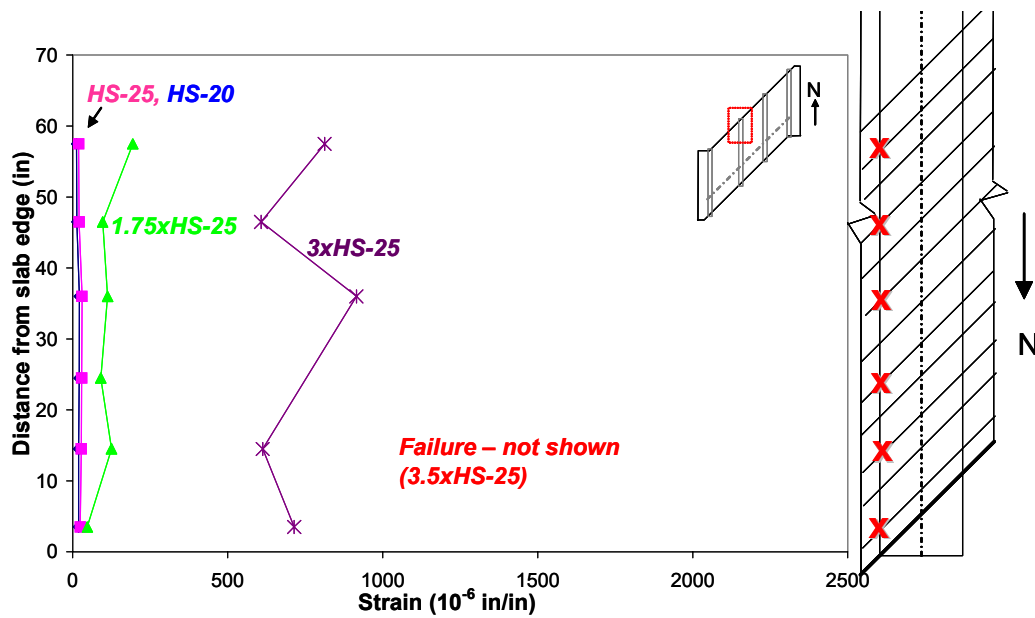
(c)

Figure 5-44 cont'd. Strain profile, UTSE, positive-moment region: (a) midspan, bottom bars; (b) west side of girder, top bars; (c) east side of girder, top bars

5.5.4   Crack Maps

In Figure 5-45, Figure 5-46, and Figure 5-47, crack maps of the top, bottom, and side of the test section are drawn for 0.8 x HS-25 (first cracking), 1.7 x HS-25 (major change in stiffness), and 3.5 x HS-25 (failure). The term "major change in stiffness" is defined and discussed in Section 5.4.1.1.

At 0.8 x HS-25, two small, hairline flexural cracks were visible on the top of the slab over the west-exterior girder (Figure 5-45a, Figure 5-46a, and Figure 5-47a). One crack was primarily perpendicular to the slab end, and the other was primarily parallel to the girder.   No new cracks were visible on the bottom or side of the slab. All cracks were of hairline width at 0.8 x HS-25.

At the major change of stiffness, 1.7 x HS-25, more extensive cracking was observed (Figure 5-45b, Figure 5-46b, and Figure 5-47b). On the top side of the slab, multiple flexural cracks developed over the exterior girder, and generally oriented perpendicular to the slab end. At 1.75 x HS-25, the widest cracks over the exterior girder were 0.007 in. (0.2 mm) wide. Over the west interior girder, two flexural cracks formed parallel to the girder, and propagated until they became continuous with the previously formed cracks in the test area to the south. Both cracks over the west interior girder were 0.004 in. (0.1 mm) wide. On the underside of the slab, a series of flexural cracks formed perpendicular to the slab end. The widest measured crack beneath the slab was 0.009 in. (0.2 mm). Several flexural cracks seen from beneath could also be viewed on the side face of the slab. The widest of these was 0.005 in. (0.1 mm) wide.

The crack map at failure shows the existing cracks during testing, and cracks formed at failure at 3.0 x HS-25. On the top of the slab at the west exterior girder, a series of torsional cracks formed parallel to the girder at the slab end, and propagated into the slab perpendicular to the slab end (Figure 5-45c, Figure 5-46c, and Figure 5-47c). On the top of the slab over the west interior girder, flexural cracks formed parallel to the girder, extending to the test area to the south. Beneath the slab, a series of flexural cracks formed primarily parallel to the girders. Near the west exterior girder, cracks on the bottom of the slab propagated perpendicular to the cracks on the top; this suggests that they are associated with torsion.
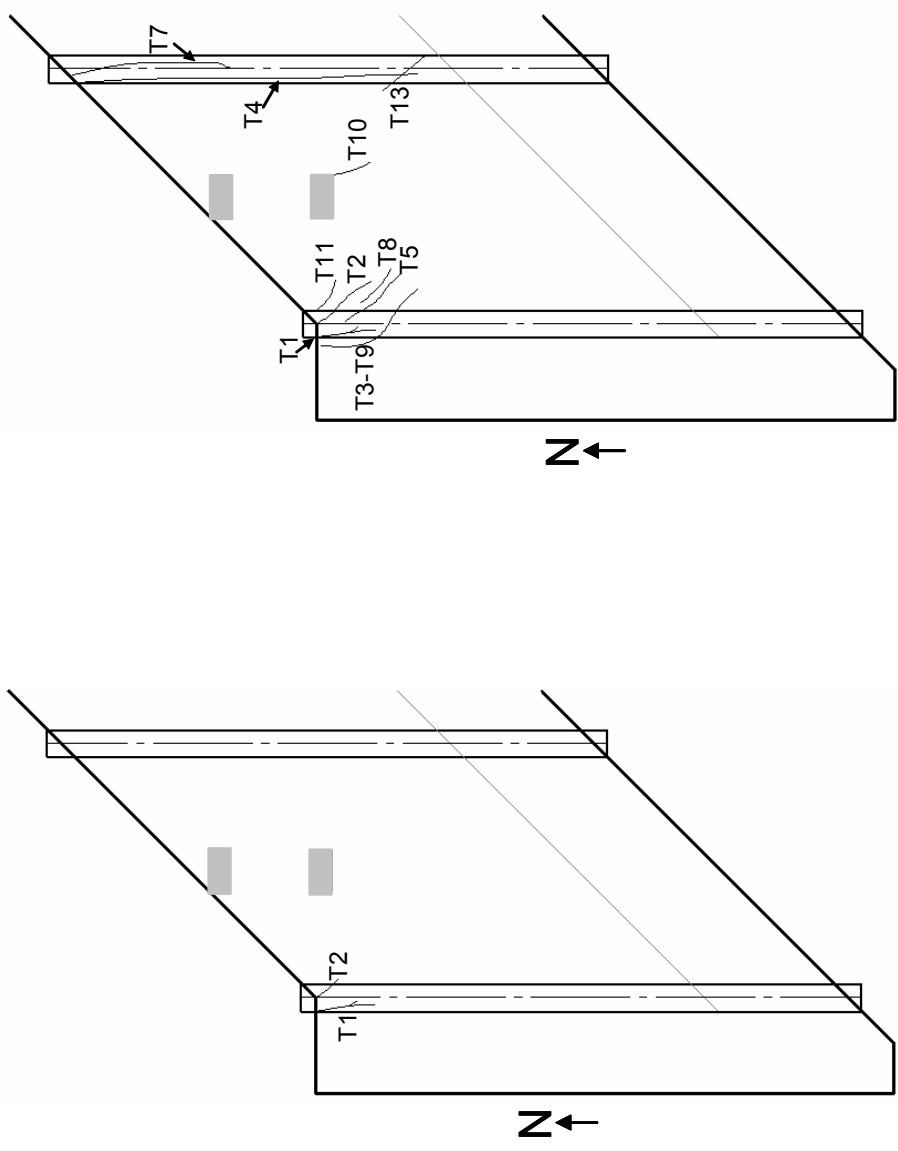
(a) 0.8 x HS-25 (first cracking)

(b) 1.7 x HS-25 (major change in stiffness)

Figure 5-45 Crack map and key, UTSE, positive-moment region; top view of slab

153

(c) 3.5 x HS-25 (failure)

(d) Key to crack lengths and widths (HL=hairline crack)
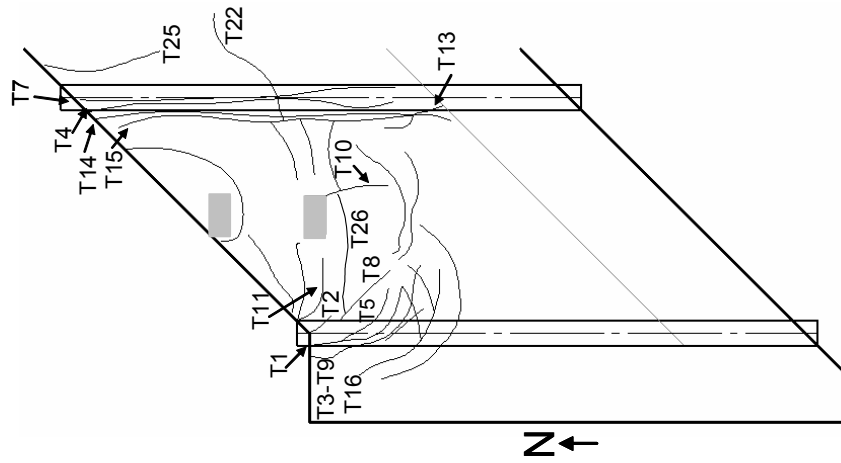
Crack Name	Load = 0.78xHS-25		Load = 1.7xHS-25		Load = 3.5xHS-25	
	Width (in)	Length (in)	Width (in)	Length (in)	Width (in)	Length (in)
T1	HL	13.5	0.007	21	0.015	50
T2	HL	10	0.007	31.5	0.01	31
T3-T9					0.01	76.5
T4			HL	22.5	0.015	127
T5			0.002	17.5	0.01	182.5
T6-T7			0.004	96	0.025	130.5
T8			0.002	125.5	0.007	35
T10			HL	23	0.015	80
T11			HL	30	0.01	32
T12			HL	15.5	0.01	22
T13			HL	4	0.005	20
T14			HL	11.5	0.012	146
T15					0.01	103.5
T16					0.01	68.5
T22					0.015	96.5
T23					0.005	34
T25					0.005	20
T26					0.005	50.5

Figure 5-45 cont'd.   Crack map and key; UTSE, positive-moment region; top view of slab

154
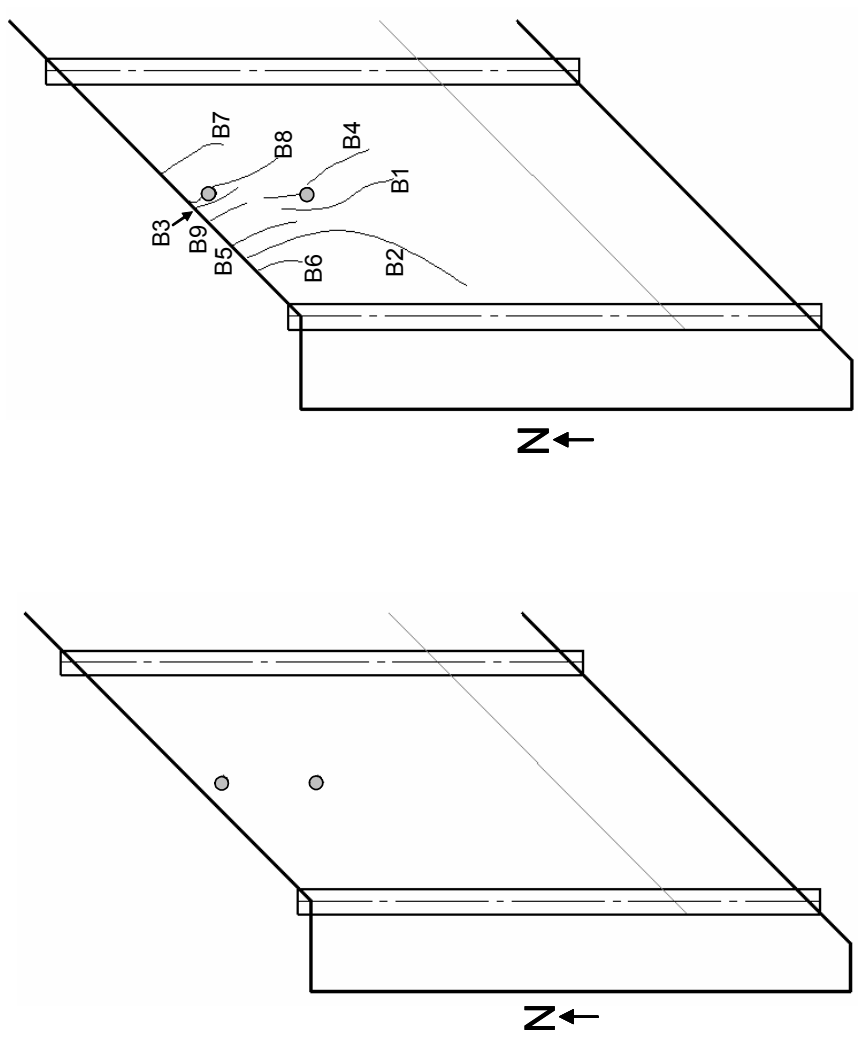
(a) 0.78 x HS-25 (first cracking) (b) 1.7 x HS-25 (major change in stiffness)

Figure 5-46 Crack map and key, UTSE, positive-moment region; bottom view of slab

155

Crack Name	Load = 0.78xHS-25 Width (in)	Length (in)	Load = 1.7xHS-25 Width (in)	Length (in)	Load = 3.5xHS-25 Width (in)	Length (in)
B1			0.005	103	0.020	103
B2			0.007	97	0.030	138
B3			0.002	44	0.160	121
B4			0.002	39	0.130	63
B5			0.002	16.5	0.005	16.5
B6			0.009	96.5	0.050	96.5
B7			HL	16	0.005	41
B8			HL	10	0.010	102
B9			HL	19	0.007	19
B10					0.030	-
B11					0.002	57
B13					0.002	23.5
B14					0.003	46.5
B17					HL	1.5

(d) Key to crack lengths and widths (HL=hairline crack)

(c) 3.5 x HS-25 (failure)

Figure 5-46 cont'd. Crack map and key, UTSE, positive-moment region; bottom view of slab

156

(a) 0.78 x HS-25 (first cracking)

(b) 1.7 x HS-25 (major change in stiffness)

(c) 3.5 x HS-25 (failure)
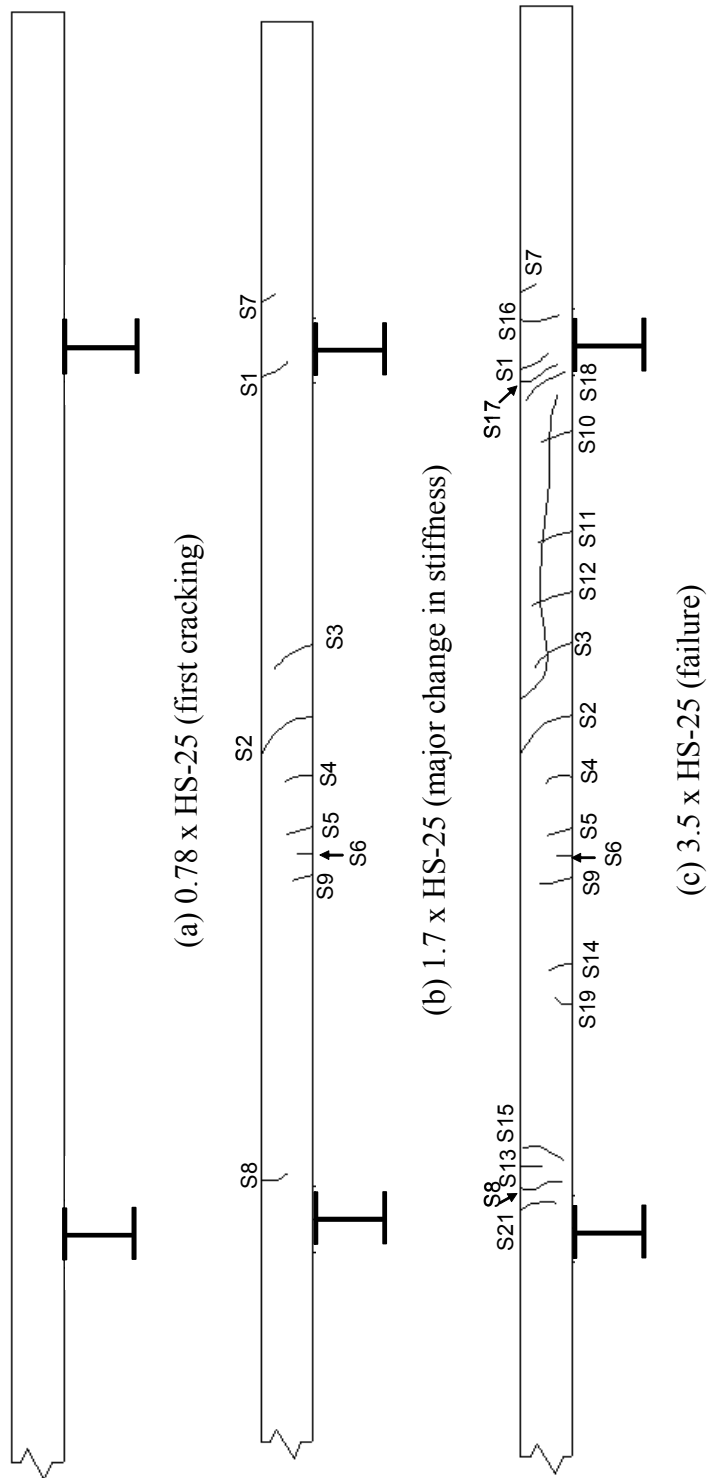
Figure 5-47 Crack map and key; UTSE, positive-moment region; side view of slab

157

	Load = 0.78xHS-25		Load = 1.7xHS-25		Load = 3.5xHS-25	
Crack Name	Width (in)	Length (in)	Width (in)	Length (in)	Width (in)	Length (in)
S1			0.005	6	0.020	7
S2			0.005	7.5	0.040	12
S3			HL	3	0.005	6
S4			0.003	3	0.013	5
S5			HL	3	0.009	6
S6			HL	2	0.003	3
S7			HL	3	0.007	3.5
S8			HL	2.5	0.010	6
S9			HL	3	0.005	4
S10					HL	6
S11					HL	6
S12					0.060	12
S13					0.005	3
S14					0.003	2
S15					0.005	4.5
S16					0.020	4
S17					0.005	5.5
S18					0.007	8.5
S19					0.002	2.5
S21					0.010	6.5

(d) Key to crack lengths and widths (HL=hairline crack)

Figure 5-47 cont'd. Crack map and key, UTSE, positive-moment region; side view of slab

5.5.5   Appearance after Failure

At 3.5 x HS-25, failure was initiated by punching shear at the loaded point closest to the edge of the slab (Figure 5-48, Figure 5-49, Figure 5-50). From the top of the slab, the failure surface extended around the loaded point to the slab edge on both sides. From the side of the slab, shear cracks extend from the top of the slab to the bottom on both sides of the loaded point. The failure surface is easily visible from beneath the slab.

(a) Facing west
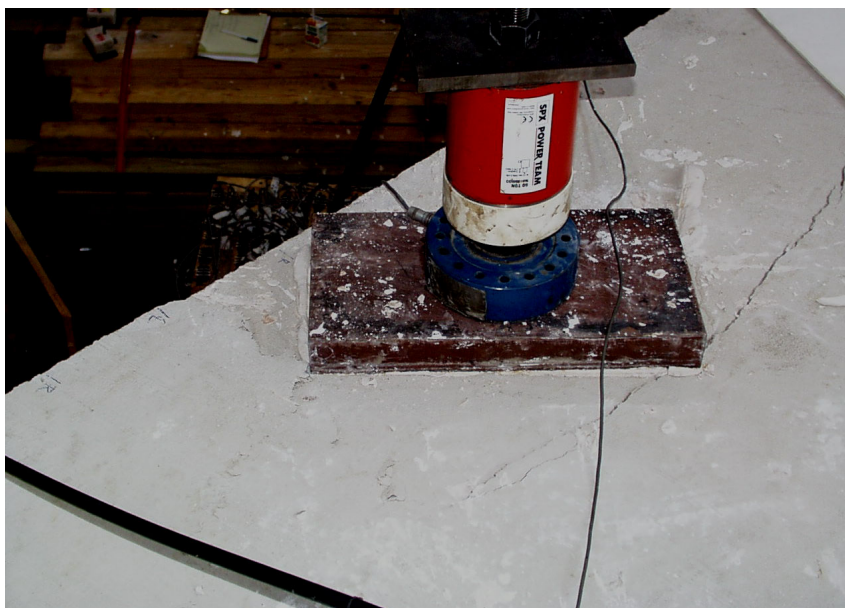
(b) Facing north

Figure 5-48   Failure surface at top of slab

159

(a) Facing south

(b) Facing south

Figure 5-49 Failure surface at side of slab

Figure 5-50 Failure surface at bottom of slab, facing north

5.5.6 Summary of UTSE End Detail, Positive-Moment Region Test

The 10-ft (3-m) girder spacing, UTSE detail test area was loaded with the AASHTO tandem load configuration placed to maximize positive moments in the end detail region. At 1.7 x HS-25, flexural cracks on the bottom surface began to propagate into the IBTS, positive-moment test region. To prevent further damage to the neighboring test area, the specimen was unloaded.

At 0.8 x HS-25, cracking was first observed on the top of the slab over the exterior girder. Cracking at loads just below the HS-25 design load level, this test area had the lowest first-cracking load observed in this research program. At first cracking, three flexural cracks formed on the top of the slab only. Coinciding with the incidence of first cracking, the first change in stiffness in the load-

161

deflection response occurred around 0.8 x HS-25. The second major change in stiffness at 1.7 x HS-25 was the result of numerous cracks forming and propagating in the slab.

The interior-bay loaded point failed in punching shear at 4.3 x HS-25 (54 kips). The UTSE, positive-moment region had higher reserve strength than the IBTS positive moment. The reasons for this difference are discussed further in Section 5.6. The relative midspan edge deflection was 0.05 in. (1.3 mm) at HS-20 and 0.08 in. (2 mm) at HS-25. At failure, the midspan relative edge deflection was 1.75 in. (44 mm). The maximum recorded strains occurred at midspan in the transverse reinforcement, reaching 5% of the yield strain (115 $\mu\varepsilon$) at HS-20 and 10% of the yield strain (220 $\mu\varepsilon$) at HS-25. During failure, the maximum recorded strains were 99% of yield strain (2170 $\mu\varepsilon$), measured at midspan.

5.6 DISCUSSION AND COMPARISON OF 45º SKEW SPECIMEN TEST RESULTS

Figure 5-51 shows deflection envelopes for all four test areas on the 45º skew test specimen. Overall, the tests maximizing negative moments behaved similarly, and the tests maximizing positive moments behaved similarly. In the negative-moment tests, reserve strength was higher, stiffness was greater, and deflections were smaller than in the positive-moment tests. In the positive-moment test regions, first cracking was observed earlier, and tensile strains were higher for respective end detail tests.

162
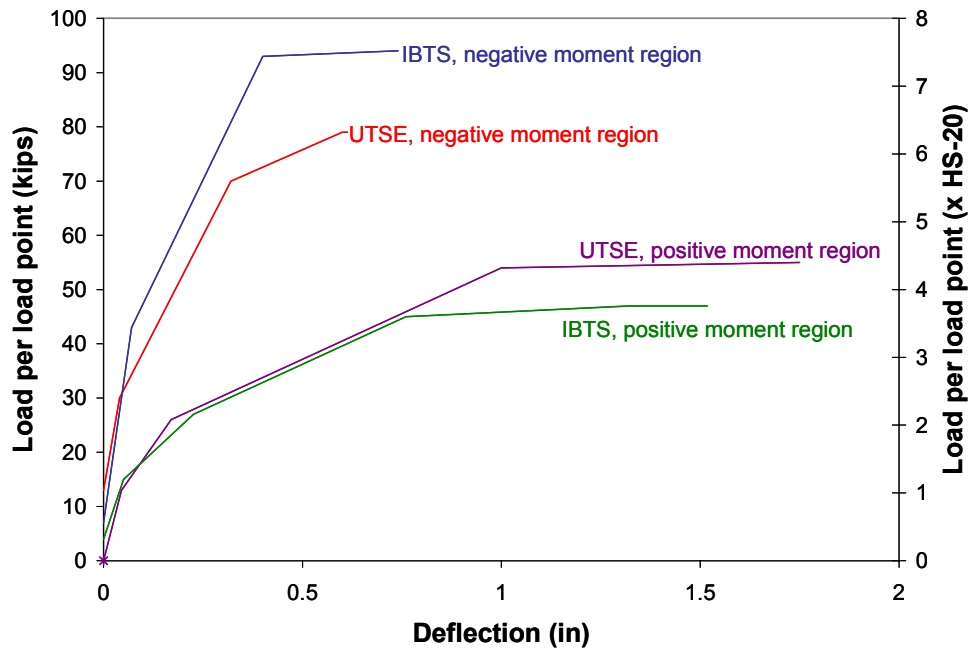
Figure 5-51 Deflection envelopes, all tests

5.6.1   Negative-Moment Tests

Results from tests maximizing negative moment are summarized in Table 5-2 and Table 5-3.   Overall, the two negative moment tests areas behaved similarly under AASHTO design loads. Deflections at the HS-20 load level were larger in the IBTS test region than the UTSE test region, and both were extremely small (less than l/2000 for all tests) compared to the girder spacing.   Tensile strains at HS-20 and HS-25 load levels were negligible, as was the difference in strains at HS-20 and HS-25 load levels. Before failure, transverse reinforcement yielded in tension at the negative-moment section of the IBTS detail, but did not yield in the UTSE detail. For both test areas, cracking was first observed well past the design load range. Due to the decreased slab depth, cracking was first observed in the UTSE detail at a lower load than in the IBTS detail.

Table 5-2 Summary of IBTS end detail, negative-moment region

| IBTS | IBTS end detail, negative-moment region | | | |
| | Deflections | | | Maximum strains (% of steel yield strain) |
Load Step	Maximum relative deflection (in)	Cracked (Yes/No)	Clear span to relative deflection ratio	
HS-20	0.025	No	3840	1.0
HS-25	0.026	No	3692	1.2
1.2xHS-25	0.03	No	3200	1.5
1.75xHS-25	0.04	No	2400	2.3
3xHS-25	0.1	Yes	960	24
Failure	0.83	Yes	116	300

Table 5-3 Summary of UTSE end detail, negative-moment region

| UTSE | UTSE end detail, negative-moment region | | | |
| | Deflections | | | Maximum strains (% of steel yield strain) |
Load Step	Maximum relative deflection (in)	Cracked (Yes/No)	Clear span to relative deflection ratio	
HS-20	0.006	No	16000	1.0
HS-25	0.007	No	13714	1.3
1.2xHS-25	0.008	No	12000	1.5
1.75xHS-25	0.032	Yes	3000	5.0
3xHS-25	0.16	Yes	600	42
Failure	0.32	Yes	300	89

Figure 5-52 shows the locations of major cracks at failure in both of the tests where negative moment was maximized. For the 8-ft (2.4-m) girder spacing, IBTS test area, a punching-shear failure initiated at the interior load plate of the interior bay, where the slab depth was 8 in. (203 mm). The failure surface formed at this interior plate, and propagated toward the exterior plate. Upon reloading of the IBTS test area, punching-shear failure occurred around the load point in the east-exterior bay, where the slab depth was 10 in. (254 mm).

At the 8-ft (2.4 m) girder spacing, UTSE detail test area, where the slab thickness was 8 in. (203 mm), punching shear failure occurred around the loaded point in the interior bay. Of all of the locations where load was applied in this test area, this load plate was closest to the edge and had the smallest shear perimeter calculated in accordance with AASHTO LRFD Bridge Design Specifications and ACI 318-02 provisions. Upon reloading, a punching-shear failure initiated at both loaded points in the exterior bay.

In test areas where negative moment was maximized, failure mechanisms and failure loads were similar. At locations where only a single load plate was applied in a bay, a punching shear failure surface formed around the plate toward the edge of the slab in shapes that were similar from test to test. At locations where two load points were applied in a bay, punching shear failure occurred on the side of the load points closest to a girder. In the IBTS detail test section, punching shear failure began at the location with the 8-in. (203-mm) depth of concrete.

Punching shear and beam shear capacities can be calculated using design provisions detailed in the ACI-318 code. Design provisions and predictions of capacity for all tests on this specimen are discussed in Section 5.6.2.2.

UTSE

N

IBTS

change in
slab depth

■ loading plate where first punching
   shear failure occurred

▬ loading plate where second
   punching shear failure occurred

— failure surface as seen from
   top of slab

— failure surface as seen
   from bottom of slab
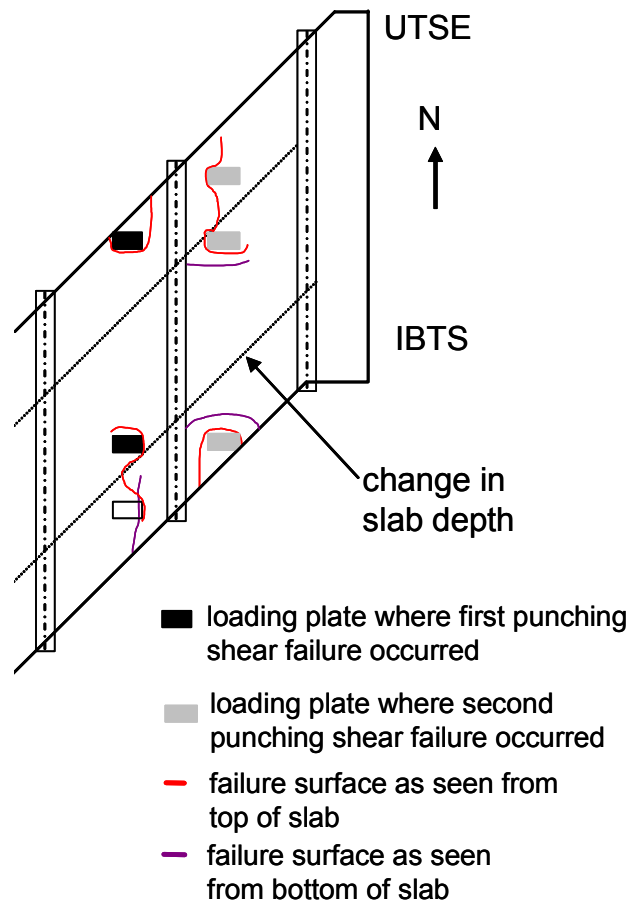
Figure 5-52 Locations of punching shear failure, negative-moment tests

5.6.2   Positive-Moment Tests

Table 5-4 and Table 5-5 summarize the results obtained from the tests maximizing positive moment. The IBTS end detail was stiffer than the UTSE detail, as evidenced by the load and edge deflection measurements. Deflections at HS-20 load levels were 16 times larger in the UTSE test region than the IBTS test region; both were extremely small, however, compared to the girder spacing (l/2000 for UTSE and l/32000 for IBTS). Tensile strains at HS-20 and HS-25 load levels were negligible, and the difference in strains in reinforcement at HS-

20 and HS-25 load levels was negligible as well. At failure, reinforcing steel at the midspan of the IBTS bay had yielded in tension, and a single reinforcing bar in the UTSE bay had yielded. For both test areas, cracking was first observed in the design load range (at HS-25 for IBTS and HS-20 for UTSE). First cracking occurred at a negligibly lower load in the UTSE section. In both tests, first cracking caused a very small change in slab stiffness. The second change in stiffness coincided with multiple cracks forming and widening, and did not occur until approximately 1.6 x HS-25.

Overall, the end details performed well when subjected to positive bending in a bay with 10-ft (3.0-m) girder spacing. Although cracking occurred at the HS-20 and HS-25 load levels, the cracks were few and narrow, and tensile strains and deflections were extremely small. For both test areas, cracks were short, narrow, and few until approximately 1.6 x HS-25, at which point the cracks began to develop more frequently.

Table 5-4 Summary of IBTS end detail, positive-moment region

IBTS	IBTS end detail, positive-moment region			
	Deflections			Maximum strains (% of steel yield strain)
	Maximum relative deflection (in)	Cracked (Yes/No)	Clear span to relative deflection ratio	
Load Step				
HS-20	0.003	No	32000	4.2
HS-25	0.006	Yes	16000	6.4
1.2xHS-25	0.1	Yes	960	15
1.75xHS-25	0.23	Yes	417	41
3xHS-25	-	-	-	-
Failure	1.52	Yes	63	395

Table 5-5 Summary of UTSE end detail, positive-moment region

| UTSE | UTSE end detail, positive-moment region | | | |
| | Deflections | | | Maximum strains (% of steel yield strain) |
Load Step	Maximum relative deflection (in)	Cracked (Yes/No)	Clear span to relative deflection ratio	
HS-20	0.05	Yes	1920	4.8
HS-25	0.08	Yes	1200	10
1.2xHS-25	0.1	Yes	960	14
1.75xHS-25	0.22	Yes	436	25
3xHS-25	0.82	Yes	117	73
Failure	1.74	Yes	55	99

Figure 5-53 shows the locations of major cracks at failure in both of the tests where positive moment was maximized. The IBTS test area failed in beam shear, at a load close to that predicted by the corresponding provisions of ACI 318-02 and the AASHTO LRFD Bridge Design Specifications. The UTSE area failed in punching shear, at a load close to that predicted by the corresponding provisions of ACI 318-02.

Under AASHTO design loads on 10-ft (3-m) girder spacings, the UTSE end detail had higher capacity than the IBTS end detail in the specimen tested. The depth of concrete plays a primary role in the shear strength of a section, and the IBTS section is 2 in. (51 mm) deeper than the UTSE section. For failure surfaces with an identical plan view shape in an IBTS section and a UTSE section, a higher beam-shear capacity and punching shear capacity would be expected in the IBTS section due to its greater depth. The difference in capacity may be explained by differences in test area geometry and the effects of torsion, topics discussed in Sections 5.6.2.1 and 5.6.2.2.

UTSE

N
↑

IBTS

■ load plate where punching shear failure occurred

☐ load plate

— failure surface as seen from top of slab

— failure surface as seen from bottom of slab
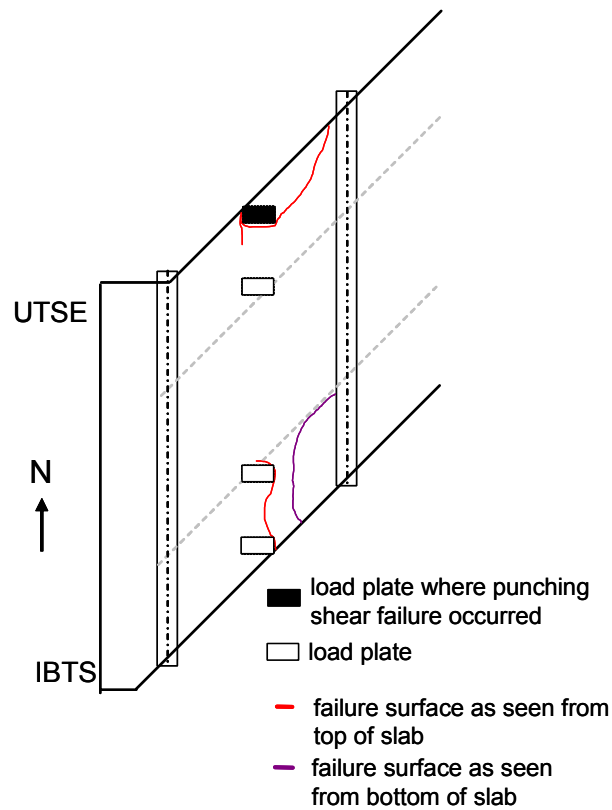
Figure 5-53 Locations of punching-shear and beam-shear failure in positive-moment tests

5.6.2.1   Shear and Slab Geometry

Although the test data are too limited to provide a precise explanation of the differences in capacities and failure modes, two possible factors influencing the failure loads of the test section are related to the geometry of the test specimen, the location of the critical section for shear and the predicted shear stress at that critical section.

The critical section for beam shear is different on either side of the load points. Due to the slab end geometry and the load configuration, one potential beam shear failure plane is shorter than the other, leading to a lower calculated

shear resistance. As illustrated in Figure 5-54, the critical plane is on the west side of the UTSE detail load points and on the east side of the IBTS detail load points. The difference in critical locations for shear is important when combined with a simple linear-elastic analysis of shear stresses on either side of the load points. Figure 5-54 shows two elastic analyses idealizing the edge detail as a wide beam. In one analysis, the interior girder acts like a fixed support; in another, like a simple support. The actual support conditions and flexural restraint of the interior girder are expected to be somewhere between these two conditions, possibly closer to the fixed support condition. Because of the differences in end fixity, the shear stresses on the east side of the load points could be up to 38% greater than the shear stresses on the west side of the load point. Though this simple model may not be an exact representation of the actions occurring in these sections, it illustrates how shear forces may have differed in the UTSE and IBTS end details.

Combining the two effects, the IBTS detail would experience higher shear forces at a location where the length of the critical section for beam shear is shorter. The UTSE detail would experience lower shear forces at the shorter critical section or higher shear forces at the longer critical section. Although the UTSE detail failed in punching shear, a small beam-shear crack formed after punching shear failure, indicating that the failure load was in the vicinity of the beam-shear failure load when punching shear failure was experienced.

UTSE

5.25'

6.9'

N

5.25'

6.9'

IBTS

P

0.31P

0.69P

P

0.5P

0.5P
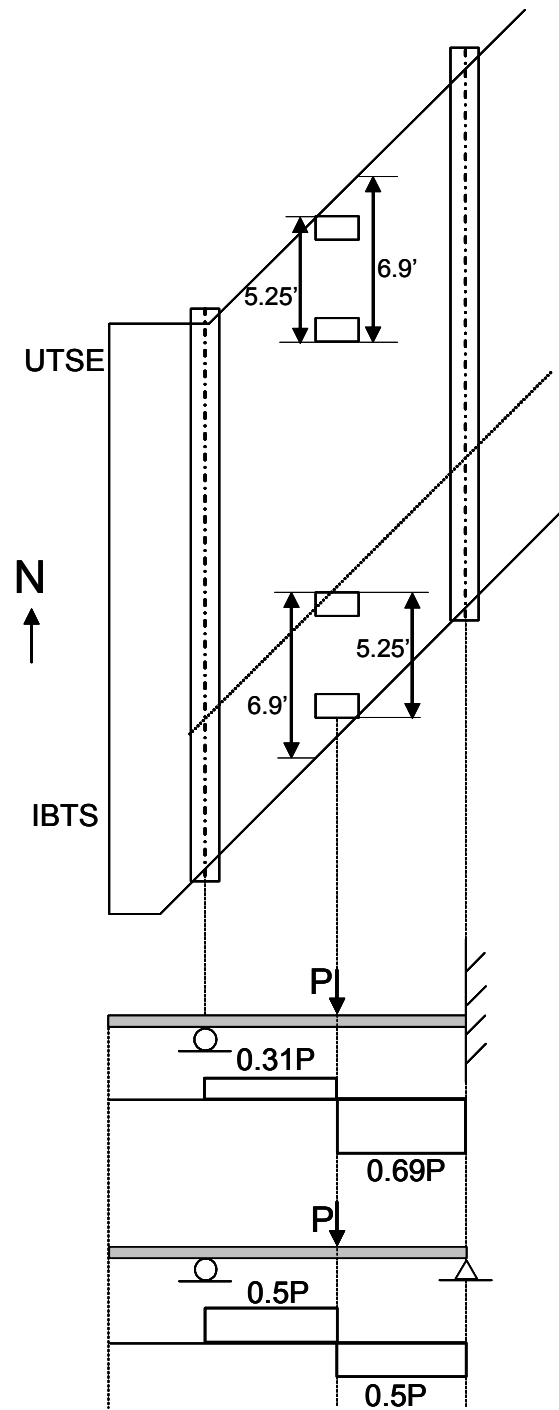
Figure 5-54 Elastic shear distribution, positive-moment tests

171

5.6.2.2 Torsion

Torsion has likely contributed to the difference in failure mode and capacities of the 10-ft (3-m) bays. Although somewhat more limited in the 8-ft (2.4-m) bays, torsional cracking was observed in every test area. These cracks appeared on the receding corners of each bay (Figure 5-55), longitudinally behind the load points. These cracks indicate that torsion could have affected the capacities and distribution of stresses in the receding corners of the test areas with 10-ft (3-m) girder spacing.

Torsional moments may have also affected the capacity of the positive-moment test areas, because the failure surface formed on an existing torsional crack in the IBTS, positive-moment test area. To fully understand the effects of torsion on beam shear and punching shear, investigations are needed beyond the scope of the current investigation.
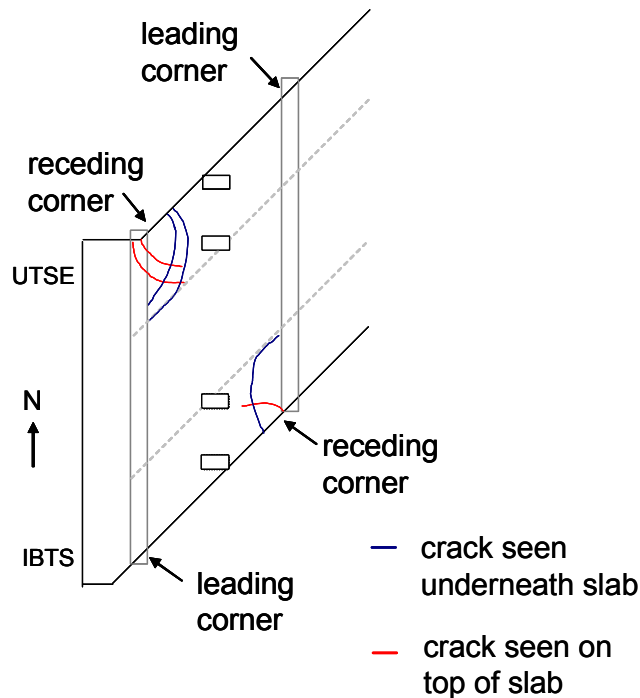
Figure 5-55 Torsional cracks in 10-ft bays

5.6.3 Observed Beam-Shear Capacity of Bridge Slab Compared to Calculated Nominal Capacity by AASHTO and ACI Provisions

The beam-shear strength of bridge slabs is addressed in Section §5.8.3.3 of the AASHTO LRFD Bridge Design Code and reviewed here. That section requires that Equation 5-1 be used for calculating the nominal beam-shear capacity of a nonprestressed section without shear reinforcement. In that equation, b is the length of the critical perimeter, a minimum distance of d/2 from the load plate; d is the distance between the extreme compression fiber and longitudinal reinforcement in tension; f_c' is the specified compressive strength of concrete in psi at 28 days; and β is 2 for a non-prestressed section. These provisions are identical to those of ACI 318-02 Section §11.8.6 .

$$V_c = \beta \sqrt{f_c'} \cdot b_y d_y \qquad\qquad \textbf{\textit{Equation 5-1}}$$

Using Equation 5-1, one-way nominal shear capacities for the positive moment tests were calculated for a section 68 in. (1727 mm) wide, for both the IBTS and UTSE end details. The predicted nominal capacity of the IBTS section was 72 kips (320 kN). Using the two bounding cases illustrated in Figure 5-54, elastic analysis predicts the shear force at the location of failure to be between 47 kips (209 kN) for simple supports and 69 kips (307 kN) using a fixed support. This indicates that the AASHTO beam shear prediction is slightly unconservative.

The predicted capacity of the UTSE section was 55 kips (245 kN). Again using the two bounding cases, elastic analysis predicts that the shear force at failure at the location of the beam-shear crack would be between 55 kips (245 kN) using simple supports and 34 kips (151 kN) using a fixed support. Because the slab at the interior girder has a fixity closer to that of a fixed support than a simple support, this calculation is also slightly unconservative.

173

5.6.4 Observed Punching-Shear Capacity of Bridge Slab Compared to Calculated Nominal Capacity by AASHTO and ACI Provisions

Nominal punching-shear capacity is calculated using Section 5.13.3.6 of the AASHTO LRFD Bridge Design Code, repeated in Equation 5-2:

$$v_c = \min\{4\sqrt{f_c'}\ ;\ (\frac{1}{2}+\frac{1}{B})4\sqrt{f_c'}\}$$

Equation 5-2

These equations are the same as those proposed by ACI 318-02 in section §11.12 for a uniform shear distribution (Equation 5-3). ACI 318-02 has one additional equation, however, and requires that punching shear capacity be computed as the minimum of the terms in Equation 5-3:

$$v_c = \min\{4\sqrt{f_c'}\ ;\quad (\frac{\alpha_s}{(b_o/d)}+2)\sqrt{f_c'}\ ;\quad (\frac{1}{2}+\frac{1}{B})4\sqrt{f_c'}\}$$

Equation 5-3

where f_c' is the specified concrete compressive strength; b_o is the length of the critical perimeter; d is the effective depth of the slab, α_s is 40 for interior loading cases and 30 for edge loading cases; and B is the ratio of the length of the longest side of the loaded area to the shorter side. Based on these parameters, the nominal punching-shear capacity of the slab is:

$$V_c = v_c b_o d$$

Equation 5-4

ACI 318-02 and the AASHTO LRFD Bridge Specification provisions require the critical perimeter to be calculated at a distance d/2 from the edge of the loading point. For loading at the edge of a skewed slab, the minimum critical perimeter, shown in Figure 5-56, is perpendicular to the slab ends on both sides of the loading plate.

174
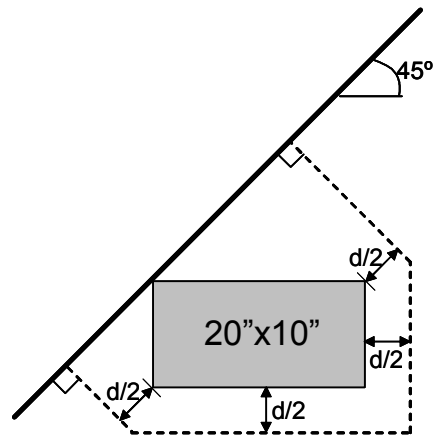
Figure 5-56 Critical perimeter used to determine punching-shear capacity with uniform stress distribution on the perimeter of the critical section

Figure 5-57 compares the observed punching-shear capacities from the 45° skew span tests against the nominal capacity by ACI 318-02 provisions (Equation 5-3 and Equation 5-4), assuming a uniform shear distribution on the perimeter of the critical section. For the tests on the 45° skew specimen, the assumption of a uniform stress distribution results in unsafe predictions of punching-shear capacity. The punching capacity of the bridge slab, loaded with an AASHTO load configuration, is only about 45% to 85% of that predicted by ACI 318-02 and AASHTO LRFD provisions, assuming a uniform shear stress distribution.
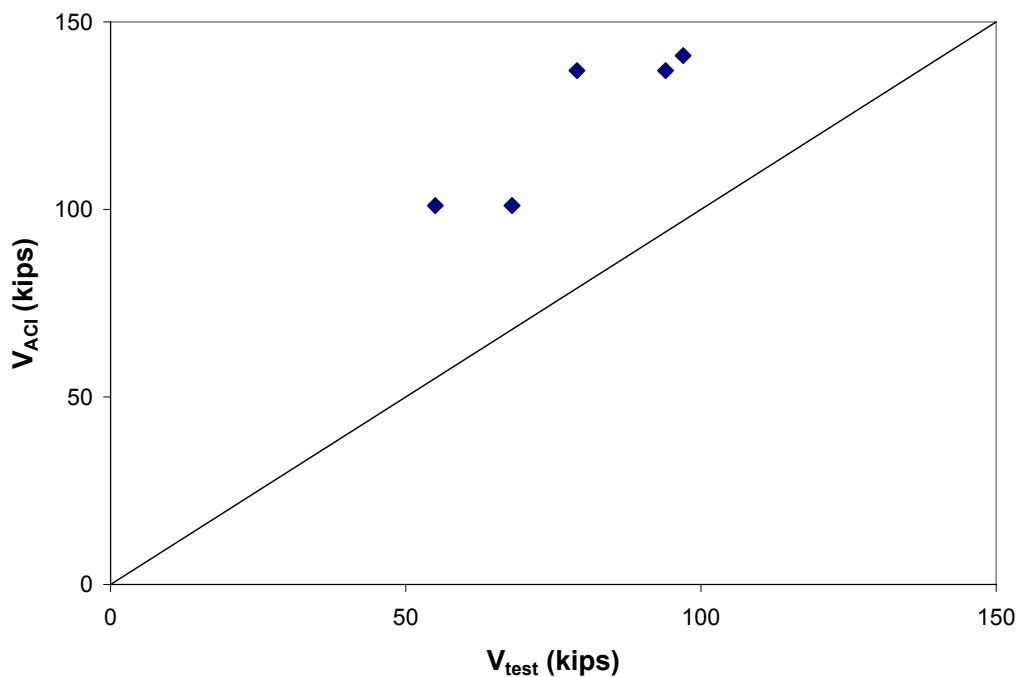
Figure 5-57 Comparisons of ACI 318-02 predictions with experimental results

The shape of the critical section assumed in the previous analysis for punching shear did not adequately predict the shape of the failure surface for the edge loading configuration in the 45º skew specimen. Figure 5-58 shows the shape of a typical failure surface, as observed from the top of the slab. In the observed failure surfaces, the critical perimeter was longer than that used in the previous calculations. For the failure surface shown in Figure 5-58, the centroidal axis of the critical perimeter does not coincide with the centroidal axis of the loaded area, resulting in unbalanced moments. ACI 318-02 uses an eccentric shear model to account for this, assuming that a portion of the unbalanced moment is transferred through an eccentricity of shear around the loaded area. Although beyond the scope of this phase of this project, a more accurate prediction of ultimate strength might be attained by varying the shape of the

176

critical perimeter and applying the eccentric shear model. Currently AASHTO LRFD Bridge Design Specifications do not include an eccentric shear model.

45°

observed shape of failure surface

20"x10"
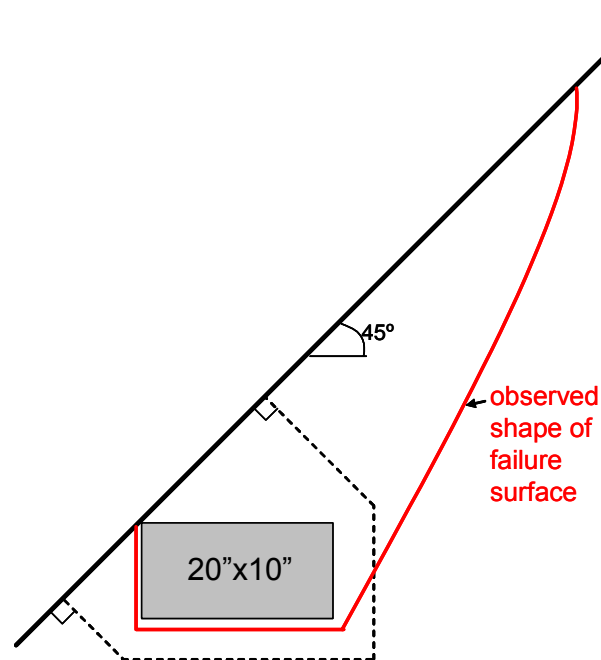
Figure 5-58 Comparison of critical section based on ACI 318-02 and typical failure surface

5.7   SUMMARY

The four tests areas on the 45º skew specimen were constructed as follows:

- IBTS end detail, negative-moment region
- UTSE end detail, negative-moment region
- IBTS end detail, positive-moment region
- UTSE end detail, positive-moment region

Each was loaded with the AASHTO design tandem load configuration. Deflections, reinforcing bar strains, and crack development and propagation are discussed for each test section.

Overall, the UTSE and IBTS end details performed well at HS-20 and HS-25 load levels. At these loads, reinforcing bar strains were insignificant, cracking was minimal, and deflections were extremely small relative to girder spacing (between l/2000 and l/36000). Only the UTSE detail, positive moment test area cracked at the HS-20 load level. The IBTS detail, positive moment test area cracked at the HS-25 load level.

Test areas had high reserve strength: the negative moment tests failed at around 6.0 x HS-25, and the positive moment tests failed at around 4.0 x HS-25. All test areas failed in punching shear, with the exception of the IBTS detail, positive-moment test area, which failed in beam shear.

In UTSE end detail sections, cracks were narrower and more numerous than cracks formed in the IBTS end detail sections. Tensile strains in the transverse reinforcement were significantly lower in the UTSE end detail tests, and no tensile strain measured strains exceeding yield in these sections. The two end details had essentially identical load-deflection responses Because shear failures occurred in all test areas, the IBTS end detail should have the highest reserve strength, because of its greater section depth. In the tests maximizing negative moments, the IBTS end detail had higher reserve strength than the UTSE end detail. In the tests maximizing positive moment, the IBTS end detail had a somewhat lower capacity than the UTSE end detail, due to the geometry of the test specimen causing the formation of torsional cracks at the location of beam-shear failure.

CHAPTER 6

Results from Overhang Tests

6.1 INTRODUCTION

Full-scale tests were conducted to study the performance of standard TxDOT details for overhangs. A total of four overhang areas were tested. As in TxDOT design standards, "breakbacks" (explained below) were constructed in the acute-angle corners of the slab. Because overhangs were not tested in the 0º skew specimen, two tests were developed to simulate a 0º skew overhang in the obtuse-angle corners of the slab. In this chapter, results from those tests are presented and discussed.

6.1.1 Breakback Corners

For slabs constructed with skews greater than 15º, TxDOT design standards require breakbacks at bridge slab corners. "Breakback" is the term used by TxDOT to describe an alternate, simplified method of constructing the acute-angle corners of a skewed slab (Figure 6-1). In this detail, the slab edge is perpendicular to the girders for a transverse distance of 2 ft (607 mm), beyond which it is skewed. All transverse reinforcement in the overhang is parallel to the slab edge.
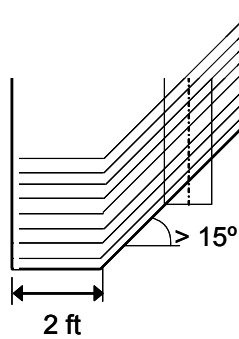
Figure 6-1 Breakback overhang layout

6.1.2 Simulated 0º Skew Corners

In the 0º skew specimen, overhangs were constructed but not tested, so the obtuse-angle overhang corners in the 45º skew specimen were built to simulate corners with zero skew. These corners are similar to the breakback corners, but the reinforcement is bent at the centerline of the girder. A layout of these corners as built in the specimen is shown in Figure 6-2.
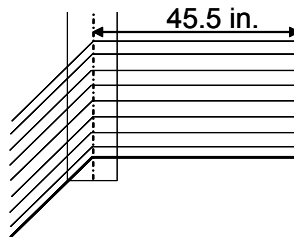
Figure 6-2 Simulated zero skew overhang

6.1.3 Overhang Test Areas

For the 45º skew specimen, four overhang tests were performed:

- 45º skew breakback overhang, IBTS detail
- 45º skew breakback overhang, UTSE detail
- Simulated 0º skew overhang, IBTS detail

180

- Simulated 0º skew overhang, UTSE detail

Two overhangs incorporated the UTSE detail, and the other two, the TxDOT IBTS detail. In the UTSE overhangs, 12 transverse reinforcing bars were placed 2.3 in. (58 mm) from the top of the slab, and 12 were placed 1.63 in. (41 mm) from the bottom of the slab. All transverse edge reinforcement in the UTSE detail was continuous into the overhangs, parallel to the slab edge. To illustrate how the transverse reinforcement is bent in the overhangs, a plan view of the top mat of the UTSE transverse reinforcement is shown in Figure 6-3(a) and (b).

| (a) | (b) |
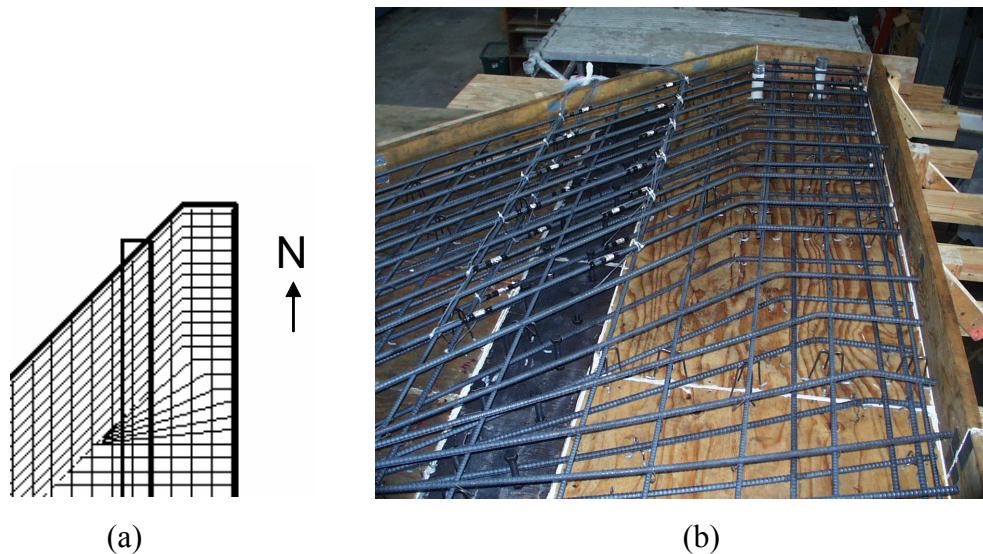
Figure 6-3 UTSE overhang reinforcement, top and bottom mats: (a) plan view drawing; (b) picture

In the TxDOT detail, the depth of the slab was reduced from 10 in. in the IBTS end detail to 8 in. in the overhang. This 2-in. (508 mm) reduction prevented the bottom transverse reinforcement from continuing into the overhang. Instead, four No. 5 bars were placed parallel to the edge in the overhang, 1.63 in. (41 mm) from the bottom of the slab. The 8 transverse reinforcing bars in the top mat were 2.3 in. (58 mm) from the top of the slab, and were continuous into the overhang.

6.1.4 Overhang Length

The standard overhang length of a TxDOT highway bridge is 3 ft (914 mm), measured from the centerline of the girder to the slab edge. Designs using AASHTO provisions do not require the center of the loading footprint to be placed in the outer 2 ft (607 mm) of the overhang. The 2-ft (607-mm) distance represents the nominal width of a guardrail (1 ft, 304 mm) and the distance from the edge of a group of tires to the center (1 ft, 304 mm). Therefore, in a standard 3-ft (914 mm) overhang, the center of a load plate could be placed at most 1 ft (305 mm) from the centerline of the beam. For the 20- by 10-in. (508- by 254-mm) loading plate footprint required by AASHTO, most of the loading plate would be located directly over the beam, a case not of interest for this research (Figure 6-4a).
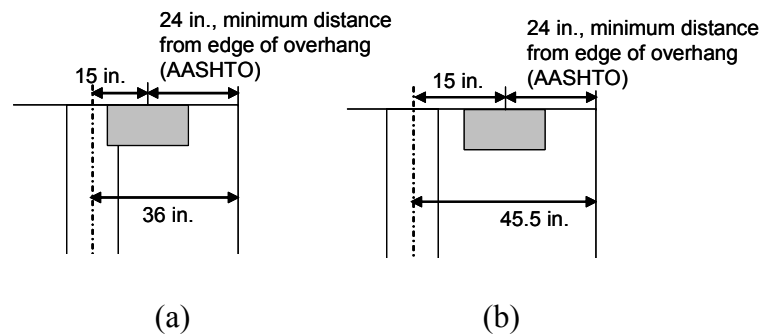
Figure 6-4 Loading plate location: (a) standard 36-in. overhang; (b)45.5-in. overhang

In a horizontal curved bridge with a radius of 600 ft (183 m), overhangs might be as much as 45.5 in. (1155 mm) wide measured from the edge of the girder. Figure 6-4(b) shows the location of the loading footprint for a 45.5-in (1155 mm) overhang. This extreme, rare case was the basis for the construction of the 45.5-in (1.15 m) overhangs in the 45º skew specimen, enabling the load plate to be placed further toward the edge of the overhang. The capacity of the

extended overhang was tested with the center of the load plate placed 24 in. (610 mm) from the edge of the overhang, as shown in Figure 6-5.

(a)	(b)
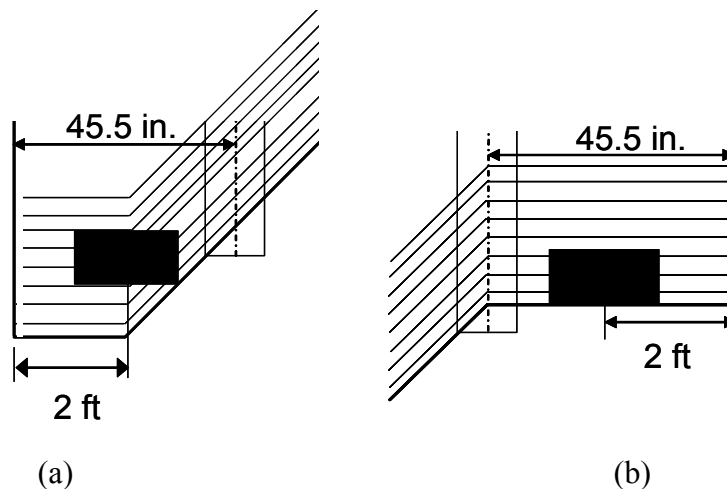
Figure 6-5 Loading plate location: (a) breakback corner; (b) simulated 0° skew corner

6.1.5   AASHTO Loads on Overhangs

Two configurations of AASHTO design loads were considered for this project: the AASHTO truck with a single axle; and the AASHTO truck with two tandem axles. These two loading configurations are discussed in more detail in Section 3.2.3. Using either of these configurations, only a single load plate placed on the overhang is considered. Because the single-axle load is the higher of the two configurations, it is the basis for the HS-20 loads for the overhang tests. Throughout Chapter 6, the load reported as HS-20 is 16 kips (71 kN) per load plate. This is a change from Chapter 5, where HS-20 loads were 12.5 kips (56 kN) per load plate, based on the tandem-axle loading configuration.

6.2 BREAKBACK OVERHANG, IBTS END DETAIL

The breakback corner built with the IBTS end detail was loaded until it failed in beam shear along the girder at 2.75 x HS-20, or 45 kips (200 kN). Figure 6-6 shows where the instrumentation was located and where load was applied. Strain gauges placed on either side of the girder on the top and bottom mats of transverse reinforcement were monitored during testing. Deflection measurements were made at the corner of the slab with linear potentiometers and string potentiometers. Because the spans between the girders had been tested before the overhangs, the slab at the overhang girder was severely cracked near the overhang test sections and in the neighboring span regions. Due to this previous cracking, a discussion of first cracking is less relevant in a discussion of overhang test results than in the span test results and is omitted from this chapter.
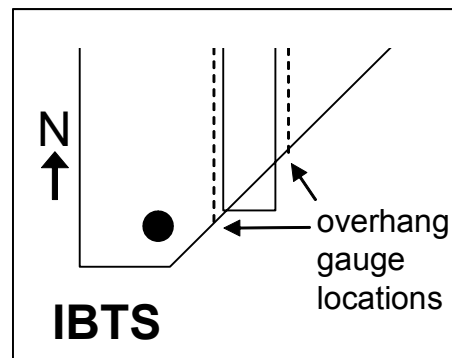
Figure 6-6 Breakback IBTS overhang

6.2.1 Load-Deflection Behavior

All deflections presented in this chapter are tip deflections, measured at the corner of the slab. The initial stiffness of the load-deflection plot may have been greater than the stiffness recorded during testing. Figure 6-7 shows that tip deflection for the breakback IBTS corner was 0.21 in. (5 mm) at HS-20 and 0.27

in. (7 mm) at HS-25. At 1.75 x HS-25, it was 0.76 in. (19 mm). The largest
deflection measured before failure was 1.34 in. (34 mm).
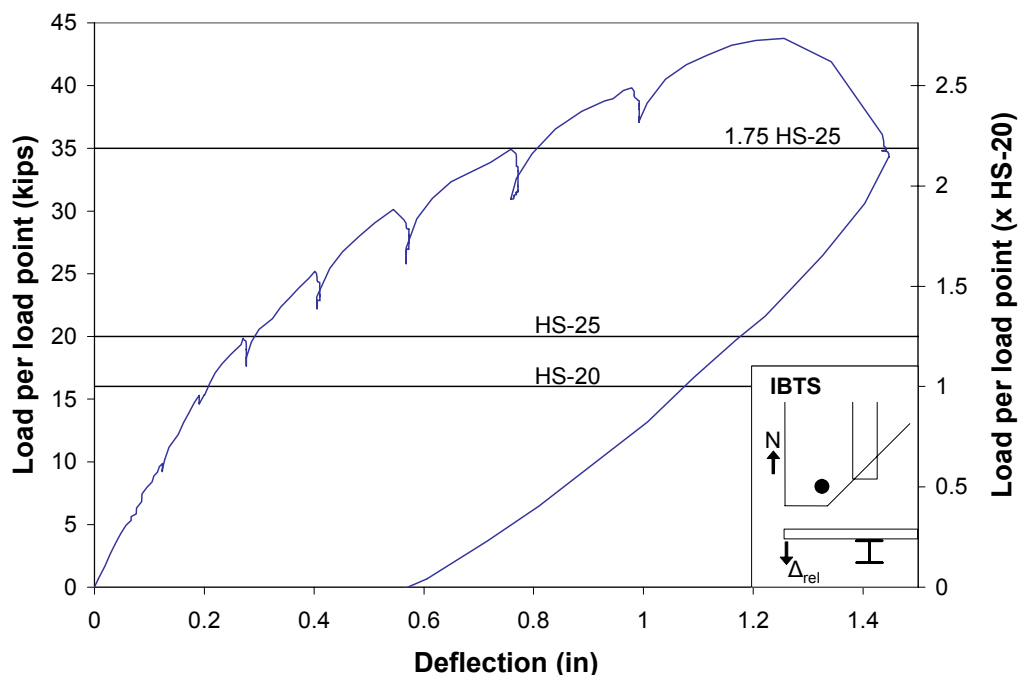
Figure 6-7 Tip deflection, breakback IBTS overhang

6.2.2   Load-Strain Response

Figure 6-8(a) and (b) show tensile strain measured at gauges on either side
of the east-exterior girder. The largest residual strain measured in this test area
from previous tests was 20$\mu\varepsilon$, less than 1% of the yield strain. For all gauges
installed over the overhangs, residual strain was equally small, less than 10% of
the yield strain. Because tensile strains less than 10% of yield are insignificant,
residual strains were not included in strains reported for overhang tests. The
strain plotted is from the gauge indicating the largest strains. For most tests, this
was the strain gauge at the transverse reinforcing bar closest to the edge. Yield
strain was determined by tensile tests on steel reinforcement (Section 4.5.1).

185

Because the load point was located on the west side of the girder, strains on the west side are discussed first. At HS-20, the maximum strain on the west side of the girder was 18% of yield strain (386$\mu\epsilon$), increasing to 25% of yield (540$\mu\epsilon$) at HS-25. At 1.75 x HS-25, the strain increased to 83% of the yield strain (1815$\mu\epsilon$). Instrumented reinforcement first yielded on the west side of the girder at 2.0 x HS-25 (40 kips). The maximum strain on the west side of the girder was 1.3 ϵ_y (2900 $\mu\epsilon$).

On the east side of the girder, the maximum strain at HS-20 was 30% of yield (665 $\mu\epsilon$) and at HS-25, 37% of yield strain (810 $\mu\epsilon$). At 1.75 x HS-25, it was 77% of yield strain (1700 $\mu\epsilon$). Reinforcement on the east side of the girder first yielded at 2.1 x HS-25 (43 kips). The largest strain measured before failure was 1.06 ϵ_y (2330 $\mu\epsilon$).
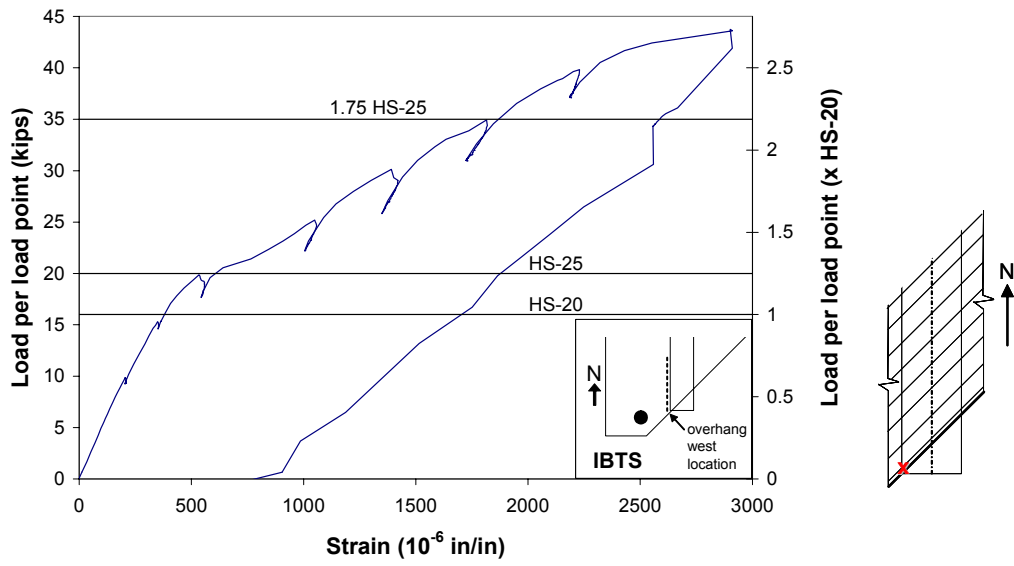
(a)

Figure 6-8 Load-strain response, breakback IBTS overhang: (a) west side of girder, top mat; (b) east side of girder, top mat

(b)
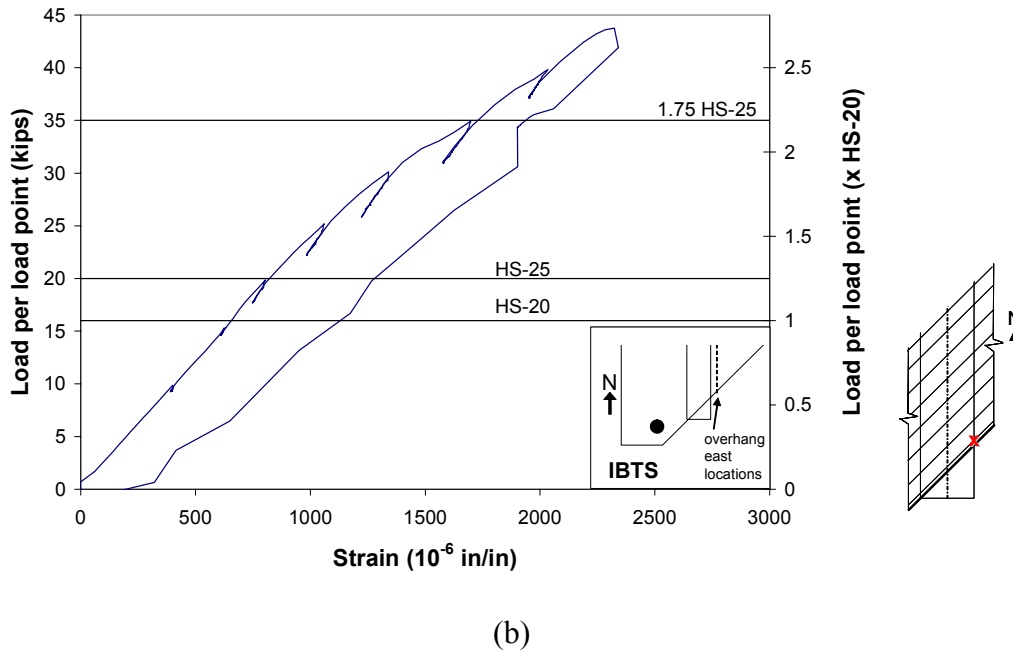
Figure 6-8 cont'd. Load-strain response, breakback IBTS overhang: (a) west side of girder, top mat; (b) east side of girder, top mat

6.2.3 Strain Profiles

Strain profiles were used to compare strain readings from reinforcing steel in the test area on both sides of the girder, and to summarize the distribution of strain in the end section. The profiles show the strain in the reinforcement at explicit load steps. A more detailed discussion of strain profiles is given in Section 5.2.3.

As shown in Figure 6-9(a) and (b), tensile strains were greater closer to the slab edge, and as applied loads increased, the gradient increased. Up to failure, strain levels were small in the end detail, and yielding of reinforcement was limited to only three bars in the end detail. In addition, tensile strain levels measured on the east side of the girder were similar to corresponding strain levels on the west side.
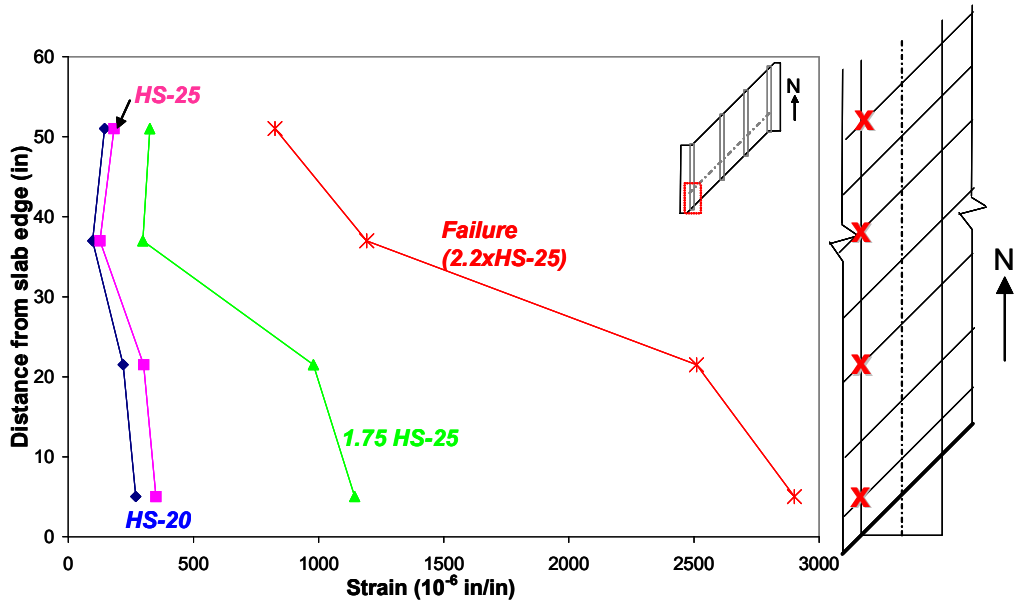
(a)
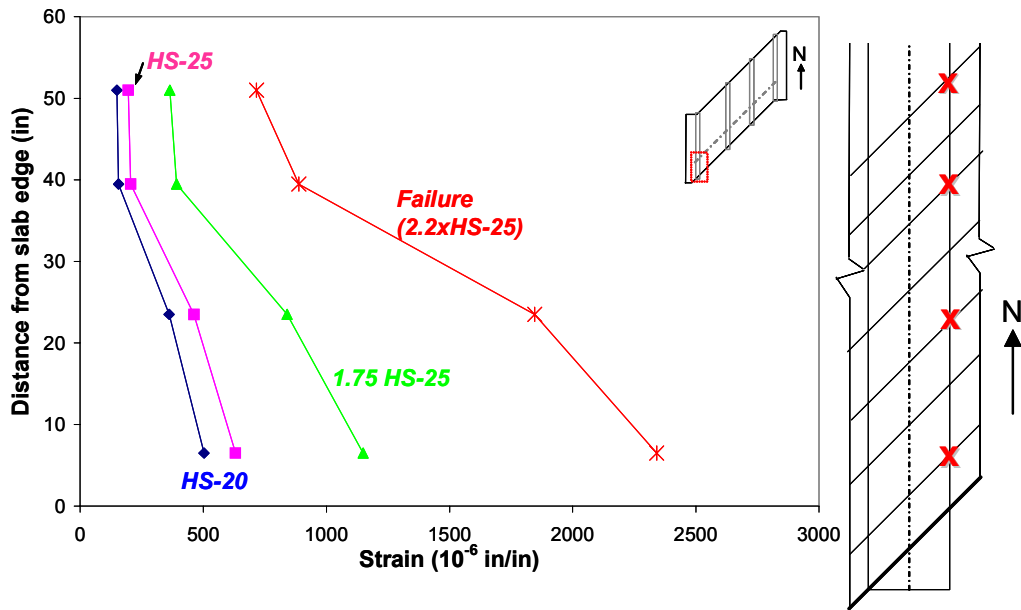
(b)

Figure 6-9 Strain profiles, breakback IBTS: (a) west side of girder, top mat; (b)

east side of girder, top mat

189

6.2.4   Crack Maps

Tests were performed on the overhangs after all span tests were completed, so the slab was severely cracked near the overhang test sections and in neighboring span regions. Because of previous cracks in overhang areas, a discussion of first cracking is less relevant than in the slab end tests. Although the loads at which first new cracks were observed is reported, crack maps are not drawn for first cracking as in Chapter 5. Instead, the formation of crack patterns in each overhang test area is discussed, and crack maps are drawn only at failure.

Figure 6-10(a), (b), and (c) show three views of the breakback IBTS overhang at failure load levels. The chart in Figure 6-10(c) shows the lengths and widths of cracks, as measured during testing. Cracks in the overhang area are frequently curved, complicating measurement of their length. During testing, lengths were carefully measured in segments along each curved crack; nevertheless, the lengths reported here and in the rest of the chapter are approximate. At 1.0 x HS-20, cracks that had formed during previous testing began to widen. New cracks were first observed in the test area at 1.3 x HS-25. As load was increased, cracks formed on the top of the deck perpendicular to the skewed end in the overhang, but parallel to the girder above the girder (Figure 6-10a). A single torsional crack formed below the deck, perpendicular to the cracks visible on the top. Both flexural, torsional, and shear-induced cracking is evidenced by the cracking patterns visible after failure.

(a) top view

(b) bottom view
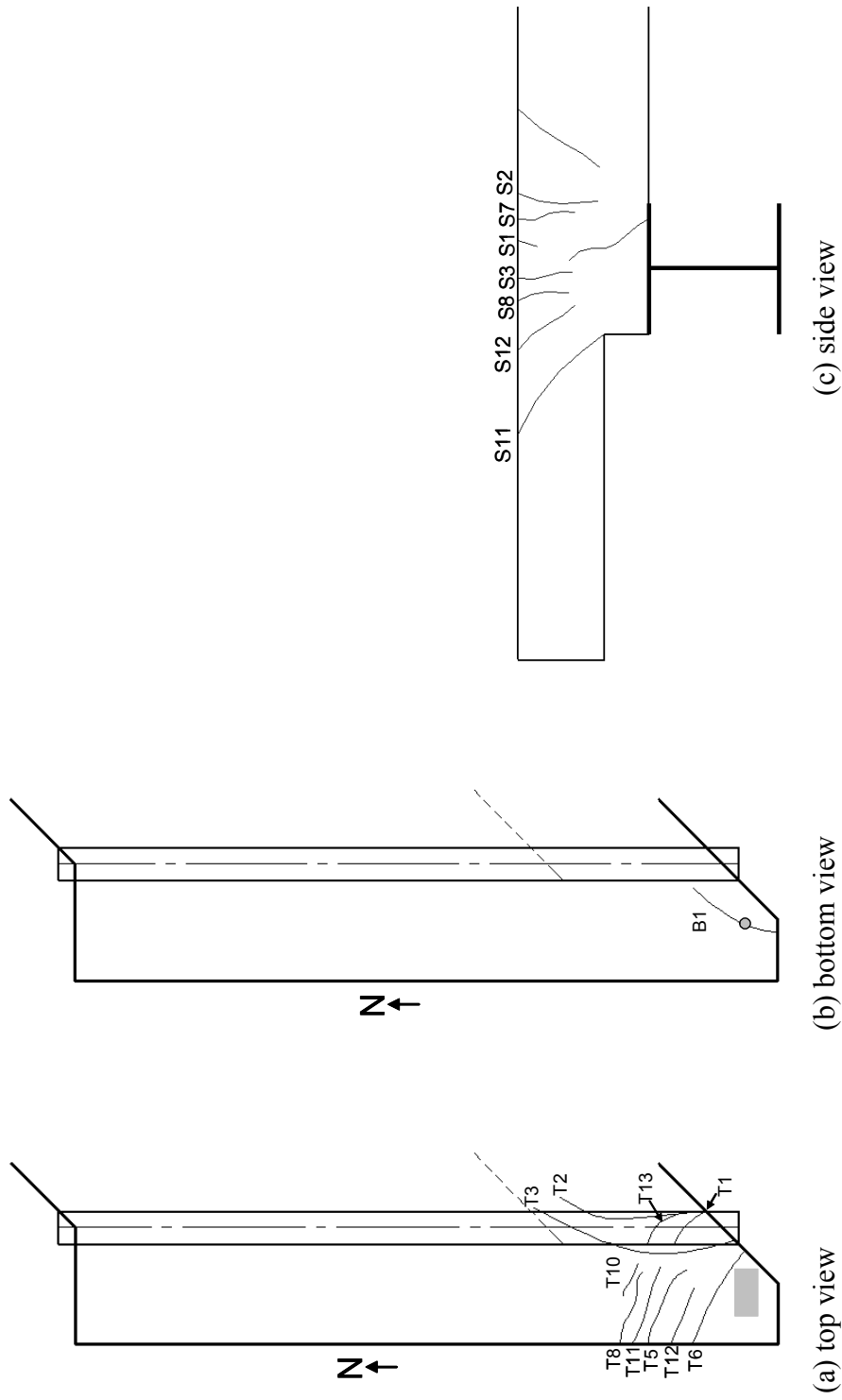
(c) side view

Figure 6-10 Crack map at failure, breakback IBTS overhang: (a) top view; (b) bottom view; (c) side view, facing north; (d) key to crack widths and lengths at failure

191

Top of Deck		
Crack Name	Width (in)	Length (in)
T1	0.010	19
T2	0.040	121
T3	0.030	142
T4	0.013	28
T5	0.013	33.5
T6	0.010	48.5
T8	0.013	50.5
T10	0.005	18
T11	0.009	40
T12	0.010	36
T13	0.007	21.5

Bottom of Deck		
Crack Name	Width (in)	Length (in)
B1	0.01	46

Side of Deck		
Crack Name	Width (in)	Length (in)
S1	0.04	10
S2	0.03	6.5
S3	0.013	9
S7	0.007	5
S8	0.005	4
S11	0.025	11.5
S12	0.025	5.5

Figure 6-10 cont'd. Crack map at failure, breakback IBTS overhang: (a) top view; (b) bottom view; (c) side view, facing north; (d) key to crack widths and lengths at failure

192

6.2.5 Appearance after Failure

Figure 6-11 and Figure 6-12 show the breakback IBTS overhang at failure. The failure surface could be clearly seen only from the side of the deck. At failure, a shear crack, originating from the bottom of the slab, propagated to the corner of the load plate at the top of the deck (Figure 6-12). This crack originated at the change in slab depth at the edge of the girder, but could not be seen from beneath the slab. Although the existing cracks on the top of the slab opened wide during failure, the shear crack visible on the side of the deck was not visible from the top.

The overhang failed in one-way shear at a section beneath the east side of the load plate (the side of the load plate closest to the girder). The failure surface was visible primarily from the side of the deck; from beneath the slab, only a short length of the failure surface (less than 2 in. or 51 mm) could be seen.
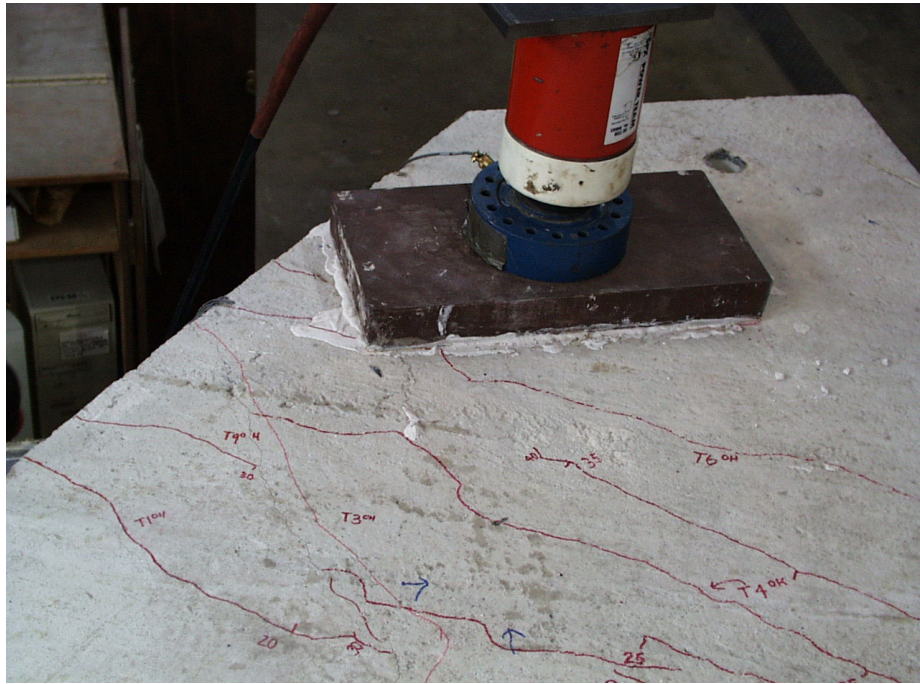
Figure 6-11 Failure of breakback IBTS overhang, top view, facing south

Figure 6-12 Failure of breakback IBTS overhang, side view, facing northeast

194

6.2.6   Summary of Breakback IBTS Overhang Test

The breakback IBTS overhang failed in one-way shear at 2.2 x HS-25 (45 kips). Cracks formed parallel to the skewed slab edge. Yielding of reinforcement in tension was first detected at 2.0 x HS-25 (40 kips) on the west side of the girder (the side closest to the load plate). The tip deflection at HS-20 was 0.21 in. (5 mm) and at HS-25 was 0.27 in. (7 mm). Crack patterns indicate that torsion played an important role in the inelastic range of the load-deflection response.

6.3   BREAKBACK OVERHANG, UTSE END DETAIL

A sketch of the breakback corner built with the UTSE end detail is shown in Figure 6-13. Strain gauges on either side of the girder at the top and bottom mats of transverse reinforcement were monitored during testing. Deflections were measured at the corner of the slab with linear potentiometers and string potentiometers. The area was loaded until it failed in one-way shear at 1.8 x HS-25, or 36 kips (160 kN).
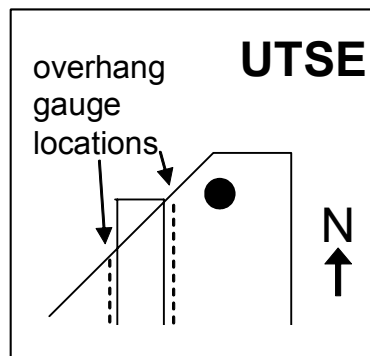
Figure 6-13 Breakback UTSE overhang

6.3.1   Load-Deflection Behavior

Figure 6-14 shows load versus corner deflection for the breakback UTSE overhang. The tip deflection measured at HS-20 was 0.3 in. (8 mm), and at HS-25, 0.41 in. (10 mm). At 31 kips (138 kN), both the string potentiometer and the

195

linear potentiometer malfunctioned, possibly due to the loss of connection between the instrumentation and computer. Just before the malfunction, the measured tip deflection was 0.8 in. (20 mm).
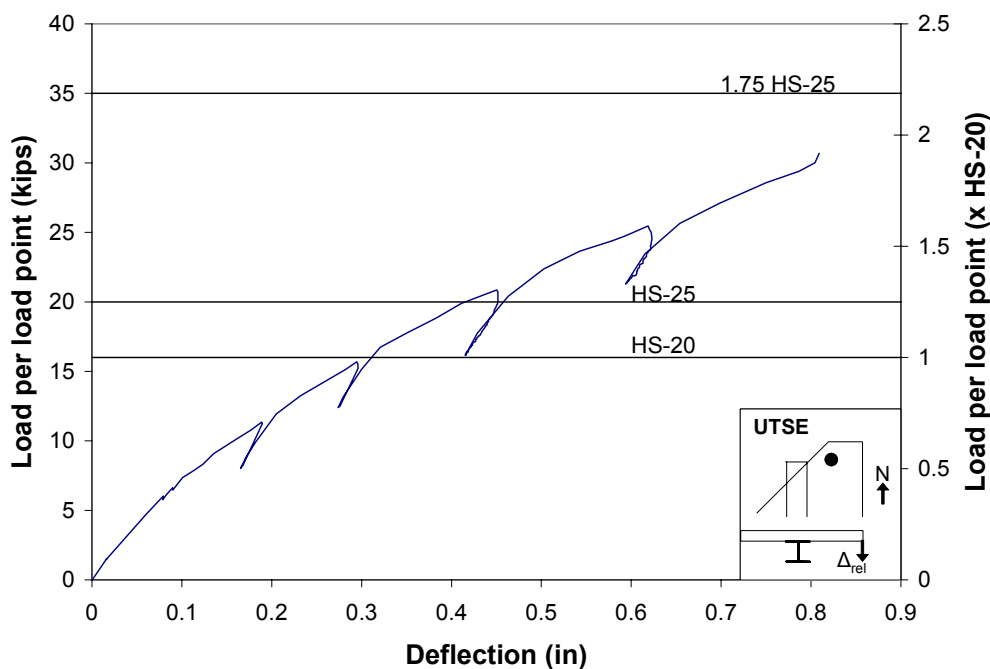
Figure 6-14 Tip deflection, breakback UTSE overhang

6.3.2 Load-Strain Response

Figure 6-15(a) and (b) show the strain measured at gauges on either side of the east exterior girder. The strain plotted is from the gauge that read the largest strains for the majority of the test, as indicated in the graphic to the right of the plot. For this overhang test, the critical gauges were at locations closest to the slab edge.

At HS-20, the maximum strain measured on the east side of the girder was 41% of yield strain (910 με), and the strain measured on the west side of the girder was 19% of yield (415 με). At HS-25, the maximum strain on the east side

of the girder increased to 53% of yield strain (1170 με), and the maximum strain on the west side of the girder was 28% of yield strain (605 με). First measured yield of reinforcement occurred at 2.1 x HS-20 (34 kips) on the east side of the girder. The largest strain measured before failure was 1.2 ε_y (2530 με), measured on the east side of the girder.
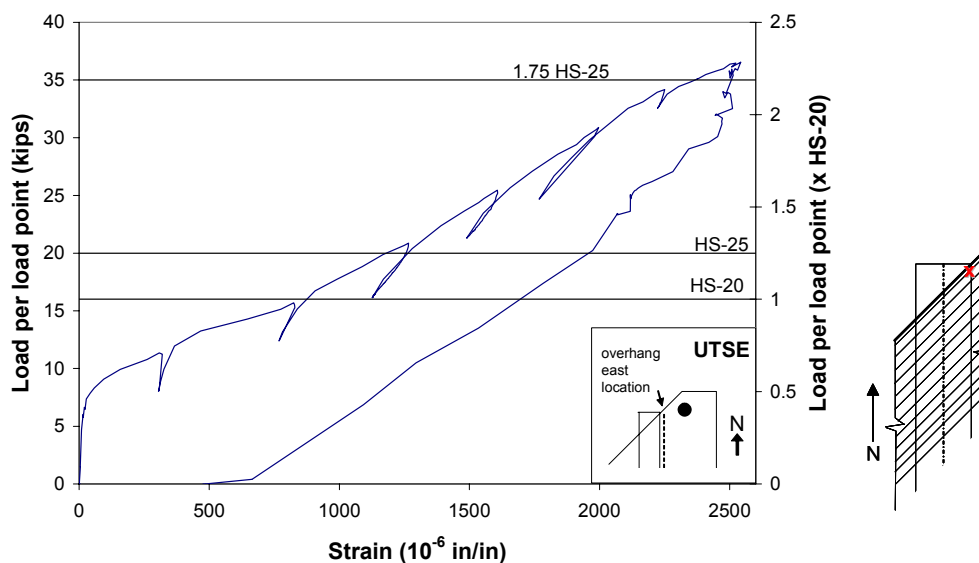
(a)

Figure 6-15 Load-strain response, breakback UTSE overhang: (a) east side of girder, top mat; (b) west side of girder, top mat
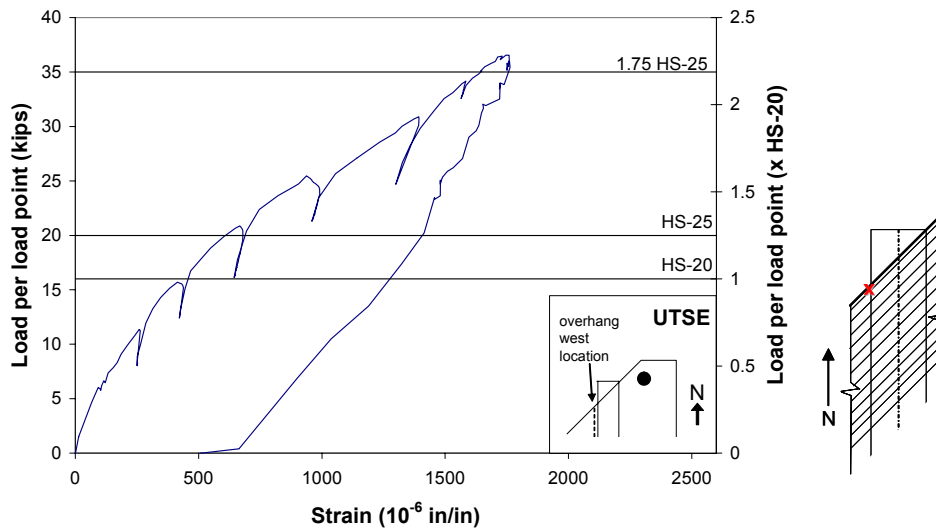
(b)

Figure 6-15 cont'd. Load-strain response, breakback UTSE overhang: (a) east side of girder, top mat; (b) west side of girder, top mat

6.3.3 Strain Profiles

Figure 6-16(a) and (b) show tensile strains measured on the east and west side of the girder at design load and at overload levels up to failure. For these two sections, strain decreased nearly linearly with longitudinal distance into the slab, and the gradient increased as applied loads increased. On the east side of the deck, strains at HS-25 were as much as 2.25 times the corresponding strains at HS-20. On the west side, strains at HS-25 were as much as 1.44 times the corresponding strains at HS-20. On the east side of the girder, only the reinforcing bar closest to the slab edge reached yield strain.
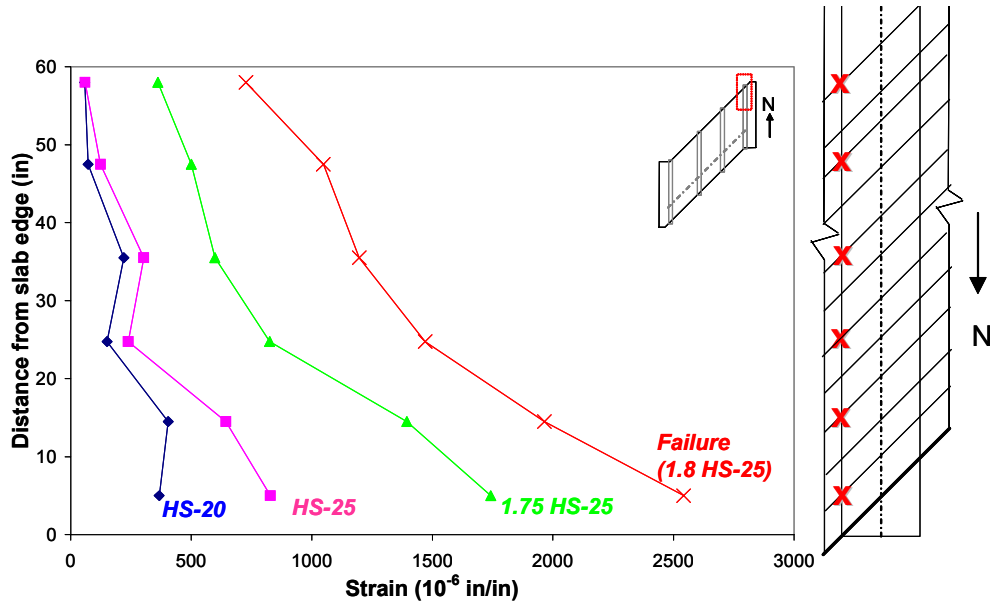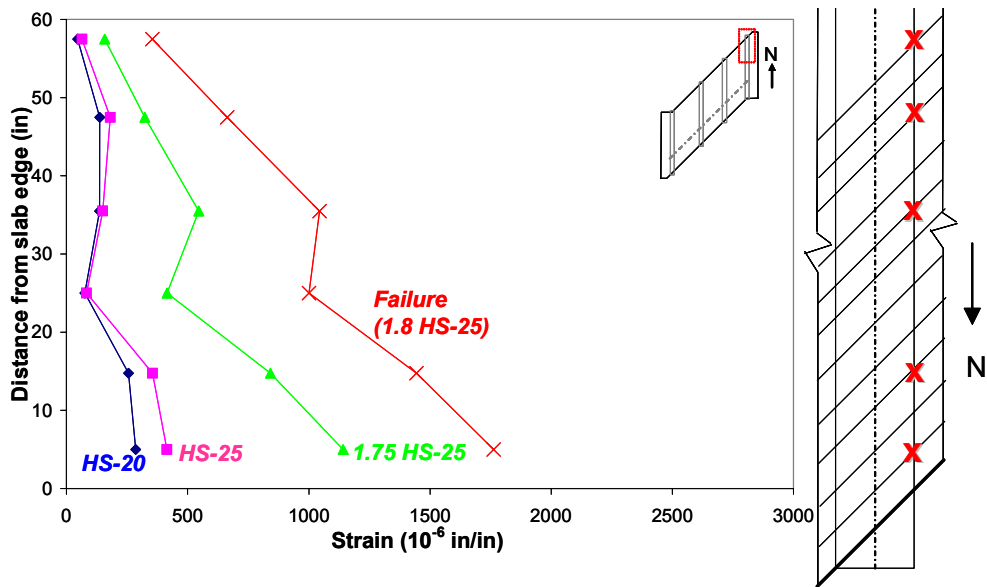
Figure 6-16   *Strain profiles, breakback UTSE overhang: (a) east side of girder, top mat; (b) west side of girder, top mat*

199

6.3.4 Crack Maps

During testing, cracks were first observed at 0.7 x HS-20 on the top and side of the deck. As applied loads were increased, cracks formed primarily perpendicular to the skewed slab end and parallel to the girder over the girder (Figure 6-17). The pattern of cracks visible on both the top and side of the deck indicate flexural and torsional cracking. Flexural and torsional cracks formed on the top of the deck, were visible on the side of the deck, but did not propagate through to the bottom of the deck. Shear cracks were visible on the side of the deck at failure, and are best illustrated in the pictures taken at failure (Figure 6-19).

(a) top view

(b) bottom view
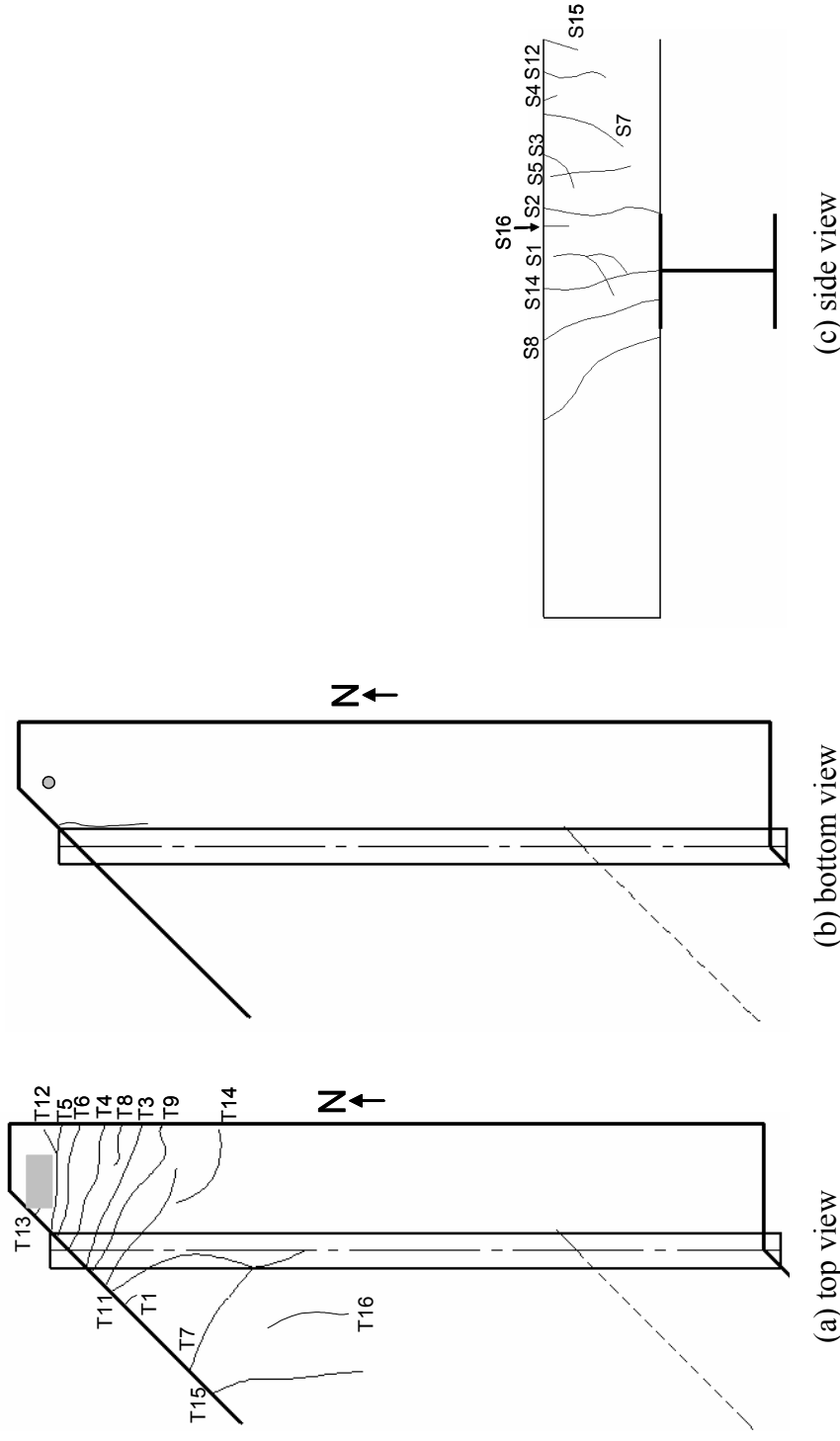
(c) side view

Figure 6-17 Crack maps at failure, breakback UTSE overhang, top view of slab: (a) top view; (b) bottom view; (c) side view, facing south; (d) key to crack lengths and widths at failure

201

Top of Deck			Bottom of Deck			Side of Deck		
Crack Name	Width (in)	Length (in)	Crack Name	Width (in)	Length (in)	Crack Name	Width (in)	Length (in)
T1	0.007	26				S1	0.007	9
T2	0.007	52				S2	0.003	6.5
T3	0.005	64.5				S3	0.007	4.5
T4	0.009	45				S4	HL	1.5
T5	0.030	25				S5	0.007	6
T6	0.009	50				S6	0.02	6
T7	0.003	-				S7	0.003	8
T8	0.007	30.5				S8	0.003	5.5
T9	0.007	73				S12	0.002	5
T11	0.002	4				S14	0.007	6.5
T12	0.003	10.5				S15	HL	4
T13	HL	4				S16	0.002	5.5
T14	0.002	71.5						
T15	0.003	57.5						
T16	HL	29.5						

(d) key to crack lengths and widths at failure, breakback UTSE overhang, top view of slab: *(a) top view; (b) bottom view; (c) side view, facing south; (d) key to crack lengths and widths at failure, *HL = hairline*

Figure 6-17 cont'd. Crack maps at failure, breakback UTSE overhang, top view of slab: (a) top view; (b) bottom view; (c) side view, facing south; (d) key to crack lengths and widths at failure

6.3.5 Appearance after Failure

Figure 6-18, Figure 6-19, and Figure 6-20 show the slab after failure. The shape of the failure surface indicates that this area failed in one-way shear. During failure, a large shear crack formed on the side of the deck, propagating from the edge of the girder leading up to the corner of the load plate (Figure 6-19). No cracks formed on the bottom of the deck during testing; just before failure, however, a failure surface formed beneath the slab at the intersection of the girder and slab (Figure 6-20). Cracking on the bottom of the deck ids difficult to identify in the pictures taken after failure, so the locations of cracks is shown in Figure 6-17b (crack map of the bottom of the deck).

Figure 6-18 Failure of breakback UTSE overhang, top view of slab, facing north

Figure 6-19 Failure of breakback UTSE overhang, side view of slab, facing south

Figure 6-20 Failure of breakback UTSE overhang, bottom view of slab, facing southwest

6.3.6   Summary of Breakback UTSE Overhang Test

The breakback UTSE overhang had the lowest capacity of all the overhang corners tested, failing in punching shear at 2.3 x HS-20 (36 kips). Yield

of reinforcement first occurred at 2.1 x HS-20 (34 kips). The maximum measured strain, on the east side of the girder, was 115% of the yield strain. Strains at HS-25 were as much as 2.3 times strains at HS-20.

6.4   SIMULATED 0º SKEW OVERHANG, IBTS END DETAIL

Two overhangs were constructed to simulate overhangs in a 0º skew slab. The simulated 0º skew overhang built with the IBTS end detail, shown in Figure 6-21, was loaded at the location shown in the figure. As in the tests on breakback overhangs, strain gauges were installed in the simulated 0º skew overhangs on either side of the girder at every other bar of the top and bottom mats of transverse reinforcement. Again, as in the overhang breakback tests, tip deflections were measured at the corner of the slab. This test area was loaded until it failed in punching shear at 2.6 x HS-25, 51 kips (227 kN).
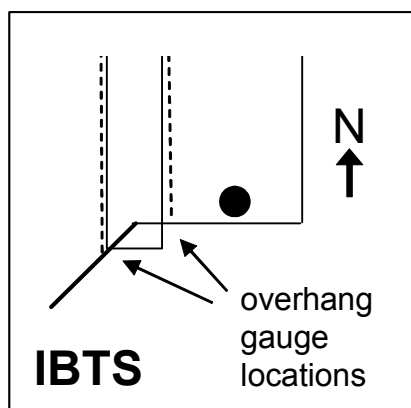
Figure 6-21 Simulated 0º skew IBTS overhang

6.4.1   Load-Deflection Behavior

The load versus tip deflection response was approximately linear up to HS-25 load levels (Figure 6-22). The tip deflection at HS-20 was 0.12 in. (30 mm), and at HS-25, 0.2 in. (51 mm). The tip deflection at 1.75 x HS-25 was 0.65 in. (17 mm). The tip deflection just before failure was 2.2 in. (56 mm).
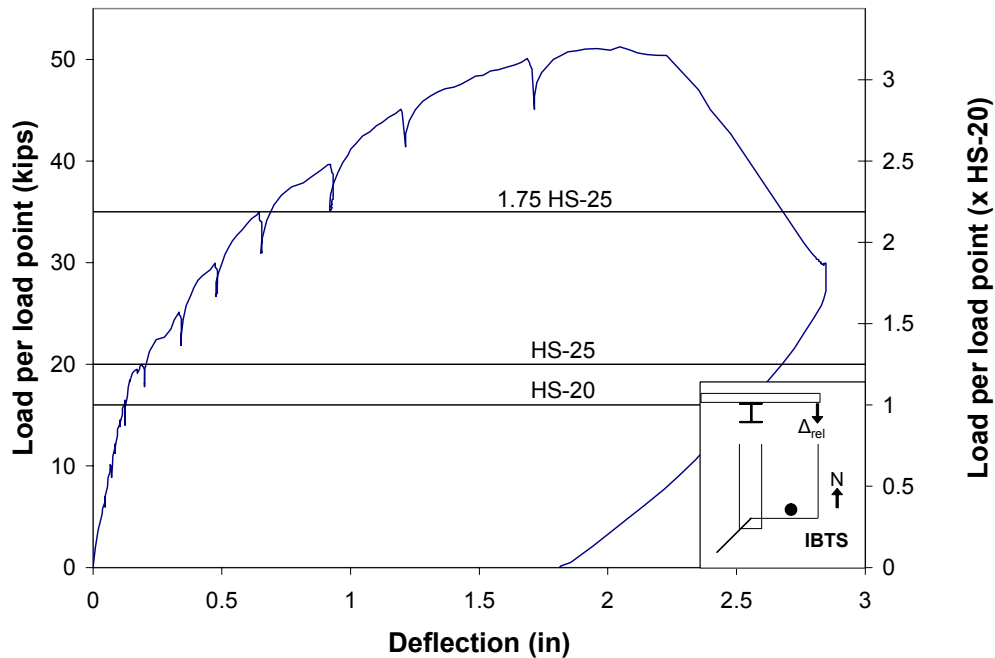
Figure 6-22 Tip deflection, simulated 0º skew IBTS overhang

6.4.2   Load-Strain Response

Figure 6-23(a), (b), and (c) show the tensile strains measured at gauges on either side of the east exterior girder. At load levels near 1.85 x HS-25 (37 kips), multiple gauges near the slab edge malfunctioned due to extensive cracking in the gauge area. On the east side of the girder, the critical gauge (that indicating the largest strain throughout testing) was the gauge closest to the slab edge, The gauge closest to the slab edge that continued to function throughout testing was the one shown in Figure 6-23(b). None of the gauges measuring tensile strain reached yield strain, either due to malfunctioning or to failure of the overhang.

At HS-20, measured tensile strains were insignificant (less than 5% of yield strain). At HS-25, the maximum strain on the east side of the girder increased to 18% of yield strain (400 με), and the maximum strain on the west

side of the girder was 5% of yield strain (105 µε). At 1.75 x HS-25, the maximum strain measured on the east side of the girder was 73% of yield strain. The largest strain measured was 75% of yield strain (1645 µε) measured at 1.85 x HS-25. Though the strain gauges indicated values less than yield strain throughout testing, the tensile strains at failure may have reached yield strain.
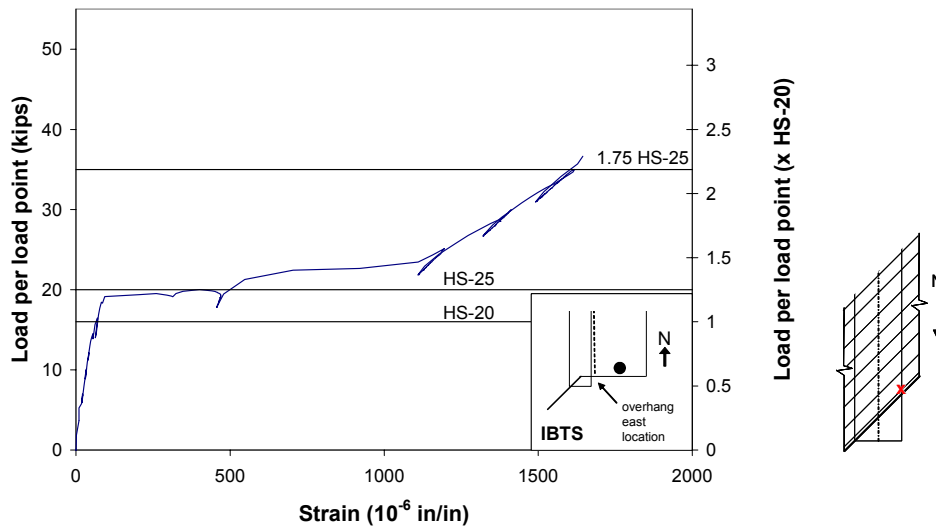
(a)

Figure 6-23 Load-strain response, simulated 0° skew IBTS overhang: (a) east side of girder, top mat, gauge at edge; (b) east side of girder, top mat, interior gauge; (b) west side of girder, top mat

(b)

(c)
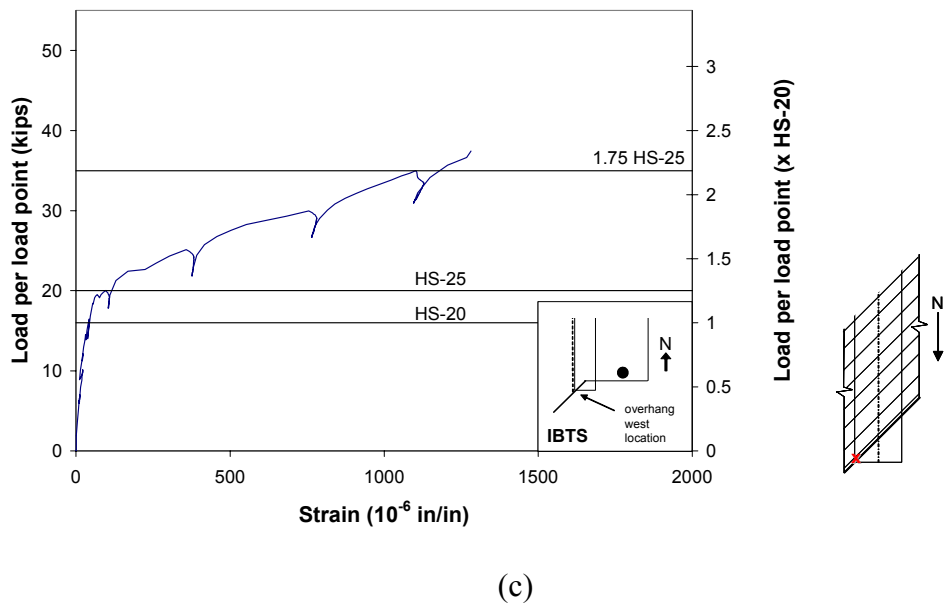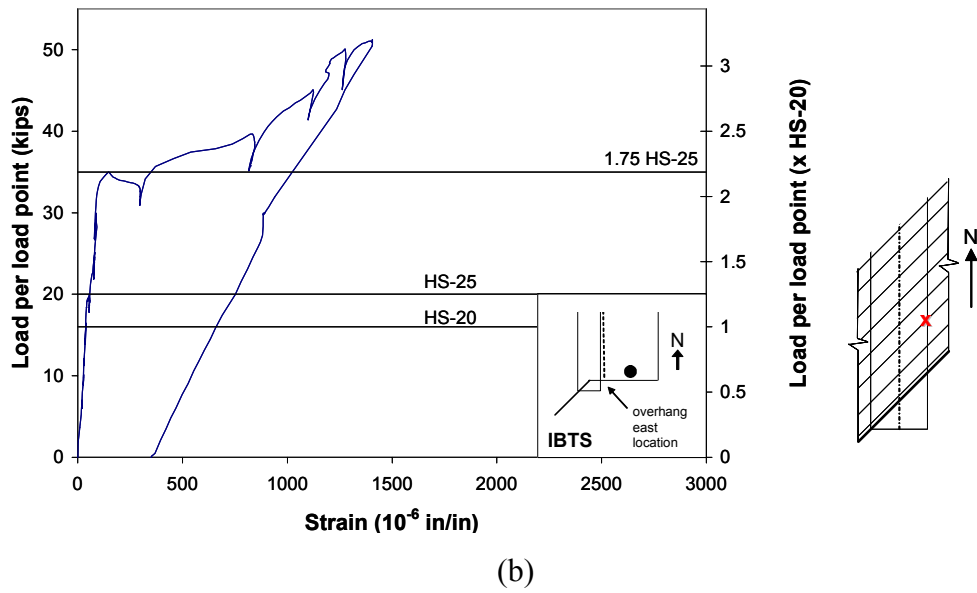
Figure 6-23 cont'd. Load-strain response, simulated 0° skew IBTS overhang:
(a) east side of girder, top mat, gauge at edge; (b) east side of girder, top mat,
interior gauge; (b) west side of girder, top mat

6.4.3   Strain Profiles

Figure 6-24(a) and (b) show tensile strains at every second transverse reinforcing bar on the east and west side of the girder. At these two gauge locations, tensile strains were insignificant at HS-20 and HS-25 load levels (less than 10% of yield strain), and were distributed nearly uniformly though the end section. At 1.75 x HS-25, strain levels at the slab edge were larger than strain levels at the interior of the deck, and varied almost linearly through the deck. Most tensile strain readings at failure are not included here due to gauge malfunctions caused by extensive cracking in the test area (6.4.2).

(a)
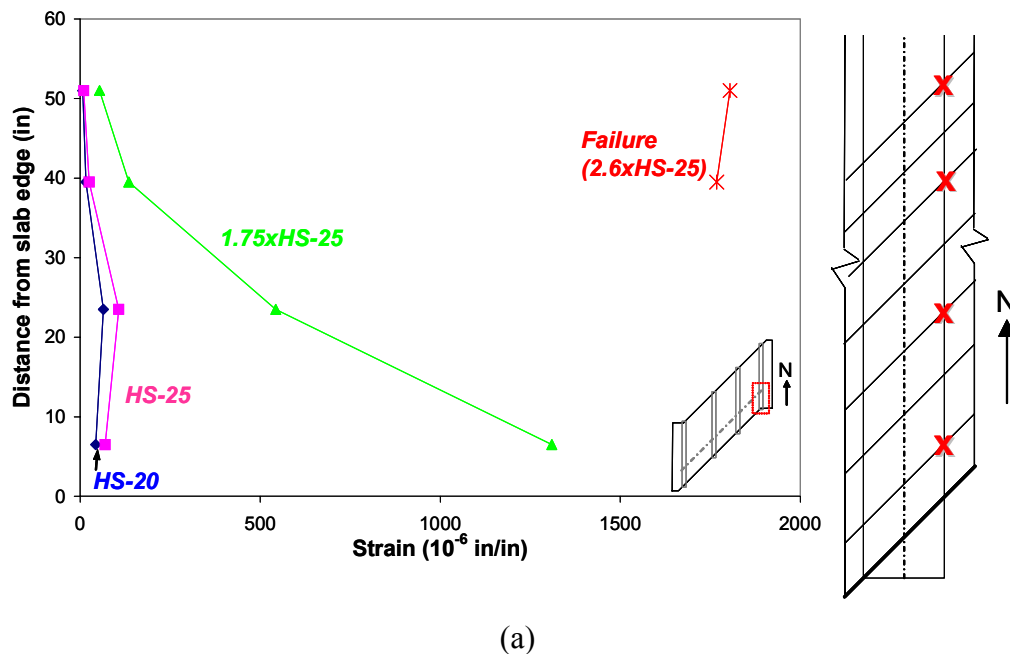
Figure 6-24 Strain profile, simulated 0º skew IBTS overhang: (a) east side of girder, top mat; (b) west side of girder, top mat

209
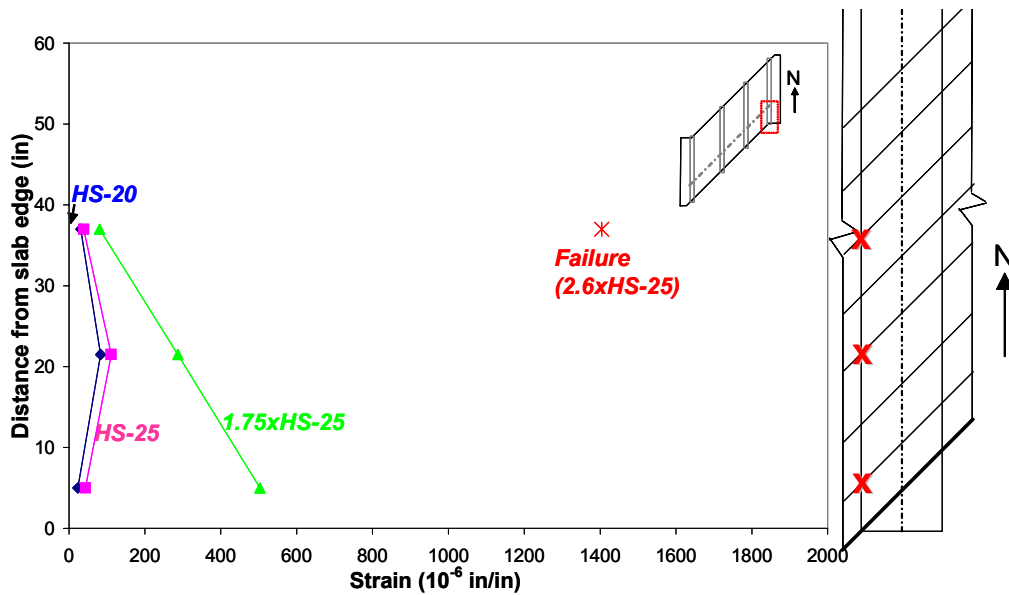
(b)

Figure 6-24 cont'd. Strain profile, simulated 0° skew IBTS overhang: (a) east side of girder, top mat; (b) west side of girder, top mat

6.4.4 Crack Maps

In the simulated 0° skew, IBTS overhang, flexural and torsional cracks were visible on the top and bottom face of the slab before failure (Figure 6-25a, b, and c). Over the girder, flexural cracks formed parallel to the girder at the HS-25 load level, widening to more than 0.25 in. (13 mm) just before failure, and causing severe damage near the girder. Torsional cracking, identified by bottom cracks oriented perpendicular to top cracks, was also pronounced.
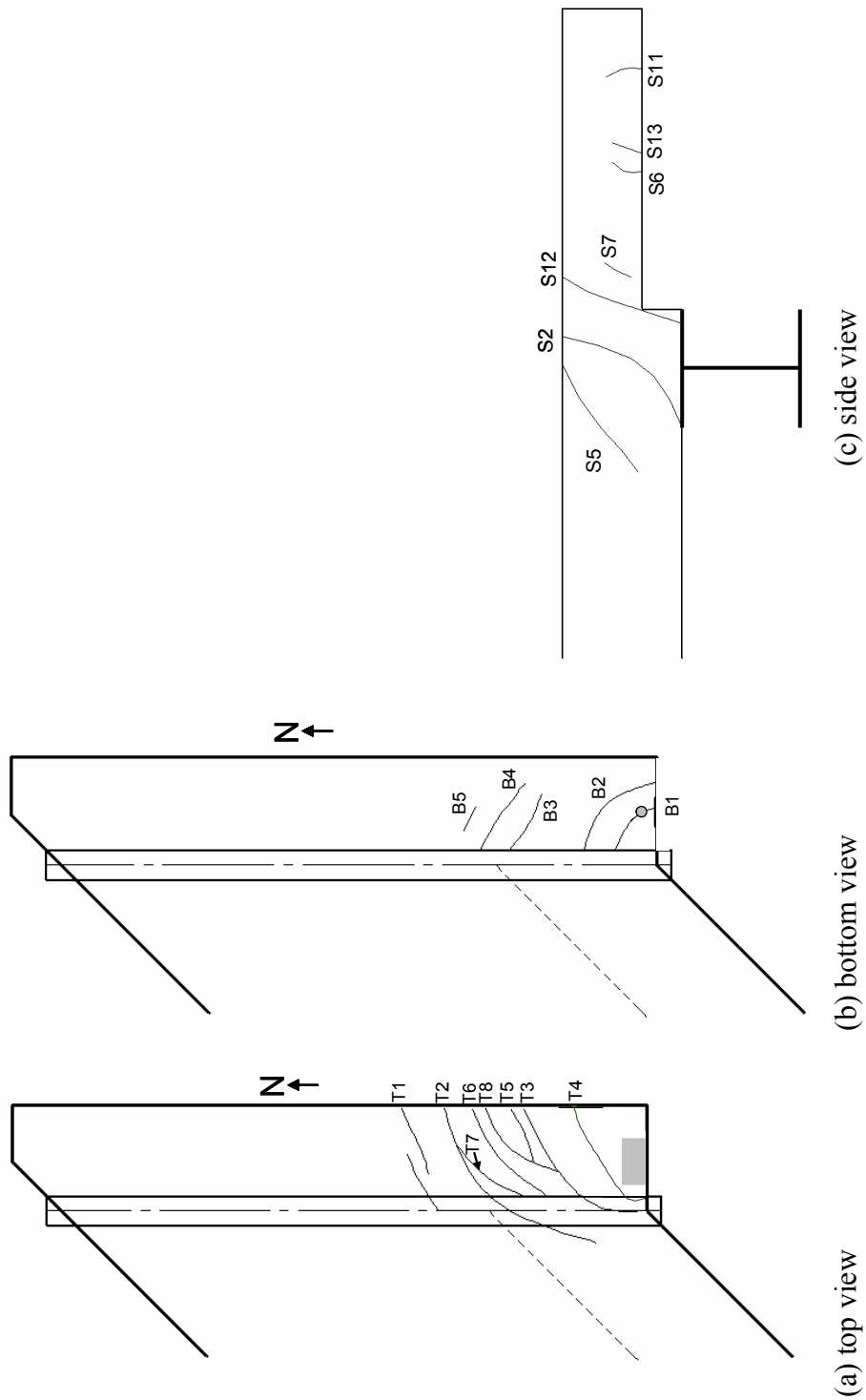
(a) top view

(b) bottom view

(c) side view

Figure 6-25 *Crack maps at failure, simulated 0° skew IBTS overhang: (a) top view of slab; (b) bottom view of slab; (c) side view of slab, facing north; (d) key to crack widths and lengths*

211

Top of Deck			Bottom of Deck			Side of Deck		
Crack Name	Width (in)	Length (in)	Crack Name	Width (in)	Length (in)	Crack Name	Width (in)	Length (in)
T1	0.009	85	B1	0.015	18	S2	0.02	10.5
T2	0.016	180	B2	0.015	46	S5	0.06	12.5
T3	0.250	75	B3	0.007	40	S6	0.003	4.5
T4	0.125	63	B4	0.005	20	S7	0.02	3.5
T5	0.030	60.5	B5	HL	8	S11	0.005	4.5
T6	0.040	69				S12	0.005	12
T7	0.007	32				S13	0.007	4.5
T8	0.007	42						

(d) key to crack widths and lengths at failure, *HL = hairline

Figure 6-25 cont'd. Crack maps at failure, simulated 0° skew IBTS overhang: (a) top view of slab; (b) bottom view of slab; (c) side view of slab, facing north; (d) key to crack widths and lengths

212

6.4.5 Appearance after Failure

Figure 6-26, Figure 6-27, and Figure 6-28 show the slab after failure. The shape of the failure surface indicates that this area failed in punching shear. During failure, a shear crack was visible on the top of the slab around the load plate. This failure surface extended from the free edge of the overhang to slab edge over the girder. From the south side of the deck, a large shear crack could be seen propagating from the crack on the top of the slab; on the east side of the deck, the same shear crack can be traced to the bottom of the deck (Figure 6-28). Although extensive torsional cracking was visible on the top and bottom of the deck during testing, torsional moments did not initiate failure. The failure surfaces on the bottom and on the top surfaces of the deck are parallel to each other, and clearly indicate a two-way shear failure.

Figure 6-26 Failure of simulated 0º skew ITBS overhang, top view of slab, facing east

213

(a) Facing north

(b) Facing northwest

Figure 6-27 Failure of simulated 0º skew IBTS overhang, side view of slab

Figure 6-28 Failure of simulated 0º skew IBTS overhang, bottom view of slab facing west

6.4.6   Summary of Simulated 0º Skew IBTS Overhang Test

The simulated 0º skew IBTS overhang failed in punching shear at 2.6 x HS-25 (51 kips). Tip deflection was 0.12 in. (3 mm) at HS-20 and 0.2 in. (5 mm) at HS-25. Extensive cracking occurred over the girder during testing, causing several strain gauges to malfunction at approximately 1.8 x HS-25. No strain gauge reached yield strain in reinforcement before malfunctioning or before specimen failure, and the maximum strain in this test area, 73% of yield strain, was measured at 1.8 x HS-25. Strains at HS-20 and HS-25 were small (less than 10% of yield strain).

6.5   SIMULATED 0º SKEW OVERHANG, UTSE END DETAIL

The simulated 0º skew UTSE overhang failed in punching shear at 2.7 x HS-25, or 54 kips (240 kN). The graphic of the simulated 0º skew slab corner built with the UTSE end detail, shown in Figure 6-29, illustrates the locations of strain gauges, installed at every second transverse reinforcing bar. As in all other

overhang test areas, deflections were measured at the corner of the slab with linear potentiometers and string potentiometers.
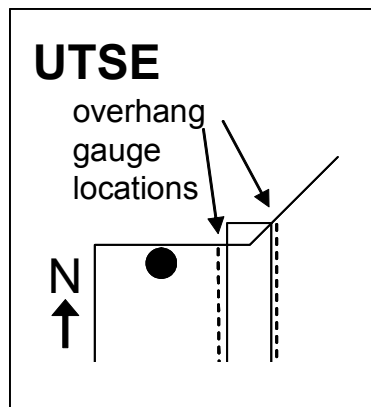
Figure 6-29 Simulated 0º skew UTSE overhang

6.5.1   Load-Deflection Behavior

The load-deflection behavior of the overhang tip, shown in Figure 6-30, indicates that the slab stiffness remained nearly linear up to HS-25 load levels. The measured tip deflection was 0.15 in. (4 mm) at the HS-20 load level and 0.21 in. (5 mm) at the HS-25 load level. At 1.75 x HS-25, the tip deflection was 0.62 in. (16 mm). The last tip deflection measured before failure was 2.7 in. (69 mm).
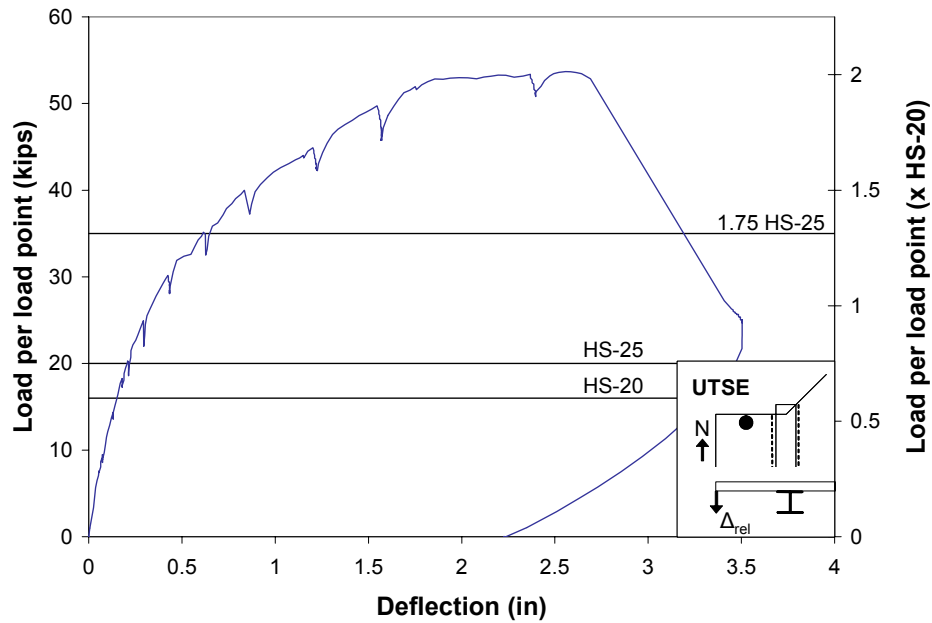
Figure 6-30 Tip deflection, simulated 0° skew UTSE overhang

6.5.2   Load-Strain Response

Figure 6-31(a) and (b) show the strain indicated by gauges on either side of the east exterior girder. At HS-20 load levels, all measured tensile strains were small (less than 5% of yield strain). At HS-25, the maximum strain on the east side of the girder increased to 8% of yield strain (175 με), and the maximum strain on the west side of the girder increased to 10% of yield strain (220 με). At 1.75 x HS-25, the maximum strain measured on the east and west side of the girder was 40% of the yield strain (850με). At 2.7 x HS-20 (43 kips), many gauges on the east side of the girder malfunctioned due to extensive cracking along the girder in this test area. At 3.2 x HS-20, the reinforcing bar closest to the slab edge on the west side of the girder yielded, reaching 2.2 ε_y before failure.

217
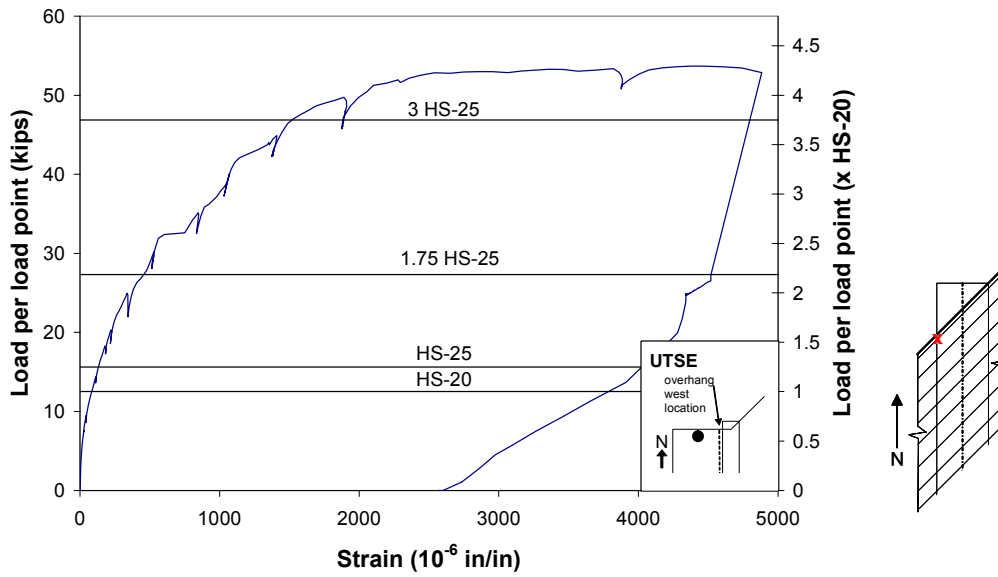
(a)
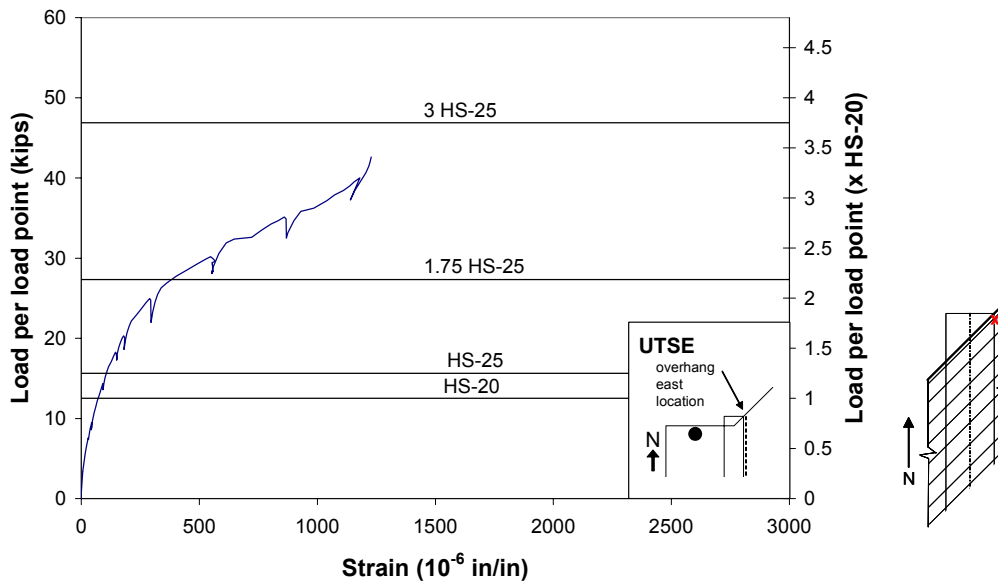
(a)

Figure 6-31 Load-strain response, simulated 0º skew UTSE: (a) west side of girder, top mat; (b) east side of girder, top mat

218

6.5.3 Strain Profiles

Figure 6-32(a) and (b) show strains on the east and west side of the girder at the simulated 0° skew UTSE overhang. At HS-20 and HS-25 load levels, strains are distributed nearly uniformly through the end detail. As load levels increased, strains at the edge of the slab became larger than strains at the interior of the slab. On the east side of the deck, strains at HS-25 were as much as 2 times the corresponding strains at HS-20. On the west side, strains at HS-25 were as much as 1.7 times the corresponding strains at HS-20.
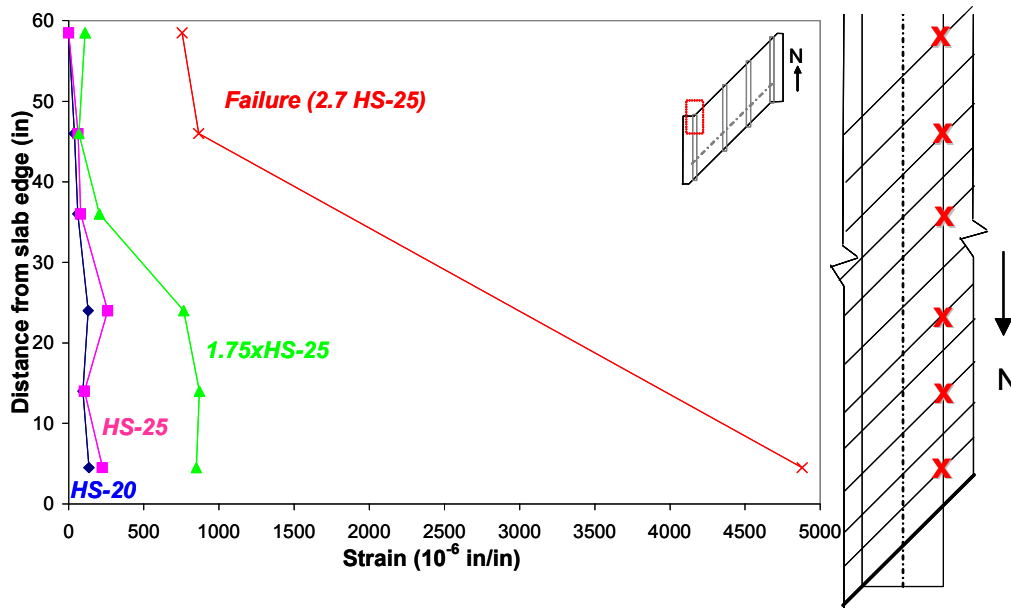
(a)

Figure 6-32 Strain profile, simulated 0° skew UTSE overhang: (a) west side of girder, top mat; (b) east side of girder, top mat
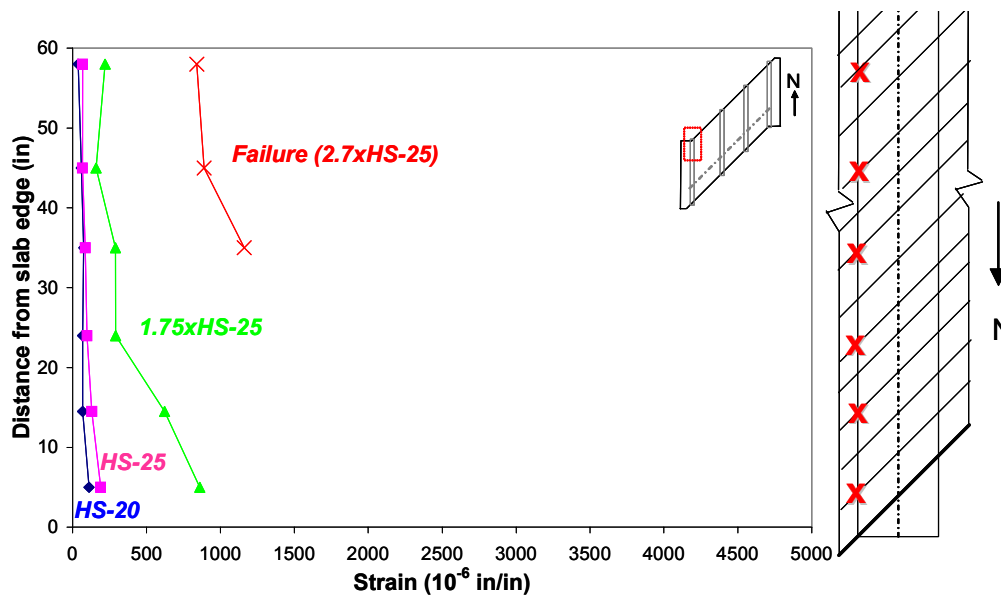
(b)

Figure 6-32 cont'd. Strain profile, simulated 0º skew UTSE overhang: (a) west side of girder, top mat; (b) east side of girder, top mat

6.5.4   Crack Maps

The crack maps shown in Figure 6-33(a), (b), and (c) illustrate the locations of cracks at failure. Extensive torsional cracking occurred above and below the overhang. Torsional cracks on the bottom of the deck extended farther into the interior of the deck than did torsional cracks on the top of the deck. A single shear crack, labeled S8, formed between the girder and the east edge of the load plate (Figure 6-33c, d)

(a) top view

(b) bottom view
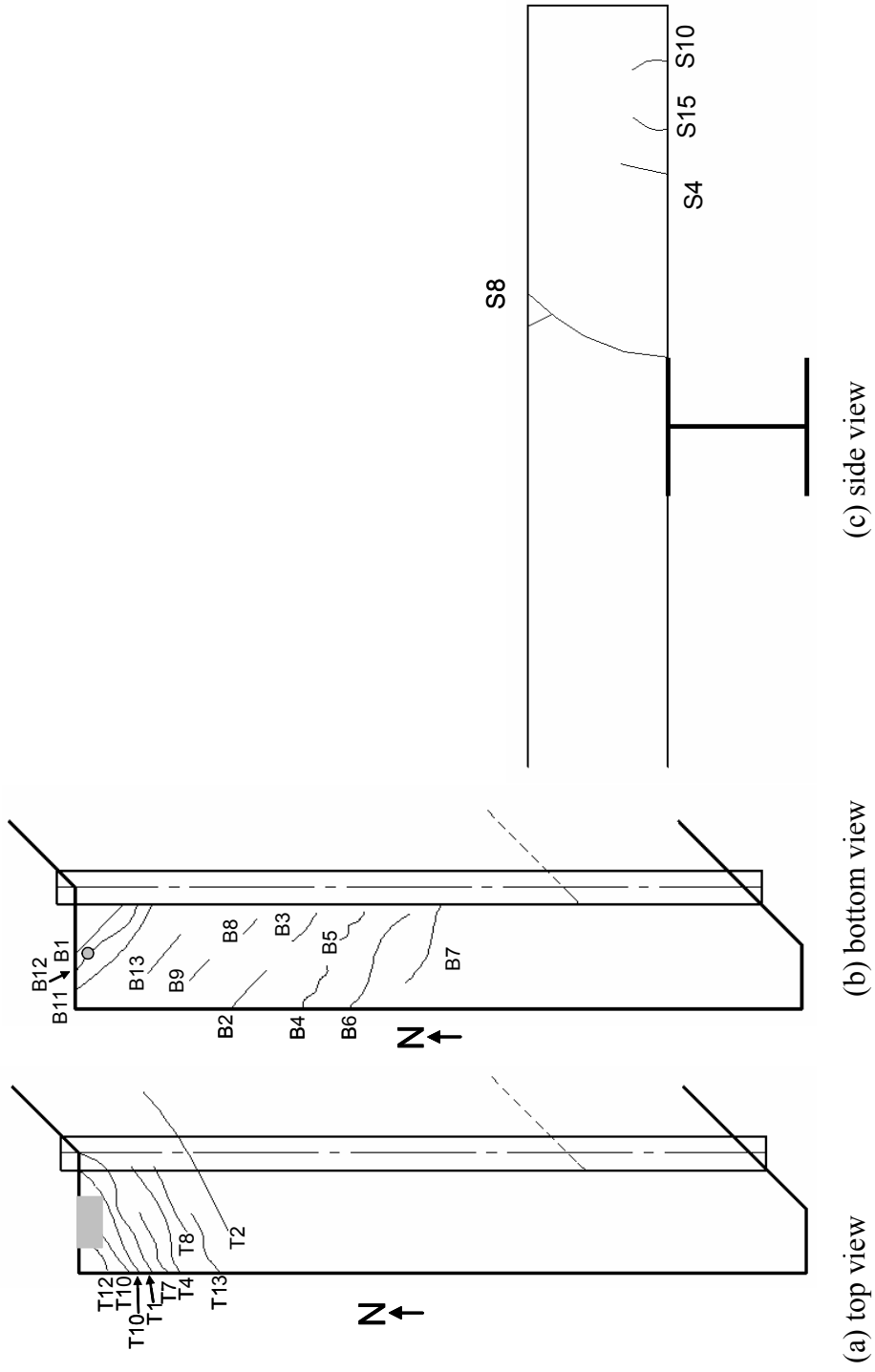
(c) side view

Figure 6-33 Crack maps at failure, simulated 0° skew UTSE overhang: (a) top view of slab; (b) bottom view of slab; (c) side view of slab, facing north; (d) key to crack widths and lengths at failure

221

Top of Deck				Bottom of Deck				Side of Deck		
Crack Name	Width (in)	Length (in)		Crack Name	Width (in)	Length (in)		Crack Name	Width (in)	Length (in)
T1	0.050	89		B1	0.01	21		S4	0.007	5
T2	0.050	98		B2	0.002	17		S8	0.005	10
T4	0.016	69		B3	0.002	17		S10	0.003	3
T5	0.050	61		B4	0.002	19		S15	0.003	3.5
T6	0.025	68		B5	0.002	21				
T7	0.060	93		B6	0.002	48.5				
T8	0.007	43.5		B7	HL	34				
T10	0.025	41		B8	HL	22.5				
T12	0.009	14		B9	0.002	15.5				
T13	0.005	22		B11	HL	26.5				
				B12	0.002	25				
				B13	HL	21				

(d) key to crack widths and lengths, *HL = hairline

Figure 6-33 cont'd. Crack maps at failure, simulated 0° skew UTSE overhang: (a) top view of slab; (b) bottom view of slab; (c) side view of slab, facing north; (d) key to crack widths and lengths at failure

222

6.5.5 Appearance after Failure

Figure 6-34, Figure 6-35, and Figure 6-36 show the slab after failure. Although torsional cracking was most extensive in this test section, extending well into the south side of the deck, the shape of the failure surfaces indicates that this area failed in punching shear rather than torsion. The intersections of the failure surface with the top and bottom of the deck are parallel to each other, and indicate that a punching shear failure surface formed from the free edge of the overhang to the slab edge above the girder.

Figure 6-34 Failure of simulated 0° skew UTSE overhang, top view of slab,
facing north
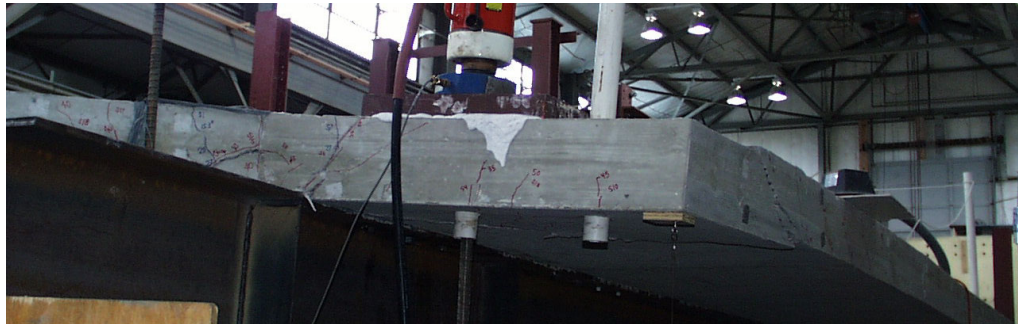
(a) Facing south
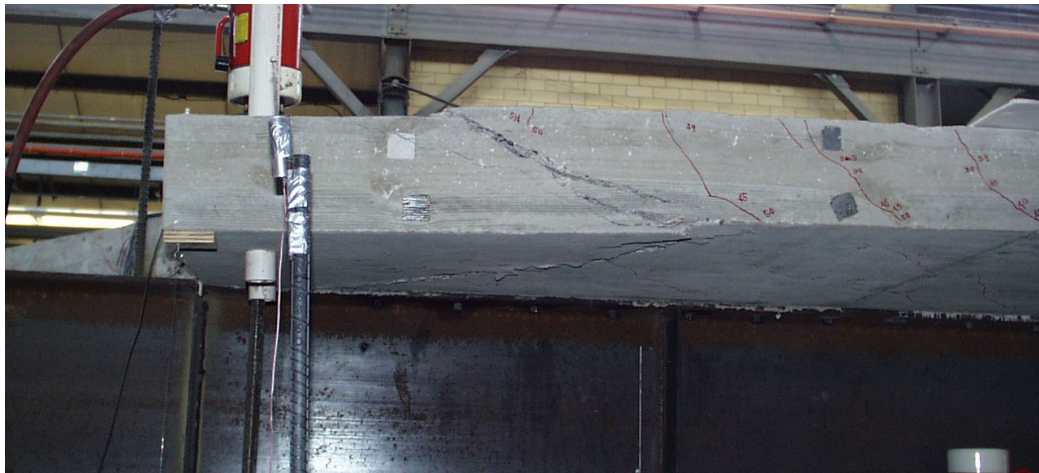
(b) Facing east

Figure 6-35 Failure of simulated 0º skew UTSE overhang, side view of slab

Figure 6-36 Failure of simulated 0º skew UTSE overhang, bottom view of slab, facing east

6.5.6   Summary of Simulated 0º Skew UTSE Overhang Test

The simulated 0º skew UTSE overhang failed in punching shear at 2.7 x HS-25 (54 kips). Tip deflection was 0.15 in. (4 mm) at HS-20 and 0.21 in. (5 mm) at HS-25. Steel reinforcement yield was not detected at a single location on the west side of the girder, but the maximum measured strain on the east side of the girder was 2.2 times the yield strain. While strains at HS-25 were up to twice the corresponding strains at HS-20, all were less than 10% of yield strain.

6.6   DISCUSSION AND COMPARISON OF OVERHANG TEST RESULTS

Results from overhang tests are summarized in Table 6-1. At failure, both the IBTS and the UTSE breakback overhangs failed in one-way shear at the girder at load levels near 2.0 x HS-25. Both the IBTS and UTSE simulated 0º skew

225

overhangs failed in punching shear at load levels near 2.6 x HS-25. Additionally, strain levels and tip deflections were similar for both breakbacks and both simulated 0º skew overhangs.

Table 6-1 Summary of results from overhang tests

	Failure load (kips)	Failure mechanism	Strain (% of yield strain)			Tip Deflection (in)		
			at HS-20	at HS-25	at failure	at HS-20	at HS-25	at failure
Breakback-IBTS	44 (2.2xHS-25)	one-way shear	30	38	132	0.21	0.28	1.3
Breakback-UTSE	37 (1.9xHS-25)	one-way shear	38	53	116	0.30	0.41	-
Simulated 0 Skew-IBTS	51 (2.6xHS-25)	punching shear	3.2	18	-	0.12	0.20	2.2
Simulated 0 Skew-UTSE	54 (2.7xHS-25)	punching shear	6.2	9.7	-	0.15	0.22	2.7

The choice of the IBTS versus UTSE detail has only an insignificant effect on overhang capacity and failure mode. Both breakback overhangs behaved similarly, and both simulated 0º skew overhangs behaved similarly. As in the interior span tests, cracks in the UTSE overhang were more closely spaced and narrower than those in the IBTS overhang. Though the crack patterns were not identical, differences between them were slight. Overall, the similarities in response indicate that the choice of reinforcement details at the overhang (IBTS versus UTSE) have little effect on overhang behavior.

In contrast, pronounced differences in behavior were observed between breakback overhangs and simulated 0º skew overhangs. In overhangs with the same end detail (IBTS or UTSE), cracks at loads near failure in the simulated 0º skew overhangs were significantly wider than in the breakback overhangs. This may be due to the location of the bend in the reinforcement, as shown in Figure

6-37. In the breakback overhang, this bend occurs beneath the middle of the load plate. In the simulated 0° skew overhangs, the bend occurs over the girder. As applied loads are increased, the top reinforcement in the simulated 0° skew overhang begins to straighten out, producing local forces in the concrete perpendicular to the skew edge and cracking along the bars as shown in Figure 6-34. These local forces cause much damage over the girder where wide cracks were observed. The resulting reduction in the flexural capacity of the overhang at the girder significantly influenced the behavior of the overhang at failure load levels and was probably decreased the overhang capacity. In a true 0° skew deck overhang, the reinforcement would not have been bent at the overhang, and this effect would not have been present.
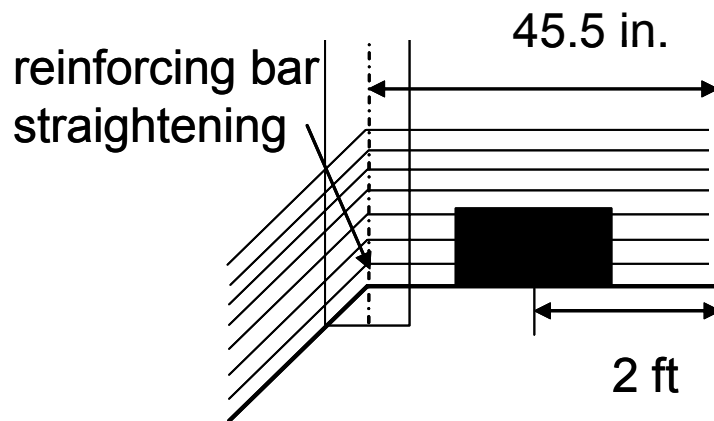
Figure 6-37 Location of reinforcement straightening, simulated 0° skew overhang

At equivalent load levels, reinforcing-bar strains in the breakback details were as much as 10 times the corresponding strains in the simulated 0° skew overhangs. Although external applied moments are the same for both configurations, the different orientation of the reinforcement in the two sections results in different resistances against the external applied moment. The most efficient orientation of the reinforcement would be perpendicular to the girder, as

227

in the simulated 0º skew overhang reinforcement orientation, but without the bends in the bars. The orientation of the reinforcement in the breakback overhang results in a reduced efficiency, increased stress, and increased strain.
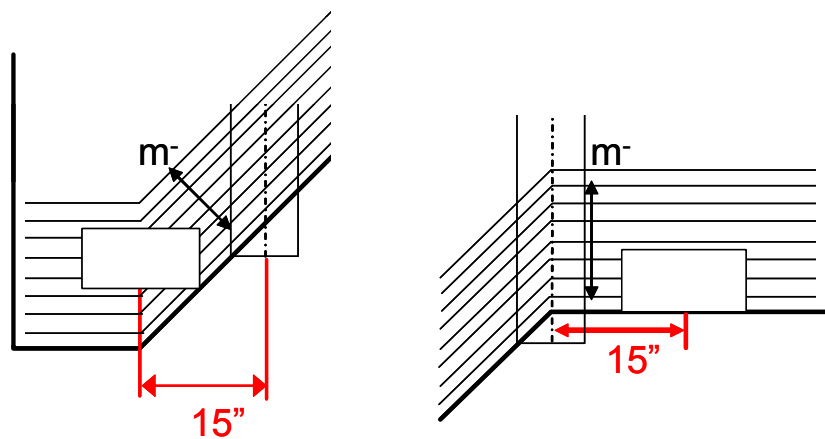
(a) Breakback overhang   (b) Simulated 0º skew overhang

Figure 6-38 Length of reinforcement between load plate and girder

At service load levels, tip deflections were significantly larger in the breakback overhangs than in the simulated 0º skew overhangs, due to the lower longitudinal stiffness of the breakback overhang. At loads near failure, however, tip deflections in the simulated 0º skew overhangs were much larger than those of the breakback overhangs. This can be attributed to the extensive cracking experienced in the simulated 0º skew overhangs, and not in the breakback overhangs.

Crack patterns in the breakback and simulated 0º skew overhangs indicate that moments were distributed differently in the different overhang corners, but that flexural and torsional cracks formed in every test section. In the breakback overhangs, flexural cracking was observed over the girder. Torsional cracks, oriented perpendicular to the skewed slab edge, were visible primarily on the top

228

of the deck. No cracking was visible on the bottom of the breakback overhangs, with the exception of a single crack in the IBTS breakback overhang.

In the simulated 0º skew overhangs, flexural cracks formed over the girder, and multiple torsional cracks formed on the top and bottom of the deck. While all overhang crack patterns indicated torsional cracking, more torsional cracks formed in the simulated 0º skew overhangs. When cracking over the girder became extensive, the flexural capacity of the section was severely reduced, forcing the redistribution of forces in the form of torsion.

6.7   SUMMARY

The four overhang corners on the 45º skew specimen were tested to failure. The two acute slab corners were constructed with breakbacks, a detail used by TxDOT. The two obtuse slab corners were constructed to simulate the overhangs in a 0º skew slab, as the overhangs were not tested in the 0º skew specimen. To test the worst-case overhang length, the length of both overhangs was extended from the standard 36 in. (914 mm) to 45.5 in. (1156 mm).

Based on the test results, the choice of the IBTS versus UTSE end detail has little effect on the behavior or capacity of the overhang corner. Regardless of the edge detail, the capacity of the breakback overhangs was about 2.0 x HS-25, and the capacity of the simulated 0º skew overhangs, about 2.6 x HS-25.

In the tests performed in overhangs constructed to simulate 0º skew overhangs, reinforcement was bent over the girder. During testing, the tensile reinforcement attempted to straighten out at the bend, causing severe cracking over the girder and a torsional redistribution of forces. This probably decreased the capacity of the section, and would not have been observed in a true 0º skew overhang.

CHAPTER 7

Comparison of Responses, 0º Skew Specimen and 45º Skew Specimen

7.1 INTRODUCTION

Test data gathered from the 0º and 45º skew specimens enable comparison of the response of slab ends with varying skews. In this chapter, failure modes, capacities, and service-load level behavior are compared for the two specimens, and trends evident from those comparisons are discussed. Tests maximizing positive moments and tests maximizing negative moments are addressed separately as positive moment loading tests and negative moment loading tests, respectively. Following the comparison of results, the applicability of the test results to slab-end design is discussed.

7.2 COMPARISON OF TESTS WITH NEGATIVE MOMENT LOADING

In both specimens, negative moment was maximized over a girder between two 8-ft (2.4-m) bays. In the 0º skew specimen, four point loads were applied in the end region in negative moment loading tests. In the 45º skew specimen, only three loads could be applied simultaneously in the AASHTO tandem configuration in negative moment loading tests. In tests maximizing negative moment, slab skew angle had little effect on the behavior of the end regions. Test areas with the IBTS end detail behaved similarly in the 0º and 45º skew specimens, and those with the UTSE end detail behaved similarly for both skew angles.

For all negative moment loading tests, test areas constructed with the same end detail had nearly identical initial slab edge stiffness, deflections at HS-20 and HS-25 load levels, and deflections at failure (Figure 7-1a, and b). In addition, relative edge deflections measured at HS-20 and HS-25 load levels were extremely small compared to the girder spacing (less than l/3800). For the 45º skew specimen, relative edge deflections were also extremely small compared to the clear span at the slab end (Section 3.3.1.1).
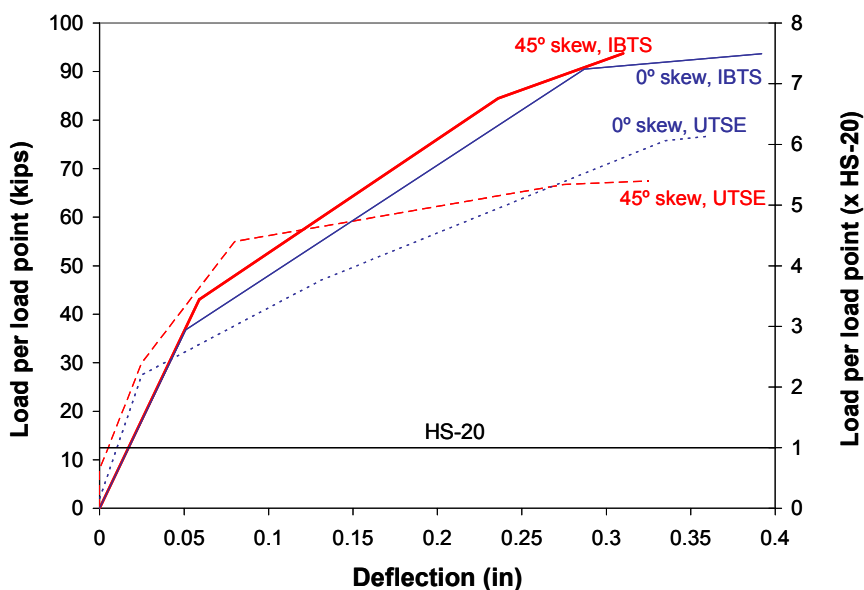
(a)

Figure 7-1 Deflection envelopes for tests maximizing negative moment: (a) up to failure; (b) focused on initial slab stiffness
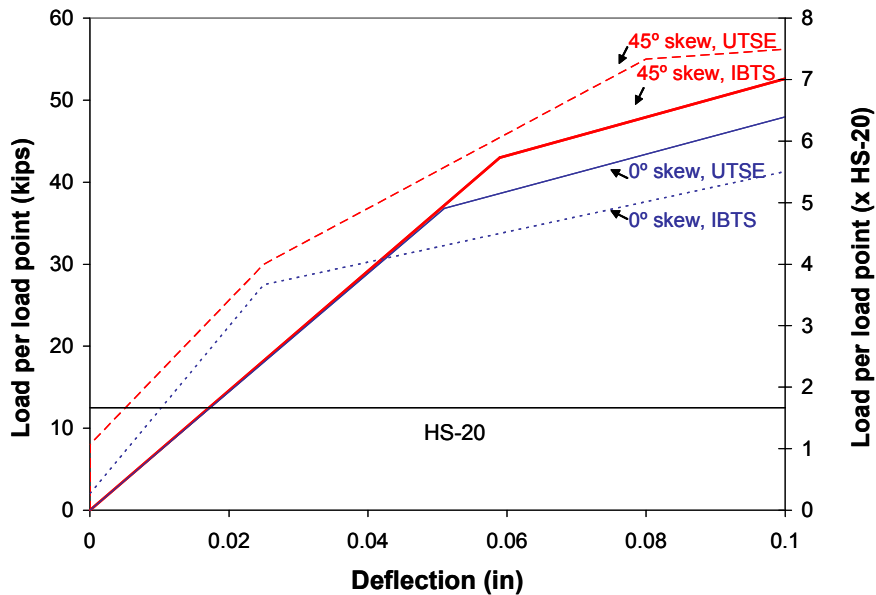
(b)

Figure 7-1 cont'd. Deflection envelopes for tests maximizing negative moment:
(a) up to failure; (b) focused on initial slab stiffness

For all tests with negative moment loading, the first observed cracks were short: top cracks were less than 2 ft (0.6 m) long, and bottom cracks were less than 5 ft (1.5 m) long. In all tests with negative moment loading, cracks were first observed at load levels of at least 1.9 x HS-20 (24 kips, 105 kN) (Figure 7-2a).

For slab ends constructed with either the IBTS or the UTSE detail, the first observed cracks in the test section did not coincide with a change in slab end stiffness. The first major change in slab stiffness occurred at higher load levels, coinciding with the initiation of multiple new cracks and the propagation and widening of the short, existing cracks. The load at which the first change in stiffness was observed, referred to in Chapter 5 as the significant cracking load, varied little for test regions constructed with the same slab end detail (Section 5.2.1.1, Figure 7-2b). In all tests with negative moment loading, fewer, narrower

232

cracks formed on the top of the slab than on the bottom of the slab. Significant cracking occurred at loads levels of at least 2.0 x HS-20 (25 kips, 110 kN).

All test areas failed in punching shear at load levels greatly above the HS-20 and HS-25 design load levels (Figure 7-2c). Failure loads for end areas with the IBTS detail were around 7.5 x HS-20 (90 kips, 400 kN), and failure loads for end areas with the UTSE end detail were at least 5.5 x HS-20 (70 kips, 305 kN).
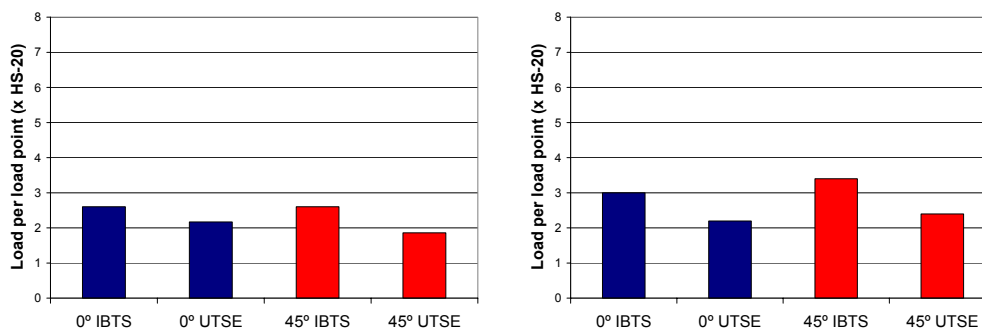
(a) First cracking loads

(b) Developed cracking loads
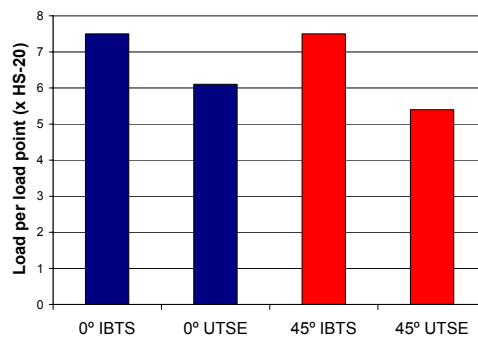
(c) Failure loads

Figure 7-2 Comparison of behavior of negative-moment test regions: (a) first cracking loads; (b) developed cracking loads; (c) failure loads

In all test areas where negative moment was maximized, strains measured in the transverse reinforcement were extremely small at HS-20 and HS-25 load levels (less than 7% of the yield strain). In the IBTS end detail test region, while

233

yield strain was not recorded on any instrumented reinforcing bar up to 3 x HS-25 (38 kips, 170 kN), some reinforcing bars did yield at some locations before failure. In the test regions of both specimens with the UTSE end detail, the largest strain measured in transverse reinforcement before failure was 90% (1980 $\mu\varepsilon$) of yield strain. Summaries of strains at various overload levels are shown for the 45º skew specimen in Section 5.6.1 of this thesis, and for the 0º skew specimen in Section 5.6 of Ryan (2003).

7.3 COMPARISON OF POSITIVE MOMENT LOADING TESTS

In both specimens, positive moment was maximized at midspan in the 10-ft (3.0-m) bay. In both the 0º skew and 45º skew specimens, two point loads were placed at midspan in the AASHTO tandem configuration. In 10-ft (3.0-m) girder spacings, skew angle had a noticeable effect on the behavior of test areas at failure load levels, but only an insignificant impact on service-level behavior.

All tests with positive moment loading showed nearly identical initial slab edge stiffnesses, deflections at HS-20 and HS-25 load levels, and ultimate deflections (Figure 7-3a, b, and c). For all tests maximizing positive moment, relative edge deflections measured at HS-20 and HS-25 load levels were extremely small compared to the girder spacing (less than l/1700).
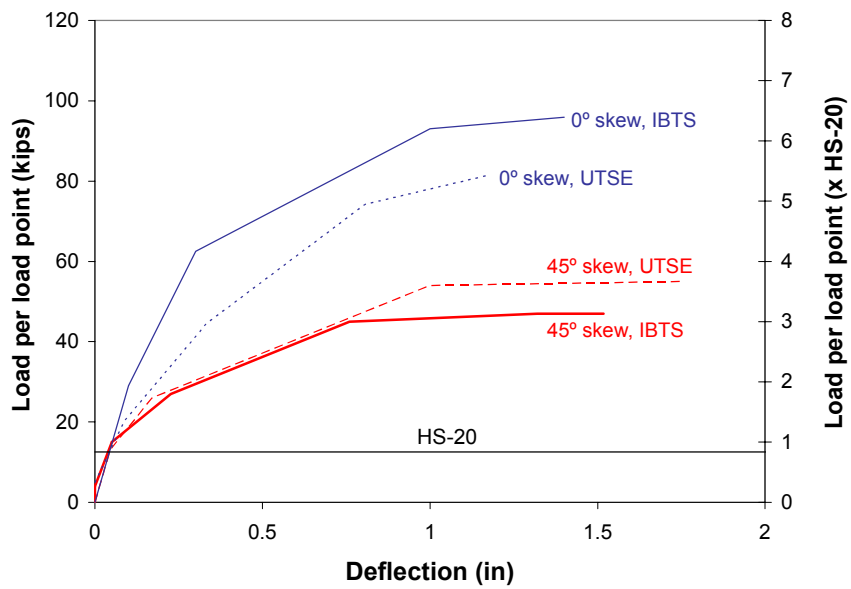
(a)
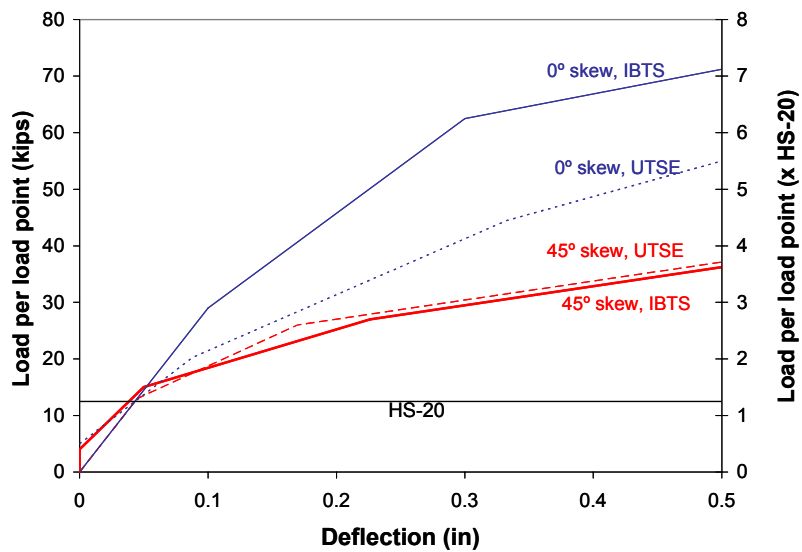
(b)

Figure 7-3 Deflection envelopes for tests with positive moment loading: (a) up to failure; (b) focused on initial slab stiffness

235

In tests with positive moment loading, the load levels at the first observation of cracking closely coincided with load levels at developed cracking, the observation of a small change in stiffness in the load-edge deflection response (Figure 7-4a, b). With the exception of the 45º skew, UTSE region, first cracking on the top side of the slab usually occurred at larger loads than first cracking on the bottom of the slab. Generally, only a few, narrow cracks were observed on the bottom of the slab at load levels between 1 x HS-20 (12.5 kips, 55 kN) and 1.5 x HS-20 (19 kips, 83 kN) (Figure 7-2a). The first cracks changed the slab stiffness only slightly, and cracking did not become extensive until higher load levels. At loads around 2 x HS-25 (25 kips, 110 kN), a larger change in slab stiffness was detected, caused by extensive crack formation and widening. Based on the crack patterns observed in the test areas just before failure, fewer, narrower cracks formed on the top of the slab than on the bottom of the slab.

Failure loads for 45º skew test areas were around 7.0 x HS-20 (88 kips, 390 kN), and for 0º skew test areas, around 4.0 x HS-20 (50 kips, 220 kN) (Figure 7-4c). While the 45º skew, IBTS test area failed in one-way shear, all other tests with positive moment loading failed in punching shear. Based on the AASHTO LRFD and ACI 318-02 provisions, nominal shear capacities are proportional to effective depth of concrete, and for identically shaped failure surfaces, the UTSE end region would have a lower punching shear and one-way shear capacity than the IBTS end region. For the 45º skew specimen, the capacity of the UTSE end region was higher than the capacity of the IBTS end region, when positive moment was maximized. This discrepancy is attributable to the geometry of the test specimen and the consequent torsional moments (Section 5.6.2.2). While test data from this investigation are too limited to quantify the torsional moments occurring in the skewed slab bays, the effects of torsion are noticeable in the cracking patterns and failure surfaces in the 45º specimen (Figure 5-35, Figure 5-

36, Figure 5-45, Figure 5-46, Figure 5-55).   Similar torsional effects were not detected in the response of the 0º skew specimen (Ryan 2003).

(a) First cracking loads   (b) Developed cracking loads
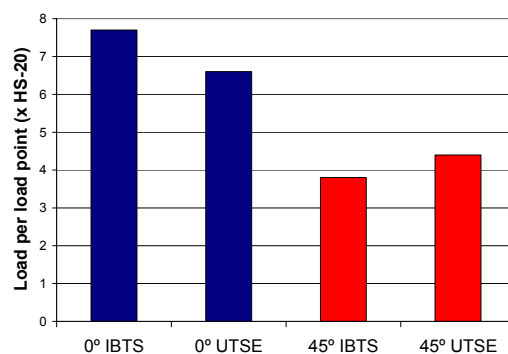
(c) Failure loads

Figure 7-4 Comparison of behavior of positive-moment test region: (a) first cracking loads; (b) developed cracking loads; (d) failure loads
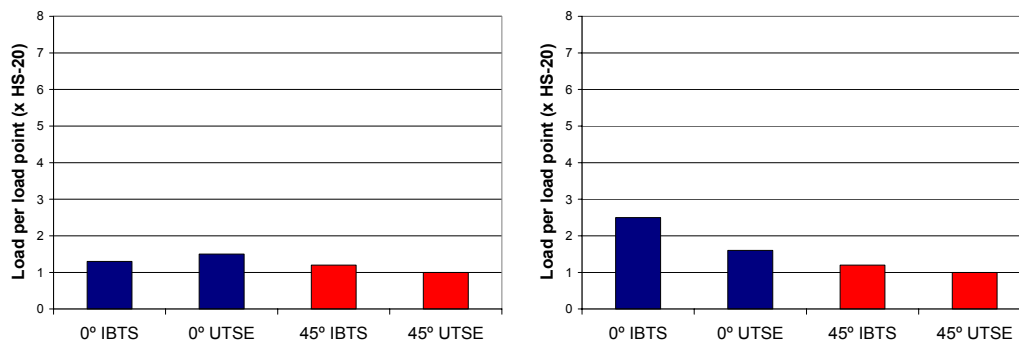
In 45º skew specimen, where positive moment was maximized, strains measured in the transverse reinforcement were extremely small at HS-20 and HS-25 load levels, between 5% and 10% of the yield strain. In the 45º skew, IBTS end detail test region, while strains up to 4 times yield strain were measured in transverse reinforcement at midspan, no reinforcement reached yield strain at the instrumented locations over the girder. In the 45º skew, UTSE end detail test regions, most transverse reinforcement did not yield at midspan, and no

237

instrumented reinforcing bar reached yield strain at locations near the girder. Summaries of strains at overloads are shown for the 45º skew specimen in Section 5.6.2 of this thesis

Summaries of strains at overloads are shown for the 0º skew specimen are shown in Section 5.6 of Ryan (2003), but are not included in this chapter and are not compared to the results from the 45º skew specimen. Test protocol was changed after the construction of the 0º skew specimen, and the locations on strain gauge instrumentation in positive moment tests were no longer critical sections. Initially, the 10-ft (3.0-m) girder spacing test areas was to be loaded such that positive moment was maximized at a location east of midspan. Instrumentation was cast into the slab to capture the strains at this location. After the first test on the 0º specimen caused a punching shear failure in the interior bay, and the loading location in the 10-ft (3.0-m) bays had to be changed. The new loading location changed the anticipated location of maximum positive moment to midspan. Because the slab was not instrumented at midspan, the strains measured may not be the maximum strains occurring in the test area and are not reported here.

7.4   COMPARISON OF RESPONSES OF IBTS AND UTSE END DETAILS

The primary aim of this study was to understand the behavior of slab ends at expansion joints constructed with the IBTS end detail; an alternate, simpler detail, named the UTSE detail, was also investigated. Overall, the UTSE end detail performed well under service load: only the 45º skew, 10-ft (3.0-m) girder spacing UTSE test area cracked at the HS-20 design load level. All other UTSE test sections cracked at loads higher than the HS-25 design load level. For the UTSE detail slab ends tested, failure loads levels were higher than 4.0 x HS-20 (50 kips, 220 kN) and as high as 6.0 x HS-20 (75 kips, 335 kN).

238

All test sections with both UTSE and IBTS end details failed due to punching shear or one-way shear. According to the punching-shear provisions of the AASHTO LRFD and ACI 318-02, shear capacity is proportional to the distance from the extreme compressive fiber to the centroid of the tensile reinforcement. This distance in the IBTS detail is 2 in. (50.4 mm) greater than the corresponding distance in the UTSE detail. Based on this punching-shear model, for two identical punching shear failure surfaces, the capacity of an IBTS section should be higher than that of a UTSE section. The test results support this hypothesis, as the punching shear capacity of UTSE detail slab ends was less than the punching shear capacity of IBTS detail slab ends for similarly configured test sections.

While punching-shear capacity depends on section depth, it may also be influenced by the section's flexural reinforcement ratio (CEB-FIP 6.4-18). The flexural reinforcement ratio of the UTSE detail was higher than that of the IBTS detail, and this was likely to have increased the punching-shear capacity of the former. The tests performed were too limited to allow for study of the relationship between reinforcement ratio and punching shear capacity. All tests results, however, indicated that regardless of whether the IBTS or UTSE end detail was used, the reserve strength of the slab ends greatly exceeds AASHTO design load levels.

At load levels around HS-20 and HS-25, tensile strains levels in corresponding UTSE and IBTS test sections were the same. After cracking, however, tensile strains measured in the UTSE test sections were smaller than those measured in the IBTS test sections. Tensile strains in the reinforcement in UTSE test sections did not exceed yield strain at any instrumented location. A single reinforcing bar reached yield strain in only in the 45º skew, 10-ft (3.0-m) girder spacing, UTSE detail test section.

239

In both the 45º skew specimen and the 0º skew specimen, more numerous, closely spaced, narrower cracks formed in the UTSE test sections, than in corresponding IBTS test sections.

7.5 DESIGN GUIDELINES FOR SLAB ENDS AT EXPANSION JOINTS

AASHTO design provisions require that bridge slabs be designed for both the service limit state (addressing stresses, deformations, and crack widths), and for the strength limit state (addressing strength and stability). One objective of this study was to provide guidance for designing slabs using the IBTS or UTSE end details.

In the design of a typical TxDOT bridge deck, the combination of girder spacing and skew angle must be chosen so that the IBTS or UTSE slab end will perform adequately under AASHTO design loads at serviceability load levels and failure load levels. Of particular interest is the effect on each detail of a hypothetical increase from HS-20 to HS-25 design load levels. In this section, the change in overall performance of IBTS and UTSE slab ends under that hypothetical increase is addressed. In addition, based on the results of tests on the IBTS and UTSE end details, the effects of varying end skew angle and girder spacing on cracking loads, deflections, reinforcing bar stress levels, and failure loads are addressed.

Previously, tests have been categorized by the placement of the AASHTO design load, maximizing either positive or negative moment. In the 0º skew specimen, loads were applied in the 8-ft (2.4-m) bays in the AASHTO design load configuration in two locations, one to maximize negative moment and one to maximize positive moment. At the same load level, maximizing negative moment in the test section frequently resulted in larger tensile strains, deflections, and crack widths than did maximizing positive moment in the test section, so the

240

slab was ultimately loaded to failure in a load configuration placed to maximize negative moment. In the 8-ft (2.4-m) bays of the 45° skew specimen, loads were placed to maximize negative moment only. In further discussions in this chapter, discussions of behavior in 8-ft (2.4-m) bays will refer to tests performed to maximize negative moment.

In all 10-ft (3.0-m) bays, test sections were loaded at midspan, maximizing positive moment. In further discussions, discussions to the behavior of slab ends in 10-ft (3.0-m) girder spacings will refer to tests maximizing positive moment.

The designer should not expect increased slab capacity or improved behavior for loads applied to girder spacings less than 8 ft (2.4 m). Because the AASHTO design tandem has a set axle length of 6 ft (1.8-m), and because the critical loading location for girder spacings 8 ft (2.4 m) or less maximizes negative moment over a girder, decreased girder spacing is likely to have only minimal effect on deck performance, regardless of slab-end details.

7.5.1   Crack Formation

In the discussion of crack formation, two behaviors must be considered in design: first cracking and the beginning of developed cracking. During testing, the slab specimens were closely observed to identify cracks, but the first cracking loads reported are only approximate. Test areas were loaded in 5-kip (22-kN) increments, and cracks could have first been visible at loads up to 5 kips (22 KN) lower than those reported here. Additionally, variations in material properties of concrete produce variations in observed cracking loads in otherwise identical specimens.

Test data gathered in this study indicate that a hypothetical increase in design loads from HS-20 to HS-25 would have little effect on the formation of cracks in decks with girder spacings of 10 ft (3.0 m) or less and skews of 45° or

241

less. First cracking loads are reported in Table 7-1 and Table 7-2 below. Based on these results, slab ends with the IBTS or UTSE detail can be expected to remain uncracked under HS-20 and HS-25 design loads for 0º skew slabs and slabs constructed with 8-ft (2.4-m) girder spacings. For specimens tested with 10-ft (3.0-m) girder spacings, first cracking loads are reduced, but still remain at or above HS-20. In the specimens tested, the combination of 10-ft (3.0-m) girder spacing and 45º skew resulted in the lowest first-cracking loads. Although the 10-ft (3.0-m), 45º skew, UTSE detail test area cracked at 1.0 x HS-20, these hairline cracks were short (less than 3 ft, or 915 mm, long).

Table 7-1 First cracking loads, IBTS end detail

IBTS	Skew Angle	
Girder Spacing	*0º skew*	*45º skew*
8-ft, negative bending	2.6xHS-20	2.7xHS-20
10-ft, positive bending	1.3xHS-20	1.2xHS-20

Table 7-2 First cracking loads, UTSE end detail

UTSE	Skew Angle	
Girder Spacing	*0º skew*	*45º skew*
8-ft, negative bending	2.2xHS-20	1.8xHS-20
10-ft, positive bending	1.5xHS-20	1.0xHS-20

For all tests, cracks were first observed at loads between 1.0 x HS-20 (12.5 kips, or 55 kN) and 3.0 x HS-20 (38 kips, or 167 kN). Developed cracking patterns, however, did not form until higher loads. The term "developed crack pattern" refers to a change in the crack formation behavior and must be observed in the context of the overall behavior of the slab end as applied loads are

increased. In all tests, at first cracking, only short (less than 5 ft, or 1.5 m), hairline cracks were observed. In the 10-ft (3.0-m) girder spacings, where positive moment was maximized, these first cracks caused a minor reduction in the stiffness of the slab edge. In the 8-ft (2.4-m) girder spacings, where negative moment was maximized, these first cracks did not produce a noticeable change in slab end stiffness. After first cracking, as applied loads were increased, crack widths and lengths grew modestly, with the initiation of only a few additional cracks. All tests maintained nearly linear load-deformation behavior until the load level labeled "developed cracking," a term used to describe the cracking required to initiate a noticeable change in slab edge stiffness. "Developed cracking" loads were all greater than 1.5 x HS-20 (19 kips, or 83 kN), and are shown in Figure 7-2 and Figure 7-4. At "developed cracking" loads, a more developed crack pattern began to emerge, initiating a reduction in slab edge stiffness. With the addition of load past the developed cracking load level, cracks grew much faster than before under the same load increments. Although additional cracks formed after "developed cracking" loads, test observations indicate that those cracks do not reduce slab capacity. For all tests performed on the UTSE and IBTS details, crack widths at load steps closest to "developed cracking" load levels are shown in Table 7-3 and Table 7-4. These widths were measured from the tests performed, and are intended to serve only as a comparative index of crack severity.

Table 7-3 Largest measured crack width at the initiation of a developed crack pattern, 8-ft girder spacing, negative bending

End Detail	End Skew	Largest measured crack width (in)		
		Top of slab	*Bottom of slab*	*Side of slab*
IBTS	*0°*	0.002	0.003	0.004
	45°	0.005	0.009	0.003
UTSE	*0°*	0.003	0.004	0.005
	45°	0.003	0.002	0.002

Table 7-4 Largest measured crack width at the initiation of a developed crack pattern, 10-ft girder spacing, positive bending

End Detail	End Skew	Largest measured crack width (in)		
		Top of slab	*Bottom of slab*	*Side of slab*
IBTS	*0°*	N/A	0.005	0.005
	45°	0.005	0.007	0.005
UTSE	*0°*	HL	0.002	0.002
	45°	0.007	0.009	0.005

7.5.2   Reinforcement Strain

Lists of maximum tensile strains measured at HS-20, HS-25, and overload load levels are given for the 0º skew specimen in Ryan (2003) and for the 45º skew specimen in Sections 5.6.1 and 5.6.2 of this thesis. For all tests performed on both the IBTS and UTSE slab ends, tensile strains measured in each test section were less than 10% (220 µε) of the yield strain at the HS-25 load level. For all tests, the strain levels at both HS-20 and HS-25 load levels were insignificant, and the increase in tensile strain between HS-20 and HS-25 load levels was insignificant as well. In the IBTS slab ends, tensile strains exceeded yield strain in at least one location in every test region. In the UTSE slab ends, no strains greater than the yield strain were measured in any test section.   The

maximum tensile strain measured in every test section before failure is summarized in Table 7-5. As with all measured test data presented in this chapter, these data are intended to summarize the magnitude of strains, and are not intended to predict exact strains in other structures. Strains reported from 0º skew specimen, 8-ft (3.0-m) girder spacing test areas may not be the maximum strains occurring in the transverse reinforcement in the slab end. Strain gauges were attached at locations above the centerline of the girder, but larger strains probably occurred at locations along either edge of the girder. These strains are included in this chapter, but are only intended as a relative guide to maximum measured strain in 0º skew test areas.

Table 7-5 Maximum measured tensile strain at failure, IBTS detail test areas

IBTS

Girder Spacing	End Skew	Largest tensile strain (multiples of yield strain)
8-ft, negative bending	0º	1.1*
	45º	3.0
10-ft, positive bending	0º	N/A
	45º	4.0

* Strain measurement made at centerline of girder and may not be the maximum strain

Table 7-6 Maximum measured tensile strains at failure, UTSE detail test areas

UTSE

Girder Spacing	End Skew	Largest tensile strain (multiples of yield strain)
8-ft, negative bending	0º	0.88*
	45º	0.89
10-ft, positive bending	0º	N/A
	45º	1.00

* Strain measurement made at centerline of girder and may not be the maximum strain

7.5.3   Slab Edge Deflection

Lists of relative edge deflections measured at midspan at HS-20, HS-25, and overload load levels are given for the 0º skew specimen in Ryan (2003) and for the 45º skew specimen in Sections 5.6.1 and 5.6.2 of this thesis. Increasing design loads from the HS-20 level to the HS-25 level had an insignificant effect on the relative slab edge deflection measured in all test areas. In 8-ft (2.4-m) girder spacings, where negative moments were maximized over a girder, maximum deflections were extremely small relative to the girder spacing (l/3800 to l/16000). For negative bending tests in 8-ft (2.4-m) bays at both skews, edge deflections were smaller for the UTSE slab ends. For positive bending tests in 10-ft (3.0-m) bays at both skews, edge deflections were smaller for the IBTS slab ends. The maximum service-deflection allowed by AASHTO LRFD provisions (AASHTO 2.5.2.6.2) is l/800. For negative-bending tests performed on 8-ft (2.4-m) girder spacings, slab edge deflections reached this level at loads ranging between 1.75 x HS-25 (22 kips, or 97 kN) to 3 x HS-25 (38 kips, or 165 kN). For positive-bending tests performed on 10-ft (3.0-m) girder spacings, slab-edge deflections reached this level at loads of about 1.2 x HS-25 (15 kips, or 67 kN) to 1.75 x HS-25 (22 kips, or 97 kN).

While increased end skew angle had an insignificant effect on maximum slab edge deflections in 8-ft (2.4-m) bays, it resulted in increased slab-end deflections in 10-ft (3.0-m) bays. For all combinations of slab-end detail and girder spacing, midspan edge deflections were acceptably small at HS-20 and HS-25 design load levels. At load levels below the significant cracking loads, as discussed in Section 7.5.1, slab-edge deflections remained small.

246

7.5.4　Predictions of Slab End Capacity

All slab areas tested failed in punching shear, with the exception of the 45º skew, IBTS detail, 10-ft (3.0-m) girder spacing test area, which failed in beam shear. The AASHTO LRFD provisions (AASHTO 5.13.3.6.3) can be used to predict the punching-shear capacity of slab ends and the beam shear capacity of the thickened end region. Additionally, flexural capacity can be predicted using yield-line analysis and the strip method. The relevancy of these methods is addressed later in this thesis (Section 7.5.4.3) for slabs designed with IBTS and UTSE slab ends.

7.5.4.1　*Punching-Shear Capacity*

Using Equations 5-3, 5-4, and 5-5, punching-shear capacity of IBTS and UTSE slab ends was calculated assuming a uniform distribution of shear stress. For the observed failure capacities of all sections tested, these predictions were unconservative. The nominal punching-shear capacities calculated for IBTS and UTSE end details in both the 0º and 45º skew specimens were 1.25 to 1.85 times the observed capacities.

For 0º skew slab ends, the ACI 318-02 eccentric-shear model (ACI 11.12.6.3)conservatively predicts the punching shear capacities measured from the tests performed on slab ends with UTSE and IBTS end details (Ryan 2003, and Section 5.7 of this thesis). The eccentric shear model is not included in AASHTO LRFD. For 45º skew specimens, nominal capacities calculated using the eccentric-shear model are closer to the tested capacities, but the necessary calculations are complex and beyond the scope of this phase of this project. The punching shear strength of sections in the 45º skew specimens is discussed in Section 5.6.4 of this thesis.

7.5.4.2 Beam-Shear Capacity

The 45º skew, IBTS detail, 10-ft (3.0-m) girder spacing test section failed in beam shear. In this test area, a section, nearly the length of the thickened end, failed along the axis of highest shear as predicted by a simple elastic analysis. If the thickened end region is assumed to behave as a wide beam, the beam-shear capacity predicted using AASHTO LRFD and ACI 318-02 provisions is between 0.65 to 0.95 times the tested capacity (Section 5.6.3).

Based on the nominal beam-shear capacity predicted for the 45º skew, IBTS detail, 10-ft (3.0-m) girder spacing test, the prediction of the beam-shear capacity may seem conservative. This approach becomes less conservative when applied to the 0º skew specimen, however. The single beam-shear failure occurred across the thickened end section, in the longitudinal section. The length of the section in the 0º skew slab end would be 4 ft (1.2 m), a distance that increases with increasing skew (Figure 7-5). Using these failure planes, the nominal beam-shear capacity predicted for the 10-ft (3.0-m) girder spacing, IBTS detail with a 45º skew, would be greater than the beam-shear capacity predicted for the same configuration at a 0º skew (Appendix B). This does not agree with the results of the tests of this study. The 0º skew, 10-ft (3.0-m) girder spacing, IBTS detail failed in punching shear at 7.7 x HS-20 (96 kips, or 430 kN), or about 1.8 times the predicted nominal capacity in beam shear. The discrepancy between the test results and the predicted nominal capacity indicates that the complex interactions between bending, torsion, and shear in the 45º skew specimen influenced the failure mode and ultimate strength of the IBTS and UTSE sections.
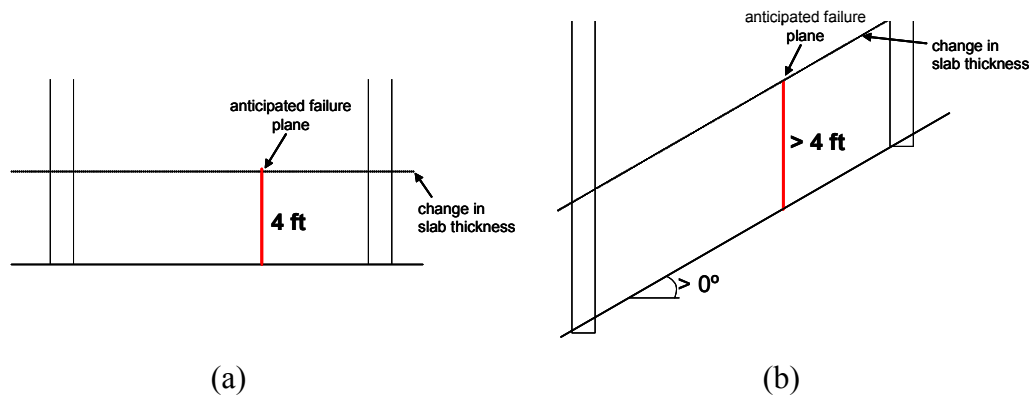
248

(a)   (b)

Figure 7-5 Anticipated beam-shear failure planes; (a) 0º skew, (b) skew greater than 0º

7.5.4.3 Flexural Capacity

Both upper-bound methods, such as the yield-line method, and lower-bound methods, such as the Hillerborg strip method, can be used to predict flexural capacity. Flexural capacity may not be a primary concern, though, as all IBTS detail and UTSE detail test areas failed in shear.

7.5.4.3.1 Yield-Line Analysis

For many reasons, a yield-line analysis may not be prudent for bridge slab ends designed with the IBTS or UTSE end details. First, yield-line analysis predicts capacity of slabs at the formation of a collapse mechanism. None of the IBTS or UTSE slab ends formed a collapse mechanism, as all failed in shear. The yield-line model does not predict punching shear behavior, but the method could still be employed to verify that flexural failure would not occur before punching-shear failure. Second, the use of yield-line analysis for IBTS or UTSE bridge slabs ends is questionable due to the difficulty in quantifying boundary conditions or collapse mechanisms, as necessary for this method. Solutions become increasingly misleading if the boundary conditions chosen do not best describe

the configuration being analyzed. For bridge slab ends, the restraint provided along girders is neither fully fixed nor simply supported, and modeling it as either may result in misleading results. Third, yield-line analysis gives upper-bound solutions, and predicted capacities could be excessively high if the selected yield-line pattern is not the critical one. And fourth, for skewed slab ends, finding the yield-line pattern that will result in the lowest predicted capacity requires the optimization of multiple variables of complex geometries, a time-consuming process that may not be successful.

To illustrate the problems inherent in using yield-line analysis to predict the capacities of deck configurations such as those investigated in this thesis, it is useful to present the results of such an analysis as applied to simple examples from this study. A sample of a yield line analysis is shown below in A yield-line analysis was performed for all test areas in both specimens. For the simpler geometry of the 0º skew slab ends, the yield-line mechanism shown in Figure 7-6 predicted a collapse load of 105 kips (467 kN) per load point in the 8-ft (2.4-m) girder spacing and 95 kips (423 kN) per load point in the 10-ft (3.0-m) girder spacing. Though yield-line analysis predicted collapse loads near the observed punching shear failure loads, the crack patterns in the test specimen were at failure were far from forming a complete flexural yield line pattern. The complexity of yield line patterns for the 45º skew specimen slab ends is vastly increased for skews of 45º, and no yield-line analysis resulted in reasonable predictions.
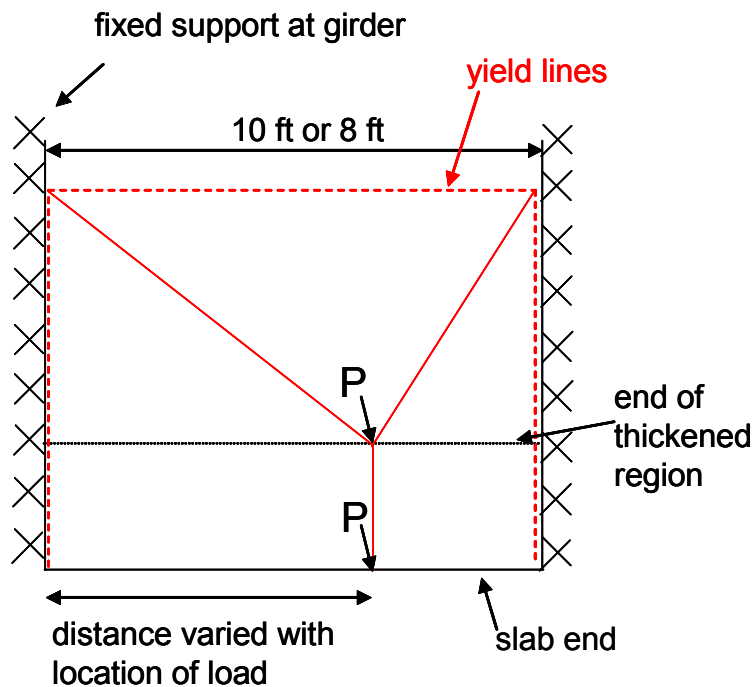
fixed support at girder

yield lines

10 ft or 8 ft

P

P

end of
thickened
region

distance varied with
location of load

slab end

Figure 7-6 Yield-line mechanism, 0° skew slab end

7.5.4.3.2 Hillerborg Strip Method

The Hillerborg Strip Method is a lower bound method which should produce conservative results. The method allows designers to assume a distribution of moments in a slab and distribute reinforcement to adequately resist flexure. For slabs designed by the strip method, a good assumption of the distribution of forces in slabs results in the placement of reinforcement so that crack widths and deflections remain small. While even a poor assumption of the distribution of forces results in reinforcing details that provide adequate resistance against failure, crack widths and deflections may be excessive.

251

For bridge slabs designed with the IBTS and UTSE end details, the distribution of forces in the slab end can be difficult to quantify, as the interaction of the combination of bending, shear, and torsion actions is complex. If designers wish to implement a third, alternate reinforcing detail, all forces can be assumed to be distributed in a single strip the width of the slab end detail, effectively designing the slab end like a wide beam. Although using a single strip may result in excess flexural capacity for slabs that are likely to fail in punching shear, the resulting service-level crack widths and deflections should be small.

7.6 SUMMARY

Comparisons have been made for the IBTS and UTSE end details constructed at both a 0º skew and 45º skew. For girder spacings of 8 ft (2.4 m) or less, AASHTO design tandem load was placed to maximize negative bending of the slab. For girder spacings of 10 ft (3.0 m) or greater, the AASHTO design tandem load was placed to maximize positive bending.

For tests maximizing negative bending, tensile strain and midspan edge deflection measured at HS-20 and HS-25 load levels were insignificant (less than 10% of yield strain and less than l/800 times the span). At failure, maximum measured tensile strains in the IBTS end detail were larger for the 45º skew than for the 0º, but reinforcement in end details constructed a both skews did not yield at many locations. The increase in skew from 0º to 45º had nearly no effect on the initial slab edge stiffness for IBTS and UTSE slab ends in the 8-ft (2.4-m), negative bending tests. First cracking was observed at loads in excess of 2.5 x HS-20 (31 kips, or 140 kN) for the IBTS slab end and 1.8 x HS-20 (23 kips, or 100 kN) for the UTSE slab end. For negative bending tests conducted at 8-ft (2.4-m) girder spacings, increasing slab end skew had little effect on load levels at first observed cracking. In these tests, the IBTS slab ends failed at loads around 7.5 x

HS-20 (94 kips, or 420 kN), and the UTSE slab ends failed in punching shear at loads levels in excess of 5.5 x HS-20 (69 kips, or 305 kN).

In the positive bending tests conducted in 10-ft (3.0-m) bays, increasing end skew had little effect on the maximum measured tensile strain and midspan edge deflection measured at HS-20 and HS-25 load levels (less than 10% of yield strain and less than l/800 times the span). Neither the increase in skew from 0º to 45º nor the use of the either the IBTS or UTSE detail had a significant effect on the initial slab edge stiffness for slab ends in the 10-ft (2.4-m) bays. For test regions where positive moment was maximized, first cracking was observed at lower loads for the 45º skew slab ends than for the 0º skew slab ends. For the 45º skew specimen, first cracking was observed at the HS-25 load level in the IBTS slab end and at the HS-20 load level in the UTSE slab end. For 10-ft (3.0-m) bays, while skew angle had a large effect on the capacity of the slab ends, no slab end with either detail failed at a load level below 3.5 x HS-20 (44 kips, or 195 kN).

CHAPTER 8

Summary, Conclusions, and Recommendations

8.1 SUMMARY

The Texas Department of Transportation (TxDOT) currently uses, for most of its bridges, the "IBTS" standard detail for bridge slab ends at expansion joints. That detail has evolved as a way of achieving increased transverse stiffness at slab ends, without using diaphragms. In the ITBS detail, slab ends are stiffened by a 2-in. (51-mm) increase in slab thickness and a slightly reduced reinforcement spacing for skewed slabs.

The IBTS end detail may not be easy to construct, because the thickened edge requires additional formwork. If the reserve strength of the free edge of the bridge deck is adequate, the thickened edge may be unnecessary for capacity. To investigate this, an alternate and possibly more economical detail was designed with a flexural capacity similar to that of the IBTS detail but without a thickened edge. Designated the Uniform Thickness Slab End (UTSE) detail, it was also instrumented and tested, and its performance was compared with that of the IBTS detail.

The primary objective of this study was to investigate the behavior of slab ends constructed with the IBTS detail and with a simpler, alternate detail (UTSE detail). Two full-scale specimens have been constructed to test both details, a 0º skew test specimen and a 45º skew specimen, and loads were applied in the AASHTO design load configurations. For both specimens, negative moments and positive moments were maximized in 8-ft (2.4-m) and 10-ft (3.0-m) bays,

254

respectively.   In the 45º skew specimen, additional overhang tests were performed.

8.2   CONCLUSIONS

Based on the results of the tests performed on the slab ends of both specimens, the following conclusions can be drawn about the general behavior of slab ends with skew no greater than 45º and girder spacing no greater than 10 ft (3.0 m):

- Service-level behavior:
  - An increase in applied loads from HS-20 to HS-25 load levels resulted in a nearly proportional increase in midspan edge deflection and strain in reinforcement.
  - At both HS-20 and HS-25 load levels, tensile strains in transverse reinforcement and the deflection-to-girder-spacing ratio were both extremely small (always less 10% of yield strain and l/800 respectively).
  - Slab ends remained uncracked beyond the HS-20 design load level, with the exception of the 45º skew, 10-ft (3.0-m) girder spacing, UTSE detail test area, which cracked at 1.0 x HS-20 (13 kips, or 56 kN).
  - After first cracking, the further initiation and propagation of cracks was minimal until load levels at or above 2.0 x HS-20 (25 kips, or 110 kN).
  - Initial slab edge stiffness was nearly the same for all combinations of skew angle and end detail for 8-ft (2.4-m) and 10-ft (3.0-m) girder spacings under positive and negative bending.

255

- o For highly skewed slabs, applied loads were resisted partially through torsion, affecting the cracking patterns and possibly the capacities of the IBTS and UTSE deck ends.
- Failure-level behavior:
  - o IBTS or UTSE slab ends loaded with AASHTO design load configurations usually failed in punching shear, with the exception of the 45º skew, 10-ft (3.0-m) bay constructed with the IBTS end detail, which failed in one-way shear; the slab ends tested did not fail in flexure.
  - o In 8-ft (2.4-m) bays, under negative moment loading, the capacity of IBTS slab ends exceeded 7.5 x HS-20 (94 kips, or 420 kN) load levels, and the capacity of UTSE slab ends exceeded 5.3 x HS-20 (66 kips, or 295 kN).
  - o Although increased skew angle decreased slab-end capacity in 10-ft (3.0-m) bays, those capacities equaled or exceeded 3.8 x HS-20 (48 kips, or 210 kN).
- Effects of skew:
  - o For negative moment loading over a girder in 8-ft (2.4-m) bays, skew had only an insignificant effect on service-level behavior (cracking, reinforcement strain, and deflection) and capacity of the IBTS and UTSE slab end details.
  - o For positive moment loading in 10-ft (3.0-m) girder spacings, increased skew resulted in increased service-level deflections and reinforcement strains, but tensile strains and deflection-to-span ratios were less than 10% and l/800 respectively at HS-25 load levels.

- For highly skewed slab ends, forces in the end region were distributed through a combination of flexural bending, torsional bending, and shear. This distribution caused 45º skew slab ends to experience more severe cracking and have lower ultimate capacities than slab ends with zero skew.

- Comparisons of IBTS and UTSE End Details:
  - Cracks in UTSE end details were more numerous, more closely spaced, and narrower than cracks formed in corresponding IBTS end details.
  - The load-deflection response of decks with the two details was nearly indistinguishable at HS-20 and HS-25 load levels.
  - Before cracking, strains were similar in corresponding UTSE and IBTS slab ends.
  - After cracking and up to failure, tensile strains in UTSE details never exceeded yield strain, and at failure were significantly less than strains in the IBTS details (usually between 33% and 25% of failure strains in IBTS details).
  - All IBTS and UTSE slab ends tested failed at loads greater than 3.8 x HS-20 (48 kips, or 210 kN), but the punching shear capacity of UTSE slab ends was less than that in corresponding IBTS slab ends. Because nearly all slab ends failed in punching shear, the reduced depth of the UTSE end detail resulted in a lower capacity.

8.2.1 Behavior of Overhangs

Using the AASHTO LRFD bridge specifications, a 10- by 20-in (254- by 508-mm) loading plate, when placed on a standard 3-ft (914-mm) overhang in

257

accordance with AASHTO design provisions, must be placed at a location over the girder. Because this case is not of interest, 45.5 in. (1157 mm) overhangs were tested in the 45º skew specimen, representing overhangs in a bridge with a horizontal curve of 600 ft (183 m). Based on the tests of breakback overhangs (Section 6.1.1) and overhangs constructed to simulate 0º skew overhangs, the following conclusions can be drawn:

- Breakback overhangs in 45º skew specimens failed in one-way shear at approximately 2.0 x HS-20 (25 kips, or 110 kN), and breakbacks in simulated 0º skew specimens failed in punching shear at about 2.6 x HS-20 (33 kips, 145 kN).

- The use of the IBTS and UTSE end details in spans resulted in slightly different overhang reinforcement arrangements, but these had nearly no effect on the ultimate capacity of a section.

- Cracks in UTSE-detail overhangs were narrower and more closely spaced than those in corresponding IBTS-detail overhangs, a trend also observed in the span tests.

- In the tests performed in overhangs constructed to simulate 0º skew overhangs, reinforcement was bent over the girder. During testing, the tensile reinforcement attempted to straighten out at the bend, causing severe cracking over the girder and a torsional redistribution of forces. This probably decreased the capacity of the section, and would not have been observed in a true 0º skew overhang.

8.3 DESIGN RECOMMENDATIONS

The following recommendations are based on the test data gathered for slabs with skew of 0º and 45º and girder spacing of 10-ft (3.0-m) or less.

8.3.1 Recommendations For Implementation

- For 0º skew slabs, punching shear capacity should be checked using the eccentric shear model of ACI 318-02.

- Bridge slabs designed with the IBTS and UTSE slab ends performed well at HS-20 and HS-25 load levels. The increase in design load from HS-20 to HS-25 does not result in significant changes in performance.

- For bridge slabs constructed with girder spacing less than 10 ft (3.0 m) and skews less than 45º, cracking can be assumed to be minimal or non-existent under HS-20 and HS-25 applied loads. When slab ends are subjected to overloads, cracking is minimal until approximately 2.0 x HS-20 (25 kips, or 110 kN).

8.3.2 Recommendations for Further Research

- For 0º skew slabs, punching shear capacity should be checked using the eccentric shear model of ACI 318-02. For other skewed slabs, the implementation of this model is complex and requires further investigation.

- One-way shear capacity should be checked using AASHTO LRFD design provisions but may result in predicted capacities that are excessively conservative (too low). This procedure resulted in reasonable predictions for the single test where one-way shear failure occurred, but gave results that were too low in some test areas where punching shear failure occurred. The applicability of the AASHTO one-way shear model should be investigated further.

- Precast-prestressed (PCP) panels are commonly to form slab interiors. The use of PCP panels at UTSE slab ends is possible and

259

could result in a reduction of construction costs. The use of PCP panels at UTSE slab ends requires further investigation.

APPENDIX A

Supplemental Strain Data

A.1 Introduction

The 45º skew specimen was instrumented with more than 250 strain gauges, and for each test area, gauge output was monitored for as many as 80 gauges. In Chapter 5, the inclusion of load-strain plots was limited to the most critical locations. Compression strains were not reported at all. In this appendix, additional plots of tensile reinforcement strains are presented. Not shown are data gathered from strain gauges that malfunction during testing or read strains less than 15% of yield strain. All strain gauges installed on bars in compression read strains less than 15% of yield strain and are not included. As in Chapter 5, graphics to the right of the plot show where gauges were located in the test section and where the test region was located in the specimen. For test regions, the axes are identical for all plots from a single test area to allow strain levels to be compared.
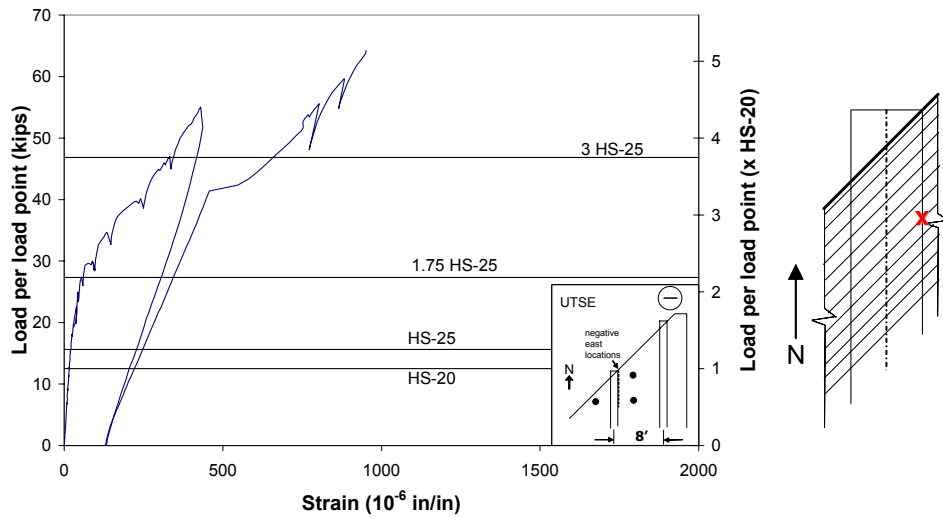
A.2 IBTS END DETAIL, NEGATIVE-MOMENT REGION
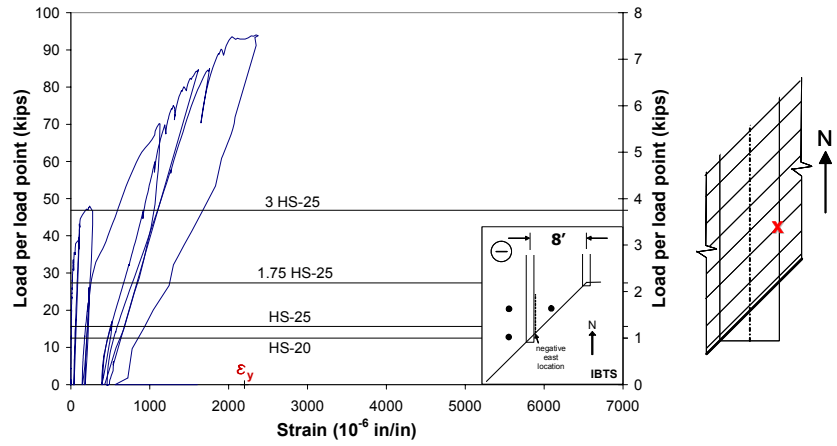
(a)
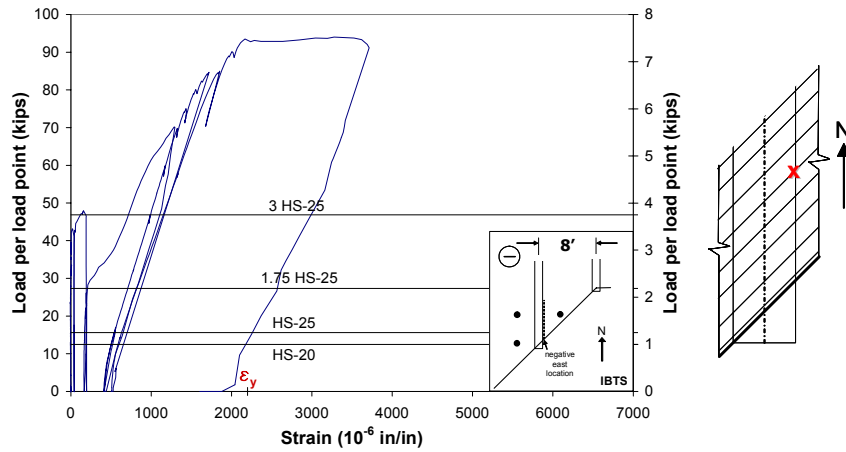
(b)

Figure A-1 Load-strain response, IBTS, negative-moment region, locations on
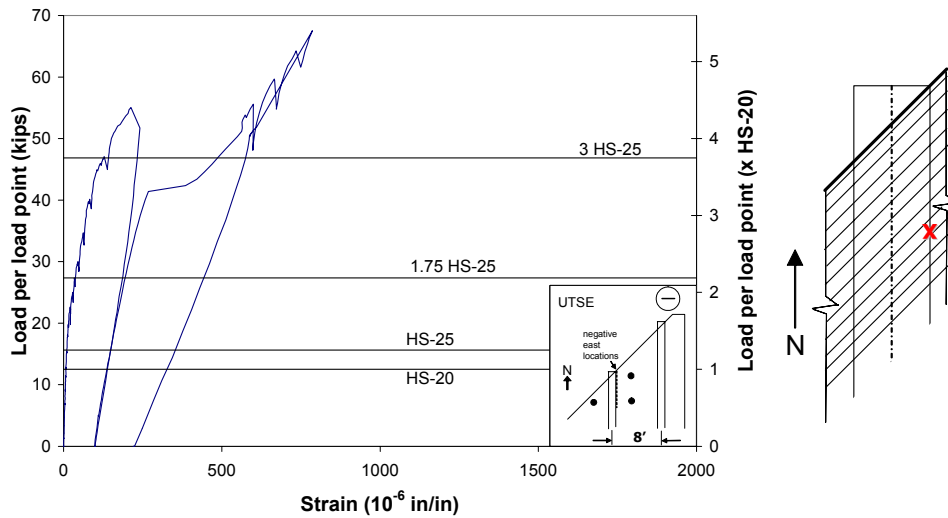*east side of east-interior girder, top mat*

262
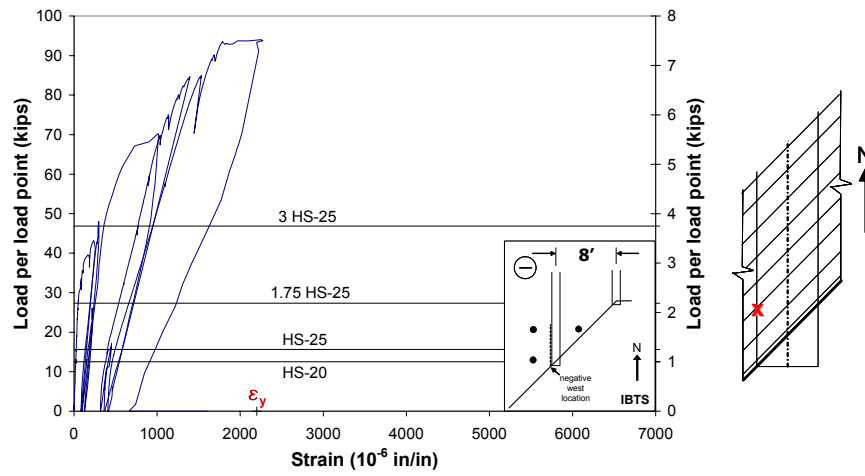
(a)
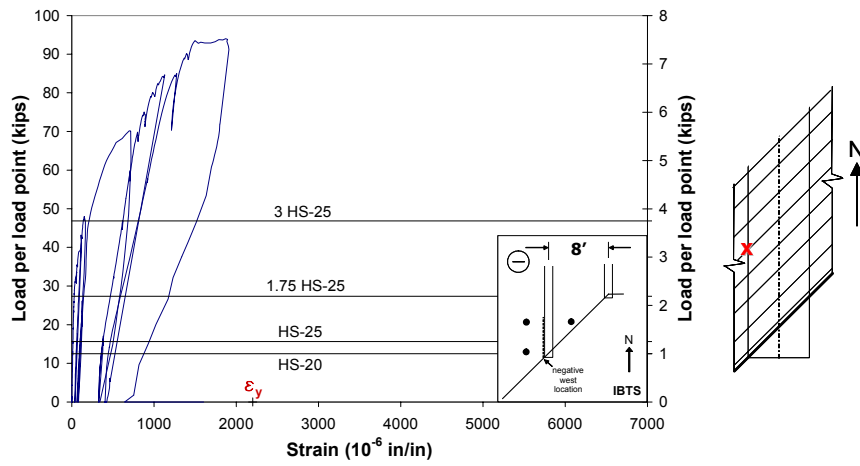
(b)

Figure A-2 Load-strain response, IBTS, negative-moment region; locations on
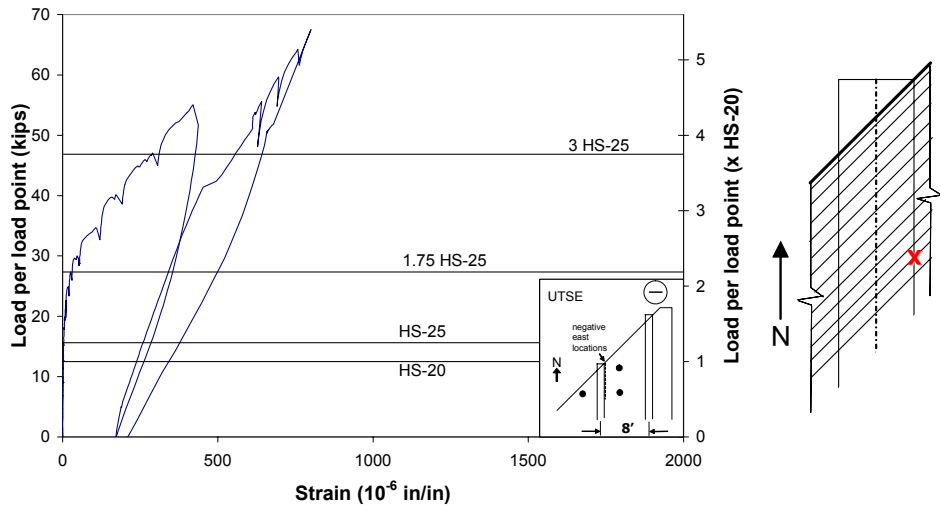
*west side of east-interior girder, top mat*
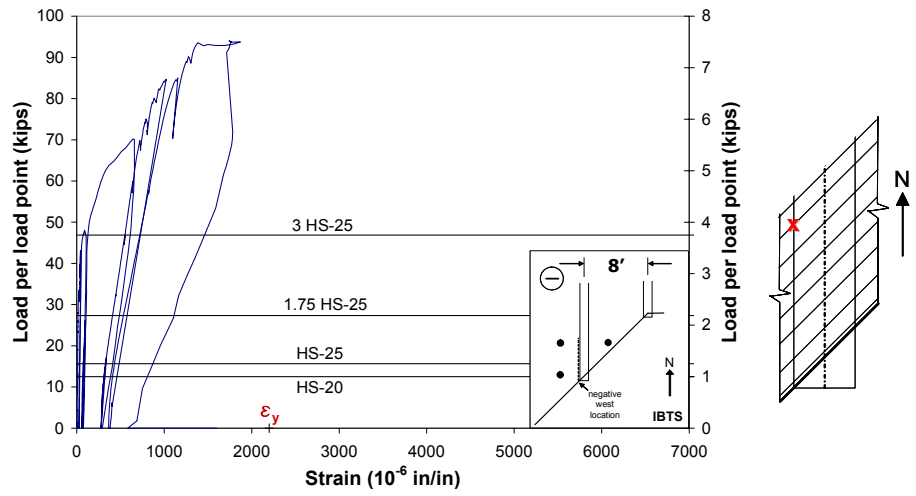
(c)
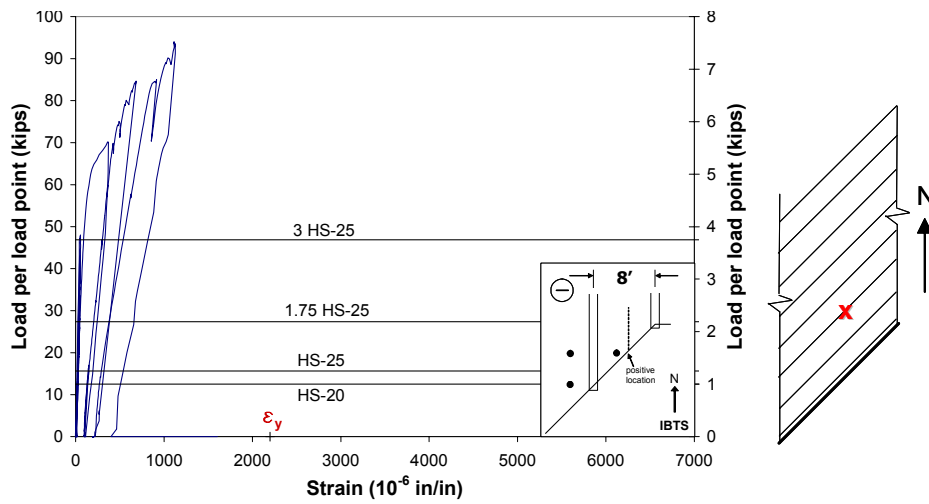
(a)

Figure A-3 Load-strain response, IBTS, negative-moment region; locations at midspan, bottom mat

264
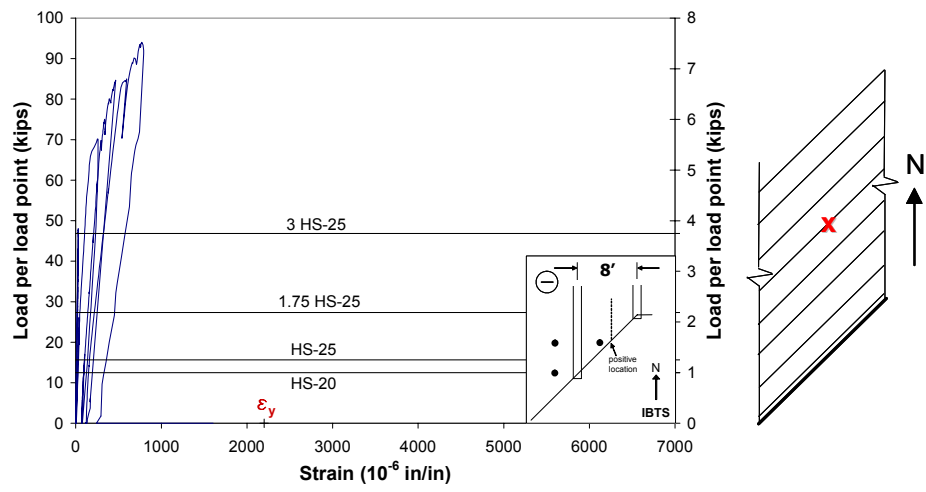
(b)
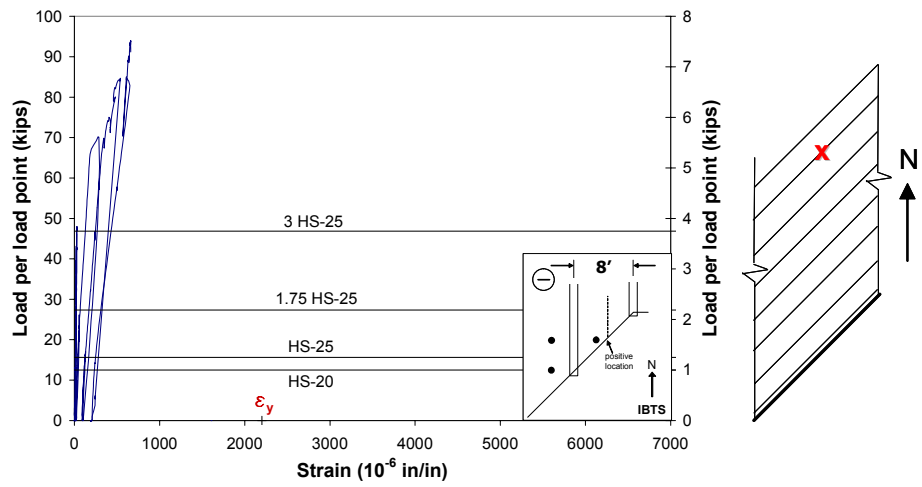
(c)

Figure A-3 cont'd. Load-strain response, IBTS, negative-moment region;

locations at midspan, bottom mat

265

A.3   UTSE End Detail, Negative-Moment Region
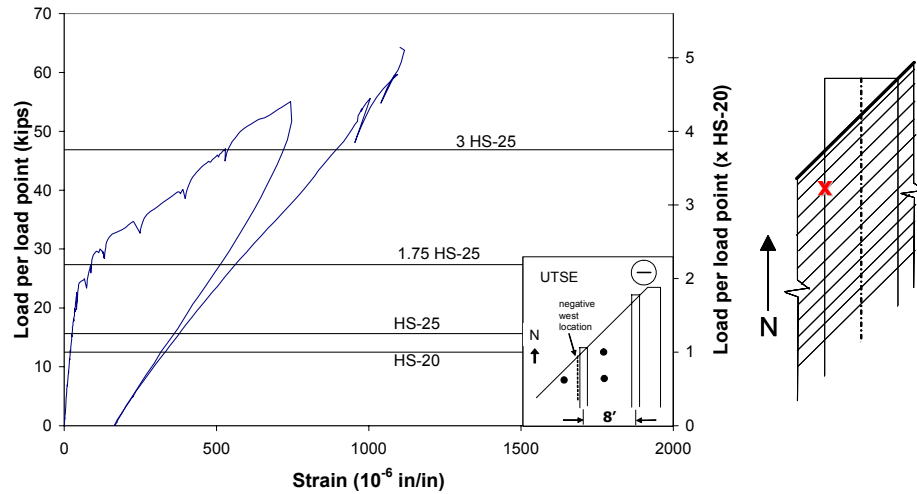
(a)
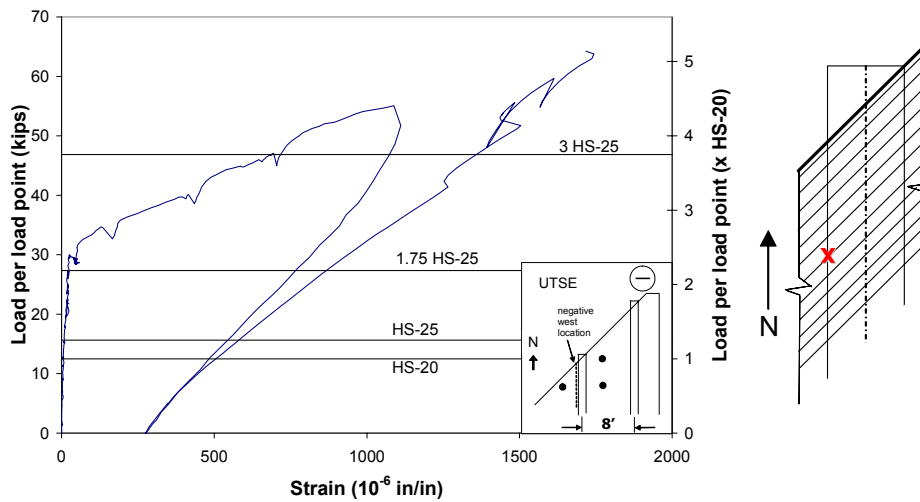
(b)

Figure A-4 Load-strain response, UTSE, negative-moment region; locations on west side of east-interior girder, top mat
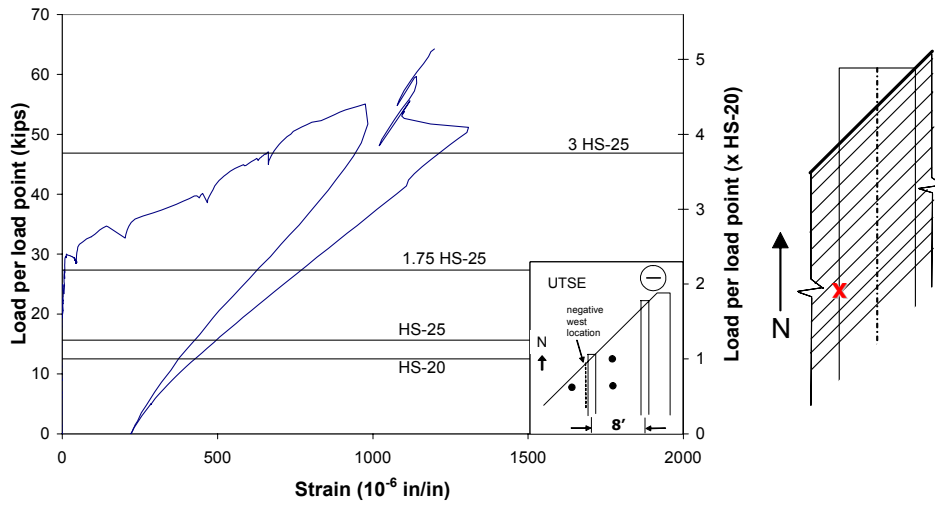
(c)
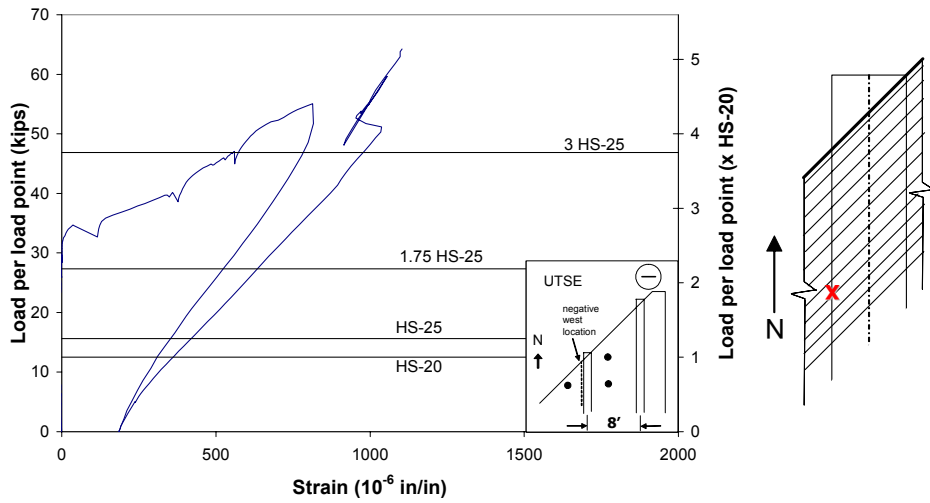
(d)

Figure A-4 cont'd. Load-strain response, UTSE, negative-moment region; locations on west side of east-interior girder, top mat
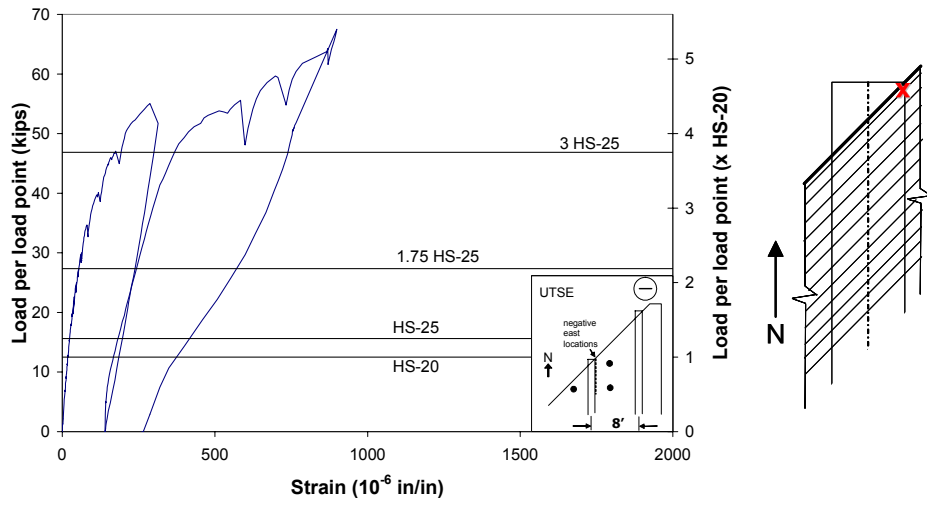
(a)
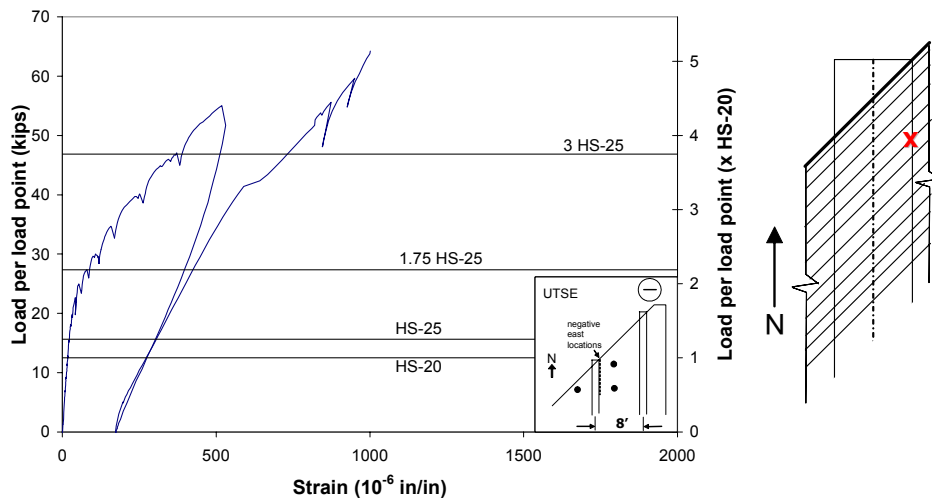
(b)

Figure A-5 Load-strain response, UTSE, negative-moment region; locations on east side of east-interior girder, top mat

(c)

(d)

Figure A-5 cont'd. Load-strain response, UTSE, negative-moment region; locations on east side of east-interior girder, top mat

(e)

Figure A-5 cont'd. Load-strain response, UTSE, negative-moment region; locations on east side of east-interior girder, top mat
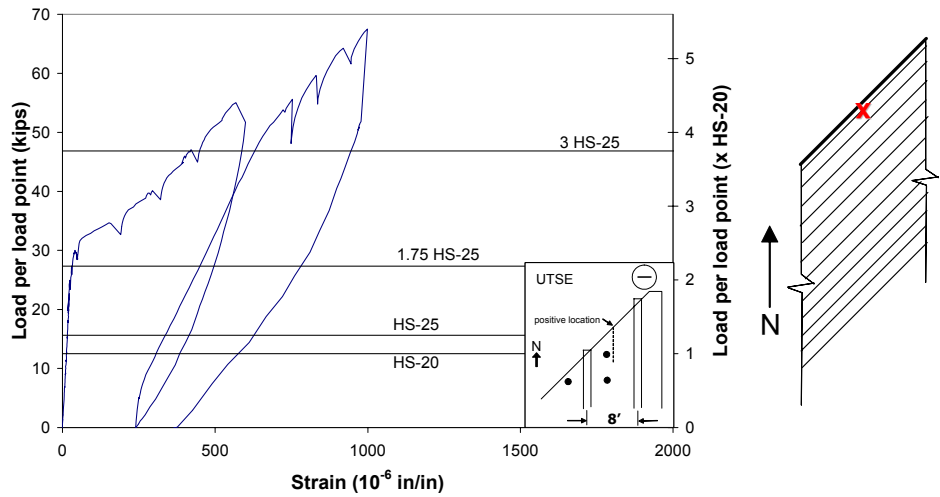
(a)

Figure A-6 Load-strain response, UTSE, negative-moment region; location at midspan, bottom mat

270

A.4 IBTS END DETAIL, POSITIVE-MOMENT REGION
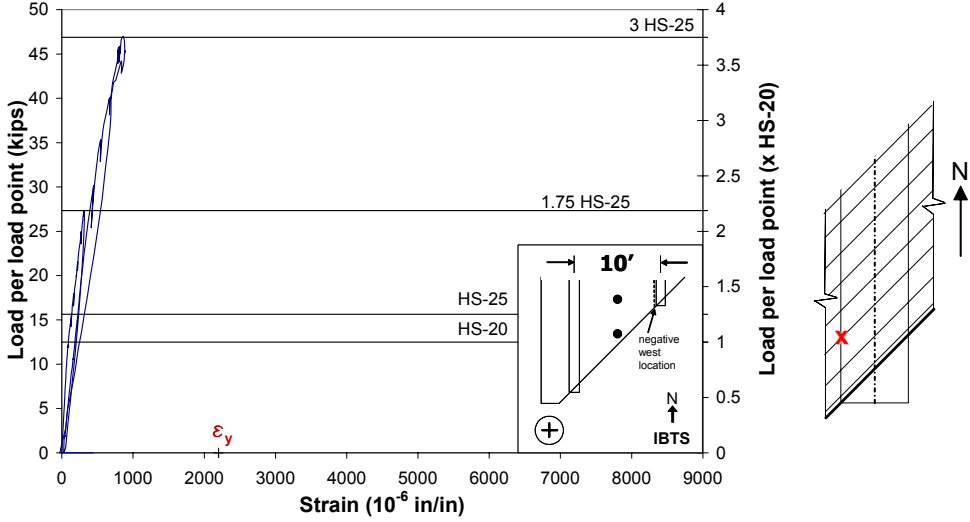
(a)
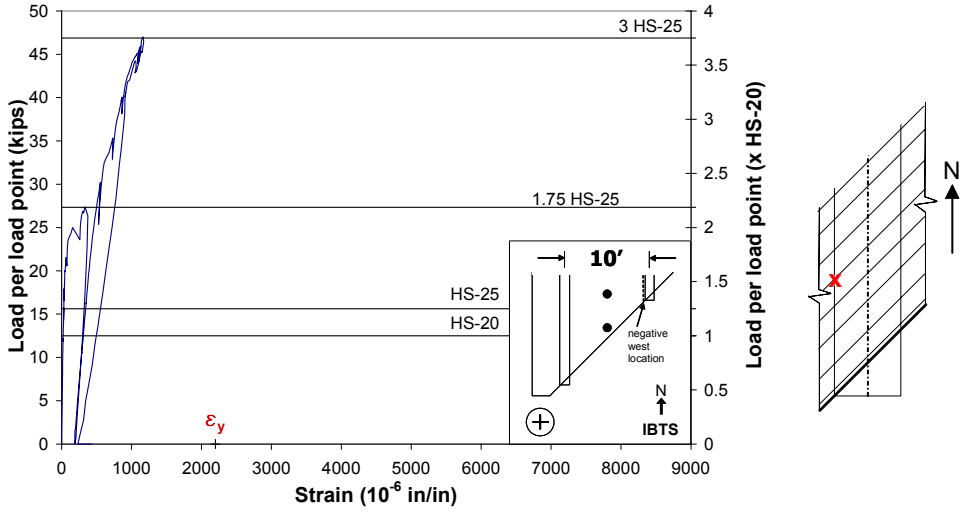
(b)

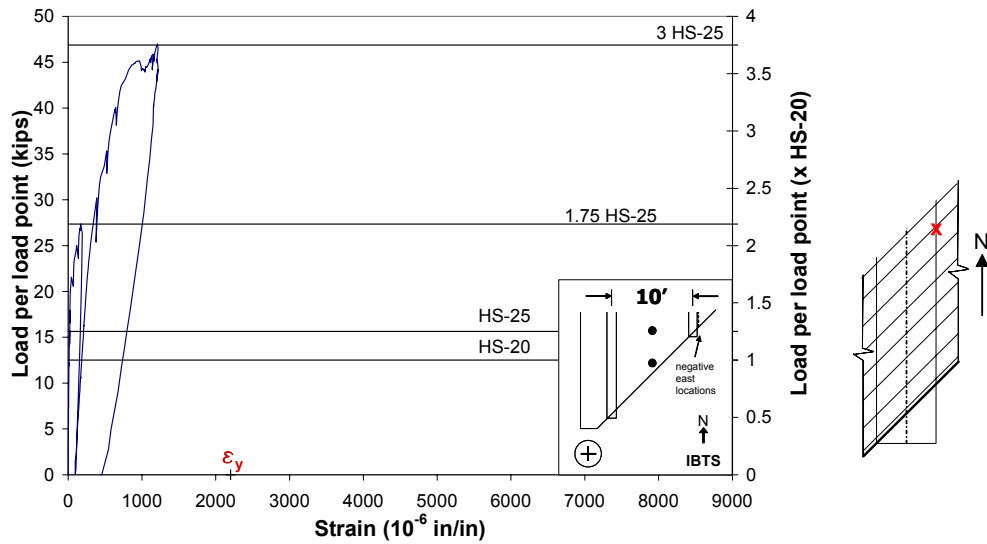*Figure A-7 Load-strain response, IBTS, positive-moment region; location on west side of girder, top mat*
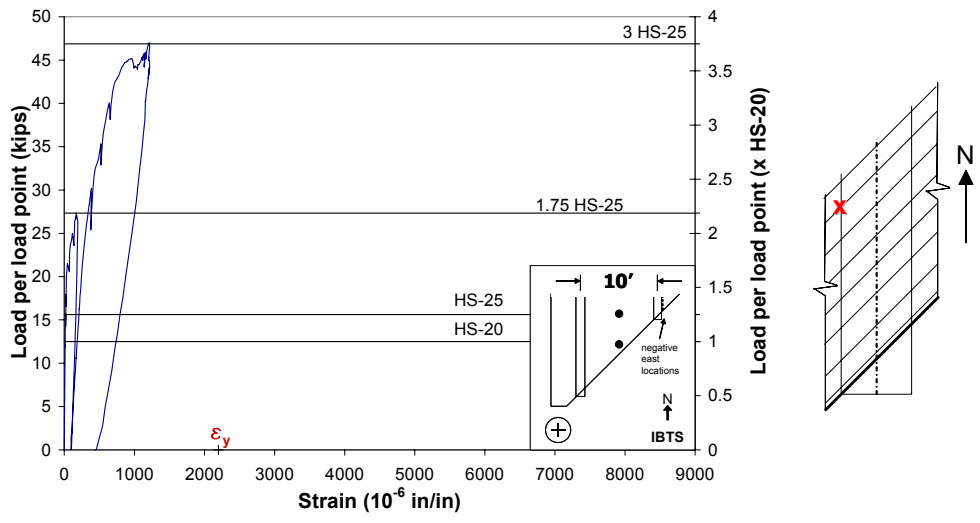
(c)

*Figure A-7 cont'd. Load-strain response, IBTS, positive-moment region;
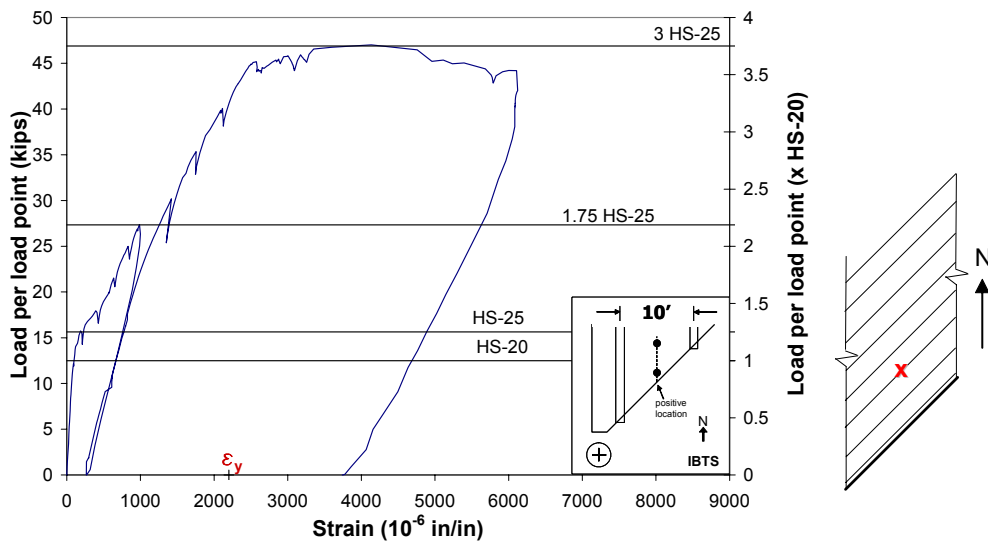location on west side of girder, top mat*
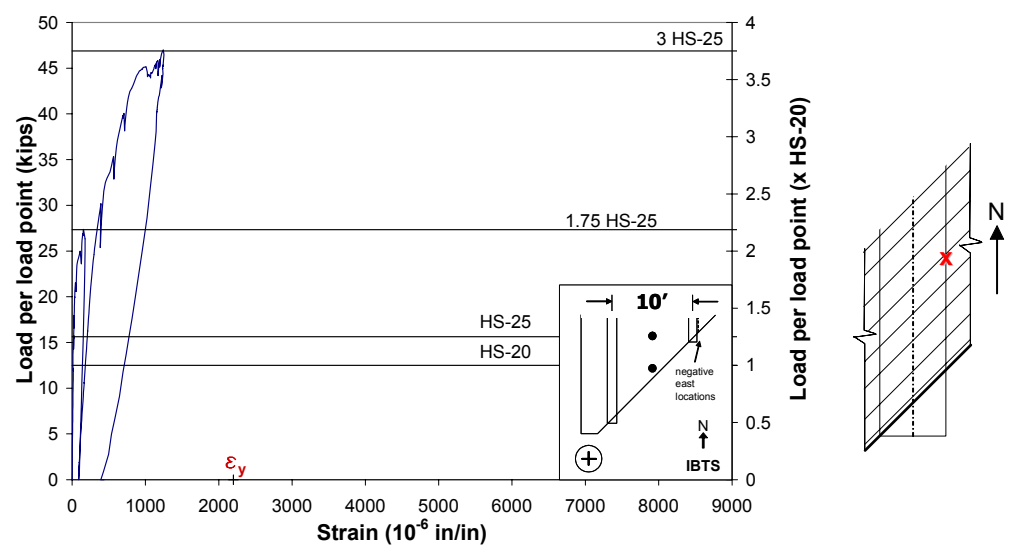
(a)

*Figure A-8 Load-strain response, IBTS, positive-moment region; location on
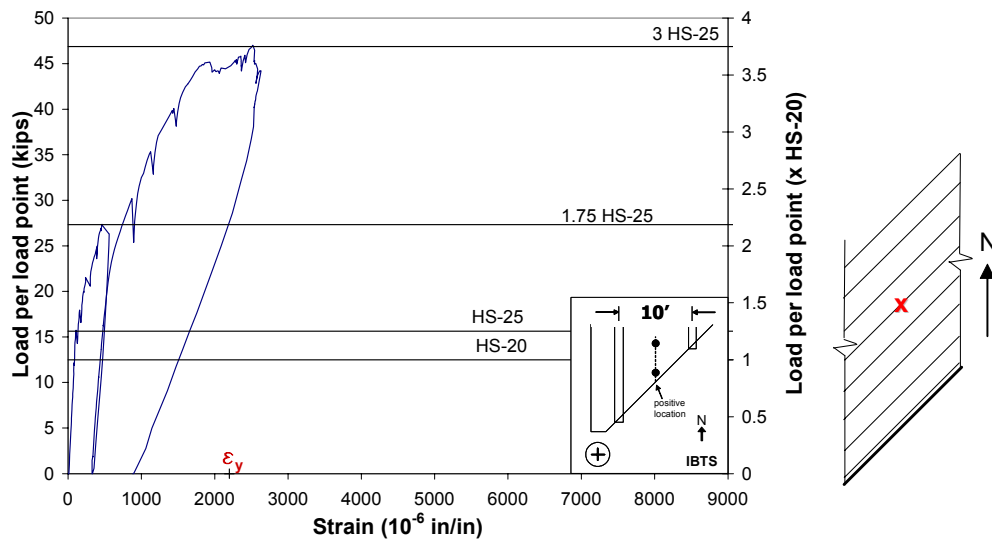east side of girder, top mat*

(b)

Figure A-8 cont'd. Load-strain response, IBTS, positive-moment region; location on east side of girder, top mat
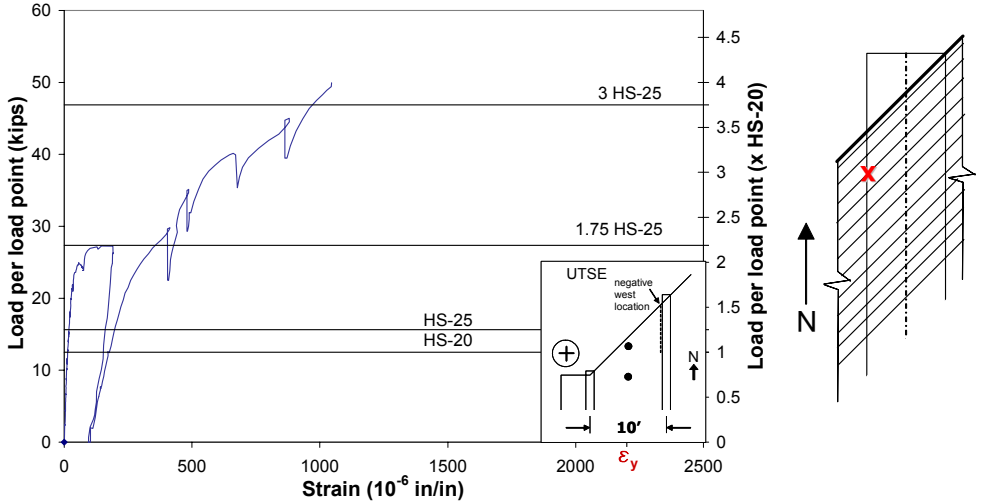

(a)

Figure A-9 Load-strain response, IBTS, positive-moment region; location at midspan, top mat
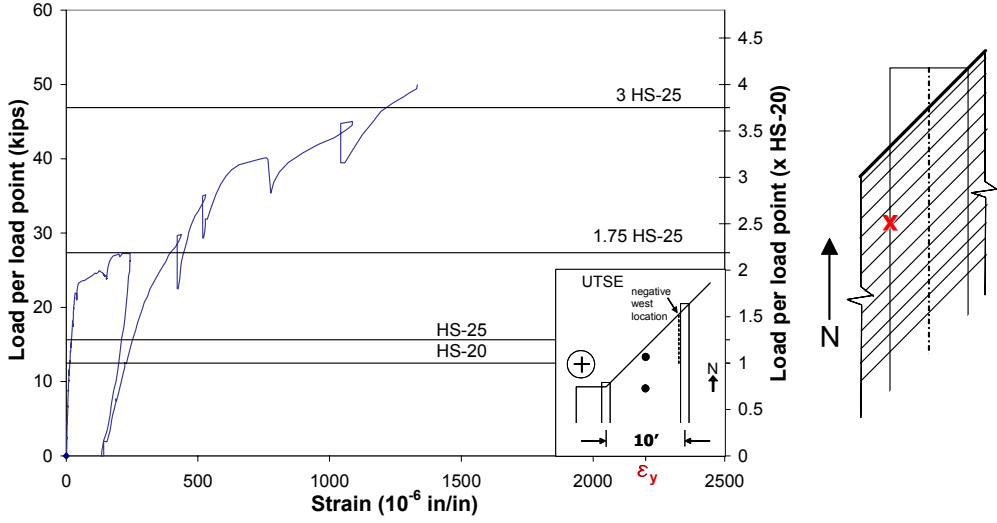
273

(b)

Figure A-9 cont'd. Load-strain response, IBTS, positive-moment region;

location at midspan, top mat

A.5 UTSE End Detail, Positive-Moment Region

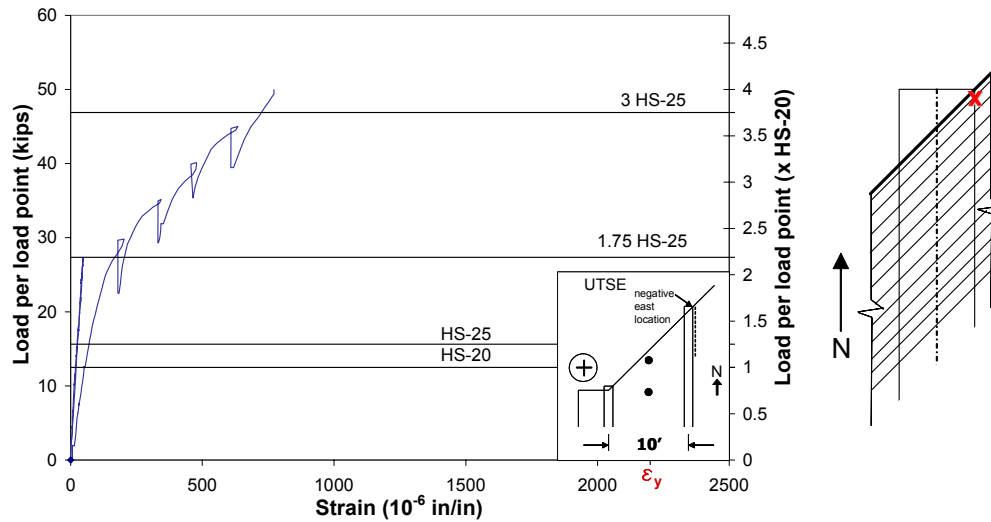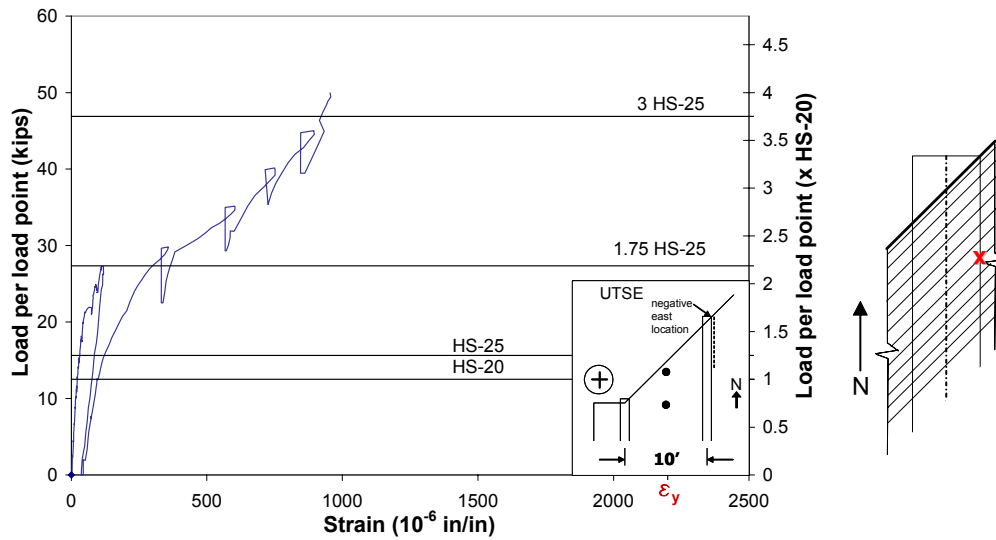(a)

(b)

Figure A-10 Load-strain response, UTSE, positive-moment region; locations

on west side of girder, top mat

275
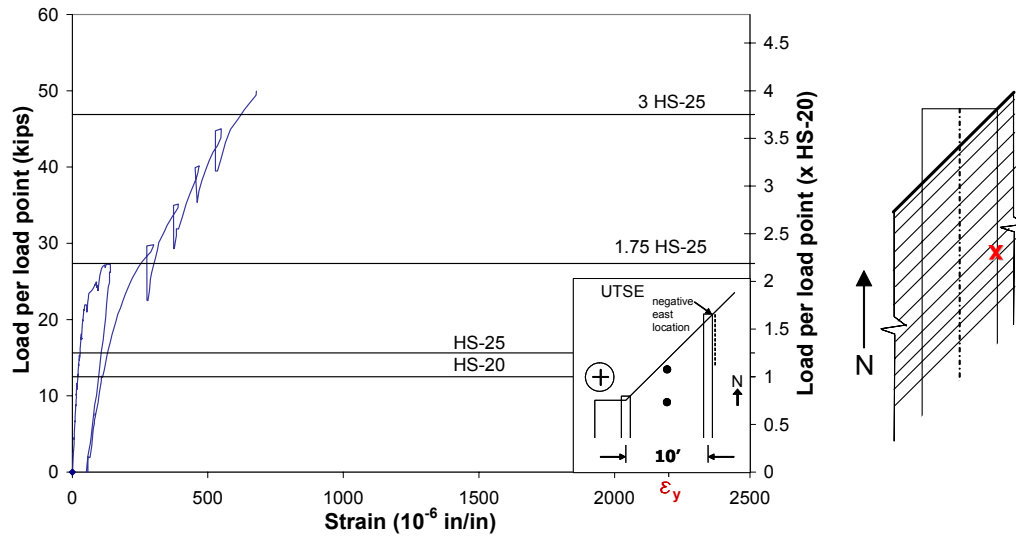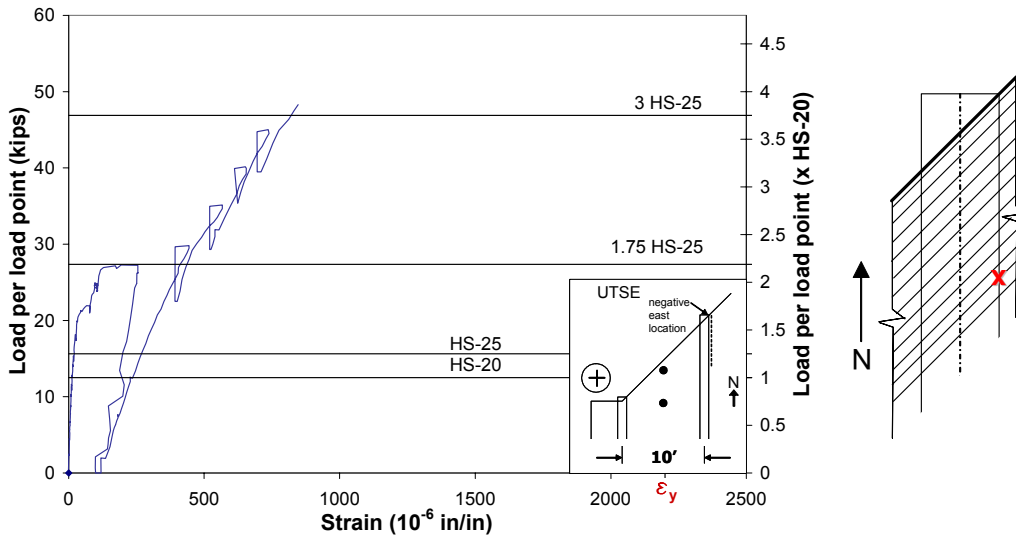
(a)

(b)

Figure A-11 Load-strain response, UTSE, positive-moment region; locations

on east side of girder, top mat
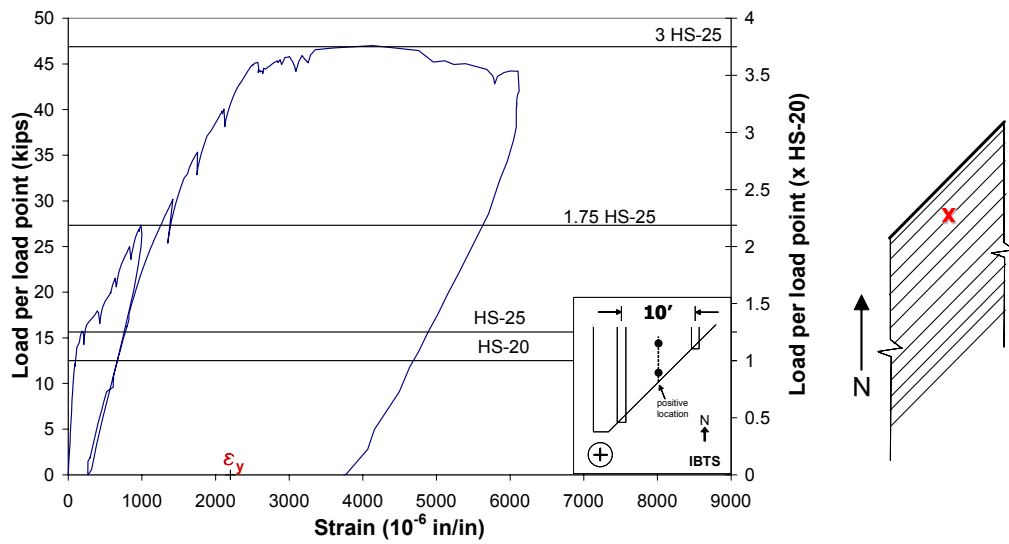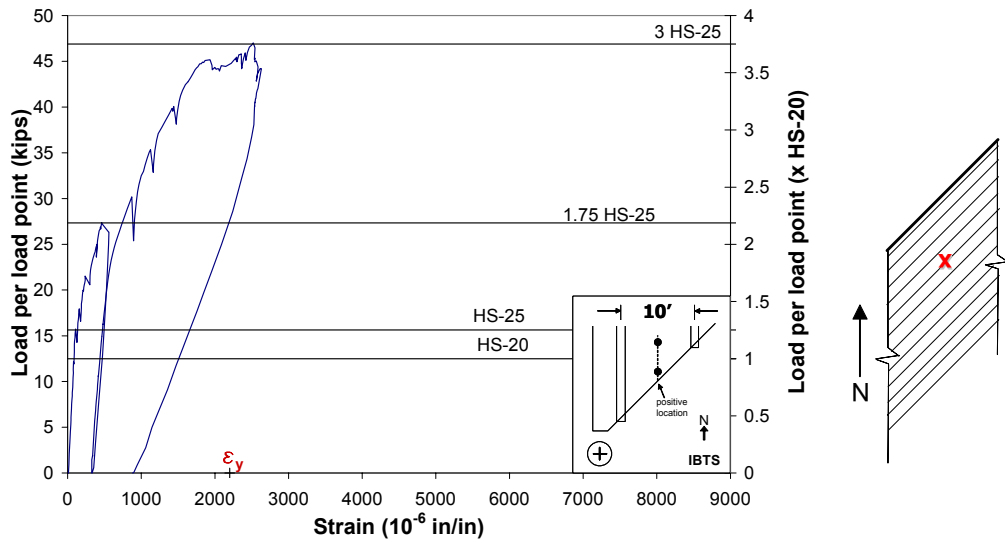
276

(c)

(d)

Figure A-11 cont'd. Load-strain response, UTSE, positive-moment region;

locations on east side of girder, top mat

277

(a)

(b)

Figure A-12 Load-strain response, UTSE, positive-moment region; locations at midspan, bottom mat

278

References

1. American Association of State Highway and Transportation Officials (1998), *AASHTO LRFD Bridge Design Specifications*, 2nd Edition.

2. ACI Committee 318 (2002), "Building Code Requirements for Structural Concrete (ACI 318-02) and Commentary (318R-02)," American Concrete Institute, Farmington Hills, Mich., 319 pp.

3. Azad, A., Baluch, M., Al-Mandil, M., Sharif, A., and Kareem, K. (1993), "Loss of Punching Capacity of Bridge Deck Slabs from Crack Damage," *ACI Structural Journal*, Vol. 90, No. 1, Jan.-Feb., pp. 37-41.

4. Azad, A., Baluch, M., Abbasi, M., and Kareem, K. (1994), "Punching Capacity of Deck Slabs in Girder-Slab Bridges," *ACI Structural Journal*, Vol. 91, No. 6, Nov.-Dec. pp. 656-661.

5. Batchelor, B., and Hewitt, B. (1976), "Tests of Model Composite Bridge Decks," *ACI Structural Journal*, Vol. 73, No. 6, Jun., pp. 340-343.

6. Batchelor, B., Hewitt, B., Casgoly, P., and Holowka, M. (1978), "Investigation of the Ultimate Strength of Deck Slabs of Composite Steel/Concrete Bridges," *Transportation Research Record*, No. 664, p. 162-170.

7. Bazant, Z., and Cao, Z. (1987), "Size Effect in Punching Shear Failure of Slabs," *ACI Structural Journal*, Vol. 84, No. 1, Jan.-Feb., pp. 44-53.

8. Beal, David B. (1982), "Load Capacity of Concrete Bridge Decks," <u>Proceedings</u>, ASCE, No. ST4, Apr., pp. 814-831.

9. Cao, L., Allen, J., Shing, P., and Woodham, D. (1996), "Behavior of RC Bridge Decks with Flexible Girders," *Journal of Structural Engineering*, Vol. 122, No. 1, Jan., pp. 11-19.

10. Christiansen, K. (1963), "The Effect of Membrane Stresses on the Ultimate Strength of the Interior Panel in a Reinforced Concrete Slab," *The Structural Engineer*, Vol. 41, No. 8, Aug., pp. 261-265.

11. Csagoly, P., Holowka, M., and Dorton, R., (1978), "The True Behavior of Thin Concrete Bridge Slabs," *Transportation Research Record*, No. 664, pp. 171-179.

12. Dorton, R., Holowka,M., and King, J. (1977), "The Conestogo River Bridge – Design and Testing," *Canadian Journal of Civil Engineering*, Vol. 4, No. 1, pp. 18-39.

13. Ebeido, T., and Kennedy, J. (1996), "Punching Strength of Deck Slabs in Skew Composite Bridges," *Journal of Bridge Engineering*, Vol. 1, No. 2, May, pp. 59-65.

14. Fang, I., Worley, J., Burns, N., and Klingner, R. (1990), "Behavior of Isotropic R/C Bridge Decks on Steel Girders," *Journal of Structural Engineering*, Vol. 116, No. 3, Mar., pp. 659-678.

15. Fang, I., Lee, J., and Chen, C. (1994), "Behavior of Partially Restrained Slabs under Concentrated Load," *ACI Structural Journal*, Vol. 91, No. 2, Mar.-Apr., pp. 133-139.

16. Fenwick, R., and Dickson, A. (1989), "Slabs Subjected to Concentrated Loading," *ACI Structural Journal*, Vol. 86, No. 6, Nov.-Dec., pp. 672-678.

17. Gamble, L., Sozen, M., and Siess, C. (1962), "Tests of a Modified Reinforced Concrete Two-Way Slab," *Journal of the Structural Division*, ASCE, Vol. 95, No. ST6, June, pp. 1097-1116.

18. Graddy, J., Kim, J., Whitt, J., Burns, N., and Klingner, R. (2002), "Punching-Shear Behavior of Bridge Decks under Fatigue Loading," *ACI Structural Journal*, Vol. 99, No. 3, May-Jun., pp. 257-266.

19. Hewitt, B., and Batchelor, B. (1975), "Punching shear strength of restrained slabs," *Journal of the Structural Division*, ASCE, Vol. 101, No. ST9, Sept., pp. 1837-1850.

20. Jackson, P. (1990), "The Global and Local Behavior of Bridge Deck Slabs," *The Structural Engineer*, Vol. 68, No. 6, Mar., pp. 112-116.

21. Jiang, D., and Shen, J. (1986), "Strength of Concrete Slabs in Punching Shear," *Journal of Structural Engineering*, Vol. 112, No. 12, Dec., pp 2578-2591.

22. Kuang, J., and Morley, C. (1992), "Punching Shear Behavior of Restrained Reinforced Concrete Slabs," *ACI Structural Journal*, Vol. 89, No. 1, Jan.-Feb., pp. 13-19.

23. Law, S., Ward, H., Shi, G., Chen, R., Waldron, P., and Taylor, C. (1995), "Dynamic Assessment of Bridge Load-Carrying Capacities," *Journal of Structural Engineering*, Vol. 121, No. 3, Mar., pp. 478-495.

24. Miller, R., Aktan, A., and Shahrooz, B. (1994), "Destructive of Decommissioned Concrete Slab Bridge," *Journal of Structural Engineering*, Vol. 120, No. 7, Jul., pp. 2176-2197.

25. Moehle, J., Kreger, M., and Leon, R. (1988), "Background to Recommendations for Design of Reinforced Concrete Slab-Column Connections," *ACI Structural Journal*, Vol. 85, No. 6, pp. 636-644.

26. Ockleston, A. J. (1955), "Load Tests on a Three Storey Reinforced Concrete Building in Johannesburg," *The Structural Engineer*, Oct., pp. 304-322.

27. Ockleston, A. J. (1958), "Arching Action In Reinforced Concrete Slabs," *The Structural Engineer*, Jun., pp. 197-201.

28. Park, R., and Gamble, L. (2000), *Reinforced Concrete Slabs*, John Wiley and Sons, New York.

29. Petrou, M., and Perdikaris, P. (1996), "Punching Shear Failure in Concrete Decks as Snap-Through Instability," *Journal of Structural Engineering*, Vol. 122, No. 9, Sept., pp. 998-1005.

30. Petrou, M., Perdikaris, P., and Duan, M. (1996), "Static Behavior of Noncomposite Concrete Bridge Decks under Concentrated Loads," *Journal of Bridge Engineering*, Vol. 1, No. 4, Nov., pp. 143-154.

31. Ryan, J. (2003), "Zero-skew Bridge Deck Behavior at Expansion Joints," Master's Thesis, The University of Texas at Austin, Texas, Aug., 319 pp.

32. Youn, S., and Chang, S. (1998), "Behavior of Composite Bridge Decks Subjected to Static and Fatigue Loading," *ACI Structural Journal*, Vol. 95, No. 3, May-Jun., pp. 249-258.

Vita

Elizabeth Michelle Griffith, the daughter of Mike and Judy Woodward, was born in Huntsville, Texas on March 3, 1978. She grew up in LaGrange, Texas, where she completed high school in 1996. In 1996, she entered the University of Texas at Austin, where she received a Bachelor of Science degree in civil engineering in 2001. In January, 2002, she entered The Graduate School at The University of Texas at Austin. In May, 2002, she married Joel Griffith.

Permanent Address: 209 Richard Road

La Grange, Texas 78945

This thesis was typed by the author.